UNIVERSITAT DE BARCELONA

Enhanced hyaluronidase and tumor neoepitope expression by oncolytic adenoviruses

Martí Farrera Sal

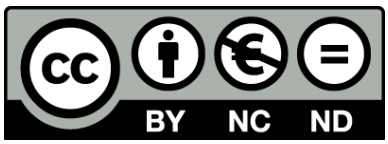

UNIVERSITAT DE BARCELONA

FACULTAT DE FARMÀCIA I CIÈNCIES DE L'ALIMENTACIÓ

PROGRAMA DE DOCTORAT EN BIOTECNOLOGIA

ENHANCED HYALURONIDASE AND TUMOR NEOEPITOPE EXPRESSION BY ONCOLYTIC ADENOVIRUSES

MARTÍ FARRERA SAL

2020

UNIVERSITAT DE BARCELONA

FACULTAT DE FARMÀCIA I CIÈNCIES DE L'ALIMENTACIÓ

PROGRAMA DE DOCTORAT EN BIOTECNOLOGIA

ENHANCED HYALURONIDASE AND TUMOR NEOEPITOPE EXPRESSION BY ONCOLYTIC ADENOVIRUSES

MARTÍ FARRERA SAL

2020

Memòria presentada per Martí Farrera Sal per optar al grau de Doctor/a per la Universitat de Barcelona

Coodirectors: Dr. Ramon Alemany i Bonastre

Dra.Míriam Bazán-Peregrino

Bazan, Miriam
Firmado digitalmente por Bazan, Miriam
Fecha: 2020.07.21 19:44:01 +02'00'

Tutora: Dra. Josefa Badia Palacin

Josefa Badia Palacin
Firmado digitalmente por Josefa Badia Palacin
Fecha: 2020.07.14 16:05:09 +02'00'

Autor: Martí Farrera Sal

TABLE OF CONTENTS

LIST OF FIGURES

LIST OF TABLES

ABBREVIATIONS

%	Percentage
ºC	Centigrade degrees
Δ24	*delta*24 mutation, deletion of 24 bp in E1A protein
µg	microgram
µL	microliter
µM	micrometer
AAALAC	Association for Assessment and Accreditation of Laboratory Animal Care
ACK	Ammonium-chloride-potassium
ACT	Adoptive T cell therapy
Ad	Adenovirus
ADP	Adenovirus Death Protein
ALL	Acute Lymphocytic Leukemia
AML	Acute myeloid Leukemia
APC	Antigen-Presenting Cell
ATCC	American Type Cell Culture
ATP	Adenosine triphosphate
BAC	Bacterial Artificial Chromosome
BCA	Bicinchoninic Acid Assay
BiTE	Bispecific T-cell engager
bp	base pairs
BSA	Bovine Serum Albumin
$CaCl_2$	Calcium chloride
CAF	Cancer-Associated Fibroblast
CAR	Coxsackievirus B and Adenovirus Receptor
CCE	Clarified Cell Extract
CD3	Cluster of differentiation 3
CD4 and 8	Cluster of differentiation 4 and 8
cDNA	complementary DNA
CE	Cell Extract
CEA	Carcinoembryonic antigen
CFSE	Carboxyfluorescein succinimidyl ester
Cm	Chloramphenicol

cm	centimeter
CMV	Cytomegalovirus
CO_2	Carbon dioxide
CPE	Cytopathic effect
CRC	Colorectal cancer
CsCl	Cesium chloride
CTL	Cytotoxic T Lymphocyte
CR	Complement Receptors
CRAd	Conditionally Replicative Adenovirus
CsCl	Cesium chloride
CTL	Cytotoxic T Lymphocyte
CTLA-4	Cytotoxic T-Lymphocyte-Associated Protein 4
DAB	3,3'-Diaminobenzidine
DAMP	Damage-Associated Molecular Pattern
DC	Dendritic cell
DMEM	Dulbecco's Modified Eagle's Medium
DMSO	Dimethyl sulfoxide
DNA	Deoxyribonucleic Acid
dNTP	Nucleoside triphosphate
EC_{50}	Half maximal effective concentration
ECM	Extracellular matrix
EDTA	Ethylenediaminetetraacetic acid
EGFR	Epidermal growth factor receptor
ELISA	Enzyme-Linked ImmunoSorbent Assay
EPCAM	Epithelial cell adhesion molecule
EphA2	EphA2 Ephrin receptor tyrosine kinase A2
ER	Endoplasmic Reticulum
FACS	Fluorescence Activated Cell Sorting
FAP	Fibroblast activation protein
FBiTE	FAP-BiTE
FasL	Fas Ligand
FBS	Fetal Bovine Serum
FDA	Food and Drug Administration

FX	Coagulation factor X
g	acceleration of gravity
g	gram
GM-CSF	Granulocyte Macrophage-Colony Stimulating Factor
h	hour
H_2O_2	Hydrogen peroxide
HCl	Chloridric acid
HEK293	Human Embryonic Kidney 293
HEPES	4-(2-hydroxyethyl)-1-piperazineethanesulfonic acid
Her2	Human EGF receptor 2
HMGB1	High Mobility Group Box 1 Protein
HSPG	Heparan Sulphate Glycosaminoglicans
HSV	Herpes Simplex Virus
hTERT	Human telomerase reverse transcriptase
HVR	Hypervariable region
Hyal	Hyalurodinase
IC_{50}	Inhibitory Concentration 50
ICD	Immunogenic Cell Death
IFN	Interferon
Ig	Immunoglobulin
IL	Interleukin
IP	Intraperitoneal
IRES	Internal Ribosome Entry Site
IT	Intratumoral
ITR	Inverted Terminal Repeats
IU	International Units
IV	Intravenous
IVIS	*In Vivo* Imaging System
K	Kozak sequence
Kan	Kanamycin
kb	kilobase
KC	Kupffer Cell
KRAS	V-Ki-ras2 Kirsten rat sarcoma viral oncogene homolog

L	Liter
LAG-3	Lymphocyte activation gene 3
LITR	Left Inverted Terminal Repeat
mAb	Monoclonal antibody
MDSC	Myeloid-derived suppressor cell
mg	milligram
MHC-I	Class I Major Histocompatibility Complex
min	minute
miRNA	MicroRNA
mL	milliliter
MLP	Major Late Promoter
MLU	Major Late transcription Unit
mm	millimeter
mm^3	cubic millimeter
mM	Millimolar
MMP	Matrix Metalloprotease
MOI	Multiplicity of Infection
mRNA	Messenger Ribonucleic Acid
MSC	Mesenchymal Stem Cell
MV	Maeslas virus
NAbs	Neutralizing antibodies
NaCl	Sodium chloride
NaH_2PO_4	Monosodium phosphate
Na_2HPO_4	Disodium phosphate
NaOH	Sodium hydroxide
NDV	Newcastle Disease Virus
NF-κB	Nuclear factor Kappa-light-chain-enhancer of activated B cells
ng	nanogram
NK	Natural Killer
nm	Nanometer
NOD-scid	Non-obese diabetic
NSCLC	Non-Small Cell Lung Carcinoma
NSG	Nod Scid Gamma

OAd	Oncolytic adenovirus
OCT	Optimum Cutting Temperature compound
OD	Optical Density
OV	Oncolytic virus
PAMP	Pathogen-Associated Molecular Pattern
pA	Polyadenylation sequence
PAMP	Pathogen-Associated Molecular Pattern
PBMCs	Peripheral blood mononuclear cells
PBS	Phosphate Buffered Saline
PCR	Polymerase Chain Reaction
PD-1	Programmed cell death protein-1
PD-L1	Programmed cell death Protein Ligand-1
pg	Picogram
pmol	Picomol
PRR	Pattern Recognition Receptor
PS	Penicillin-Streptomycin
PSA	Prostate-Specific Antigen
PTEN	Phosphate and tensin homolog
Rb	Retinoblastoma
RGD	Arginine-glycine-aspartic acid
RITR	Right Inverted Terminal Repeat
RLU	Relative light units
RNA	Ribonucleic Acid
rpm	revolutions per minute
RPMI	Roswell Park Memorial Institute
RT	Room Temperature
RT-PCR	Real-Time PCR
scFv	Single chain fragment variable
Scid	Severe combined immunodefiency
SA	Splicing Acceptor
SD	Standard Deviation
SDS	Sodium dodecyl sulfate
SEM	Standard Error of the Mean

ssDBP	Single-stranded DNA binding proteing
Strep	Streptomycin
TAA	Tumor-Associated Antigen
TAE	Tris-Acetate-EDTA
TAM	Tumor-Associated Macrophage
TAP	Transporter Associated to Antigen Processing
TCR	T Cell Receptor
TE	Tris-EDTA
TGF-β	Transforming Growth Factor-β
TIL	Tumor-Infiltrating Lymphocytes
TIM-3	T-cell immunoglobulin and mucin-domain containing-3
TNF-α	Tumor Necrosis Factor alpha
TP	Terminal Protein
TRAIL	TNF-related apoptosis-inducing ligand
Treg	Regulatory T cell
Tris	Tris(hydroxymethyl)aminomethane
TU	Transducing Unit
V	Volt or Volume
VEGF	Vascular Endothelial Growth Factor
vp	viral particle
VSV	Vesicular Stomatitis Virus
VV	Vaccinia Virus
wt	wild type

Amino acids

F Phe, phenylalanine	**S** Ser, serine	**Y** Tyr, tyrosine	**K** Lys, lysine	**W** Trp tryptophan
L Leu, leucine	**P** Pro, proline	**H** his, histidine	**D** Asp, aspartic acid	**R** Arg, arginine
I Ile, isoleucine	**T** Thr, threonine	**Q** Gln, glutamine	**E** Glu, glutamic acid	**G** Gly, glycine
M Met, methionine	**A** Ala, alanine	**N** Asn, asparagine	**C** Cys, cysteine	**V** Val, valine

Nucleotides

A adenine	**T thymine**	**G guanine**	**C cytosine**	**U uracil**

SUMMARY

The oncolytic viruses (OVs) preferentially infect tumor and selectively replicate in cancer cells without harming normal tissues. OVs have been tested in clinical trials as monotherapy or combined with chemotherapy, radiotherapy, and immunotherapy. Nonetheless, the intratumoral spreading and the immune response hamper the treatment efficacy. In this thesis, these two challenges have been addressed in three separate chapters.

First, VCN-01, a hyaluronidase-expressing oncolytic adenovirus, was tested in a clinical trial in pancreatic cancer patients. We assessed the immune response triggered by VCN-01 as monotherapy or in combination with chemotherapy. We reported an early anti-viral immune response induction of IL-6, IL-10, IFNγ, IDO1, IP-10, and sLAG-3 in serum, independently of chemotherapy. We found a correlation between treatment toxicity and the IL-6 and IL-10. Furthermore, the triggered anti-viral immune response such as IFNγ, sLAG-3, and neutralizing antibodies anti-Ad5 was associated with better antitumor activity in patients.

The neoepitope vaccines have been tested in patients with limited clinical responses. We hypothesized that an oncolytic adenovirus (OAd) encoding for tumor neoepitopes could be a very effective vaccine platform. The expression of tumor neoepitopes may trigger immune response towards tumors, improving OAd therapy, and bypassing the limitations of current vaccines. We provided a proof-of-concept that OAds expressing tumor neoepitopes can induce immune responses against encoded neoepitopes in naïve mice. However, no antitumor activity was observed in a murine pulmonary adenocarcinoma model.

Finally, VCN-01 exhibited enhanced intratumoral spreading and potent antitumor efficacy in different models due to PH20 expression. However, higher hyaluronidase activity than VCN-01 may further treatment efficacy. Higher transcription of hyaluronidase was achieved by two different strategies: after *E1a* via P2A (self-cleaving peptide of porcine teschovirus-1) and after fiber via splice acceptor of Ad40 long fiber. These hyaluronidase-expressing OAds also showed improved antitumor efficacy compared to VCN-01. Furthermore, we postulated that intratumoral hyaluronidase expression may enhance T cell accumulation within tumors. As hyaluronidase activity also facilitates drug delivery into the tumors, these novel hyaluronidase-expressing OAds emerged as candidates to be combined with other treatments with limited efficacy in cancers with dense stroma.

RESUM

Els virus oncolítics (OVs) són capaços de infectar les cèl·lules tumorals i replicar específicament en elles, sense malmetre teixits sans. Els OVs s'han testat en assajos clínics com a monoteràpies o combinats amb quimioteràpia, radioteràpia i immunoteràpia. En base a aquesta experiència s'han identificat la distribució intratumoral i la resposta immunològica com els principals impediments per l'eficàcia d'aquests tractaments. En aquesta tesis, hem abordat en tres capítols diferents estratègies per millorar aquests dos factors.

Primerament, el VCN-01, un adenovirus oncolític que expressa hialuronidasa, s'ha testat en assajos clínics en fase I en pacients amb càncer pancreàtic. Hem analitzat la resposta immune produïda per VCN-01 com a monoteràpia o en combinació amb quimioteràpia. Hem detectat una forta resposta immunològica transitòria després de la injecció de VCN-01 amb increments en serum de IL-6, IL-10, IFNγ, IDO1, IP-10 i sLAG-3. Hem correlacionat els nivells de IL-6 i IL-10 en sèrum amb la toxicitat del tractament. A més a més, La resposta immune anti-viral en forma de IFNγ, sLAG-3, i anticossos contra Ad5 està associada amb una millor eficàcia antitumoral en pacients.

Les vacunes de neoepítops s'han testat recentment com a teràpies antitumorals en pacients, però amb escasses respostes clíniques. En aquesta tesis hipotetizem que els adenovirus oncolítics (OAds) poden expressar neoepítops tumorals actuant com a plataforma de vacunació, i augmentant la resposta immune contra el tumor. En el segon capítol s'exposa com a prova de concepte la capacitat dels OAds d'induir resposta immune contra neoepítops tumorals expressats des del virus en ratolins. No obstant, no s'ha millorat la eficàcia antitumoral en un model murí d'adenocarcinoma pulmonar.

VCN-01 presenta una millor biodistribució en el tumor i una gran eficàcia en diferents models *in vivo,* gràcies a l'expressió de la PH20. Hem aconseguit generar dos virus amb major transcripció de hyaluronidasa que VCN-01, mitjançant dues estratègies: després de *E1a* via P2A (un pèptid del teschovirus-1 porcí) o després de la fibra mitjançant un acceptor de *splicing* de la fibra llarga de l'Ad40. Aquests virus tenen una millor eficàcia antitumoral que VCN-01. A més a més, hem demostrat que l'expressió d'aquest enzim des del tumor pot afavorir l'acumulació de cèl·lules T en el propi tumor. Donat que la hyaluronidasa també afavoreix l'extravasació de fàrmacs en els tumors, els OAds generats en aquesta tesi podrien ser uns excel·lents candidats per combinar amb teràpies que tinguin una eficàcia limitada en tumors amb un estroma dens.

GENERAL INTRODUCTION

1. CANCER IMMUNOLOGY

Cancer cells accumulate mutations that overcome cell division control; resulting in uncontrolled cell proliferation [1]. The original focus of cancer cells forms the primary tumor that can invade surrounding tissues and eventually spread through the lymphatic system or blood to distant sites emerging as a new tumor, known as metastasis.

Cancer cells have DNA-repair defects that cause genetic instability. The tumor mutational burden (TMB) is a measure of accumulated mutations in a cancer type. Genetic alterations result in mutated or aberrant proteins and their abnormal expression, ending in cellular stress [2]. There are two types of tumor antigens: the tumor-associated antigens (TAAs), and tumor-specific antigens (TSA). The TAAs are normal proteins aberrantly expressed in cancer cells. For instance, the prostate-specific antigen is overexpressed in some prostate tumors. In contrast, TSAs are exclusively expressed in tumors as a consequence of a specific-tumor mutation. Mutated proteins can be processed and presented on the major histocompatibility complex (MHC) on the cancer cell surface and elicit immune responses, called neoantigens or neoepitopes. Moreover, another potential source of TSAs in virally-associated tumors (i.e., Epstein-Barr virus related to head and neck cancers) are epitopes derived from viral open reading frames (ORFs).

The innate and the adaptive immune system work together to detect and eliminate transformed cells, a process known as cancer immunosurveillance. The antitumor response starts with the detection of danger signals (danger-associated molecular patterns, DAMPs) by innate immune cells. Natural killer (NK) cells and γδ-T cells monitor the cell surface for aberrant protein expression or cell stress markers and eliminate tumor cells directly [3,4] (**Figure 1,** step 1). The death of cancer cells releases tumor antigens (TAAs and TSAs) that are uptaken by antigen-presenting cells (APCs), the dendritic cells (DCs), macrophages, or B cells. Subsequently, they process and present or cross-present the antigens on MHC-I and MHC-II to induce an adaptive response (**Figure 1**, step 2). The nature of molecules available during APC maturation

determines the type of T CD4$^+$ cell (or T helper cell, Th) and T CD8$^+$ induced response. The surrounding DAMPs such as protein HGMB1, heat-shock proteins, and ATP promote a Th response type I (Th1), characterized by Th1-polarized DCs or M1 macrophages. The Th1 signals, secreted by matured APCs, consist of pro-inflammatory cytokines: interleukin (IL) 12, type I interferons (IFN), and tumor necrosis factor (TNF) among others [5,6].

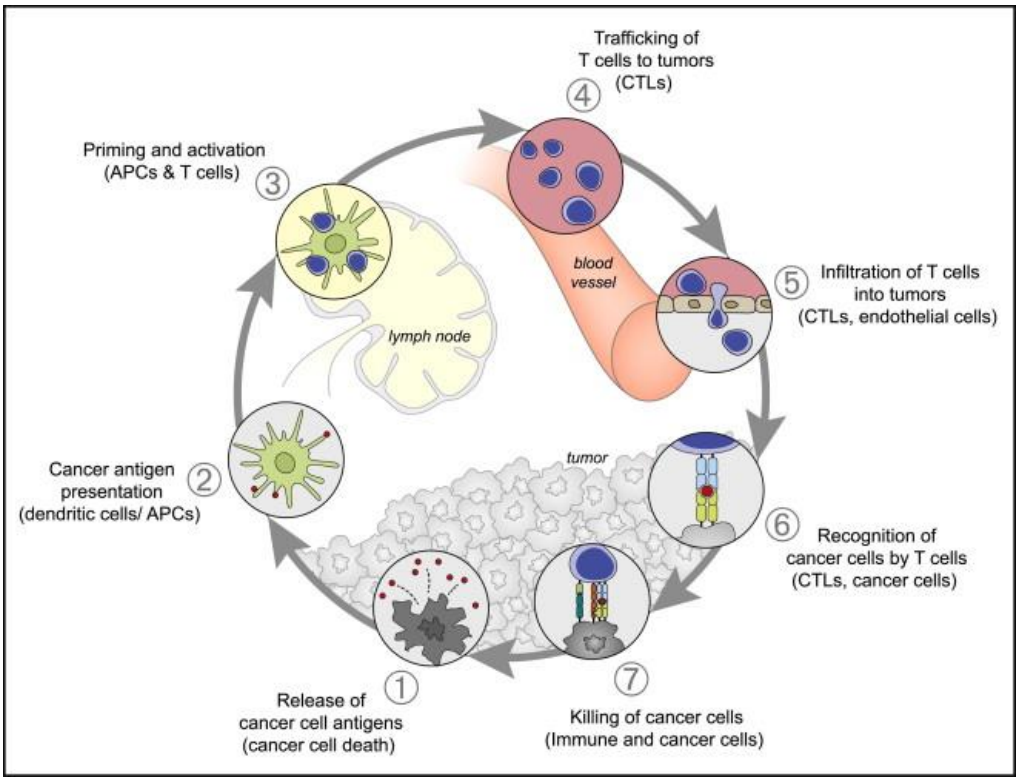

Figure 1. The cancer-immunity cycle. (1) The cancer cell death by cell stress process or innate immune system releases tumor-derived antigens. **(2)** These antigens are captured by antigen-presenting cells (APCs) that maturate and circulate to the draining lymph node. **(3)** At the lymph node, these APCs can prime and activate tumor-specific T-cells. **(4)** The activated CD4$^+$ cells (Th cells) and CD8$^+$ cells (CTLs) are mobilized to the tumor site via a chemokine gradient. **(5)** The lymphocytes extravasate into the tumor, and **(6)** the infiltrating CTLs can recognize cancer-antigens presented in the MHC-I of tumor cells. **(7)** This recognition activates the CTLs inducing the cancer cell killing. Image from [7]

Tumor-antigen-loaded DCs migrate to draining lymph nodes where will interact with T cells (**Figure 1**, step 3). The MHC-presented peptides in DCs would be recognized by specific T cell receptors (TCRs), initiating a signaling cascade that activates the T cell. The costimulatory signals impact in the triggered T-cell response. The Th1 polarized-DC promotes the generation of Th1 $CD4^+$ cells and cytotoxic $CD8^+$ T cells (CTLs). Subsequently, these T cells are mobilized from the lymph node to the tumor site via a gradient of T cell attracting chemokines, including chemokine C-C motif ligand 2 (CCL2), CCL5/RANTES, chemokine C-X-C motif ligand 9 (CXCL9), and CXCL10 (also known as IP-10) [8] (**Figure 1**, step 4 and 5).

At the tumor, the infiltrating CTLs cells can directly recognize and kill cancer cells [9] (**Figure 1**, step 6 and 7). The specific neoantigen-CTLs response has been reported as the predominant in a melanoma patient [10], suggesting that neoepitopes play a pivotal role in antitumor immunity. Apart from the T cell response, plasma B cells infiltrate the tumor margins, in few numbers compared to the T cells, producing cytokines and antibodies. Antibodies enhance the antitumor response by inducing antibody-dependent cellular cytotoxicity (ADCC), phagocytosis, complement activation, and favoring antigen-presentation by DCs. Moreover, B cells form tumor-associated tertiary lymphoid structures (TLS), which support the maturation of B cells and T cells within the tumor microenvironment [11]. Thus DCs provide initial T cell activation in the lymph nodes, and B cells can maintain additional T cell population expansion intratumorally in the TLS [12,13].

If the triggered immune response is enough, the body remains free of cancer in a stage known as the elimination phase (**Figure 2-A**). The immunosurveillance process continuously occurs, as a constant immune selective pressure. Eventually, the cancer cells evolve to evade the immune response, resulting in an equilibrium phase between dying tumor cells and surviving tumor cells (**Figure 2-B**). During this phase, only the immunosuppressive or less immunogenic tumor cell clones survive. This process is known as tumor immunoediting [14], and it leads to the escape phase, where the cancer cells finally evade the immune response forming a tumor (**Figure 2-C**).

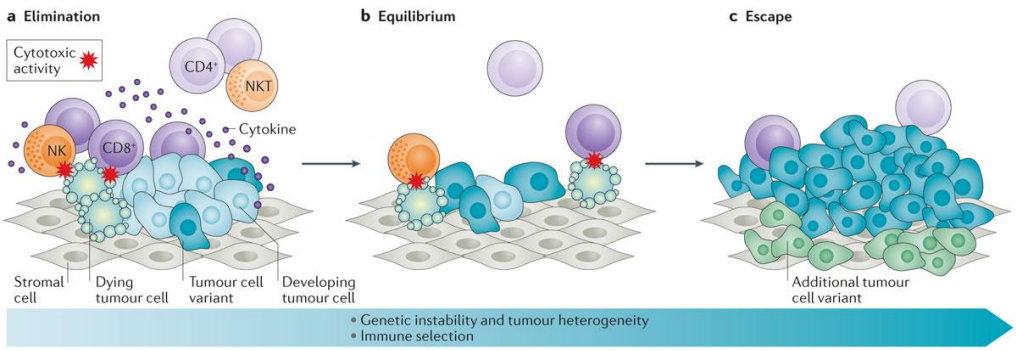

Figure 2. Immunoediting phases. (A) Elimination phase where the immune system detects and eliminates cancer cells, and the body remains free of tumors. **(B)** The equilibrium phase in which some tumor cell variant appears and can evade the immune system attack. This is considered the initial stages of clinically detected tumors. **(C)** The escape phase where the immune system is not able to control tumor growth. Image adapted from [15]

During the transition between equilibrium and elimination phase, cancer cells establish a tumor microenvironment (TME) where the function of immune cells is attenuated. The edited tumor cells and stromal cells (endothelial or epithelial cells and fibroblasts) produce factors such as transforming growth factor-β (TGF-β), prostaglandin E2 and IL-10 that disrupt the APC maturation in the TME [8,15]. The DCs isolated from TME often display a partly matured, immunosuppressive phenotype with a Th2 cytokine-secreting profile [5,8]. The secreted TGF-β inhibits the DCs migration to the lymph node. Even they eventually reach the lymph node, these Th2-DCs induce tolerance, anergy, or the production of regulatory T $CD4^+$ cells (Tregs) and regulatory B cells (Bregs) [11]. The Tregs and myeloid-derived suppressor cells (MDSCs) are recruited to the tumor site and produce indoleamine-2,3-dioxygenase (IDO) and TGF-β inducing attenuation of T cell responses [16]. Tregs consume IL-2, which is indispensable for T cell activation. MDSCs produce arginase and nitric oxide to deprive the amino acids that T cells need to proliferate [8,17]. Bregs are generated in the TLS or recruited into the tumor and produce IL-10 and TGF-β, which convert macrophages into the pro-tumoral M2 phenotype.

Moreover, the tumor infiltration of effector T-cells (CTLs and Th1 cells) is inhibited by repressing the chemokine gradient [5,18]. In the case that effector T cells could infiltrate or have already infiltrated in the tumor become anergic (or exhausted) by the persistent exposure to the antigen in the strongly immunosuppressive conditions. As a result, Th cells and CTLs isolated from TME present an exhausted phenotype, characterized by high-level expression of immune checkpoint receptors such as cytotoxic T-lymphocyte-associated protein 4 (CTLA-4) and programmed cell death protein 1 (PD-1). The interaction between these receptors and their ligands up-regulated in tumor cells, stromal cells, or immunosuppressed APCs inhibits T cell responses. Furthermore, cancer cells can also directly escape T-cell recognition downregulating MHC class I or disabling the antigen processing machinery [19,20]. Even more, the accumulated mutations in genes related to cell death reduce the immunogenicity of the process [21].

Despite the evasion mechanisms, CTLs and Th1 helper cells are still considered to essential for antitumor immunity [22]. Their infiltration in the TME is associated with a good prognosis in various types of cancer [23]. Proper activation of these cells is crucial for the antitumor response; the understanding of tumor mechanisms to suppress these cells offers many targets for cancer therapy.

2. CANCER IMMUNOTHERAPIES

The treatments aiming to trigger the immune system against the cancer cells are termed immunotherapies. Multiple strategies have been developed to target the TME, cancer cells, or immune cells and revert the tumor immunosuppression.

The immune checkpoints are co-stimulatory and co-inhibitory molecules upon interaction with their ligands leads to T cell exhaustion or stimulation, thereby modifying the antitumor immune response (**Figure 3**). One of the most successful approaches has been the use of antibodies to block immune checkpoint inhibitors. A variety of immune checkpoint antibodies have been approved for the treatment of melanoma, head and neck cancers, hepatocellular cancer, Merkel cell carcinoma,

cervical cancer, small cell lung cancer, and others (except pancreatic cancers) [24]. Remarkably, the best responses have been published targeting the PD-1/PD-L1 axis. The greatest clinical activity has been shown in tumor histologies with a high mutation load and T cell infiltrates (commonly named hot tumors). In contrast, those tumors without pre-existing T cells (cold tumors) have not been sensitive to these therapies [25,26].

The adoptive cell transfer (ACT) of tumor-infiltrating lymphocytes (TILs), based on the *ex vivo* isolation and expansion of TILs and their re-infusion into the patient, showed a promising 40% of durable clinical responses in patients with metastatic melanoma. Moreover, antitumor responses have been reported in selected cases of patients with cholangiocarcinoma, colorectal cancer, and breast cancer [27]. Another approach is the chimeric antigen receptor (CAR) T cell therapy. CAR T cells are genetically modified to recognize TAAs specifically. CAR are chimeric molecules composed of an extracellular single-chain (ScFV, derived from an antibody) that binds to TAA, a transmembrane domain, and an intracellular module that activates the T cell upon receptor engagement. CAR T therapy reported outstanding responses for hematological malignancies leading to their FDA approval for lymphoblastic leukemia and large B-cell lymphoma [28,29]. However, limited success has been reported in treating solid tumors in clinical trials [30,31].

Engagers are molecules that bind target cells to immune cells independently of MHC, forcing the release of cytotoxic molecules to kill the target cell. An example is the bi-specific T-cell engagers (BiTEs), which are composed of two ScFV connected through a linker. One of the ScFV binds to a TAA on target tumor cells, and the second binds to T cell CD3, thereby forcing an immunological synapse that ends in the tumor cell death by T cell independently of TCR recognition [32].

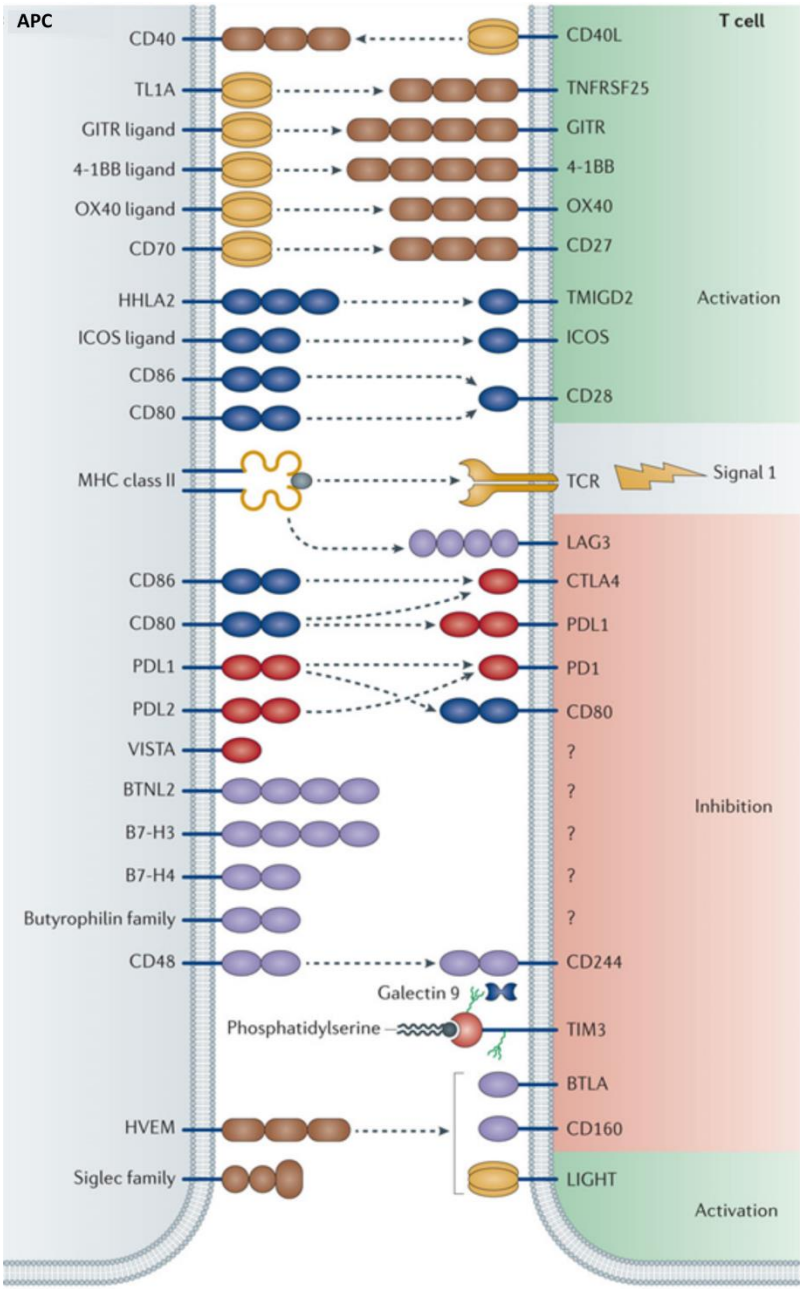

Figure 3. Immune checkpoint axis between T cells and antigen-presenting cells (APCs). The T cell receptor (TCR) starts the signaling cascade upon its interaction with antigen-MHC complex (signal 1). Additional interactions between ligands and activating (green shading) or inhibitory (red shading) receptors are crucial for further regulating T cell activation and tolerance. The second signals include co-stimulatory ligands and receptors (blue), immune checkpoint ligands and receptors (red), tumor necrosis factor receptor superfamily (TNFRSF; brown) members and their trimeric TNF superfamily

ligands (light brown), and additional members of the immunoglobulin superfamily (purple). Image from [33].

2.1 CANCER VACCINES

As we have seen antitumor immune responses are related to the induction of CTLs and Th1 cells against tumor antigens. Thus, major efforts have been made to develop tumor vaccines capable of inducing these responses. Therapeutic vaccines based on TAAs have obtained disappointing results, mainly due to the central tolerance mechanisms [34,35]. Moreover, as TAAs are expressed, even in low levels, in normal tissue, their targeting resulted in autoimmune toxicities [1].

The use of tumor-specific antigens was a more suitable strategy for therapeutic vaccination. The firsts successes were in viral-associated tumors. Patients with vulvar intraepithelial neoplasia induced by the human papillomavirus 16 (HPV16) were vaccinated with synthetic long peptides (SLP). Complete and partial responses were reported in those patients with smaller lesions [36,37]. HPV vaccines have been approved for cervical cancer [38], and recently to a subset of HPV-induced head and neck cancers. However, for the non-viral tumors, vaccination was not a therapeutic option.

The immunotherapeutic potential of targeting neoantigens has been persistently postulated. Neoantigens are tumor-specific, and their targeting should be safe and elicit immune responses that are not subjected to the central immune tolerance, unlike the TAAs. However, technical difficulties in identifying specific tumor mutations impaired this strategy. Recent technological innovations and the raising clinical data pointing specific tumor neoepitope-T cell responses prompted the neoepitope personalized vaccine approach.

Clinical trials provided a proof of concept that neoepitope vaccination can enhance the frequency of neoantigen responses following immunization. Nevertheless, this induction of T cell response is rarely translated into a clinical benefit as monotherapy

[39]. Several challenges and technical issues need to be addressed to become an efficient therapy.

One of the projects of this thesis is based on neoepitope vaccination. Further details and limitations of neoepitope cancer vaccines are described in the chapter B introduction.

3. CANCER VIROTHERAPY

Conventional treatments such as chemotherapy, radiotherapy, or surgery showed successful therapeutic results in localized tumors and initial stages. However, some of them produce highly toxic side effects, and tumors are resistant to these treatments, especially at advanced stages. The mentioned immunotherapies bypassed some disadvantages of classical treatments. Nonetheless, they also presented limited efficacy in certain types of tumors, and acquired tumor resistance has been reported. In consequence, new strategies or a combination of existing therapies are an evident need in the field.

The use of oncolytic virus (OVs) emerged as an alternative for cancer treatment. OVs have the ability to selectively replicate in cancer cells without harming normal tissues [40,41]. The viral progeny produced in the initial infection is released to the extracellular media where infect surrounding cells, amplifying the initially administered dose, ideally until the eradication of the tumor mass (**Figure 4**). This is an uncommon feature in the field of pharmacology: a selective drug that amplifies itself in the tumor.

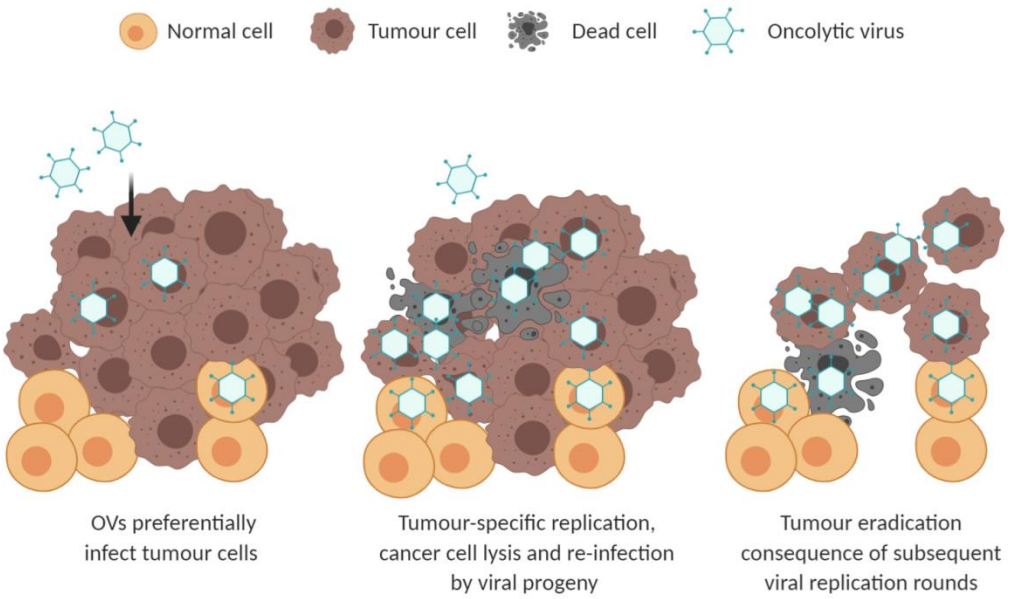

Figure 4. Principle of cancer virotherapy. The oncolytic virus infects normal and preferentially tumor cells and selectively replicates in cancer cells. If a normal cell is infected, the replication cycle is aborted. Virus replication leads to cancer cell lysis and release of the viral progeny. The newly generated viruses initiate their replicative cycles, disseminating throughout the tumor mass until its elimination. Image created with Biorender.com.

OVs have a multimodal mechanisms to eliminate cancer cells. They directly kill the tumor cell and the oncolysis releases tumor antigens, pathogen-associated molecular patterns (PAMPs), and DAMPs. Altogether, OVs induce a pro-inflammatory response that triggers antitumor immunity [42] (**Figure 5**, detailed in 5.4.1.2). Moreover, OVs can be armed with therapeutic transgenes aiming to kill bystander non-infected cancer cells.

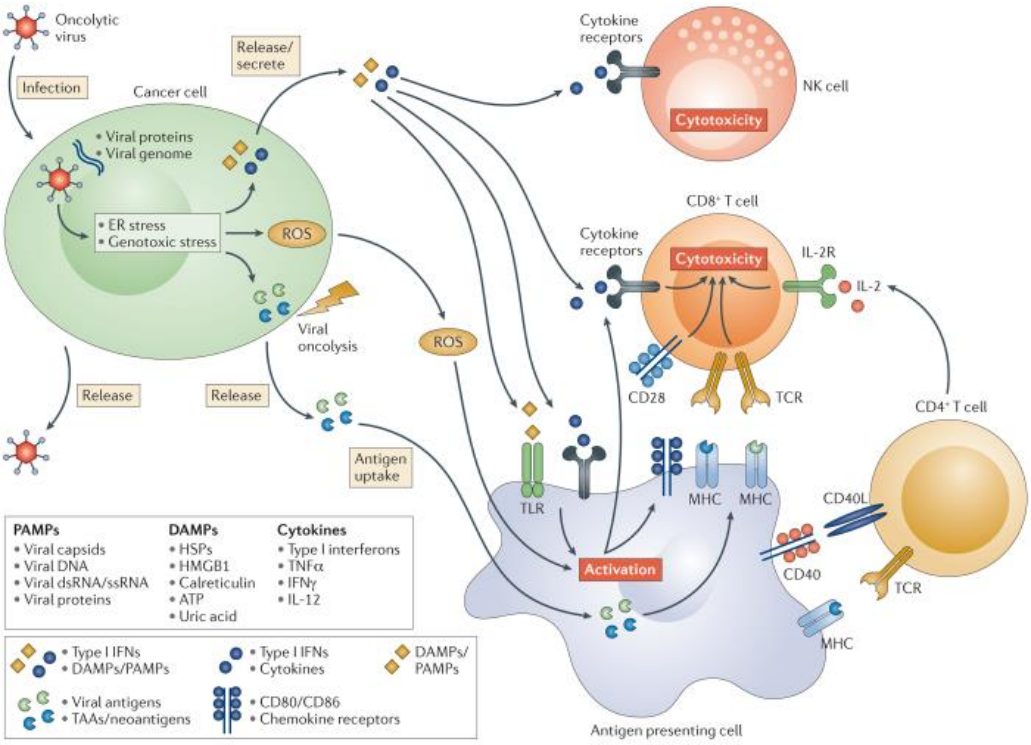

Figure 5. Mode of action of oncolytic virus. The infection and replication of oncolytic viruses leads to viral oncolysis and the release of new viruses. This induces the release of PAMPs, DAMPs, cytokines, and TAAs that are uptaken by antigen-presenting cells. It induces an anti-viral and eventually antitumor immune response that determines the therapeutic effect of virotherapy treatment. Image adapted from [42].

So far, only three OVs have been approved as commercial cancer therapies. The oncolytic adenovirus H101 (or Oncorine) became the world's first OV approved for head and neck cancer treatment in 2005 [43]. Then, Rigvir, an oncolytic reovirus approved for the treatment of advanced melanoma in Estonia, Latvia, Poland, and Belarus [44]. Most notably, T-Vec (also termed IMLYGIC or talimogene laherparepvec) is an HSV expressing the granulocyte-macrophage colony-stimulating factor (GM-CSF), and it was approved in the USA, Europe, and Australia for the treatment of advanced or non-resectable melanoma [45].

Among the OVs, adenoviruses present several features that turn them into suitable virotherapy candidates. They are safe, as they are not associated with any severe

disease in immunocompetent patients. The OAd genome is episomal, avoiding integration into host DNA. The genome encodes for an adenoviral proofreading-DNA polymerase ensuring genomic stability. OAds can infect quiescent and proliferating cells. Furthermore, they have a lytic cycle, and their replicative capacity allows to obtain high titers preparations (10^{12}-10^{13} viral particles/mL). The high production and stability are requirements for clinical setting feasibility [46,47]. Moreover, it has been widely studied as a model of DNA replication, RNA splicing, cell cycle control, and oncogenic transformation, among other viruses genomes [48,49]. As a consequence, we have vast knowledge about their molecular biology, which facilitates to modify their genome for virotherapy aims.

4. ADENOVIRUS BIOLOGY

4.1 GENERAL FEATURES AND CLASSIFICATION

Ads are non-enveloped DNA viruses members of the *Adenoviridae* family. In human, 57 serotypes have been defined by sensitivity to neutralizing antibodies and classified into seven species (A-G), based on the hemagglutination profile [50]. Ads are common human pathogens that cause a range of infections from mild, self-limited respiratory viral infections, conjunctivitis, and diarrhea to severe disseminated disease [51]. Within the same subgroup, the pathogenicity and tissue tropism is similar. The human adenovirus from specie C and serotype 5 (Ad5) infects epithelial cells from the respiratory tract, causing mild respiratory symptoms similar to a common cold. Ad5 has been the most used in the fields of gene therapy, vaccination, and cancer virotherapy. The viruses presented in this thesis are based on Ad5 serotype genome.

4.2 VIRION STRUCTURE

Ad virions are composed of 13 types of proteins, 7 of them form the capsid, and the other 6 are packaged with the linear double-stranded DNA in the core of the virion particle [52,53]. The icosahedral capsid has a 60-90 diameter and consists of 20 triangular faces, and is conformed by homopolymers of three main proteins: hexon, penton base and fiber (**Figure 6-A**). The faces and edges of the capsid are 240 copies of

hexon homotrimers. The penton base is a pentameric protein located in the 12 vertices of the capsid, where the fiber emerges. The fiber is a homotrimer in which each protein has three domains: an N-terminal tail, the shaft, and the C-terminal knob. The tail attaches the whole protein to the penton base (in the capsid vertices). The shaft is in the center of the protein and extends the fiber to the outside of the capsid. Finally, the knob plays a crucial role in the formation of fiber trimers and interacts with the cellular receptors. The fiber and the penton base are key-interactors for viral binding to the cells and determine the adenoviruses tropism [53].

In addition to these three main capsid proteins, other minority proteins such as protein pIIIa, pVI, pVIII, and pIX act as cement between hexons. The capsid encases the double-stranded viral DNA, which is associated with core proteins pV, pVII, Mu (pX), and terminal protein (TP) (**Figure 6-B**).

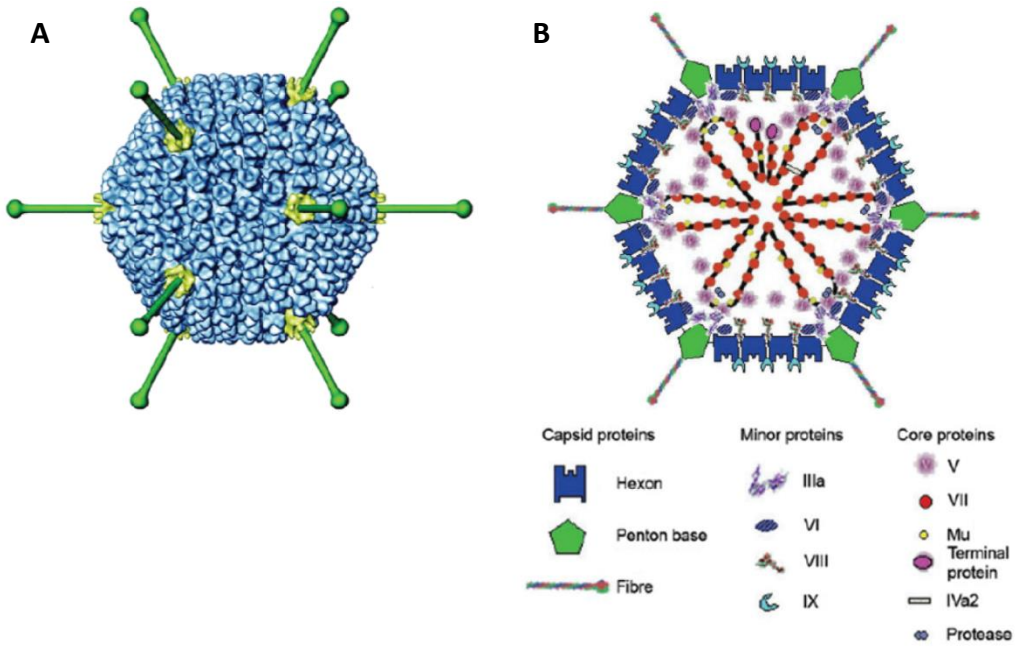

Figure 6. Adenovirus structure. (A) Virion structure at 17 Å resolution. The three main capsid proteins are depicted. The hexon protein (blue), the fiber protein (green) protrudes from the penton base (yellow) (Image from [54]). **(B)** Protein composition of adenovirus capsid. Capsid and minor protein locations are well defined, whereas the disposition of core proteins and virus DNA is conjectural (from [53]).

4.3 GENOME ORGANIZATION

The Ad5 genome is a 36 kb linear molecule of double-stranded DNA flanked by two inverted terminal repeats (ITR), which contain the viral DNA replication origins. The packaging signal (Ψ) is located at 100bp from the left ITR, and it is involved in virus encapsidation. The rest of the genetic information is organized in overlapping transcription units with different timing of use during the viral cycle. There are six early (E) transcription units (*E1A, E1B, E2, E3,* and *E4*), three delayed-early units (*IX*, *IVa2*, and *E2 late*), and one late (L) transcription unit. The late unit is under the control of the major late promoter (MLP) and is transcribed as a unique mRNA and processed to generate five families of late mRNAs by alternative splicing (*L1* to *L5*) [55]. The late mRNAs produce the structural proteins of the capsid.

In addition, Ad genome also contains the viral-associated (VA) genes that codify for two non-coding RNAs, which are involved in translational control during infection. **Figure 7** depicts a schematic representation of Ad5 genome.

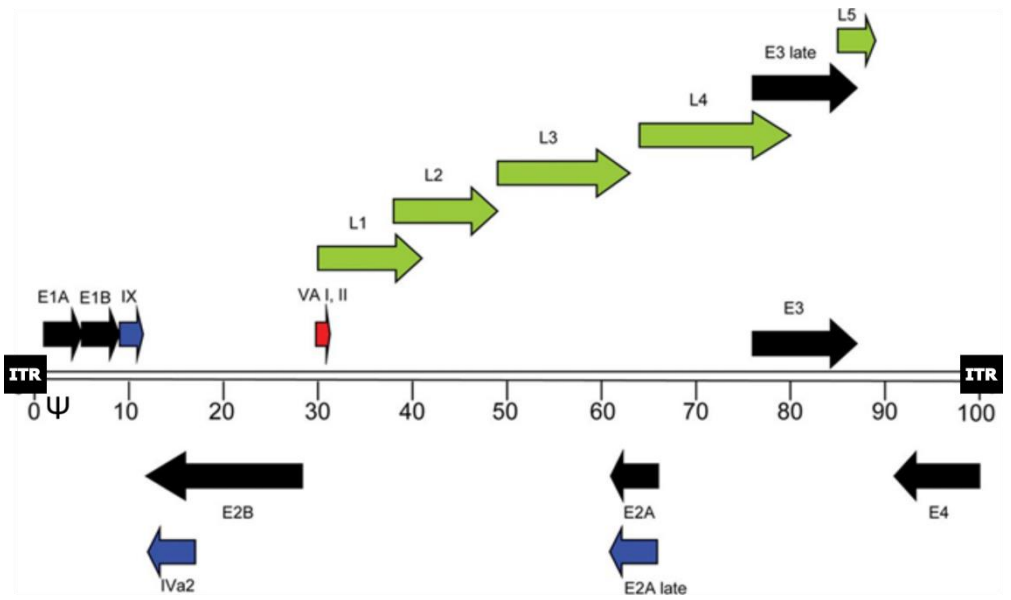

Figure 7. The Ad5 genome. Early (black), delayed-early (blue), and late (green) mRNAs are shown as arrows. Rightwards reading transcripts are shown on top, leftwards reading transcripts at the bottom.

The inverted terminal repeats (ITR), the packaging signal (Ψ), and the VA-RNAs (red) are also depicted. The genome is divided into 100 map units (approximately 350nt per map unit). Adapted from [56].

4.4 ADENOVIRUS INFECTION CYCLE

4.4.1. Adsorption and entry

Ad5 cell infection requires two steps. The primary high-affinity interaction between the fiber knob and the coxsackie adenovirus receptor (CAR) [57] (**Figure 8, step 1**). A secondary interaction between an RGD (Arg-Gly-Asp) motif from the penton base protein and the αVβ3, αVβ5, α5β1, and αvβ1 integrins is required for the viral-entry into the cell through clathrin-mediated endocytosis [58] (**Figure 8, step 2 and 3**). The protein VI mediates the endosome escape, and the virion is translocated to the nuclear pore complex through the microtubule network [59,60] (**Figure 8, step 4**). After reaching the nuclear pore complex, the capsid is completely disassembled, and the viral DNA enters into the nucleus for subsequent transcription and replication (**Figure 8, step 5**).

4.4.2. Early gene expression and DNA replication

In the nucleus, the *E1A* transcription unit is immediately expressed (6hours after infection), as its promoter only requires cellular proteins to start the transcription (**Figure 8, step 6**). *E1A*-encoded proteins promote the transcription of the rest early transcription units (*E1B, E2A, E2B, E3, and E4;* 6-12hours post-infection, **Figure 8, steps 10a/10b**) and induce the S phase into the infected cell. This is a prerequisite for Ad replication and is achieved by the sequestration of the retinoblastoma (Rb) protein family members, which inhibits the cell cycle [48,49,61]. The *E1B* gene products inhibit the cell apoptosis. The proteins from *E2* transcription units are required for the viral genome replication: the adenovirus DNA polymerase (Pol), the preterminal protein (pTP) and the single-stranded DNA binding protein (ssDBP) (**Figure 8, steps 11-14**). The *E3* gene products are responsible for the anti-viral immune response inhibition. The E3-19K retains the newly generated MHC class I molecules and related proteins (such as

MICA/B) in the endoplasmatic reticulum, preventing the viral antigen presentation on the cell surface and the NK cells activity [62,63]. Finally, the *E4* transcriptional unit is related to the viral replication, stability, and transport of viral mRNA, and it also mediates the expression of the late genes.

4.4.3. Late gene expression and virion assembly

After early phase proteins have accumulated, the viral genome replication starts (**Figure 8, steps 14-15**). Then, the major late promoter (MLP) regulates the expression of genes from the late transcription units (*L1-L5*), by generating multiple copies of a single pre-mRNA. The late pre-mRNA encodes for 15 to 20 different mRNAs processed by differential splicing and polyadenylation (**Figure 8, steps 16-19**). Most late proteins correspond to structural proteins involved in virion assembly and genome packaging in the nucleus (**Figure 8, steps 20-21**). In order to generate infectious Ad particles, a subset of the structural proteins are cleaved by Ad protease into their mature form, and the viral particles are assembled. Finally, cell lysis and progeny release occur, mediated by the adenovirus death protein (ADP) encoded in the *E3* transcription unit (**Figure 8, step 22**), the only early gene that is expressed during the late phase.

5. ONCOLYTIC ADENOVIRUSES

A fundamental requirement for an oncolytic virus is the replication restriction only in cancer cells to avoid undesired toxicity in normal tissues. Only a few viruses present natural selectivity for tumor cells (parvoviruses and reoviruses). The vast majority of viruses, including Ads, need genetic manipulation to block their replication in non-cancer cells. Two main strategies have been pursued to make the adenoviruses oncolytic viruses: transductional targeting and transcriptional targeting.

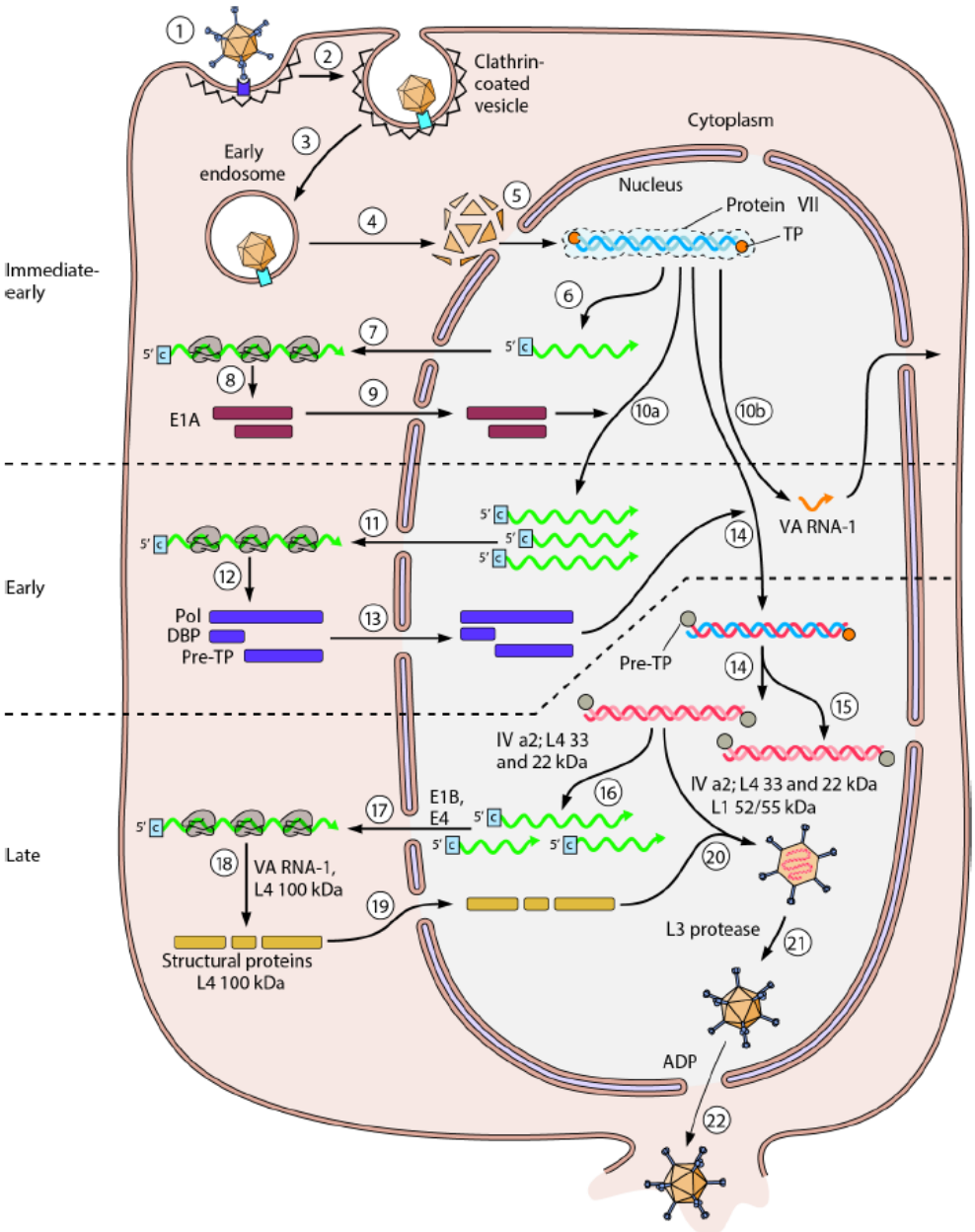

Figure 8. The infectious cycle of human adenoviruses. The infection cycle of adenoviruses can be divided into time-specific events: adenovirus cell entry (steps 1-3), capsid disassembly and genome import into the nucleus (steps 4-5), immediate-early E1A gene expression (steps 6-9), E1A-mediated transcription of viral early genes (step 10a), translation of viral early proteins (steps 11-13), viral DNA replication (steps 14-15), transcription and translation of viral late genes (steps 16-19), capsid assembly and virion maturation (steps 20-21) and progeny virus release (step 22). Image from [64].

5.1 TUMOR-SELECTIVE ONCOLYTIC ADENOVIRUSES

5.1.1. Transductional targeting

Transductional targeting strategies aim preferential infection of cancer cells rather than normal through two main approaches: ablating the native Ads tropism (detargeting) and directing the Ad to cancer-specific receptors (retargeting). One of the most used ligands to enhance tumor tropism is the RGD-4C peptide (CDCRGDCFC), which targets integrins, commonly overexpressed in different types of cancer [65,66]. The RGD in the fiber HI-loop allows the use of integrins as a primary receptor instead of CAR (without ablating native CAR binding) [67].

5.1.2. Transcriptional targeting

Detargeted and retargeted Ads can still infect normal cells. In consequence, tumor replication restriction is required. Two broad types of OAds have been developed according to the transcriptional targeting strategy.

The first type is OAds with modified or deleted viral gene sequences important for replication in normal cells but dispensable in tumor cells. For instance, an adenovirus unable to replicate in normal cells but with a productive lytic infection in cells having the Rb pathway inactivated, a common defect of human cancers [68]. The deletion of 24-base pairs in the *E1A* region impedes the E1A binding with the pRb [69]. The E1A-mediated sequestration of pRb releases the E2F transcription factor, leading to S-phase induction and viral replication in normal cells. However, in tumors, the pRb pathway is deregulated, resulting in constitutively E2F-mediated transcription of cell cycle control genes. Thus, in normal cells, the Δ24-E1a protein fails to interact with the pRb protein, resulting in halted viral gene transcription and replication (**Figure 9**). Conversely, in a cancer cell, without a functional Rb, the S phase genes are constitutively promoted by the free E2F allowing the viral gene transcription and replication. Several similar transcriptional targeting approaches have been described [70–72].

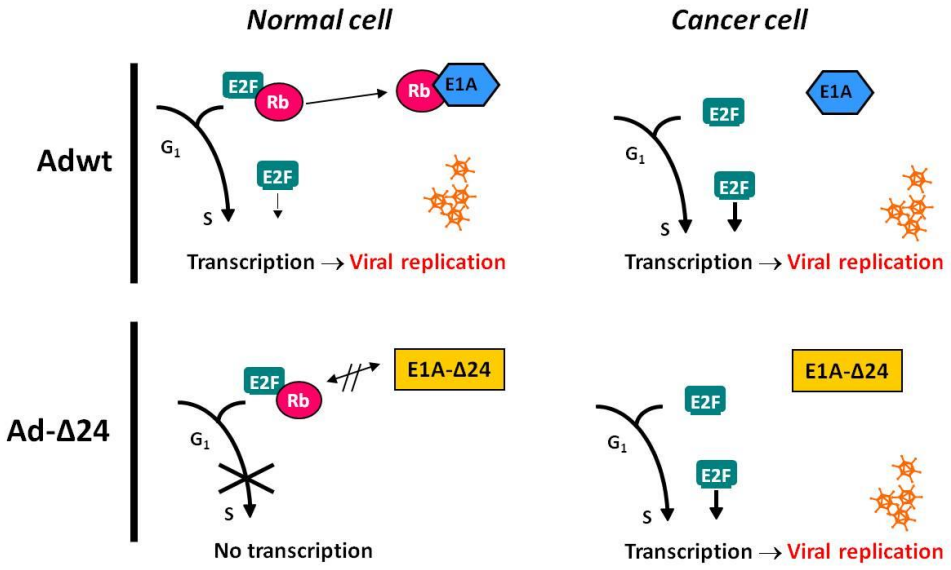

Figure 9. Δ24 selectivity mechanism. E1A protein binds and inactivates Rb to induce S phase of cell cycle and viral replication. In tumor cells, this function is redundant since the Rb pathway is truncated, and E2F is already free. In normal cells, Δ24 deletion avoids the dissociation of Rb and E2F, and no viral replication occurs. Image from [73].

The second strategy to transcriptionally target OAds is the insertion of tissue/tumor-specific promoters to restrict essential genes for viral replication (normally *E1A, E1B, E2* or *E4* promoters). The viral cycle depends on E1A activation, thereby replacing the *E1A* promoter for another cellular promoter activated in deregulated tumors would lead to specific viral replication.

A more recent strategy is the use of micro RNAs (miRNAs) to control viral transcription. They can regulate post-transcriptional gene expression by binding the 3' untranslated regions (UTRs) of mRNA, preventing the translation and inducing its degradation. Adenoviral genomes have been engineered to express the targeting sequences for these miRNAs in essential viral genes impeding the replication [74–76]. This strategy is based on differential expression of miRNAs between normal cells (high) and cancer cells (low), due to cancer cells' downregulation of miRNA machinery [77].

5.2 ICOVIR15 AND ICOVIR15K

ICOVIR15 (ICO15) [78] and ICOVIR15K (ICO15K) [79] are two oncolytic adenoviruses designed in our group that combine three targeting approaches. We use these viruses as platforms to test novel modifications, as presented in this thesis.

Two transcriptional targeting approaches have been implemented in these viruses. Firstly, the endogenous promoter of *E1A* has been modified by incorporating eight extra E2F-responsive sites organized in four palindromes and one extra Sp-1-binding site [80] (**Figure 10-A**). The E2F is free in cancer cells and activates the *E1A* transcription, triggering essential genes for viral replication, such as *E4*. The E4-6/7 proteins form a complex with the cellular E2F to efficiently activate the E2F promoter and the viral E2a promoter, resulting in a positive feedback loop. Similarly, the Sp-1 interacts cooperatively to activate transcription [81]. The E2F and Sp-1 extra binding sites in the *E1A* promoter confers an enhanced *E1A* expression in tumor cells, compared to the adenovirus wild-type (Adwt). Then to selectively restrict the replication, the viruses contain the previously described Δ24 deletion in E1A, which impairs the replication cells without Rb pathway alterations (**Figure 10-B**).

Different transductional targeting strategies have been applied in each OAd. The ICO15 contains the mentioned RGD ligand inserted in the HI loop of the fiber knob [67,82]. In contrast, ICOVIR15K combines a liver detargeting and a tumor retargeting approach. The Ad fiber shaft contains a KKTK domain that putatively binds to heparin sulfate glycosaminoglycans (HSG) in the hepatocytes, conferring a hepatic tropism. Our group demonstrated that the replacement of this KKTK domain by the RGD motif improved the tumor: liver ratio *in vivo* in the context of a non-replicative adenovirus [83] (**Figure 10-C**). ICOVIR15K showed increased bioavailability after systemic administration and greater antitumor efficacy *in vivo* compared to ICOVIR15 [79].

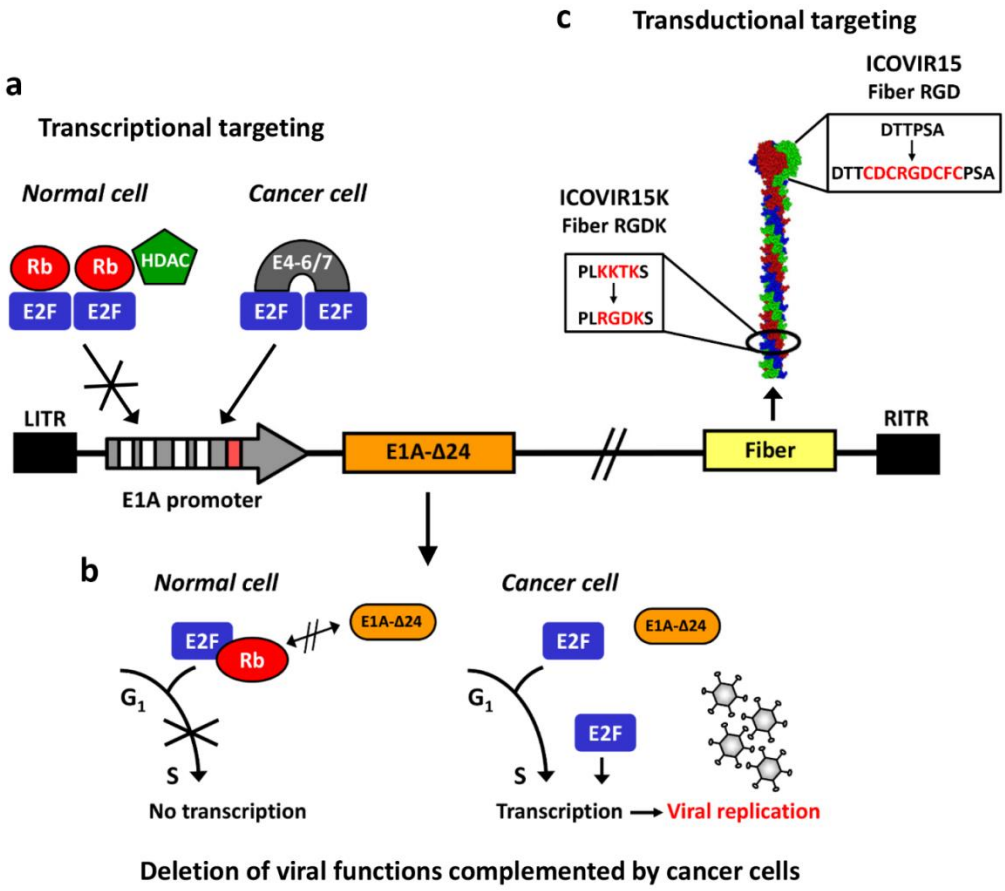

Figure 10. The modifications in ICOVIR15 and ICOVIR15K genomes. Both oncolytic adenoviruses contain the modified *E1A* promoter with four E2F boxes (white squares) and one Sp1 box (red square), and the truncated E1A-Δ24 protein to confer selectivity for tumor cells. In ICOVIR15, the RGD motif is inserted in the HI-loop of the fiber *knob* (fiber RGD), whereas in ICOVIR15K is inserted in the fiber *shaft* replacing the KKTK domain (fiber RGDK). Image from [84].

5.3 CLINICAL EXPERIENCE WITH ONCOLYTIC ADENOVIRUSES

The first oncolytic adenovirus (OAd) tested in clinics was the mutant ONYX-015, an E1B-55K deleted virus to, theoretically, restrict its replication in p53 deficient cells, such cancer cells [70]. After promising preclinical data, ONYX-015 was tested in different types of cancer. However, the best clinical results were reported in phase I and phase II clinical trials in head and neck patients. They received intratumoral injection of the virus and systemic combination of chemotherapy [85]. The phase I proved the clinical safety [85], and the phase II reported with 14% of complete or partial regressions in

treated lesions, and 41% of stable disease [86]. Unfortunately, phase III was canceled due to corporate takeover.

However, Chinese scientists patented an OAd with a similar E1B-55K mutation and an extra E3 deletion, called H101 or Oncorine, and performed a phase III clinical trial in China to study the effectivity in combination with chemotherapeutic regimens. A total of 160 patients were enrolled with an overall response of 78.8% combined with cisplatin and 5-fluorouracil agents. The results lead to the approval for nasopharyngeal carcinoma treatment by the Chinese government regulators. It was the first clinical trial demonstrating antitumoral efficacy of an OAd, and the first world-approval of an OV. Nonetheless, controversial issues were claimed in the scientific community about the small cohort of patients, the lack of a head to head comparison against the standard of care, and the problematic or incomplete follow-up of the patients [43,87]. Moreover, further studies revealed that tumor selectivity of the E1B-55K virus was not as simple as p53 targeting [88], and reduced oncolytic potency of ONYX-015 and H101 in several types of cancer was related to their genomic deletions [87].

As a consequence, the field sought for improved OAds with higher anti-cancer potency and selectivity. The second-generation OAds targeting pRb pathway for tumor selectivity (E1AΔ24,**Figure 9**) and enhanced tumor targeting (RGD in the fiber HI-loop) were developed and tested in clinics. An example is the ICOVIR-5 [89], generated in our group, tested intravenously in phase I clinical trial in cutaneous and uveal melanoma. Although no responses were detected 4 out 12 patients were positive for viral genomes in metastasis [90]. The results highlighted the feasibility of using OAds for the systemic treatment of metastasis.

Another relevant example is the DNX-2401 (also called Delta24-RGD [91]) tested in ovarian cancer demonstrating manageable toxicity [92]. Interestingly, in phase I clinical trial of intratumoral injected recurrent malignant gliomas, 20% of 25 patients survived more than 3 years, and 3 patients presented more than 95% of regression. The authors postulated that the long-term survival in recurrent gliomas was a consequence of a

direct oncolytic effect of the virus followed by elicitation of immune-mediated antitumor responses [93]. These results lead DNX-2401 to receive the fast-track status and orphan drug designation by the FDA and EMA for the treatment of malignant glioma [94].

Other examples of the firsts steps in clinics with second-generation OAds are the CG7870 or ColoAd1. The CG7870 [95] was injected intravenously in phase I clinical trial and dose-escalation had to be halted at $6x10^{12}$ vp due to severe adverse effects. The only reported response was a drop on the tumor marker PSA in 3 out of 8 patients treated with the highest dose [96]. The ColoAd1 or Enadeontucirev is a chimeric adenovirus between serotype 11 and serotype 3 generated by "directed-evolution" (Ad11/3, [97]). Enadenotucirev has been tested intravenously in phase I/II clinical trial with several different cancer types. They demonstrated manageable toxicity of intravenously repeat-dose schedule. The dosing consisted of a low dose on day 1 followed by higher doses at day 3 and 5. The virus was detected by IHQ in the tumor lesions [98], but not relevant results were published regarding responses [99].

Taking all data together, we can assume that OAds treatment produced manageable adverse effects and triggered some clinical responses, especially in intratumorally injected tumors. Furthermore, the experience in the first clinical steps pointed out some challenges that the field needs to solve to become an efficient anti-cancer therapy (detailed in 5.4).

Nowadays, new OAds encoding for transgenes have been developed to bypass some treatment limitations or to enhance anti-cancer therapy. To date, more than 40 clinical trials with oncolytic adenovirus have been registered. We summarized the active or completed clinical trials with engineered OAds as monotherapy or in combination with chemotherapy, radiotherapy, and immunotherapies in **Table 1**.

Table 1. Summary of active and completed clinical trials with OAds.

OAd	Clinical trial	Phase	Cancer	Combination	Admin
DNX-2401	NCT03178032	I (C) [100]	DIPG	-	IT
	NCT00805376	I (C) [93]	MG	-	IT
	NCT01956734	I (C)	GBM	TMZ (oral)	IT
	NCT02197169	I (C)	GBM and GS	IFNg (IT)	IT
	NCT03896568	I (R)	AA, GBM, GS, MG	Loaded MSCs	IV
	NCT03714334	I (NR)	GBM	-	IT
	NCT02798406	II (NR)	GBM and GS	Pembrolizumab (IV)	IT
DNX-2440	NCT03714334	I (NR)	GBM	-	IT
Delta24-RGD	NCT01582516	I/II (C)	GBM	-	IT
CRAd-Survivin-pk7	NCT03072134	I (C)	MG	Loaded NSC+SoC	IT
ICOVIR-5	NCT01864759	I (C) [90]	Melanoma	-	IV
	NCT01844661	I/II (C) [101]	Recurrent/Metast	Loaded MSCs (CELYVIR)	IV
OBP-301	NCT03190824	II (NR)	Melanoma	-	IT
TILT-123	NCT04217473	I (R)	Melanoma	Monotherapy +/- TIL therapy	IT
LOAd703	NCT03225989	I/II (R)	Panc, Ov, CC, BiC	SoC or GE immune-conditioning	IT
	NCT04123470	I/II (R)	Melanoma	Atezolizumab (IV)	IT
ORCA-010	NCT04097002	I/II (R)	Prostate	-	IT
CAdVEC	NCT03740256	I (R)	HER2+	Ad-specific HER2 CAR T cells (IT)	IT
CG7870	NCT00116155	I/II (C) [102]	Prostate	-	IV
CG0070	NCT00109655	I (C) [103]	BC	-	IT
	NCT02365818	II (C) [104]	BC	-	IT
ONCOS-102	NCT01598129	I (C) [105–107]	Advanced cancers	CP (oral)	IT
	NCT03514836	I/II (R)	Prostate cancer	CP+DCVAC/PCa (SC)	IT
	NCT03003676	I (NR)	Melanoma	CP (IV) + Pembrolizumab (IV)	IT
	NCT02879669	I/II (NR)	Mesothelioma	CP (IV)+Pemetrexed + Carboplatin	IT
Ad5-yCD/mut TKSR39rep-hIL12	NCT03281382	I (R)	Pancreatic	5-FC (oral)	IT
VCN-01	NCT02045589	I (C)	Pancreatic	GE+Abx (IV)	IT
	NCT02045602	I (NR)	Pancreatic	GE+Abx(IV)	IV
	NCT03799744	I (R)	HN	Durvalumab (IV)	IV
	NCT03284268	I (R)	Retinoblastoma	-	IT
ColoAd1	NCT02053220	I (C)[98,99]	CC, NCLC, BC, RCC	-	IT/IV
	NCT03916510	I (R)	Rectal Cancer	Chemoradiotherapy	IV
NG-350	NCT03852511	I (R)	Epithelial	-	IT/IV
NG-641	NCT04053283	I (R)	Epithelial	Chemo or Immunotherapy	IT/IV

Phase: C, completed; R, recruiting; NR, non-recruiting. **Cancer:** DIPG, difuse intrinsic pontine gliomas; MG, malignant gliomas ; GBM, glioblastoma; GS, gliosarcoma; AA, anaplastic astrocytoma; Panc, pancreatic; Ov, ovarian; CC, colorectal; BiC, biliary carcinoma; HN, head and neck squamous carcinoma; NCLC, non-small cell lung cancer; BC, bladder cancer; RCC, renal carcinoma. **Combination:** TMZ,temozolomide ; MSC, mesenchymal stem cells; NSC, neural stem cells; TIL, tumor infiltrating lymphocytes; SoC, standard of care; GE, gemcitabine; CP, cyclophosphamide; Abx, abraxane ®

5.4 CHALLENGES FOR ONCOLYTIC ADENOVIRUSES

Despite the promising expectations in OAd therapy for cancer treatment, the first clinical trials reported limited clinical responses, especially as monotherapy agents. The tumor delivery and targeting (**Figure 11**, boxes 1-4, red zone), the intratumoral spreading (**Figure 11**, boxes 5-8, yellow zone), and the immune response in the tumor (**Figure 11**, boxes 9-12, blue zone) were identified as the main challenges for virotherapy efficacy.

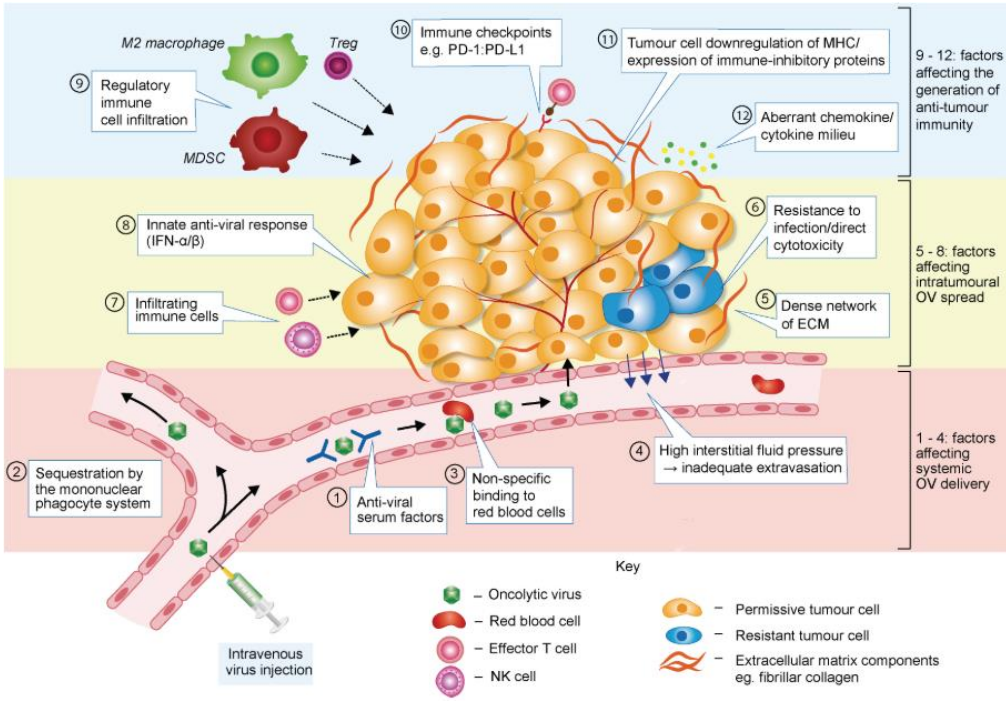

Figure 11. Challenges to effective OVs therapy *in vivo*. When delivered to tumors via the bloodstream, most of the initial dose is retained by hepatic macrophages (Kupffer cells) and splenic macrophages (box 2). Moreover, OVs can be neutralized by the interaction with blood cells, the complement proteins, and neutralizing antibodies (box 1 and 3). The high interstitial fluid pressure within the tumor hampers the extravasation (box 4). If extravasation is achieved or after intratumoral injection, several factors may limit the intratumoral viral spread and therapeutic effectiveness. They are the tumor stroma (e.g., extracellular matrix (ECM)) (box 5), anti-viral activity, and cancer resistance to OAd-mediated cell killing (box 6-8). Finally, the immunosuppressive tumoral environment impairs the antitumor response induction (box 9-12). Image from [108].

5.4.1. Tumor delivery and targeting

The first generation OAds reported modest responses, despite intratumoral injections. Their infectivity relied on the CAR receptor, which is downregulated in advanced cancers [109], such as the ones that patients have in clinical trials (**Figure 11**, box 6).

The second-generation OAds solved the issue with RGD-targeting strategies.However, they presented limited activity intravenously. Upon the intravenous administration, the main part of the injected dose is immediately retained in the spleen and liver due to their large vascular fenestrations, causing mainly hepatotoxicity [110,111]. OAds are accumulated in the liver sinusoids and interact with different cell types, especially with liver macrophages (Kupffer cells) (**Figure 11**, box 2).

Humans are commonly exposed to Ad5 wild-type infection (up to 90% seroprevalence depending on the region). Thus patients commonly present circulating neutralizing antibodies (NAbs) against capsid proteins inactivating the OAds virions [112,113]. NAbs, natural antibodies (IgMs), complement proteins opsonize the virus and enhance Kupffer cell-mediated clearance [114,115] (**Figure 11**, box 1). Moreover, the capsid interaction with coagulation factors increase the liver to tumor-targeting ratio [116,117]. OAds attach to human erythrocytes via CAR, but its effect on viral bioavailability is still controversial [118,119] (**Figure 11**, box 3). Finally, the high interstitial fluid pressure within the tumor impairs the OAd extravasation from the vasculature [120] (**Figure 11**, box 4).

Several strategies have been tested in pre-clinical and clinical settings to overcome the mentioned challenges. Chemical shielding of the Ad capsid with synthetic polymers or albumin [121–123], and the replacement of HVR from one Ad serotype to another have been published to evade NAbs [124]. Alternatively, taking advantage of the tumor homing and NAb protection that some cellular carriers confer, our group tested in clinics patient-derived autologous mesenchymal stem cells (MSCs) infected with ICOVIR-5 achieving clinical responses [101].

5.4.2. Intratumoral spreading

Once the OAds reach the tumor, their intratumoral spreading is hampered by the tumor stroma composed of different types of cells (such as cancer-associated fibroblasts (CAFs), immune cells, and others) and the extracellular matrix (ECM). The low rate of tumor regressions in immune-deficient pre-clinical models highlighted the relevance of the tumor stroma. The ECM is formed by a dynamic network of macromolecules playing a significant role in cancer progression. The quantity and composition of the cancer ECM is associated with cancer progression and patient prognosis. Moreover, the ECM acts as a physical barrier avoiding drug dispersion and adenoviral spreading [125].

For instance, the collagen excludes the oncolytic viruses based on their size. Thus treating the tumors with collagenase improved the virus distribution and enhanced the antitumor efficacy. Similarly, ECM-degrading enzymes are commonly exploited to enhance viral penetration in solid tumors [126]. Hyaluronic acid (HA) is one of the critical components of the ECM. The characteristics of HA are detailed in the introduction of chapter C of this thesis. Briefly, HA impairs the adenovirus spreading within the tumor. The co-injection of OAd with hyaluronidase improved the virus spread and antitumor response in HA-containing melanoma and prostate xenograft models [127]. Based on these observations, our group developed a hyaluronidase-expressing OAd, called VCN-01 (or ICO17K), described in the next section 5.5.1.1.1.

5.4.3. Immune response

The role of the immune response in cancer virotherapy is the main controversial issue. The strong innate and adaptive responses against OAds was thought to hamper the therapy by reducing viral replication. This was based on the hypothesis that tumor regressions exclusively depends on viral oncolysis. Clinical reports of early virus clearance and relative low-rate of responses supported the postulate. Furthermore, historical observations of better responses in immunosuppressed patients also converged with the hypothesis [128].

After clinic experience, we know that the replication is limited in patients. Despite the immunosuppressive TME, the virus is cleared by the immune system. However, antitumor responses have been reported without evidence for their dependence on OAd replication in humans. Moreover, pre-clinical studies reported antitumor efficacy of non-replicative viruses in murine models. Even more provocative is the preclinical evidence that anti-viral immune response can enhance the efficacy of OV therapy in different types of viruses, yet the mechanisms remain unclear [129,130]. Perhaps more revealing are the kinetics of complete regressions in glioblastoma patients treated with DNX-2401, occurring several months post-administration after pseudoprogression without detectable viral replication [93,131]. Altogether opened a debate about the OV mode of action. The immune system, historically defined as an enemy, turned into a necessary ally for the immune-related activity of the OVs. Nowadays, the OVs are currently being designed mainly as immune-adjuvants to overturn the tumor immunosuppression, attract immune cells to the tumor, and induce anti-viral and antitumor immunity.

What it is clear is the strong immune response elicited by OVs seems to be at the same time a pro (trigger an antitumor immune response) and a con (impede sustained viral oncolysis). Thus, a balance between these two facts might be crucial for the success of the virotherapy. The antitumor and anti-adenoviral immune responses have been pivotal in this thesis and are intensely detailed in the next sections.

5.4.1.1 Immune response upon systemic administration

Upon systemic administration, Ad interacts with different cells and factors in the bloodstream that strongly impairs the tumor infection (see 5.4.1). The main part of the dosage is retained in the spleen (5%) and liver (95%). The splenic macrophages and Kupffer cells (hepatic macrophages) trap the adenoviral complexes, inducing pro-inflammatory and anti-viral signals through NFκB-dependent and interferon-dependent signaling cascades. *In vivo* studies with rodents, primates and the human clinical trials revealed the induction of a plethora of mostly pro-inflammatory mediators. Including cytokines (IL-6, TNF, IL-12, IL-1α and β), chemokines (IL-8, MIP-2, IP-10, RANTES, MIP-

1α, MIP-1β, and MCP-1), platelet-activating factor (PAF), and type-I interferons (IFN-α/β) [132]. In concrete, IL-6, IL-10, TNFα, and IL-1β cytokines have been detected in patient's serums minutes after intravascular injection [99,133,134]. Furthermore, histological evaluation of tissues revealed areas of leukocyte and neutrophil infiltration in the liver, spleen, and lung after intravenous administration, suggesting an innate-adaptive response in every infected tissue [135,136].

In detail, the innate responses to Ad comprise cellular components, called pattern recognition receptors (PRRs); they detect pathogen-associated molecular patterns (PAMPs). The toll-like receptors (TLRs), expressed mainly in immune cells, are one of the main PRRs. TLR2 can directly recognize the virion extracellularly and trigger the MyD88-signalling pathway. The FX-Ad complex is bound to the TLR4 triggering immune mediators in a murine system [137], but poorly induce inflammatory responses in human mononuclear phagocytes such as macrophages, monocytes or DCs [138] (**Figure 12**, step 1 and 5). Virions are opsonized by neutralizing, natural antibodies and the complement components in the bloodstream. The Ab-Ad complexes are detected by macrophages, monocytes, dendritic cells (DCs), and neutrophils through the Fc receptor (FcR) [115,139], triggering phagocytosis and pro-inflammatory cytokines. Moreover, macrophages recognize the Ab-Ad complexes via the intracellular antibody receptor TRIM21 [140,141], inducing interferon regulating factor (IRF) cascades. Interestingly, no differences were found in activating abilities between IgG or IgM isotypes [141]. Similarly, the Ad-C3 complex is recognized extracellularly by complement receptors (CR), such as CR1, CR3, CR4, CRIg. The CRs, together with scavenger receptors, are the principal mechanisms of Ad capture by Kupffer cells in the liver [142,143]. Moreover, systemic delivery in mice revealed that 25% of the input virus is captured by circulating neutrophils via FcR and CR1 [144] (**Figure 12**, step 2).

Despite the mentioned mechanisms, free virions are able to infect cells. The initial interaction of Ad fiber knob with CAR receptor and integrins results in NF-κB-mediated expression of chemokines and IL-1 (**Figure 12**, step 3). In murine immunocompetent models, the IL-1α is the mediator of anti-adenoviral response after Ad RGD

engagement with β3 integrins in a subpopulation of splenic macrophages (MACRO+ Macrophages). The IL-1/IL-1R pathway promotes the synthesis of chemokines that recruit neutrophils to the sites of infection [137,141,145].

After viral entry, whatever the via (infection, TLRs, and FcR-mediated phagocytosis), the cell holds intracellular PRRs to detect the Ad. The entry is generally through the endosomes, where the TLR9 detects unmethylated CpG islands in dsDNA sequences characteristic of Ad genome. Activation of TLR9, generally in plasmacytoid DCs, causes IFN type I transcription via MyD88 dependent pathway [146,147] (**Figure 12**, steps 4,5, 10, and 11). Eventually, the viral particle escapes from the endosome releasing the viral genome in the cytosol (**Figure 12**, step 6). The cytosolic dsDNA is sensed by cGAS/STING pathway (**Figure 12**, steps 7 and 10). It is expressed in immune and non-immune cells (even in some cancer cells), and its activation ends in NF-κB and IRF mediated response. Conventional DCs use this mechanism [148], and Kupffer cells activation of IRF3 ends in their necrotic cell death by an undefined mechanism. The necrosis occurs within the first-hour post-Ad injection and does not require signaling of any known mediators of necrosis cell death. The Kupffer necrosis aims to contain the viral dissemination (retaining up to 10^{11} vp/kg [149]) and induces an antiviral state in the surrounding cells. After Kupffer necrosis, a subsequent administration of Ad particles can not be trapped in the liver, and a significant part of the dose remains bioavailable [150].

Another class of PRR is nucleotide-binding oligomerization domain-like receptors (NLRs). They are also cytosolic DNA sensors found in immune cells and others such epithelial cells [151], conforming the inflammasome together with apoptosis speck proteins (ASC) and caspases. The inflammasome activation induces the IL-1β and IL-18 maturation, promoting the NF-κB signaling and pro-inflammatory necrotic cell death [141,152,153] (**Figure 12**, step 8). This can be triggered independently of MyD88 and viral replication in immune cells and human skin explants [154].

RIG-1-like receptors (RLRs) are another family of PRRs that recognize cytoplasmic viral RNAs. RIG-1 can detect cytosolic ssRNA such as the adenoviral associated RNAs (VA), the VA I and VA II in the case of viral replication, and induce an NF-κB and type I IFNs in a similar way of TLRs [146,155,156]. Moreover, the adenoviral genome can be converted into ssRNA by RNApol III, also activating the RIG-1 pathway [157] (**Figure 12**, steps 9, 5, 10, and 11).

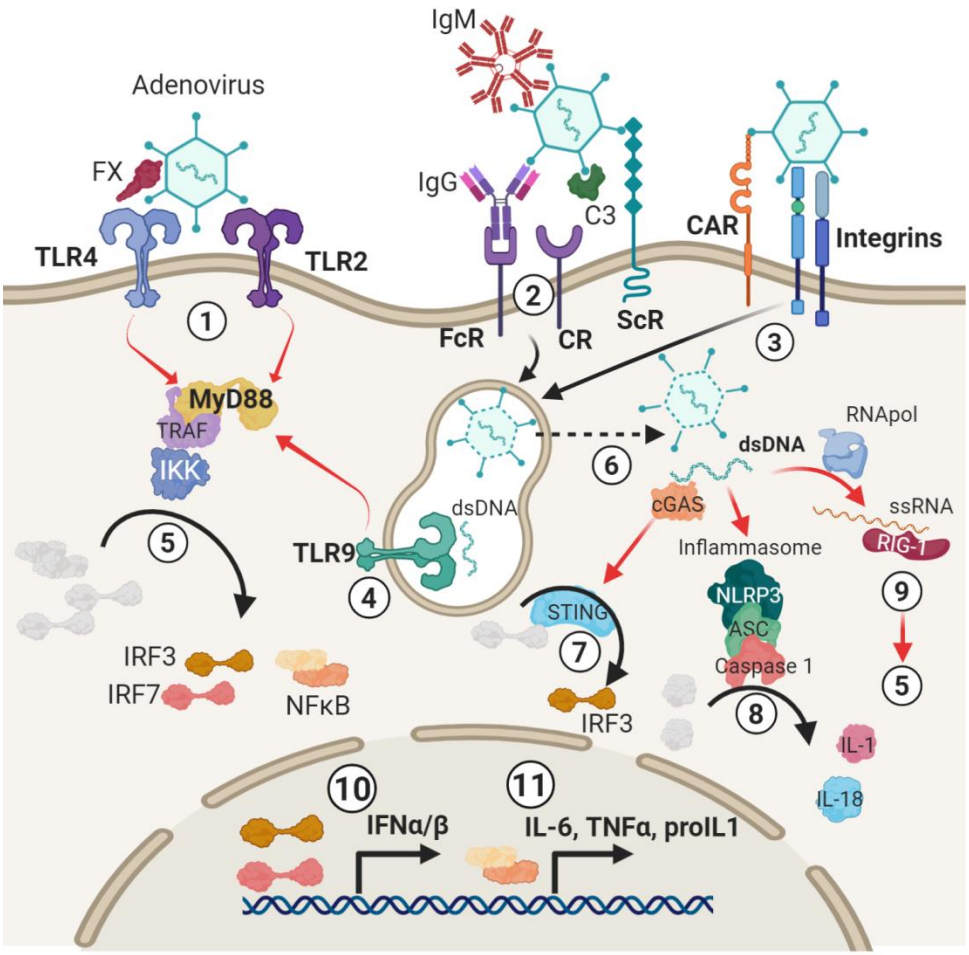

Figure 12. Anti-adenovirus immune sensing. The innate sensors to Ads could be divided into the TLR-MyD88 depending pathways or independent (cytosolic sensors). **(1)** The Ad is recognized by toll-like receptor 2 (TLR2, [158]), or the Factor X (FX)-Ad complex is detected by TLR4. Both interactions trigger the MyD88-signaling pathway. **(2)** The opsonized adenoviral particles are captured by Fc receptors (FcR), complement receptors (CR) or scavenger receptors (ScR), and phagocyted into macrophages, DCs, neutrophils, and monocytes. **(3)** Ad virions could infect cells through CAR/integrins mechanism.

(4) The internalized particles are decomposed in the endosome, and the viral dsDNA is detected by TLR9 activating the MyD88 signaling pathway. **(5)** It ends in the activation of interferon regulating factors (IRF) 3 and 7 by phosphorylation and also the activation of the NF-κB transcription factor. **(6)** Viral particles escape from the endosome and release the viral DNA in the cytosol inducing: **(7)** cyclic GMP-AMP synthase (cGAS) that homodimerizes and generates a cyclic guanine adenine monophosphate (cGAMP) which binds to adaptor STING leading to activate IRF3 [141], **(8)** the inflammasome (NLRP3, ASC, and activated caspases) cleaves pro-IL-1/18 into their active form. **(9)** The Ad genome could be transcribed into ssRNA by RNApolIII and activate the RIG-1 sensor, which induces MyD88-cascade (5). **(10)** This response ends in the IRF activation promote the IFN type I (α and β) production. **(11)** NF-κB promotes the translation of pro-inflammatory genes such as IL-6, TNFα, proIL-1β (needs from caspase 1 to activate), among others. Figure created with Biorender.com.

Altogether, FX, Ab, and complement compete to form a complex with the virion (**Figure 13**, step 1). The complexes facilitate the virus capturing. The relocalization into the cytosol triggers a pro-inflammatory response without the need for viral replication [141]. This process occurs in the Kupffer cells (**Figure 13**, step 2) and splenic marginal macrophages (**Figure 13**, step 3) due to their localization and specialization to efficiently clear the bloodstream from pathogens. Two central signaling cascades are activated through IRF and NF-κB. The IFN response functions in the autocrine/paracrine manner, promoting the interferon-stimulated genes (ISG) to eliminate virions from the cell and block the replication by inhibiting *E1A* transcription. Moreover, the Kupffer cells undergo necrotic cell death (**Figure 13**, step 4) to avoid viral dissemination and recruit more immune cells to fight the infection. In contrast, splenic macrophages require the cytotoxic neutrophil activity to be eliminated (**Figure 13**, steps 5 and 6). The NF-κB induces pro-inflammatory cytokines and chemokines to recruit neutrophils (within minutes after injection), NK cells, and lymphocytes to the infected tissue (**Figure 13**, step 7).

Moreover, it induces the DC maturation and polarization towards a Th1 response linking to the adaptive responses in the lymph nodes (**Figure 13**, step 8). Adenoviral antigens are presented by DC inducing $CD8^+$ cytotoxic T lymphocytes (CTLs), $CD4^+$ T helper cells type I (Th1) and B cells (**Figure 13**, step 9). CTLs are capable of lysing virally infected cells via MHC-I viral antigens recognition. Furthermore, CTLs can cross-react to different serotypes, unlike the NAbs. The TCD4+ Th1 cells are predominant in adenoviral responses [159], providing help for optimal CTL and B cell activation, leading

to antibody formation. Th1 cells are also critical for the generation of memory responses.

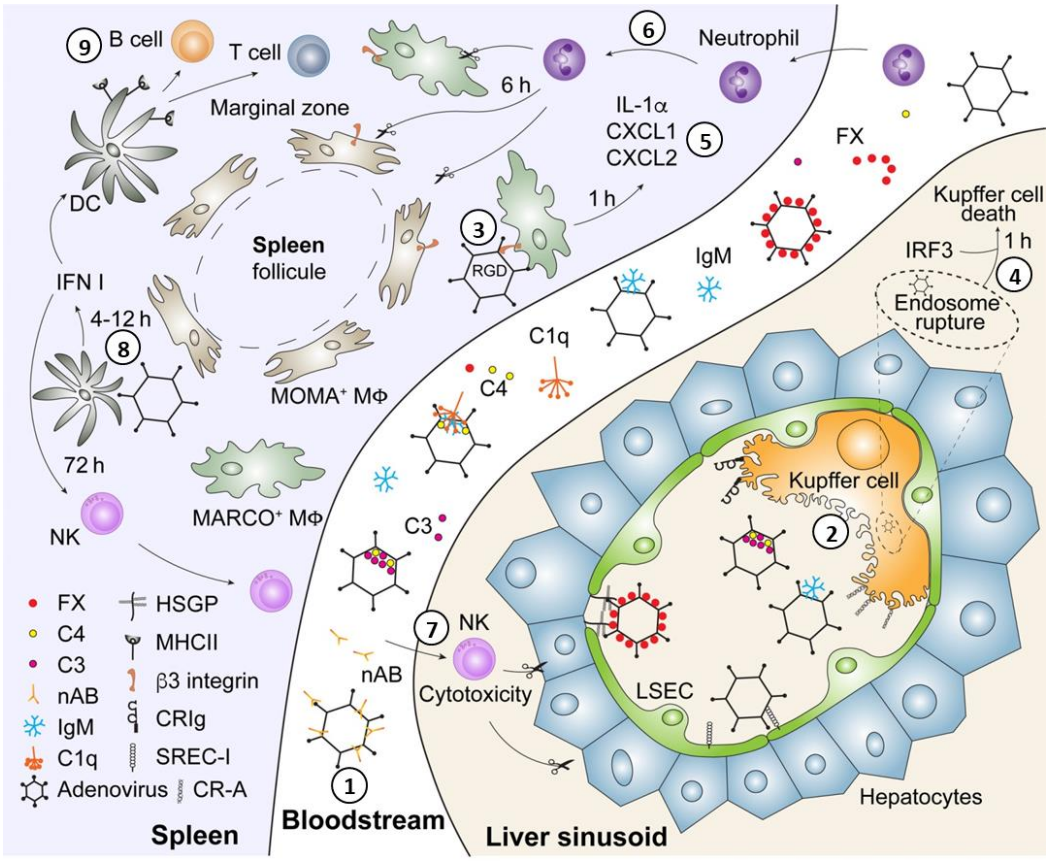

Figure 13. Immune response after systemic Ad administration. (1) In the bloodstream (white), the Ad interacts with several blood factors: neutralizing antibodies (nAB), complement components (C1q, C3, C4), natural antibodies (IgM), and Factor X (FX). **(2)** Ad particles are captured in the liver (right, brown) by Kupffer cells through the complement receptor (CRIg) and scavenger receptor (SREC-I). **(3)** A subpopulation of splenic macrophages (MARCO+ Mϕ) in the marginal zone of the spleen trap with virions via β3 integrin. **(4)** The mentioned capturing induces Kupffer cell death, and **(5)** macrophage pro-inflammatory signaling that recruits **(6)** neutrophils which eliminate the infected macrophages. **(7)** The triggered inflammation in the liver and spleen recruits NK cells and promotes **(8)** the DC maturation towards Th1 response, promoting **(9)** an anti-viral adaptive response by T $CD8^+$, T $CD4^+$ Th1 and B cells. Figure adapted from [160]

5.4.1.2 Immune response in the tumor

In the case that a free virion infects a tumor cell, the binding of fiber knob to CAR receptor induces signal transduction on infected cells that leads to MAPK and NFκB pathways activation [161]. RGD binding to αv integrins also activates these pathways. Inside the cell, the Ad dsDNA triggers the mentioned innate sensors. Although TLRs expression has been reported in epithelial cells and some cancer cells, they are commonly expressed in immune cells [162,163]. Thus, infected cancer cells trigger TLR-independent mechanisms; cGAS/STING pathway is the most relevant [164,165]. Cancer cells commonly present defects in IFN-pathways to become immunosuppressive, favoring viral persistence [166]. Furthermore, Ads evolved to bypass the anti-viral immune response. If the OAd replicates, E4 proteins hijack the machinery associated with DNA damage pathways. In parallel, E3 proteins inhibit NF-κB-induced transcription and downregulate MHC and other immune markers avoiding the immune system recognition [167]. The balance between the triggered immune response and the viral evading mechanisms determine the viral cycle. If the viral-life cycle is completed, the infected cancer cell is lysed by the oncolysis process in less than 72hours.

There are different cell death process classified according to the phenotypic changes. Some forms of programmed cell death do not trigger an immune response, such as the apoptosis of cancer cells. Nonetheless, if the cell death induces an immune stimulation is considered an immunogenic cell death (ICD). The ICD is characterized by the exposure and release of DAMPs that mobilize the immune system: ATP secretion (a “find me” signal), calreticulin surface exposure (“eat me” signal), and at later stages the release of nuclear proteins such the high mobility group box protein 1 (HMGB1) or heat shock proteins (HSP) [21,168].

The OAd-mediated oncolysis is a multi-modal cell death process involving necroptosis, pyroptosis cascades, and sustained autophagic activity [169–171]. During the OAd replication, the cancer cell releases all characteristic DAMPs for an ICD, and is phagocyted by immature DCs *in vitro,* triggering a Th1 profile [170,172,173]. Moreover, Ad-infected cells presented inflammasome activity, a consequence of the released ATP

or/and dsDNA sensing in the cytoplasm [170,174]. Besides, cancer cells undergoing either pyroptosis or autophagy, such as OAd-infected cells, enhance the recruitment and phagocytosis of APCs through the “find me” and “eat me” signals. These signals are good prognosis factors for successful immunotherapy [175,176]. Altogether, the OAd-infected cancer cells trigger an immune response via innate sensors or immunogenic cell death. It explains the limited replication and efficient viral clearance reported in clinical trials.

In any case, the debulking of tumor mass by APC-phagocytosis or direct viral oncolysis releases PAMPs (adenoviral proteins or DNA), DAMPs, and tumor antigens (TAAs, TSAs) in a pro-inflammatory context. This recruits more macrophages, DCs, NK cells, and neutrophils into the tumor, reverting the immunosuppressive status from “cold” to “hot” [177]. Moreover, the APCs maturate and cross-present tumor and viral antigens activating the adaptive immune system in the lymph nodes. Thus, the anti-viral signaling can prime the immune system for a collaterally antitumor response. OAds act as an *in situ* antitumor vaccine independently of the antigen, what it was termed antigen-agnostic tumor vaccine [178] (**Figure 14**). Reports of infected-cancer cells inducing antitumor responses support this idea [179]. Furthermore, OAd-mediated oncolysis elicits anti-neoepitopes responses in pre-clinical and clinical studies [180,181]. There is evidence that the immune-mediated response is a pivotal mechanism of OAds therapeutic activity independent of viral replication [182,183]. This changed the paradigm in the virotherapy field towards immunovirotherapy. OAds have been designed as a immune-adjuvants encoding immune-stimulatory molecules and combined with different immunotherapies.

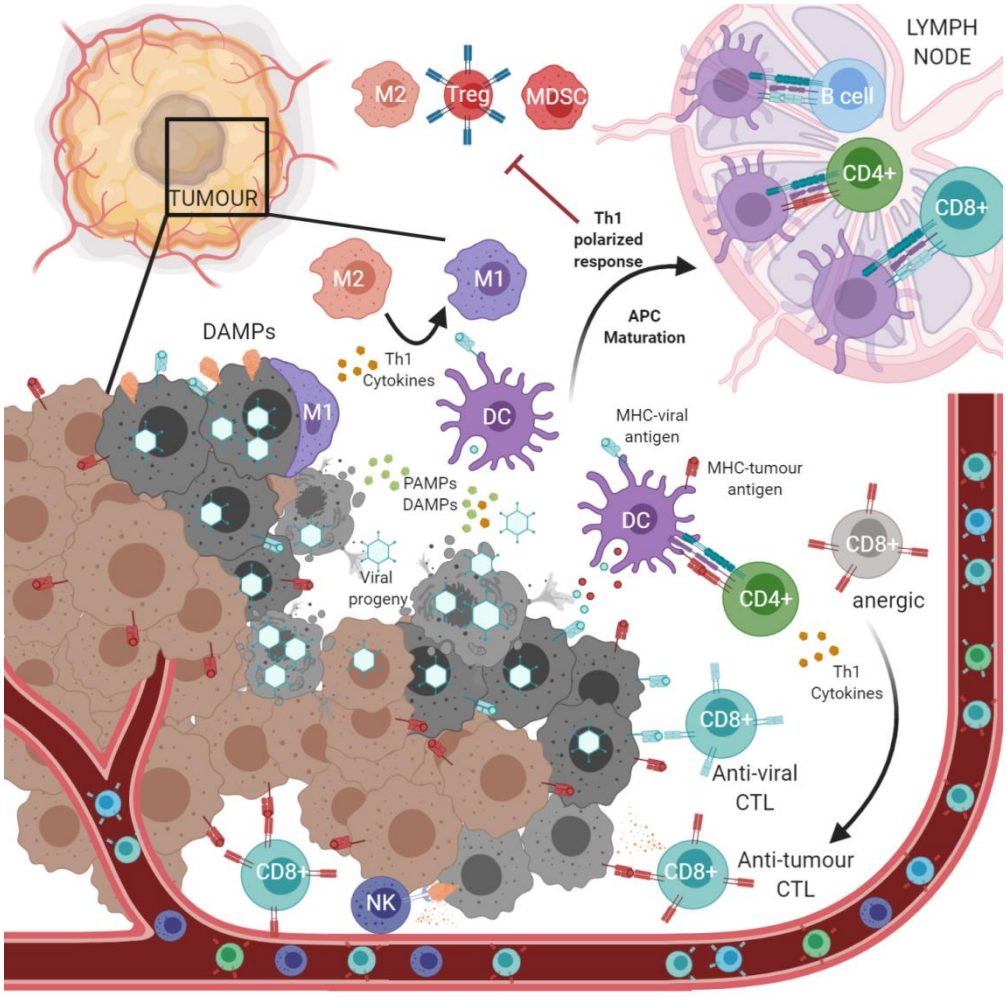

Figure 14. Overview of immunovirotherapy and *in situ* vaccination hypothesis. Tumor-infected cells express DAMPs that could recruit M1 macrophages (blue) among other innate cells and phagocyte the tumor cell (dark grey tumor cell) inducing pro-inflammatory cytokines (Th1 cytokines). In parallel, the virus induces oncolysis (light grey tumor cells) releasing the viral progeny, PAMPs (green), DAMPs (orange) and tumor (red), and viral (light blue) antigens. These are captured by DCs that mature and transit to the lymph node cross-presenting and activating antitumoral and anti-viral lymphocytes (CD8+, CD4+, and B cells). They circulate towards the tumor thanks to a chemokine gradient also induced during the pro-inflammatory response. The Th1 polarization can revert immunosuppressed phenotypes such M2 macrophages to M1 or anergic T cells to their activation. Moreover, the Th1 polarization in the lymph node avoids the maturation and differentiation of regulatory T cells (Tregs), and myeloid-derived suppressor cells (MDSCs). Image created with Biorender.com.

5.5 ARMED ONCOLYTIC ADENOVIRUSES

We described different approaches to enhance OAds tumor targeting by capsid modifications (section 5.1.1), and tumor-selective replication using promoters or gene deletions (see 5.1.2). OAds containing with these modifications, such as CV706, CG7870, AdΔ24RGD, and ICOVIR5, entered clinical trials (detailed in section 5.3). However, despite occasional striking tumor responses, clinical efficacy remained low [90,93,102,184,185]. A potency increase and bypass the clinical challenges are required to become a real and viable cancer therapy. The insertions of transgenes into OAds' genome, also known as "arming OAds" [186], aim the destruction of neighboring and distant uninfected cancer cells by transgene-encoded therapeutic proteins or RNA.

Adenovirus has several advantages compared to other oncolytic viruses for transgene insertion. All RNA viruses except orthomyxoviruses (e.g. influenza virus) and retroviruses replicate in the cytoplasm and, therefore nuclear transcriptional control elements, such as tumor-selective promoters, are non-functional. In contrast, DNA viruses except for poxviruses (e.g. vaccinia virus) replicate in the nucleus and are compatible with the use of eukaryotic promoters. Viruses with small compact genomes can not accept transgenes (picornavirus, reovirus, and parvovirus). Besides, adenovirus stands out of the rest of transgene-carrying viruses (VSV, Measles, NDV, Herpes, and Vaccinia) because it has a highly regulated temporal sequence of viral gene expression starting with E1A which allows tuning transgene expression.

5.5.1. Types of genes

OAds have been modified to encode several different types of transgenes. The function of transgenes can be considered virocentric or immunocentric. Virocentric transgenes would enhance virus cytotoxicity, yields, or spread. Immunocentric transgenes aim to enhance the immune responses elicited during the oncolysis, based on the triggered antitumor immune response is the ultimate mechanism of efficacy for OAds.

5.5.1.1 Virocentric transgenes

Virocentric transgenes aim to improve the oncolytic effect, enhance virus spread, or kill bystander non-infected cells. The prodrug-converting enzymes for molecular chemotherapy, known as suicide genes, were inserted in the first armed-OAds. The enzymes promote the conversion of intravenously administered non-toxic prodrugs to toxic drugs in adenovirus-infected cells, inducing a bystander effect with limited systemic toxicity [187–194]. Following this rationale toxins were also used to kill surrounding non-infected cells [195,196].

Apoptosis stimulates adenoviral spread through apoptotic bodies at a late stage of the virus cycle [197]. Thus, OAds armed with different apoptosis inducers have been published: p53 [198,199], TNFα [200–203], soluble apoptosis-inducing ligand (TRAIL) [204–209] and others [204,210–213].

Moreover, connective tissue, fibrosis, and extracellular matrix hamper viral spread in the tumor (as we have seen 5.4.2) [214]. OAds have been armed to digest the connective tissue with relaxin [215,216], hyaluronidase [217], or DNAse-I [218].

5.5.1.1.1 VCN-01

The hyaluronic acid (HA) hinders the intratumoral spreading of OAds, but the HA degradation significantly enhanced the viral distribution and efficacy [127]. Our group armed the ICO15 with the human PH20 hyaluronidase, generating the ICO17 [217]. Furthermore, ICO17 was significantly improved by the mentioned RGDK transductional targeting generating the ICO17K, renamed as VCN-01 [219]. VCN-01 currently being developed by VCN Biosciences S.L. has exhibited favorable toxicity profiles and potent antitumor efficacy in different mouse and Syrian hamster models of cancer [219–222]. The hyaluronidase and oncolytic activity of VCN-01 enhance the chemotherapeutic and immunotherapeutic drugs' extravasation into treated tumors (manuscript in preparation). VCN-01 is currently under clinical trial investigation to treat advanced pancreatic cancer (NCT02045602, NCT02045589), retinoblastoma (NCT03284268), and head and neck cancers (NCT03799744).

This thesis analyzed the patients' immune response in the pancreatic cancer clinical trial (Chapter A). Furthermore, an optimization of the VCN-01 hyaluronidase activity has been performed in Chapter C.

5.5.1.2 Immunocentric transgenes

Arming OAds with immune-stimulatory cytokines or redirecting immune molecules has emerged as the main approach to prevent cancer spread and recurrence by overcoming the immune tolerance in the tumor.

An example is the granulocyte-macrophage colony-stimulating factor (GM-CSF), stimulating the development, recruitment, activation, and survival of dendritic cells, which are vital for antitumor immunity. As we have seen, there are two armed-OAds with GM-CSF in clinics: ONCOS-102 [105,106,223] and CG0070 [103,224]. Similarly, other immunostimulatory cytokines have been used: IL-12 [225–227], IL-15 [228,229], IL-21 [230] or IL-24 [231–236]. Even OAds expressing combinations of immunostimulatory ligands and cytokines are being tested in phase I clinical trials: TILT-123 (expressing TNFα and IL-2, [237]) or LOAd703 (CD40L and 41BBL, [238]).

Armed-OAds evolve in parallel to the immunotherapy landscape. An OAd producing a full-length human monoclonal antibody specific for CTLA-4 was published for the first time in 2012 [239]. OAds have been designed to produce soluble ligands of immune checkpoints such as OX40L [240], GITRL [241], or a fusion protein sPD1-CD137L [242]. Even more, targeting crucial molecules for the resistance to anti-PD1/PD-L1 and anti-CTLA-4 therapies such as TGF-β has been expressed from OAds [243,244].

Moreover, the generation of bispecific T-cell engagers (BiTE) opened a new opportunity for redirecting the anti-viral lymphocytes against a TAA. OAds armed with BiTEs against EGFR or FAP have been generated in our group [245,246]. All mentioned approaches have been combined in single adenoviral agents such NG-641, armed with 4 transgenes: IFNα to drive dendritic cell priming, CXCL9, and CXCL10 to recruit T-cells and FAP-BiTE to redirect them.

MATERIALS AND METHODS

6. HANDLING OF BACTERIA

During this thesis two different *E. coli* bacteria strains were used: DH5α for DNA production and SW102 strain used for the homologous recombineering.

6.1 PREPARATION OF ELECTROCOMPETENT AND CHEMOCOMPETENT BACTERIA

6.1.1. Electrocompetence

The *E. coli* stock was conserved at -80ºC with 15% glycerol. In order to induce electrocompetence, 10mL of LB (1% Tryptone, 0.5% Yeast Extract, 0.5% NaCl) were inoculated with the stock and was grown overnight at 37ºC in agitation. Next day, the 10mL preculture was used to inoculate 1L of LB at 37ºC in agitation until it reached an OD_{600} of 0.5-0.6. Then the culture was distributed in 250 mL SORVALL bottles and kept 40 minutes on ice to stop bacterial growth. Further manipulation of bacteria was carried on at 4ºC. Bacteria were centrifuged 15 minutes at 4000*g* and 4ºC in a SORVALL centrifuge, the supernatant was discarded, and the pellet was gently washed with 4ºC cold bi-distilled water (ddH_2O). This centrifugation/washing process was repeated 3 times and in the last wash the pellet was resuspended in 45mL of water with 15% glycerol. Bacteria were centrifuged one more time and, finally resuspended in 3mL of water containing 15% glycerol. The OD_{600} of a 1:100 dilution of the suspension should be close to 1 (which is equivalent to $2.5x10^8$ bacteria/mL). Finally, the bacterial suspension was aliquoted and stored at -80ºC.

6.1.2. Chemocompetence

The *E. coli* stock was conserved at -80ºC with 15% glycerol. In order to induce chemocompetence, 5mL LB were inoculated with the glycerinate and it was grown overnight at 37ºC in agitation. Next day, 3mL of the overnight culture was used to inoculate 15mL of LB at 37ºC in agitation until it reached an OD_{600} of 0.6-0.7. Then bacteria were incubated 20 minutes on ice and centrifuged during 10 minutes at 2000*g* and 4ºC. After that, the supernatant was discarded, and the pellet was gently resuspended in 9mL of $CaCl_2$ 0.1M. It was incubated on ice for 30 minutes and then

centrifuged 10 minutes at 2000g and 4ºC. Finally, the supernatant was discarded again, and the pellet was resuspended in 4.8mL $CaCl_2$ 0.1M and 15% glycerol. Appropriate aliquots were prepared and stored at -80ºC.

6.2 TRANSFORMATION OF BACTERIA

6.2.1. Electroporation

Frozen electrocompetent DH5α aliquots (50µL) were thawed on ice and mixed with a maximum of 10 µL pre-cooled DNA (10-1000pg for retransformations or >200ng for recombinations). The mixture was gently mixed, incubated 5 minutes on ice and transferred into ice-cold 0.2 cm electroporation cuvettes and were electroporated at 50 µF, 1500 V and 125 Ω with the Electro Cell Manipulator™ ECM 630. Immediately, bacteria were recovered in 1 mL LB and incubated for 60 minutes in agitation at 37ºC. The recovered culture or an appropriate dilution of it was plated on LB plates supplemented with the corresponding selection antibiotic and incubated at 37ºC overnight. The next day, one clone was inoculated in 5mL for mini-preps, or 100-200mL midi-preps LB supplemented with the corresponding antibiotic for isolating plasmid DNA as described in section 6.3.

6.2.2. Chemical transformation

Frozen chemocompetent DH5α aliquots (50µL) were thawed on ice and mixed with 2 to 10µL of DNA and incubated for 1 minute on ice. Then a heat-shock was induced at 42ºC for 30-45 seconds flicking the tube. Once the shock finished bacteria was put on ice for 2 minutes. After that, bacteria were recovered in 1mL of LB for 1 hour at 37ºC in agitation. Later, they were centrifuged at 2000*g* during 5 minutes, the supernatant was discarded and the pellet resuspended with the remaining volume and plated on LB plates supplemented with the corresponding selection antibiotic and incubated at 37ºC overnight. The next day, desired clones were inoculated in 5mL or 100-200mL LB supplemented with corresponding antibiotic for isolating plasmid DNA as described in section 6.3.

6.3. PLASMIDIC DNA EXTRACTION FROM BACTERIAL CULTURES

Plasmid DNA was obtained from saturated *E. coli* cultures grown in LB with antibiotic according to protocols based on an alkaline lysis with SDS. DNA was prepared at small and large scale.

6.3.1. Small and large-scale plasmid DNA preparations

Small-scale plasmid DNA preparations (mini-preps) were performed following an adapted protocol described by Birnboim and Doly [247] using Qiagen midi-prep kit reagents. A colony grown in a LB-antibiotic dish was inoculated in 5mL of LB-antibiotic and incubated overnight at 32ºC (for SW102) or 37ºC (for DH5α). 500µL of the overnight culture were saved in a 1,5mL tube to prepare the glycerol stock. Rest of the culture was centrifuged at 2000g, and the pellet was resuspended in 200µL of pre-cooled solution R3 with previously added RNAse as kit indicates and incubate 5 minutes on ice. After that, 200 µL of solution L7 were added and the mixture was blended by inversion and incubated 5 minutes at RT. Finally, 200µL of pre-cooled solution N3 were added and the mixture was blended again by inversion and let it on ice during 20 minutes until a white precipitate appears. After that, it was centrifuged 10 minutes at 15000*g*. Next, the clear supernatant was collected without taking the white pellet that corresponds to cellular DNA, proteins and SDS, and 0.75 volumes (high copy) or 1.3 volumes (low copy) of isopropanol were added and vigorously mixed. Then plasmid DNA was precipitated by centrifugation during 10 minutes at 15000*g*, supernatant was discarded, and the pellet was washed with 70% ethanol. It was centrifuged again 5 minutes at 15000*g*, discarding the supernatant, and the pellet was dried and resuspended in 50 µL of TE.

Large-scale DNA preparations (midi-preps) were prepared from 200 mL (Low-copy plasmids) or 100mL (High-copy plasmids) of saturated bacteria culture using the NZYMidiprep kit (Nzytech), following manufacturer's instructions.

6.4. HOMOLOGOUS RECOMBINATION IN BACTERIA

Genetic modification of the adenovirus genome was carried out with the bacterial artificial chromosome (BAC) recombination-mediated genetic engineering (recombineering) method described by Warming et al [248]. Homologous recombination of the BACs is achieved by using *E.Coli* stain SW102, which contains the integrated temperature-sensitive defective λ-prophage. Its recombination machinery is controlled by a temperature inducible promoter, whose activation can be triggered by a temperature of 42ºC. Electroporation of the heat-shocked bacteria with a donor DNA fragment flanked by homology arms (>40bp) to the targeted site in the BAC will result in the insertion of the DNA by homologous recombination. This method has been adapted by Stanton et al [249], in order for the BAC to carry the whole adenovirus genome, a system called AdZ (Ad with zero cloning steps). *SacB* and *Ampicillin* (Amp) resistance genes from Stanton *et al.* protocol were replaced by *rpsL-neo* cassette, as it is a faster and more cost-effective method [250].

Genome modification was performed in two steps. In the first step (positive selection), the *rpsL-neo* cassette is inserted in the region of interest of the adenovirus genome. This first fragment had homology regions (about 40 bp) with the site we wanted to modify on each end. The neo gene in the *rpsL-neo* cassette confers resistance to kanamycin. Thus, positive selection can be achieved by plating the bacteria after electroporation in LB agar plates supplemented with kanamycin (kana) and chloramphenicol (Cm, the pAdZ BAC backbone confers resistance to this antibiotic). In the second step (negative selection), the heat-shocked bacteria containing the pAdZ-rpsL-neo are electroporated with the DNA of interest flanked by homology arms targeting the region where the *rpsL-neo* cassette is inserted. The *E. coli* strain SW102 is intrinsically resistant to streptomycin (Strep) due to mutations in the *rpsL* gene but introducing the wild-type *rpsL* gene into the bacteria exerts dominant phenotypic effects over mutated *rpsL* [251]. After the second transformation, recombinant clones were those that had incorporated the inserted DNA and had lost *rpsL-neo* cassette, being consequently sensitive to Kana and resistant to Strep.

The plasmid pAdZ5-CV5-E3^{+} provided by Richard Stanton was modified in order to obtain pAdZ-ICOVIR-15K and pAdZ-ICOVIR-15 plasmids, backbones that have been used for all the modifications described in this thesis. The detailed procedure for recombineering is as follows. For positive selection, glycerinates of the bacteria containing the desired backbone were inoculated in 5mL of LB media including Cm + Strep antibiotics (12.5µg/mL, and 1mg/mL, respectively) and incubated overnight at 32ºC and constant agitation. Then 25mL of LB Cm + Strep were inoculated with 0.5mL of the previous culture and incubated 32ºC with agitation until it reached an OD_{600} between 0.5-0.6. At this moment, culture was divided in two Falcon tubes with equal volumes. One of the tubes was kept on ice until further processing (non-induced). The other tube was induced by heat-shock at 42ºC for 15 minutes in a water bath with agitation, followed by chilling on ice for 15 minutes (induced). From that moment, manipulation was performed on ice in order to ensure transformation efficiency. Both cultures (induced and non-induced) were centrifuged 5 minutes at 4000*g* at 4ºC and supernatant was discarded. Bacteria pellet was resuspended in 12mL of cold ddH_2O water and centrifugation was repeated. This washing step was repeated thrice and, and finally the pellet was resuspended in approximately 300 µL ddH20. Then, 50µL-aliquots of the induced and uninduced cultures were transformed with ≥200 ng of the *rpsL-neo* DNA flanked by the desired homology arms. Bacteria were recovered in 1mL of LB and incubated 2 hours at 32ºC with constant agitation. From this recovery, 100µL were plated into LB plates containing Cm and Kan (12.5µg/mL, and 15µg/mL, respectively) and incubated overnight at 32ºC. About 20-24 hours later, the number of colonies on the plates of induced and non-induced cultures was counted to determine the recombination efficiency. Then, colonies from induced plates were picked and inoculated in 4mL LB supplemented with Cm and Kana and incubated at 32ºC and 250 rpm. Next day, mini-preps of DNA were performed (see 6.3.1). For screening of recombinant clones, 17,5µL of the mini-preps were digested with the corresponding restriction enzymes (New England Biolabs and Takara/Clonetech) in appropriate conditions and separated by electrophoresis on 1% agarose gels. Positive clones were stored at -80ºC in LB with 15% (v/v) glycerol. pAdZ-ICOVIR15 or pAdZ-ICOVIR-15K

backbones were modified with the insertion of *rpsL-neo* cassette in different desired positions using this positive selection method.

A similar procedure was followed for the second step, in which the clones obtained in the previous step were inoculated in 5mL of LB Cm + Kan and cultured overnight at 32ºC. Next day, the bacteria were made competent for its transformation by electroporation as described previously. Again, 200 ng of DNA (insert) containing the desired modification were transformed. After the recovery incubation, 100 µL from a 1:10 and 1:25 dilution were plated in LB agar supplemented with Cm and Strep and plates were incubated overnight at 32ºC. Next day, colonies were picked and inoculated in 4mL of LB-Cm + Strep and incubated overnight at 32ºC in agitation. Recombinant clones were screened and stored as above, and the correct insertion of the genes was confirmed by sequencing (929.6.4). Midi-preps from the sequenced positive clones were prepared (see section 6.3.1) and used for transfection (see section 9.2).

7. CELL CULTURE

7.1. CELL LINES

The cell lines used in this thesis for the *in vitro* and *in vivo* experiments are summarized in the following table:

Table 2. Cell lines used in this thesis.

Cell line	Tumour type	Origin	Medium	FBS
A549	Lung adenocarcinoma	Human	DMEM	10%
HEK-293	Embryonic kidney	Human	DMEM	10%
MDA-MB-231	Breast adenocarcinoma	Human	DMEM	10%
HT1080	Fibrosarcoma	Human	DMEM	10%
Sk-mel-28	Melanoma	Human	DMEM	10%
MIA PaCa-2	Pancreas carcinoma	Human	DMEM	10%

Panc-1	Pancreas carcinoma	Human	DMEM	10%
FaDu	Pharynx squamous carcinoma	Human	DMEM	10%
B16-F10	Melanoma	Murine	DMEM	10%
CMT64.6	Lung adenocarcinoma	Murine	DMEM	10%
JAWSII	Immature dendritic cell	Murine	αMEM	20%

The cancer cell lines A549, HEK-293, MDA-MB-231, HT1080, MIA PaCa-2, Panc-1, FADU, Jurkat and B16-F10 were obtained from the American Type Culture Collection (ATCC, Manassas, VA, USA). CMT.64 cell line was provided by Dr. Stephan Kubicka (Hannover Medical School, Hannover, Germany) and the most permissive clone to adenovirus infection was previously isolated and expanded by our group, generating the CMT64.6 [252].

7.2. CELL MAINTEANCE AND COUNTING

All cells were maintained in the appropriate media (Gibco, Thermo Fisher Scientific) supplemented with FBS (Gibco, Thermo Fisher Scientific) previously inactivated by heating at 56ºC for 30 minutes and 1% of penicillin-streptomycin (PS, Gibco-BRL) (100 U/mL and 100 μg/mL, respectively). They were incubated at 37ºC in a humidified atmosphere with 5% CO_2 in the presence of the medium described in **Table2**. When cultures reached 80-90% confluence, cells were washed once with PBS and detached with trypsin-EDTA. To stop the reaction, cells were resuspended to a final volume of 10 mL in the corresponding medium supplemented with 5-10% (v/v) FBS. These cell suspensions were used to split the cells 1:6 to 1:20 depending on the cell line. To determine cell numbers, the automatic counting was performed with a cell counter TC20^{TM} (Bio-Rad) according to the manufacturer's instructions.

7.3. CRYOPRESERVATION AND CELL THAWING

For long term storage, cells were collected by trypsinization and pelleted by centrifugation. Cell pellets were resuspended in cold freezing medium (90% FBS, 10% DMSO). Cell suspension was distributed in cryotubes at 1 mL/tube and placed in a Mr.

Frosty freezing container for its freezing at -80ºC for 24 hours. Next day, cryotubes were stored in a liquid nitrogen tank. For cell thawing, cells were rapidly thawed in a water bath at 37ºC. Cells were diluted in pre-warmed medium and trespassed to a 15 mL Falcon tube. Centrifugation at 1000*g* was carried out for 5 minutes and the pellet of cells was resuspended in fresh medium and seeded at an appropriate density.

7.4. MYCOPLASMA TEST

All cell lines were routinely tested for contamination of: *Mycoplasma Hyorhinis, M. Arginine, M. Pneumoniae, M. fermentas, M. orale, M. pirum, Acholeplasma laidlawii* and *Spiroplasma mirum* by qPCR using the following primers:

Table 3. **Primers for testing mycoplasma.**

Primer	Sequence (5'→ 3')
MICO-1	GGCGAATGGGTGAGTAACACG
MICO-2	CGGATAACGCTTGCGACTATG

As a template for the qPCR, 1/100 dilution of medium from cells that had been in overconfluence and absence of antibiotics for at least 7 days were used. If the result was positive, cells were discarded or treated with Plasmocin^{TM} (Invivogen) at 25 µg/mL for 2 weeks, and then the cells were tested again.

7.5. ISOLATION, CRYOPRESERVATION AND THAWING OF HUMAN PBMCS AND T CELLS

All experiments were approved by the ethics committees of the University Hospital of Bellvitge and the Blood and Tissue Bank (BST) from Catalonia. Blood samples were obtained from the healthy donors. Peripheral blood mononuclear cells (PBMCs) of healthy donors were isolated from the blood by ficoll (Rafer) density gradient centrifugation in Leucosep tubes (Greiner Bio-one) following manufacturer's recommendations. Erythrocytes were removed by incubation with ACK lysing buffer (Lonza) and thrombocytes were removed by centrifugation of the PBMCs at 1000*g* for 10 minutes and aspiration of the supernatant. T cells were isolated from blood samples

with the RosetteSep Human T-Cell Enrichment Cocktail (STEMCELL Technologies) according to the manufacturer's instructions. T cells were cryopreserved in FBS supplemented with 10% DMSO in aliquots of 5-10 × 10^7 cells/vial. For thawing, T cells cryovials were quickly thawed in a water bath at 37ºC and washed once with 10 mL RPMI supplemented with 10% FBS and 10 mM HEPES (Gibco) by centrifugation. Cells were resuspended at a concentration of 3 × 10^6 cells/mL and incubated overnight for the recovery of the cells prior to the experiments.

7.5.1. Preactivation and expansion of human T cells

T cells were isolated as described in section 2.6. For stimulation, human T cells (1 × 10^6 cells/mL) were cultured with CD3/CD28 activating Dynabeads (Thermo Fisher Scientific) at a 1:3 bead-to-cell ratio. On day 3 after bead stimulation, T-cell cultures were fed with ¾ culture volumes of fresh medium. On day 5 after bead stimulation, beads were removed by placing the cultures on DynaMag-15 magnet (Thermo Fisher Scientific) and recovering the supernatants. Cells were counted with the TC20 automated counter by setting the gates from 8 µM to 14 µM (resting T cells have a mean diameter of 6 µM, whereas proliferating T cells have a mean diameter of 10 µM), and cultures were set to 1 × 10^6 cells/mL. From this day on, cells were diluted to a concentration of 8 x 10^5 cells/mL. Cells were maintained in culture until day 10-11 after bead stimulation, when they were still in the expansion phase and just before they returned to a resting state. Aliquots (1-10 × 10^7 cells) were cryopreserved in FBS supplemented with 10% DMSO.

7.5.2. Generation of genetically-modified T cells

For the generation of luciferase-T cells, transduction with the corresponding lentiviral vectors was carried out 24 h after bead-mediated T-cell activation (see section 7.5.1). For the generation of luciferase-expressing T cells, cultures were infected with the CBG-T2A-GFP vector at MOI of 7.5. Transduced T-cell cultures were expanded and handled as described in section 7.5.1. T cell preparations were characterized for the expression of the transgene and phenotyped for CD4 and CD8 T-cell subpopulations by flow cytometry (see section 10.2.1).

7.6. RNA EXTRACTION

RNA was extracted from 4e6 cells of CMT64.6 and B16-F10 cell lines according to RNeasy Mini kit (Qiagen) protocol. Briefly, cells were trypsinized and collected as a cell pellet, then were lysed by adding buffer RLT. The lysate was loaded into QIAshredder spin column for spinning and homogenizing. Then 1 volume of Etanol (EtOH) 70% was added to the homogenized lysate and transferred into RNeasy spin column. The column was centrifuged and afterwards buffer RW1 was added and centrifuged again. RPE buffer was used to wash the spin column membrane twice. Finally, the RNA was eluted with RNase-free water.

7.6.1. RNA sequencing

After quality control assessment by electrophoresis, total RNA of CMT64.6 and B16-F10 were sequenced at "Centre Nacional d'Anàlisi Genòmica (CNAG) (stranded mRNA-seq, >135M PE reads) using Illumina HiSeq2000 at read length 2x75 bp. Data from CNAG was analyzed by Rebeca Sanz Pamplona from "Unitat de Biomarcadors I Susceptibilitat" (Institut Català d'Oncologia, ICO). FastQC software was used to assess reads quality and all evaluated parameters were satisfactory except for B16-F10 sample where four overrepresented sequences were found corresponding to Illumina single end PCR primer and TrueSeq adaptors (technical noise). A trimming of these sequences was done before RNA seq processing. Then, reads were mapped over reference mouse genome (mm10) using STAR tool. The resulting SAM file was processed with Picard tool to mark and remove duplicates. Next, we use GATK tool SplitNCigarReads which splits reads into exon segments and made a base recalibration.

7.6.1.1. Neoepitope identification

With RNAseq data a variant calling was done using GATK Unified Genotyper (variant call quality > 30). Next, clusters with at least 3 variants within a window of 35 bp was filtered. The resulting good quality variants were annotated using VEP (Variant Effector Predictor). In parallel, Cufflinks tool was used over aligned reads to extract a matrix of gene expression. As a result, for B16-F10 cell line 57161 variants were identified and

filtered (frequency > 15% and DP > 20) resulting in 10230 missense mutations. From those, 1323 transcripts corresponding to 538 genes was annotated as missense thus used for neoepitope prediction purposes. For CMT64.6 model 1310 variants were identified and filtered to 644 missense transcripts corresponding to 281 gene missense mutations used for neoepitope prediction.

7.6.1.2. Neoepitope prediction

Mouse FASTA sequences extracted from UniProt were used to translate information about DNA missense mutations into an aminoacid change level (only isoforms 1 were considered). For each missense mutation, a sequence of 27-aminoacids centred on the mutation and the corresponding wild type peptide were analyzed for potential neoantigens. NetMHCpan 2.8 Server was used to infer putative immunogenic peptides for B16-F10(19 aa; 8 or 9mer) combining information about HLAs mouse genotype (H2) and peptides harbouring missense mutations. An immunogenic epitope was defined as a mutated peptide with high affinity for one HLA allele IC_{50}<50nM or rank<2%.. Information about the level of expression of each gene generating an immunopeptide was also computed. As a result, a list of 126 putative immunogenic neoantigens was generated for B16-F10 model. For the CMT64.6 a similar process was performed with NetMHCcons 1.0 software and independently of *wild type* counterpart obtaining 26 putative immunogenic neoepitopes.

8. EXPRESSION PLASMIDS

The pGT4082 was used in this thesis as a platform of genetic modifications to insert and to test different transgenes. pGT4082 is a mammalian expression plasmid that contains a prokaryotic and eukaryotic *ori* which allow its replication in eukaryotic cells and bacteria. Moreover, codifies for an ampicillin resistant gene for its selection in bacteria. The pGT4082 constitutively expresses the Green Fluorescent Protein (GFP) under the Cytomegalovirus (CMV) promoter. The GFP cassette is flanked by the Age I and Not I unique restriction sites. Desired transgenes were cloned in place of GFP using these two restriction sites, thus all transgenes included the restriction site Age I at N-terminal and Not-I at C-terminal. Moreover all transgenes included at C-terminal a

cleavable linker of Human Rhinovirus 3C protease (HRV 3C) and 6xHistidinte-tag to detect and purify the produced protein.

The pGT4082 plasmid were digested by the restriction enzymes (New England BioLabs) and separated by gel electrophoresis, the band corresponding to the linearized plasmid (without GFP) was sliced from the gel and purified with Monarch®DNA gel extraction kit (New England BioLabs) according to manufacturer's protocol. Transgenes were synthesised by PCR as would be detailed in next sections and then digested to perform the ligation. PCRs were performed according to manufacturer's protocol (NzyTech, Ref.MB146) with the next conditions:

Table 4. PCR conditions to generate transgenes. *Mean of the melting temperatures of both primers.

Stage	Description	Temperature	Time	Cycles
1	Initial denaturation	96ºC	5 minutes	1
2	Denaturation	96ºC	30 seconds	50
	Annealing	Depending on primers*	30 seconds	
	Extension	72ºC	2 minutes	
3	Final extension	72ºC	7 minutes	1
4	Cooling	4ºC	∞	1

Then, linearized vector and digested insert were ligated with the T4 DNA Ligase (New England BioLabs) following manufacturer's instructions (molar ratio of 1:7 vector to insert). Finally chemocompetent bacteria (see 6.1.2) were transformed (explained at 6.2.2) with 2 to 5µL of the ligation and incubated overnight at 37ºC. Next day mini-preps of DNA (section 6.3.1) and analysis of restriction patterns were performed to screen the clones.

8.1. HUMAN HYALURONIDASE SPAM-1 (hPH20)

A soluble form of human hyaluronidase SPAM-1 (hPH20) was cloned as a transgene in the expression plasmid. The sequence was obtained from ICOVIR-17, where the transmembrane region was deleted by Sonia Guedan et al. as described in [253]. The transgene was generated by PCR using the sPH20 Fwd and sPH20 Rv primers (**Supplementary Table 1**, Annex) to include Age I restriction site and Kozak's signal at N-terminal and HRV 3C protease's cleavable linker, 6xHis-tag and Not I restriction site at C-terminal. The genome of ICOVIR17K was used as a templeate. Once the PCR fragment was obtained and purified it was restricted by Age-I and Not-I restriction enzymes to clone it in a linearized pGT4082, generating pGT4082-hPH20.

8.2. *APIS MELLIFERA* HYALURONIDASE (BHYAL)

A hyaluronidase from *Apis mellifera* was used as transgene, the sequence was obtained from GenBank (Gene ID: 406146). It was generated by PCR using the BHyal Fwd and BHyal Rv primers (**Supplementary Table 1**, Annex) to introduce the Age-I restriction site and Kozak's signal at N-term and HRV 3C protease's cleavable linker, 6xHis-tag and Not-I restriction site at C-term. DNA from pAdZ-ICO15K-IIIaBHyal was used as a template kindly provided by Estela Nuñez (Crisitina Fillsat's Group). Once the PCR fragment was obtained and purified it was digested to clone it in linearized pGT4082 generating pGT4082-BHyal.

8.3. SEQUENCING

Once the clones of the ligation were checked by a restriction pattern analyzes, they were sequenced to check the proper ligation and discard transgene mutations. The primers used for sequencing are detailed in Table 5 and conditions in Table 6.

Table 5. Primers for sequencing pGT4082 inserted transgenes.

Primer	Sequence 5' to 3'
CMVup Fwd	AAATGGGCGGTAGGCGTGTA

GT4082Rv	GTTTGGACAAACCACAAC

Table 6. PCR conditions for sequencing pGT4082.

Stage	Description	Temperature	Time	Cycles
1	Initial denaturation	96ºC	1 minute	1
2	Denaturation	96ºC	30 seconds	50
	Annealing	50ºC	15 seconds	
	Extension	60ºC	2 minutes	
3	Pause	4ºC	∞	1

8.4. CALCIUM PHOSPHATE TRANSFECTION

After clone confirmation a large-scale DNA preparation was performed (explained in 6.3.1) to transfect HEK-293 cells the plasmid containing the desired transgene by the calcium phosphate-based method.

Monolayers of HEK-293 cells seeded in 24-well plates, 6-well plates or p10 plates at a confluence of 60% were used. For each plasmid to be transfected the following mixture was prepared:

Table 7. Proportions of reagents depending on the plate for a calcium phosphate transfection.

Reagents	24-well plate	6-well plate	p10 plate
$CaCl_2$ 2M	3.9µL	19,5µL	62,5µL
DNA	0.6µg	3µg	15µg
H_20	up to 32.4µL	up to 162µL	up to 500uL

This solution was mixed up softly for 5 minutes, and another 1.5 mL tube containing 32.4µL, 162µL or 500µL of HBS 2X (NaCl 274 mM, HEPES 50 mM, and NaH_2PO_4 1.5 mM

in H_2O, pH adjusted to 7.05 with NaOH) was prepared depending on the plate. The solution containing the DNA was added drop by drop to the tube. The mixture was incubated for 20 minutes at RT and added drop-wise to the plate. 2 hours later calcium phosphate precipitates became visible and at 16 hours post-transfection the medium was removed and exchanged by fresh medium.

8.5. PRODUCTION OF SUPERNATANTS

HEK-293 cells were transfected according to 8.4 with desired plasmid and next day the medium was removed and exchanged by fresh Opti-MEM medium (without FBS). After 7 days post-transfection the supernatant was collected in a falcon and centrifuged at 750g during 5minutes to pellet the detached cells. The clarified supernatant was collected and then according to each experiment was concentrated or not with approximately 20x with Amicon Ultra-15 filter units with a molecular weight cutoff of 30 kDa (Merck Millipore) according to manufacturer's instructions. Aliquots of the supernatant were stored at -20ºC for future analysis.

9. RECOMBINANT ADENOVIRUSES

All adenoviruses used in this thesis are derived from the human adenovirus serotype 5 (Ad5). The viruses ICOVIR15 [78] and ICOVIR15K [254] has been previously described.

9.1. CONSTRUCTION OF TRASNGENE-EXPRESSING ONCOLYTIC ADENOVIRUS

As explained before in section 6.4 a parental backbone of pAdZ-ICOVIR15 or pAdZ-ICOVIR15K should contain *rpsL-neo* cassette in the genome position to replace it for the desired transgene. Next plasmids: pAdZ-ICOVIR15K-E1a-RpsLNeo and pAdZ-ICOVIR15-Δ6.7/19K-CMV.RpsLNeo were generated in the context of this thesis for further modifications explained in the next sections. All PCRs of the next sections were performed according to Table 4 conditions, and the product of the PCR was purified by gel electrophoresis excision according to Monarch®DNA gel extraction kit (New England BioLabs) or Qiaquick PCR product purification kit (Qiagen) depending on convenience.

9.1.1. Construction human hyaluronidase PH20-expressing oncolytic adenoviruses.

A soluble version of human hyaluronidase (hPH20) had been inserted in ICOVIR15K previously in our lab under the splicing acceptor IIIa generating the ICOVIR17K [219]. In this thesis 4 new viruses codifying for hPH20 were generated with different genome positions and splicing acceptors as described in next section.

9.1.1.1. pAdZ-ICOVIR15K-40SAPH20

pAdZ-ICOVIR17K containing the hPH20 was used as a template to generate the 40SA-PH20 transgene by PCR with the 40PH20af Fwd and 40PH20af Rv primers in **Supplementary Table 1** (Annex) adding an upstream and downstream homology arms. The left homology region included the Kozak, the 40SA splicing acceptor[255] and extra DNA base pairs from the adenovirus genome. The right homology arm included the stop codon, polyA signal and extra base pairs from the adenovirus genome. Both arms were homologous to the sequences flanking the *rpsL-neo* cassette in the pAdZ-ICOVIR15K-rpsLneo plasmid. Once the PCR was performed and the product was purified, homologous recombineering (detailed in 6.4) was done to generate pAdZ-ICOVIR15K-40SAPH20.

9.1.1.2. pAdZ-ICOVIR15K-E4.IIIaPH20 and pAdZ-ICOVIR15K-E4.40SAPH20

Exactly as 9.1.1.1 pAdZ-ICOVIR17K was used as a template for PCRs to generate the transgenes: E4.IIIaPH20 and E4.40SAPH20. Primers E4-IIIaPH20 Fw and 40PH20 Rv (**Supplementary Table 1**, Annex) generated E4.IIIaPH20 transgene with an upstream homology arm containing IIIa splicing acceptor, Kozak and extra DNA base pairs from the adenovirus. Primers E4-40PH20 Fw and 40PH20 Rv (**Supplementary Table 1**, Annex) generated E4.40SAPH20 transgene with the same upstream homology arm except for the splicing acceptor 40SA in place of IIIa. In both transgenes upstream and downstream homology arms were homologous to sequences flanking *rpsL-neo* in the pAdZ-ICOVIR15K-E4.RpsLNeo. After homologous recombineering (detailed in 6.4) pAdZ-ICOVIR15K-E4.IIIaPH20 and pAdZ-ICOVIR15K-E4.40SAPH20 were generated.

9.1.1.3. pAdZ-ICOVIR15K-E1aP2APH20

In this case the *rpsL-neo* cassette was introduced in pAdZ-ICOVIR15K generating pAdZ-ICOVIR15K-E1aRpsLneo. A PCR with the template pJet-RpsLneo and E1A-RpsL Fw and E1A-RpsL Rv primers (**Supplementary Table 1**, Annex) followed by homologous recombination with the resulting PCR fragment (see 6.4) were performed to obtain the pAdZ-ICOVIR15K-E1aRpsLneo.

Then, the transgene containing hPH20 and a P2A [256] sequence at N-terminal of hPH20 was generated by PCRs. First, an overlapping PCR with oligos E1PH20 F1 and E1PH20 F2 was done and the product was purified and used as a forward primer together with E1PH20 Rv for the second PCR (**Supplementary Table 1**, Annex). Finally, the product of the last PCR which contained two arms homologous to the sequences flanking the *rpsL-neo* cassette in the pAdZ-ICOVIR15K-E1aRpsLneo was used to recombine (explained in 6.4) to generate pAdZ-ICOVIR15K-E1aP2APH20.

9.1.2. Construction of *Apis mellifera* hyaluronidase-expressing oncolytic adenoviruses

An *Apis mellifera* hyaluronidase (BHyal) was used as a transgene. It was generated by PCR using the IIIaBHyalwt af Fw and BHyalwt af Rv primers in **Supplementary Table 1** (Annex) and a template containing BHyal kindly provided by Estela Nuñez (Cristina Fillat's Lab). Once the PCR was performed it was recombined into pAdZ-ICOVIR15K-RpsLneo to generate pAdZ-ICO15K-IIIaBHyal.

The same template was used to generate the E4-IIIaBHyalwt fragment with the E4-IIIaBHyal wt Fwd and E4-BHyalwt Rv primers (**Supplementary Table 1**, Annex). The resulting transgene was recombined into pAdZ-ICOVIR15K-E4.RpsLNeo, generating the pAdZ-ICOVIR15K-E4.IIIaBHyal.

9.1.3. Construction of tumour neoepitopes-expressing oncolytic adenoviruses

9.1.3.1. pAdZ-ICOVIR15-Δ6.7/19K-CMV.B16TMG, pAdZ-ICOVIR15-Δ6.7/19K-CMV.B16TMG2 and pAdZ-ICOVIR15-Δ6.7/19K-CMV.B16TMG2.L

pAdZ-ICO15-Δ6.7/19K-5/35-CMV-RpsLneo was generated by homologous recombineering with a PCR product generated with the primers pCMVRpsL Fwd and AfterFiRpsL Rv (**Supplementary Table 1**, Annex) and pJet-RpsLneo as a template. Then, B16FTMG transgene was generated by PCR with CMVTMG Fwd and CMVTMG Rv primers (**Supplementary Table 1**, Annex) using pSpB16TMG template. The transgene was inserted by homologous recombineering generating pAdZ-ICO15-Δ6.7/19K-5/35-CMV.B16TMG. It was modified to change the fiber introducing the *rpsLneo* cassette generated by PCR with primers FiRpsLneo Fwd and FiRpsLneo Rv (**Supplementary Table 1**, Annex) generating by homologous recombineering the ICO15-Δ6.7/19K-RpsLNeo-CMV.B16TMG next the RGD fiber generated by PCR with FiRGD Fwd and FiRGD Rv primers (**Supplementary Table 1**, Annex) was used to replace the RpsLNeo cassette obtaining pAdZ-ICOVIR15-Δ6.7/19K-CMV.B16TMG by homologous recombineering.

At this point, the *rpsLneo* cassette generated with primers CMVRpsL2 Fwd and CMVRpsLNeo2 Rv (**Supplementary Table 1**, Annex) was incorporated again after CMV promoter but this time in pAdZ-ICOVIR15-Δ6.7/19K-CMV.B16TMG generating by homologous recombineering pAdZ-ICOVIR15-Δ6.7/19K-CMV.RpsLneo. B16TMG2 and B16TMG2.L were synthesised by BaseClear Synth® with two homologous arms flanked by SmaI restriction sites. After fragments' digestion they were inserted by homologous recombineering generating pAdZ-ICOVIR15-Δ6.7/19K-CMV.B16TMG2 and pAdZ-ICOVIR15-Δ6.7/19K-CMV.B16TMG2.L.

9.1.3.2. pAdZ-ICOVIR15-Δ6.7/19K-CMV.CMT64.6TMG

The CMT64.6TMG transgene was synthesised by BaseClear Synth® with two homologous arms flanked by SmaI restriction sites. After fragment digestion, it was

inserted by homologous recombineering in pAdZ-ICOVIR15-d6.7/19K-CMV.RpsLneo generating pAdZ-ICOVIR15-Δ6.7/19K-CMV.CMT64.6TMG.

9.2. ADENOVIRUS GENERATION BY CALCIUM PHOSPHATE TRANSFECTION

Once the desired modifications have been incorporated into the viral genome, this recombinant viral DNA was introduced HEK-293 by calcium phosphate-based transfection (explained in 8.4) with the plasmid containing the viral. For the transfection with pAdZ plasmids, previous linearization of the viral genome is not required since these plasmids incorporate a self-excising system. Once the plasmid enters the cell, the endonuclease I-SceI is expressed and releases the viral genome. This system increases the efficiency of the transfection, as circular DNA is transfected more efficiently than linear DNA. After the transfection, the viral cycle begins, and after several rounds of replication (about 7 days post-transfection), foci of cytopathic effect are clearly seen. Then, cells were collected together with the supernatant (cell extract, CE) and underwent 3 rounds of freeze/thaw cycles to completely release the viral particles from the cells. This cell extract (CE) was used for further amplification steps.

9.3. CLONE ISOLATION BY PLAQUE PURIDICATION ASSAY

Serial dilutions from the transfection CE, ranging from 10^{-1} to 10^{-7}, were prepared in DMEM 5% FBS. 100µL of each dilution was used to infect one 6-well of 80% confluent A549 cells for 4 hours at 37ºC. After removing the media and washing of the cells with PBS, 3mL of a 1:1 solution of DMEM 5% FBS and 1% agarose pre-warmed was added to the cells. Once solidified, 2mL of fresh medium were added over the agarose matrix. The plates were incubated at 37ºC until the appearance of plaques was evident (5-8 days post infection). To select clones, the medium was removed, and the plaques were picked through the agarose matrix. The aspirated agarose/medium was resuspended in 500 µL of DMEM 5% FBS and used for further amplifications steps.

9.4. AMPLIFICATION AND PURIFICATION OF ADENOVIRUSES

Amplification and purification allowed us to obtain enough amounts of adenovirus and in the appropriated formulation to be used for *in vitro* and *in vivo* assays.

9.4.1. Amplification of oncolytic adenoviruses

After clone selection (explained in 9.3), 250µL from the clone suspension were used to infect a 6-well of confluent A549 cells. When cytopathic effect (CPE) was observed cells were harvested and subjected to 3× freeze/thaw cycles. From this point on, viruses were sequentially amplified by scaling up. In general, 1:20 dilutions of the viral suspension from each step were used as inoculum for the next expansion step, while the rest was stored at -80ºC as backup stocks. Infections were performed in DMEM 5% FBS and dishes were incubated until cells showed evident signs of CPE. For harvesting, infected cells were collected by pipetting and subjected to 3x freeze/thaw cycles. In the final harvesting step, cell pelleted by centrifugation and cells were resuspended in a maximum volume of 10 mL before performing freeze/thaw cycles for purification. 50mL of supernatants were also collected for the first round of ultracentrifugation.

9.4.2. Purification of oncolytic adenoviruses

Oncolytic adenoviruses were purified by cesium chloride (CsCl) density gradient centrifugation. Prior to the preparation of the CsCl gradients, cell pellets were subjected to three freeze/thaw cycles to release the viruses from the cells. Debris was cleared by centrifugation at 1000*g* for 10 minutes, and the supernatant was collected. Cell pellets were resuspended in 10mL of the supernatant stored in the last step of the amplification process, and tubes were centrifuged again to wash the pellet. This process was repeated until a final volume of 42mL of virus supernatant was reached. Discontinuous CsCl gradients were prepared in ultracentrifugation tubes (Beckman Coulter). For the first layer of the gradient, 2.5mL of a solution with a concentration of 1.35g/mL were added to the bottom of the tubes. The second layer consisted of 2.5mL of a CsCl solution at 1.25g/mL, and it was carefully added on top of the first layer. Gradients were completed by carefully adding 7.5mL of the virus on top of the second

layer of the gradient. Tubes were ultracentrifuged for 2 hours at 150000*g* (35000rpm, SW40 Ti rotor, Beckman) and 10ºC. With these conditions, viral particles are separated from cell debris according to size and appear as 2 bands at the interface between 1.25 and 1.35g/mL layers. The upper band corresponds to empty viral capsids and was removed by suction. The lower band of interest was collected and placed on ice for further purification and concentration. A second centrifugation step using a continuous CsCl gradient was performed. The solution containing the virus was brought up to 24mL with the CsCl solution at 1.35g/mL and distributed into 2 ultracentrifuge tubes. The second centrifugation was carried out overnight at the same conditions of the first one. After this, the upper band was discarded by suction and the band corresponding to the full viral particles was collected in a maximum volume of 2mL. Buffer exchange was performed by three consecutive dialysis of two hours each one with desired buffer Tris-NaCl, supplemented with glycerol to a final concentration of 5% (v/v). Then 20µL to 500µL aliquots were stored at -80ºC for long term storage. All purified viruses in this thesis are detailed in **Supplementary Table 2** (Annex)

9.5. TITRATION OF ADENOVIRUSES

9.5.1. Determination of physical viral particles by spectrophotometry

This method is used to quantify the viral particles (vp) from a purified adenovirus stock without discrimination between infective or defective particles. It is based on the determination of the absorbance of viral DNA at a wavelength of 260 nm.

Three different dilutions (1:5, 1:10, and 1:20) of the purified viral stock were prepared in lysis buffer (Tris 10 mM, EDTA 1 mM, 0.1% SDS, pH 8.0) and incubated for 10 minutes at 56ºC. Then, the OD_{260} and OD_{280} was measured using a quartz cuvette and spectrophotometer. The final concentration of the virus was calculated with the following formula, considering that the extinction coefficient of adenoviruses is 1.1 x 10^{12} per OD unit:

$$Titer\ (vp/mL) = OD_{260\,nm} \times sample\ dilution \times 1.1 \times 10^{12}$$

The ratio between the absorbance at 260 nm and 280 nm gives an idea of the integrity of the purified sample. It should be around 1.3.

9.5.2. Determination of functional viral particles by anti-hexon staining

This method is based on the detection of positive cells for the immunostaining of the viral protein hexon in monolayers of A549 cells infected with serial dilutions of the virus. This technique allows the determination of functional infective viral particles (Transducing Units, TU) in purified stocks and cell extract samples.

Serial 1:10 dilutions of the viral stock were prepared in DMEM 5% FBS in triplicates in a final volume of 100µL in 96-well plates. A549 cells (1×10^5 cells) were added to the wells in a volume of 50µL and plates were incubated for 36 hours at 37ºC. Medium was aspirated and the cells were dried for 5 minutes at RT. To fix and permeabilize the cells, 100µL/well of cold methanol were added and incubated 10 minutes at -20ºC. Methanol was removed, and wells were washed twice with PBS^{2+} containing 1% BSA. Cells were incubated for 1-2 hour at 37ºC with 1:5 diluted anti-hexon antibody obtained from the hybridoma 2Hx-2 (ATCC, Manasas, VA, USA). Cells were then washed thrice and incubated with an anti-mouse secondary antibody conjugated with the fluorochrome Alexa-488 (Thermo Fisher Scientific) diluted 1:500 for 1-2 hour. Finally, cells were washed three times and the viral titer was determined by counting stained cells using an inverted fluorescence microscope. To calculate the concentration of transducing units (TU) in the stock, the following formula was used:

$$Functional\ titer\ (TU/mL) = \frac{Mean\ of\ positive\ cells}{100\ \mu L} \times Dilution\ factor \times 1000\ \mu L$$

9.6. CHARACTERIZATION OF ONCOLYTIC ADENOVIRUSES

9.6.1. Isolation of viral DNA from infected cells (Hirt's)

This method has been used for the analysis and validation of the clones obtained in the plaque formation assay.

For this, A549 cells seeded in a 100 mm plate were infected with the corresponding adenovirus until complete CPE was observed. Cells were harvested and centrifuged 5

minutes at 1000 *g*. Supernatant was discarded and the cell pellet was resuspended in 1 mL of PBS. Cell suspension was pelleted again by centrifugation and resuspended in 350µL of ddH_20. 350 µL of Hirt's solution 2X (10 mM Tris pH 8.0, 20 mM EDTA, 1.2% SDS, and 200µg/mL of proteinase K) were added to the cell suspension and the sample was mixed and incubated for 1 hour at 56ºC. 200µL of NaCl 5 M were added dropwise while vortexing, and the mixture was incubated at 4ºC for 8-16 hours until a white precipitate (corresponding to the cellular DNA) appeared. In order to eliminate this cellular DNA, the suspension was centrifuged for 30 minutes at 15000 *g* and 4ºC and the upper clear phase containing the viral DNA was collected. Incubation with RNAse at a final concentration of 100 µg/µL was carried out for 1 hour at 37ºC. Samples were mixed with one volume phenol-chloroform and centrifuged for 5 minutes at 13000 *g*. The upper phase containing the DNA was collected, mixed with two volumes of ethanol supplemented with 2% sodium oxaloacetate and incubated for 1 hour at -20ºC. Samples were centrifuged for 20 minutes at 13000 *g*, the supernatant was discarded and pellets were washed once with 70% ethanol. Finally, the supernatant was discarded and air-dried DNA pellets were resuspended in 25µL TE pH 8.0.

9.6.2. Isolation of viral DNA from purified viral particles

This method has been used to verify the identity of each generated virus purified stock. 50 µL-aliquot of purified virus were used. Usually, an input of 2 x 10^{10} vp results in yields of 1 µg of viral DNA.

To this aliquot, we added: 16µL EDTA pH 8.0 (0.5 M), 20µL SDS (10%), 8µL Proteinase K (10 mg/mL) and up to 400µL of TE pH 8.0. Then, samples were incubated for 2 hours at 56ºC in order to dissociate viral particles. DNA was isolated by phenol-chloroform extraction and ethanol precipitation as described above. DNA pellets were resuspended in 25µL TE pH 8.0.

9.6.3. Characterization of viral genomes by restriction enzymes

Genomes of recombinant adenoviruses were characterized by restriction analysis to confirm genome stability during amplification. For this, 500 ng of adenovirus DNA was

digested with the corresponding restriction enzyme according to the manufacturer's instructions. DNA from the parental adenovirus (*i.e.* ICO15K) was included as a control for comparison. Digestion patterns were evaluated by gel electrophoresis on 1% agarose gels.

9.6.4. Characterization of viral DNA by sequencing

Adenovirus genomes were sequenced to discard potential recombinations with the wild-type *E1a* present in HEK-293 cells during the transfection–mediated adenovirus rescue, and to discard mutations in the transgenes after the amplification process in A549 cells. The primers for the sequencing of the different regions of the adenovirus genomes are described in next table.

Table 8. Primers used for adenovirus and transgenes sequencing.

Span	Primer	Sequence (5'→ 3')	To sequence
Fiber	Fiber up	CAAACGCTGTTGGATTTATG	Transgenes inserted after fiber
	Fiber down2	GGCTATACTACTGAATGAA	
E4	Ad35566F	CACCACTCGACACGGCACCA	Transgenes inserted after E4
	Ad35825R	GGGCGGAGTAACTTGTATG	
E1a	Oligo7	GGAACACATGTAAGCGACGGATGTGG	Modified *E1a* promoter
	Ad670F	ATCTTCCACCTCCTAGCCAT	Δ24 mutation

Sequencing was performed with the BigDye™ Terminator v3.1 Cycle Sequencing Kit (Applied Biosystems, Thermo Fisher Scientific). For the sequencing setup, 15µL-reaction mixes were prepared containing 100-200 ng DNA, 3.2 pmol of the primer, 3µL 5X Sequencing Buffer, 2µL Reaction Mix and ddH2O to complete the final volume. The PCR conditions are the same listed in Table 6. Reactions were sequenced by the core facility

from the translational research laboratory at the Catalan Institute of Oncology or by Stabvida (Portugal).

10. *IN VITRO* ASSAYS

10.1. RECOMBINANT ADEONVIRUS-BASED *IN VITRO* ASSAYS

10.1.1. Adenovirus-mediated cytotoxicity assay

Different human or mouse cell lines (between 1.5 x 10^4 to 3 × 10^4 depending on the cell type) were seeded in 96-well plates in DMEM supplemented with 5% FBS. Cells were infected with serial dilutions of the parental virus (i.e. ICO15K) or the modified viruses starting from 200-1000 TU/cell. At day 4-6 post-infection plates were washed with PBS and stained for total protein content with the bicinchoninic acid (BCA) kit (Pierce Biotechnology). Absorbance was determined and the percentage of cell survival was calculated by normalization to the absorbance values of uninfected wells. The inhibitory concentration 50 (IC_{50}) was calculated with GraphPad Prism v6.02 (GraphPad Software Inc.) by using a dose-response non-linear regression with variable slope.

Table 9. Detail of number of cells and initial multiplicity of infection (MOI) for cytotoxic *in vitro* assays.

Cell line	Cells per well	Initial MOI (serial dilution)
A549	30000	200 (1/5)
Sk-mel-28	20000	200 (1/5)
MIA PaCa-2	30000	200 (1/3)
FaDU	20000	600 (1/3)
HT-1080	20000	600 (1/3)
MDA-MB-231	15000	400 (1/3)
Panc-1	30000	200 (1/3)
B16-F10	15000	1000 (1/2)
CMT64.6	15000	1000 (1/2)

10.1.2. Adenovirus production assay

A549 (10^5) or CMT64.6 ($3{\cdot}10^5$) were seeded in 24-wells plates and incubated overnight. Cells were infected with parental virus and tested viruses at MOI of 20 or 400 respectively in a final volume of 500 µL for 72 hours. After incubation, the cells were collected together with the supernatant and cell extracts were prepared by 3x freeze/thaw cycles. The functional titer was determined with the anti-hexon staining method (see section 9.5.2). Results are expressed as the number of TU produced by a single cell, considering the functional titer and the number of cells at the day of the infection.

10.1.3. Production of supernatants

A549 cells ($1x10^7$) were seeded in 100 mm culture plates. When plates had 90% of confluence, medium was removed and cells were infected at MOI of 20 with ICO15K, or ICO15K-modified viruses in a final volume of 10 mL of DMEM supplemented with 5% FBS. 72h post-infection, supernatants were collected and centrifuged 5 min at 500 *g* to eliminate detached cells. Supernatants from uninfected cells were used as a mock control. For turbidimetric assays, supernatants were concentrated (approximately 20x) with Amicon Ultra-15 filter units with a molecular weight cutoff of 30 kDa (Merck Millipore) according to manufacturer's instructions. Aliquots of the supernatant were stored at -20ºC for future analysis.

10.2. PROTEIN DETECTION

10.2.1. FLOW CYTOMETRY

Flow cytometry analysis was performed with a Gallios cytometer (Beckman Coulter). The antibodies used in this thesis are listed and described in **Table 10**. Cells were washed twice with PBS and stained for viability with LIVE/DEAD fixable stain (dilution 1:1000, Thermo Fisher Scientific) for 30 min at room temperature in dark. Then, after 3 washes with PBS 5% FBS and 0,01% NaN_3, direct surface staining with corresponding antibodies were performed for 30 min on ice. All flow cytometry data were analyzed with the FlowJo software v7.6.5 and v10 (Tree Star).

Table 10. List of antibodies used for flow cytometry. Conc: Concentration

Antibody	Specie	Clone	Company	Conc.	Application
Anti-H2-Kb-FITC	Mouse	28-8-6; monoclonal	Biolegend	1:50	Murine cells characterization
Anti-H2-Db-PE	Mouse	KH95; monoclonal	Biolegend	1:40	Murine cells characterization
Anti-H2Kb-OVA257-PE	Mouse	25-D1.16; monoclonal	Biolegend	1:500	Presentation of OVA257 in H2-Kb
Anti-human CD8-APC	Mouse	SK1; monoclonal	Biolegend	1:500	Luc-expressing T cells characterization
Anti-human CD4-PerCP/Cy5.5	Mouse	OKT-4; monoclonal	Biolegend	1:500	Luc-expressing T cells characterization

10.2.2. ELISA

Non-inactivated serum samples from patients of the clinical trial NCT02045602 were analyzed for L-kyneurine and L-tryptophan ratio, as a surrogate marker of IDO activity, was measured by ELISA kit (Ref.ISE-2227, Immunosol) according to manufacturer's protocol. Serum samples were prepared by acylation reaction for kyneurine assay and precipitated and derivatized for tryptohan assay.

ELISAs for IL-6, IL-10 were performed by Silvia Torres and Rafael Moreno from Virotherapy and Immunotherapy Group (Labortori Recerca Translacional 1, LRT-1) and the results were provided by Carmen Blasco from VCN Biosciences S.L. ELISA for PAF was performed by Sara Morgado from VCN Biosciences S.L.

10.2.3. LUMINEX MULTIPLEX IMMUNOASSAY

Non-inactivated serum samples from patients treated of the clinical trial NCT02045602 were analyzed for 34 (Lm1, Ref.PPX-34-MXPRJ93) or 18 (Lm2, Ref.PPX-15-MXNKTAN) different immune soluble markers by a ProcartaPlex Multiplex Immunoassay (ThermoFisher) according to manufacturer's protocol. Briefly, the antigens standards were prepared, then magnetic capture beads were vortex for 30 seconds and 50µL were added to each well. The liquid was removed maintaining the beads bound to the

plate using a magnetic support. After that, 25µL of Universal assay plus 25µL of standards, controls, or samples were added to each well and incubated with shaking at room temperature for 120min (in Lm1) or overnight at 4ºC (in Lm2). The beads were washed twice and 25µL of detection antibody mix were added. After 30min incubation at room temperature and two washes, 50µL of Streptavidin-PE were used to mark the bound detection antibody. The samples were incubated 30min at RT and then washed twice. Finally, the beads were resuspended adding 120µL of reading buffer. Plates were stored 48h (in Lm1) or 36h (in Lm2) at 4ºC, then they were shaken at RT during 5min and the data was acquired by Magpix (Luminex xMAP Technology, Thermofisher).

10.2.4. WESTERN BLOT

Supernatants from infected or transfected cells were resolved by electrophoresis on an 8% acrylamide gel and transferred to a nitrocellulose membrane by standard methods. Then, membranes were immunoblotted with the desired primary antibody listed in the next table. Membranes were incubated overnight at 4ºC and secondary labeled with correspondent anti-mouse (DAKO, ref. P0447) and anti-rabbit (DAKO, ref. P-0448) according to the manufacturer's protocol. Bands intensity was quantified by Image Lab v6.0.1 (Bio-Rad Laboratories, Inc).

Table 11. Primary antibodies used in this thesis for Western Blot.

Antibody	Specie	Clone	Company	Concentration
Anti-HisTag	mouse	13/45/31-2; monoclonal	Dianova (DIA:900-200)	2 ug/mL
Anti-hPH20	rabbit	Polyclonal	Novusbio(ref. NBP1-81637)	0.4 ug/mL
Anti-Ad5 fiber	mouse	4D2; monoclonal	Fitzgerald (ref. 10R-A116B)	1:4000

10.2.5. TURBIDIMETRIC ASSAY OF HYALURONIDASE ACTIVITY

Supernatants of infected or transfected cells were harvested and concentrated 20-fold with Amicon Ultra-15 filter units with a molecular weight cutoff of 30 kDa (Merck Millipore) or not. Then, supernatants were mixed with hyaluronic acid (HA, Sigma) at 0,03% w/v solution in phosphate buffer (pH=5,35) and incubated overnight (12-18h) at 37ºC. Then the reaction wass stopped adding 5 volumes of acid albumin solution (24mM sodium acetate, 79mM acetic acid, and 0.1% of bovine albumin (pH=3.75)), and

the absorbance at 600nm was measured. Low absorbances indicate high hyaluronidase activity. A blank control containing fresh medium and HA solution and positive control with recombinant PH20 (Acro Biosystems, PH0-H5225) was included.

11. *IN VIVO* ASSAYS

11.1. MOUSE MODELS AND PROCEDURES

All the animal studies were performed at the IDIBELL facility (AAALAC unit 1155) and approved by the Ethics Committee for Animal Experimentation from Biomedical Research Institute of Bellvitge (IDIBELL). In all the experiments tumors were measured weekly with a digital caliper and tumor volume was determined with the equation V (mm^3) = $\pi/6 \times W^2 \times L$, where W and L are the width and the length of the tumor, respectively.

E016/18: C57BL/6J female mice of 6 week old (from Charles River) were implanted subcutaneously with CMT64.6 tumors in both flanks and randomized into groups (n≥5 animals per group) when tumors reached an average of 80mm^3. Mice were treated intravenously with $3 \cdot 10^{10}$ vp in 200µL or intratumorally (in only one tumor) with $3 \cdot 10^{10}$ vp in 30µL. Tumor volume was monitored for 25 days and then animals were sacrificed, the splenocytes were harvested (see 11.2.) and assessed by ELISPOTs.

E078/19: Nude athymic female mice (4 week-old at arrival, ENVIGO) were implanted subcutaneously with Sk-mel-28 tumors in each flank (2 tumors per animal) and when reached an average of 150mm^3 were intratumorally treated with $1 \cdot 10^9$ TU in 30µL (n=5 tumors per group). The tumors were monitored during 40 days, when they were sacrificed and tumors were collected for immunohistochemistry (IHC).

NSG2: For this study female 6-8 week-old NOD/*scid*/*IL2rg*$^{-/-}$ (NSG) mice (bred in house) with a body weight between 15 and 30ng were used. Sk-mel-28 tumors were implanted subcutaneously in mice flanks (2 tumor per animal), then animals were randomized into treatment groups (n≥7 tumors per group) when tumors reached a mean of 180mm^3. Mice were treated with an intravenous injection of $2 \cdot 10^{10}$vp /animal in 200µL,

and tumor volume was monitored twice or thrice a week for 81 days. At the endpoint, tumors were collected for immunohistochemistry analyses.

E002/20: 6-week old female athymic nude mice (ENVIGO) were implanted subcutaneously with A549 tumors in both flanks. When tumors reached 120mm^3 animals were allocated randomly into treatment groups (n≥9 tumors per group) and intravenously administrated with correspondent virus at $4{\cdot}10^{10}$ vp/animal in 200µL. Tumor volume was monitored for 112 days, when animals were sacrificed.

E138/18: 6 week old female C57BL/6J mice (Charles River) were implanted with CMT64.6 tumors (subcutaneous) in both flanks. Mice were randomly allocated into groups (n= 10 tumors per group) when tumor volume average reached 80 mm^3. Then every tumor was injected with correspondent treatment at $1{\cdot}10^9$ TUs in 30µL. Tumor volume was monitored for 18 days and mice were sacrificed to isolate splenocytes (see 11.2) for ELISPOTs.

NSG1: For this study female 6-8 week-old NOD/*scid*/*IL2rg*$^{-/-}$ (NSG) mice (bred in house) with a body weight between 15 and 30ng were used. A549 tumors were implanted subcutaneously in mice flanks (2 tumor per animal), then animals were randomized into treatment groups (n=10 tumors per group) when tumors reached a mean of 210mm^3. Mice were treated with an intratumoral injection of $2{\cdot}10^9$vp /tumor with 50U of rPH20 in 30µL. Three days post-treatment a second injection of 50U of rPH20 or PBS (30µL) was administrated in each tumor according to treatment. Four days later (7 days from first treatment),pre-activated GFP- and CBG-luciferase-expressing T cells (Luc T cells) were intravenously administrated ($5{\cdot}10^6$ cells/animal in 200µL). Mice were given an intraperitoneal injection of 15 mg/mL D-luciferin potassium salt solution (Byosinth AG) and imaged daily for 4 days using IVIS Lumina XRMS Imaging System (PerkinElmer). Tumor luminiscence was measured by selecting region of interest around the tumor contour and substracting the background. Tumor volume at the end of the experiment was recorded.

11.2. MICE IMMUNIZATION

C57BL/6J mice (female, 6 week-old, from Charles River) were injected with $3 \cdot 10^{10}$ vp intravenously (n≥3 animals per group) in 200µL and 7-days post-injection mice were sacrificed to isolate splenocytes for ELISPOT assays. Alternatively, animals from efficacy experiments (detailed in 11.1) were also assessed at the endpoint for ELISPOT assays.

11.3. ISOLATION OF MURINE SPLENOCYTES

Spleens from euthanized C57BL/6J mice were surgically resected under sterile conditions and placed in falcons containing RPMI 10% FBS until their processing. Cells strainers (70µm) were placed in a petri dish containing 5mL of RPMI 10% FBS and spleens were mechanically disrupted with the plunger of a syringe by pressing the spleen against the strainer. The medium in the petri dish was passed through the strainer to ensure complete disaggregation if the spleen. Medium was collected and centrifuged for 5 minutes at 750g. The supernatant was discarded, and red blood cells were lysed by resuspending and incubating the pellet with 5 mL of ACK lysis buffer for 5 minutes at RT. The lysis was stopped rising the falcon with complete medium. Then cells were washed three times with PBS with Pasteur pipette removing the remaining fat. Finally, splenocytes were resuspended in RPMI 10% FBS, a 1/100 dilution was counted (see 7.2) and cell concentration was adjusted as needed.

11.4. ENZYME-LINKED IMMUNOSPOT ASSAY (ELISPOT)

CTL specific responses were evaluated by anti-IFN-γ Enzyme-linked immunospot assay (ELISPOT). This method is based on the measurement of the frequency of cytokine-secreting cells at a single-cell level in response to the stimulation with a specific antigen by employing the sandwich enzyme-linked immunosorbent assay (ELISA) technique.

All steps until the development of the plates were performed under sterile conditions. 96-well polyvinylidene fluoride membrane ELISPOT plates (Multiscreen plates, Millipore, Billerica, MA) were treated with 30 µL of 35% ethanol per well for 1 minute. Then, 5 washes with ddH_2O were performed and plates were incubated overnight at

4°C with a murine IFN-γ-specific capture antibody (clone AN-18, BD 551309, San Jose, CA) at 4 µg/mL diluted in PBS at a final volume of 100 µL/well. The day after, the antibody was discarded and plates were washed 5 times with PBS and blocked with 200 µL/well RPMI+10%FBS medium for at least 1 hour at RT. During this incubation, the splenocytes were isolated (as explained in 11.2) and 100 µL of a $2.5x10^6$ cells/mL cell suspension were added to each well ($2.5x10^5$ cells/well). The peptides that were used for the stimulation of the splenocytes were: $E1b_{192}$ (VNIRNCCYI) or the correspondent according to the experiment. All the peptides were synthesised by SG Servicios Hospitalarios (Sevilla) or JPT Innovative Peptide solutions (Germany) at >75% purity and re-suspended following the manufacturer's instructions. Stimulation with the peptides was performed at a final concentration of 1 µM. Phorbol-myristate-acetate (PMA at 15 ng/mL) plus ionomycin (250 ng/mL) were used as positive control of stimulation and media only as negative control, at 100 µL/well. Plates were incubated with the splenocytes for at least 18 hours (using 9mer as stimuli) or 36hours (for 27mers) at 37°C and 5% CO_2. From that moment, sterility was not required. Cells and medium were removed and the plates were washed 5 times with PBS. Then, the biotinilated anti-murine IFNγ secondary antibody (clone RA-6A2, BD 55156, San Jose, CA) was added at a concentration of 1 µg/mL in PBS 0.5% FBS at a final volume of 100 µL/well and incubated for 1-2 hours at RT. Next, the antibody was removed and the plates were washed 5 times with PBS. The streptavidin-ALP (ExtrAvidin Ref E2636-2ML Sigma E2636, Sant Louis, MO) was then added diluted 1:2500 in PBS 0.5% FBS (100 µL/well) and then incubated for 1 hour at RT. Again, 5 washes with PBS were performed and finally 50 µL/well of the substrate BCIP/NBT solution (Ref B1911-100ML, Sigma, St. Louis, MO) was added. Plates were developed for 15-30 minutes until spots emerged and the plate was washed with tap water to stop the reaction. Plates were left to dry overnight and spots were counted using the Bioreader 6000-E (Biosys, Germany).

11.5. IMMUNOHISTOCHEMISTRY (IHC)

Paraffin-embedded blocks were cut into 4-µm thick sections with a microtome and deposited into poly-L-lysine treated slides. Sections were deparaffinized by subjecting

them to a battery of 3 xylols (7 minutes each), 2 absolute ethanol (2min), then the endogenous peroxidase activity was blocked by incubation for 30 minutes in 0.3% H_2O_2 dissolved in 100% methanol. Subsequently, 3 washes (2min) of 96% ethanol, 1 wash (2min) in ethanol 70%, and finally the sections were rehydrated by submerging them in PBS for 10min. For HA staining, sections selected for negative control were digested with 50µL of hyaluronidase (Bovine Testes hyaluronidase, Sigma H3631) at 20 U/mL for 1h at 37ºC in a sealed humidity chamber. Meanwhile, the rest of tissue sections were incubated with PBS. Then, wash slides thrice in PBS (5min/wash), and block all sections with 10% normal goat serum diluted in PBS for 1h at room temperature. Afterwards, the blocking serum was gently removed and the sections were incubated with B-HABP (Amsbio, AMS.HKD-BC41) at 5 µg/mL in PBS 0,1% BSA overnight at 4ºC in a humidity chamber. For adenovirus detection, the primary antibody used was an anti-Ad2/5 E1A antibody (Santa Cruz Biotechnology) diluted 1/200 in PBS.

After overnight incubation, slides were washed thrice with PBS for 5 minutes, and were covered with ABC complex (Avidin-Biotin-Peroxidase, ABCkit PK-4000, Vectastain) and incubated 1 hour at RT. Next, slides were washed 3 times more with PBS, 1 wash with TBS for 5 min, and developed by covering the sections with the chromogenic substrate DAB+ (Envision Kit, Dako Cytomation K3468) during approximately 15 seconds, until a brown precipitated appeared. The reaction was stopped by rinsing the slides with tap water for 10 minutes. Finally, the sections were counterstained with hematoxylin, rehydrated and mounted in DPX (VWR International).

11.6. DETECTION OF TRANSCRIPTS IN TUMORS BY REAL-TIME PCR

Frozen tumor samples were disrupted using 5mm metal beads (Geneye Ref. 77.GY-BM1005) and Ultimate sample homogenizer (UPHO, Geneye Ref.77.GY-U001) according to manufacturer's protocol. Briefly, metal beads were treated with Real DNA remove (Real Laboratory ref.RD055) for 5 min and washed with distilled water, then tissues were placed in a tube with 2 washed metal beads and 50µL of PBS. For tumor fragments, 2 cycles of of 2 min at 60 Hz were used in UPHO to disrupt the tissue. Then,

15-25 µL of homogenized tissue were used with the QiAmp DNA mini kit (Qiagen, ref.51304) to extract the DNA from these tissue according to manufacturer's protocol.

To quantify the viral genomes in the tumor, 100 ng of DNA in the presence of SYBR Green I Master (Roche) were used. Standard curves for viral genomes prepared by serial dilutions of known copy numbers of adenovirus plasmid. The primers used for the detection of virus are listed in **Table 12** and qPCR conditions in **Table 13**.

Table 12. Primers used in qPCR for detection of adenoviral genome.

Gene	Sequence 5'→3'
Ad18852	CTTCGATGATGCCGCAGTG
Ad19047R	ATGAACCGCAGCGTCAAACG

Table 13. qPCR conditions for adenoviral genome detection.

Stage	Description	Temperature	Time	Cycles
1	Activation	95ºC	10 minutes	1
2	Amplification cycles	95ºC	15 seconds	40
		60ºC	1 minute	
		72ºC	7 seconds	

12. STATISTICAL ANALYSIS

Statistical analyses were performed using GraphPad Prism software v6.02. All results were expressed as means ±SD or ±SEM, as indicated. P-value < 0.05 was taken as the level of significance. Firstly, data was assessed for normality with Shapiro-Wilk test, according to the result parametric or non-parametric test were performed. For mean comparisons between groups, the tests used were:

Table 14. Statitstical tests used for groups comparison.

	Parametric		Non-Parametric	
	Paired	**Unpaired**	**Paired**	**Unpaired**
2 groups	Two-tailed T-	Two-tailed T-	Wilcoxon	Mann-Whitney

	test (paired)	test	signed-rank test	test
>3 groups	Paired One-way ANOVA	One-way ANOVA	Kruskal-Wallis	Kruskal-wallis
Post Hoc	Tukey	Tukey	Dunn	Dunn

For *in vivo* studies, mixed 2-Way ANOVA of repeated measures was used to compare the means between all groups in every measure. Correlations of parametric data were assessed by Pearson correlations and non-parametric data by Spearman correlation. Eventually, the correlations were presented in a correlation map indicating the value of correlation according to a gradient of color (red:1, blue:-1) and the p-value<0.05 with asterisks in the map.

For the heatmaps, the Z-score was used. The Z-score was employed as a way of normalizing and comparing results. The Z-score for each patient in every analyte and timepoint was calculated by substracting to each value the mean of the analyte concentration from all timepoints, and dividing for the correspondent standard deviation. The Z-score informs if the value of a raw score is above or below the mean value. Scores above the mean have positive Z-scores and were colored in gradient of red, while those below the mean have negative Z-scores scores and were colored in gradient of blue. Scores near the mean were represented in white. According to this, increases or decreases in a particular timepoint compared to all timepoints can be evaluated in each analyte.

CHAPTER A

IMMUNE ANALYSIS OF VCN-01 TREATED PATIENTS

1. INTRODUCTION

1.1. SOLUBLE IMMUNE MARKERS

The immune responses are tightly controlled biological events to prevent adverse effects in the host. They are ligand-receptor mediated responses, including cytokines (interleukins, chemokines, interferons, and tumor necrosis factors), membrane molecules (ligands and receptors), and other components. One of the mechanisms that modulate the immune-signaling is the shedding of the immune-mediators (via proteolytic cleavage by ADAM metalloproteinase family, alternative splicing of mRNA, exon skipping, or microvessel shedding [257,258]). The activity of their soluble forms could be antagonistic or agonistic.

Similarly to cytokine receptors, soluble versions of adhesion molecules have been described in sepsis. During a prolonged inflammation, soluble isoforms of leukocyte recruitment molecules such as E-selectin, L-selectin, and P-selectin are shed and accumulated in the blood plasma, as potential biomarkers of systemic inflammation [259]. High levels of soluble sE-selectin have positively correlated with chronic inflammation and breast cancer stage and metastases [260].

Immune checkpoint molecules lead to T cell exhaustion or stimulation, thereby modifying the immune response. They have been related to infections, autoimmunity, and cancer. Most of them have been recognized as intact transmembrane proteins; however, soluble isoforms or shed variants have been described for the majority. The shedding mechanisms identified are alternative splicing and the extracellular proteolytic release via ADAM10/ADAM17 proteases activation upon TCR signaling [261,262].

The development of cancer immunotherapies (and other diseases) increased the relevance of the soluble versions of checkpoints. The most relevant therapies are the anti-PD-1/PD-L1, and anti-CTLA-4 antibodies, thereby the corresponding soluble forms have been the most studied.

sPD1 serum levels remain controversial at this moment. For instance, high sPD1 serum levels have been reported as a good prognosis in NSCLC (non-small cell lung cancer), but increased risk of HBV-related HCC (hepatocellular carcinoma), and no predictive value in OSCC (oral squamous cell carcinoma) [263–265]. In contrast, sPD-L1 is detected in healthy human serums, increasing with age. Despite not being directly associated with tumor PD-L1 expression, most of the reports conclude that high serum concentration of sPD-L1 correlates with a cancer diagnosis or worst prognosis, acting as a valuable biomarker [266].

Despite correlation studies between serum levels and disease prognosis, there is a need to fully understand the mode of action of soluble isoforms. Two mechanisms might be predicted, an intrinsic effect of shedding the molecule and extrinsic cytokine-like function, modulating other immune cells. However, this remains unclear for most of the soluble immune checkpoints. Altogether, soluble checkpoints might be important for immunotherapy, but further studies are required to elucidate their mechanisms and potential use as biomarkers or therapies.

1.2. SOLUBLE IMMUNE MARKERS ANALYSIS IN ADENOVIRUS CLINICAL TRIALS

Genetically modified adenoviruses have been widely used as therapeutic agents, particularly in gene therapy and vaccination fields. In the last decades, their application has been extended in cancer therapy. Their toxicity has been monitored and reported in all clinical trials, especially after the death of 18-years old patient, Jesse Gelsinger, in a gene therapy trial. He died 98h post-injection due to a cytokine release syndrome and multiple organ failure. The post-mortem examination detected viral DNA in most of the tissues and high serum levels of IL-6 and IL-10 (but normal TNFα), highlighting their relevance in toxicity. This clinical trial pointed out the variation in patients' response to systemically administrated adenoviral vector (the rest of 17 patients did not present these clinical signs) [267]. Since then, fully controlled dose-escalation clinical trials have been performed to test Ad agents in clinics.

Regarding cancer therapy, most of the oncolytic adenoviruses in clinics reported manageable toxicity and consistently confirmed the IL-6 increase after intratumoral or intravenous injection [90,99,107]. Moreover, IL-8 peak has been detected after the intratumoral injection of ONCOS-102 [107]. An IL-10 increase was reported in ICOVIR-5 patients after intravenous treatment [90]. Finally, TNFα, IFNγ, and MCP-1 peaked after multiple intravenous injections of Enadenotucirev (ColoAd1) [99].

Despite the mentioned reports, no profound analyses have been performed in serum's patients to evaluate other cytokines nor soluble immune checkpoints.

1.2.1. P-VCNA-001

In this chapter, we analyzed the immunologic response of patients treated intravenously with VCN-01, an oncolytic adenovirus that expresses soluble hyaluronidase PH20, from the pancreatic cancer trial (NCT02045602, also named P-VCNA-001). The clinical trial has been divided into three arms. Patients from the first arm (P-VCNA-001:I) were treated with a dose-escalation of the virus, ranging from 1e10 viral particles (vp) to 1e13 vp; however, in this thesis, only the two highest dose levels were analyzed: 3.3e12 or 1e13 vp. These two highest doses were selected from the first arm in the clinical trial as safe and tolerable. Accordingly, arm II and III, employed these two dose levels. In the second arm (P-VCNA-001:II), VCN-01 treatment was combined with the standard of care for pancreatic tumors, Gemcitabine (GE) and Abraxane (Abx). The VCN-01 was injected, and 4 hours later the GE/Abx regimen was administrated. Conversely, the third arm (P-VCNA-001:III) consisted of a delayed chemotherapy regime that started at day 8 post VCN-01 intravenous injection (**Figure 15**).

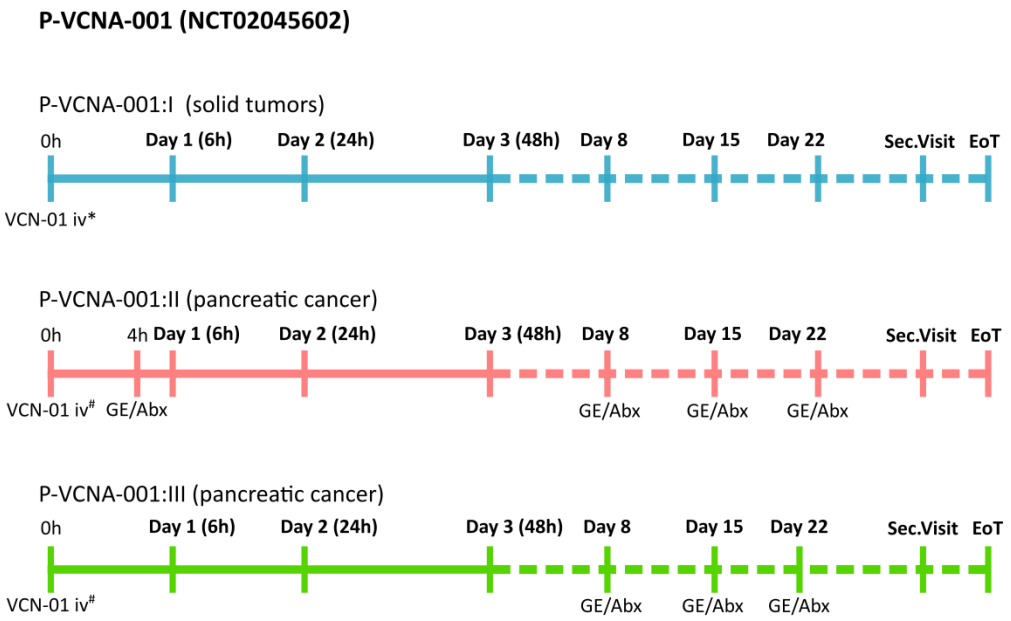

Figure 15. P-VCNA-001 clinical trial scheme with serum sample collection timepoints analyzed for immune markers. The three arms of the clinical trial are depicted. Serum samples were obtained in these depicted timepoints. In the lower part the administration timepoints of VCN-01 and chemotherapy are annotated. IV intravenous, GE: gemcitabine, Abx:abraxane.

The patient's serums were obtained during the treatment and assessed for protein levels of 34 immune markers by Multiplex Immunoassay (Luminex) with the main aim of characterizing the immune profile after VCN-01 treatments. The immune markers included cytokines (interleukins, chemokines, interferons, and tumor necrosis factors), soluble immune checkpoints, soluble adhesion molecules, and enzymes.

According to pre-clinical data in immunocompetent mice VCN-01 intravenous injection increased significantly the serum levels of IFNγ, IL-6, IP-10, and TNFα. Moreover, IL-2, IL-10, GM-CSF, and IL-1β were also evaluated [268]. Aiming to validate the data in patients, we included these markers in the multiplex panel. Moreover, depending on the set of cytokines secreted during the T $CD4^+$(Th) maturation, the phenotype and activity of Th cells vary, as depicted in **Figure 16**. Multiple cytokine combinations were assessed to profile the Th response induced by VCN-01 injection.

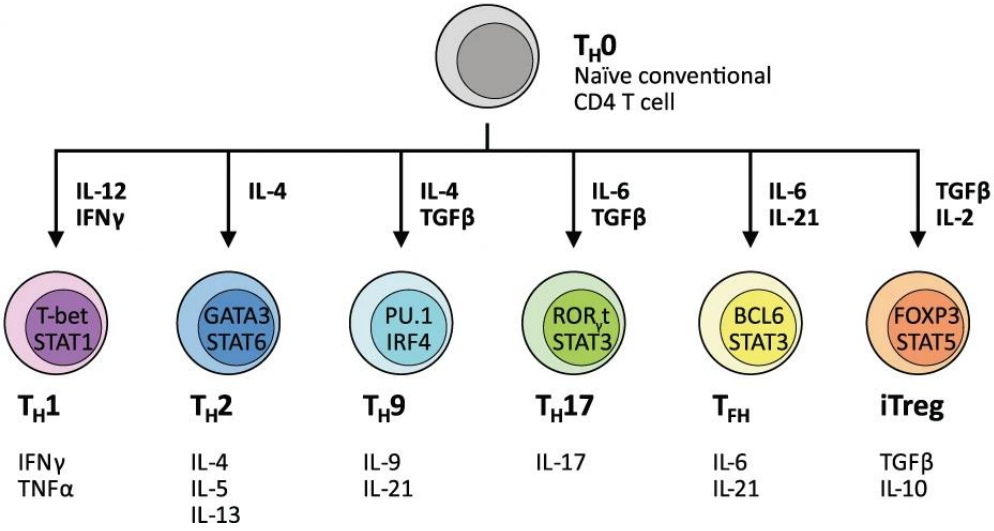

Figure 16. Diversity of CD4 subsets phenotype in immunity. Upon receiving cues from the cytokine milieu together with TCR activation, naive $CD4^+$ T cells (Th 0) upregulate expression of key transcription factors regulating subset differentiation, which in turn drives the expression of effector cytokines associated with each particular subtype. Key transcription factors and cytokines involved are indicated for individual subtypes. Th cells augment the development of the CTL response and are required for the development of $CD8^+$ T cell immunity in their role as central co-ordinators of adaptive immunity. Unlike $CD8^+$ T cells, whose primary function is to mediate cell contact-dependent cytotoxicity of infected or malignant cells, Th cell exhibit a diverse repertoire of effector functions. They exhibit considerable phenotypic plasticity and heterogeneity depending on local context and microenvironment. Th cells activated in the periphery can also differentiate into induced Tregs (iTregs), which are able to mediate immunosuppression. Image adapted from [269]

Finally, soluble adhesion molecules, immune checkpoints, and enzymes were also evaluated for the first time in patients' serums treated with an oncolytic virus. The 34 analyzed immune markers are summarized in the next table.

Table 15. The 34 immune markers analyzed in VCN-01 patient's serum.

Type	Analyte	Function
Cytokine	GM-CSF	GM-CSF is a pro-inflammatory mediator and immune regulator [270]
Cytokine	TNFα	TNFα is induced in acute responses acting as a principal mediator of inflammation [271]
Interleukin	IL-1β	IL-1β is a potent pro-inflammatory mediator that requires inflammasome processing [272]

Interleukin	IL-6	IL-6 is a pro-inflammatory regulator in infections and tissue damage [273,274]
Interleukin	IL-10	IL-10 is anti-inflammatory and promotes humoral response [275]
Interleukin	IL-12p70	IL12p70 is an immune-stimulator promoting the IFNγ production in NKs and T cells [276]
Interleukin	IFNγ	IFNγ triggers anti-pathogen activity, antigen presentation, recruitment, proliferation, and differentiation of immune cells [277,278].
Interleukin	IL-2	IL-2 promotes proliferation of effector, memory and regulatory T cells [279,280]
Interleukin	IL-9	IL-9 is pleiotropic; it has pro and anti-inflammatory roles [281].
Interleukin	IL-5	IL-5 promotes eosinophils activation and survival [282,283].
Interleukin	IL-13	IL-13 is involved in mucosal inflammation and anti-parasite responses [284]
Interleukin	IL-17A	IL-17A induces pathogen defense in mucosal and epithelial surfaces, and inflammation (related to allergies and autoimmunity)[285].
Interleukin	IL-21	IL-21 enhances the function of macrophages, NK, NKT cells, B cells. Restriction of DC maturation [286].
Interleukin	IL-22	IL-22 is involved in host defense, homeostasis, and tissue regeneration in non-hematopoietic cells [287]
Interleukin	IL-23	IL-23 stimulates memory rather naïve T cells, enhances Th17 type cell expansion, and induces the production of pro-inflammatory cytokines [288,289].
Chemokine	IL-8	IL-8 is a pro-inflammatory mediator and chemoattractant for neutrophils [290]
Chemokine	IP-10	IP-10 is a chemoattractant for macrophages, DCs, NK, B and T cells [291]
Soluble ligand	sE-selectin	sE-selectin is shed upon endothelial activation impairing T cell recruitment [260,292]
Enzyme	IDO1	IDO1 is induced by IFNγ with anti-viral and immune suppressor activities [293].
Soluble IC	sPD-1	sPD-1 competes with membrane-bound PD-1 for the same ligands, thereby avoiding the T cell inactivation through the PD-1 [266].
Soluble IC	sPD-L1	sPD-L1 binds to the PD-1 on the T cell surface inducing anergy [294,295].
Soluble IC	sPD-L2	sPD-L2 is produced by alternative splicing with a non-reported biological function [296]. Low serum levels have been related to malignancies [297,298]

Soluble IC	sCD152	sCD152 (or sCTLA-4) is produced mainly by T-regs and tumor cells (among others), impairing the co-stimulation of CD28, thereby reducing the immune response [261].
Soluble IC	sCD137	CD137 (or 4-1BB) is released (sCD137) by T cells in high activation stages to reduce the immune activity (antagonistic to CD137) [299].
Soluble IC	sTIM-3	sTIM-3 is released by protein cleavage, and it might have co-inhibitory functions [262]
Soluble IC	sLAG-3	sLAG-3 is released upon T-cell activation. It might enhance the antigen presentation[300]
Soluble IC	sGITR	sGITRL might impair NK recruitment and immune cell activation [301].
Soluble IC	sBTLA	sBTLA function has not been clearly detailed. High serum levels have been associated with sepsis severity and worse HCC prognosis [302,303].
Soluble IC	sHVEM	sHVEM might down-regulate the immune response. Marker of autoimmune disease and poor -prognosis of gastric cancer [304,305].
Soluble IC	sCD27	sCD27 is released after T cell activation involved in a positive loop for T cell stimulation. It has been used as a marker to monitor immune activation [306].
Soluble IC	sCD28	sCD28 inhibits the T cell response in vitro, and it is increased in systemic autoimmune diseases [307,308].
Soluble IC	sCD80	sCD80 is produced by alternative splicing and activates the T cell activity trough the CD28 signaling [309,310].

.

2. OBJECTIVES

The main objectives of this chapter are (1) to characterize the immunological-induced changes in VCN-01 treated patients and (2) to identify if there is any correlation between VCN-01 immunological-induced changes and toxicity or efficacy.

Hypothesis: immunological changes induced by VCN-01 in patients have an impact in either toxicity or efficacy of the treatment.

Specific objectives:

- To characterize an immune modulation at serum levels after VCN-01 intravenous injection.
- To evaluate the effect of viral dose on the serum levels of soluble immune markers induced by VCN-01.
- To evaluate the effect of chemotherapy on the serum levels of soluble immune markers induced by VCN-01.
- To identify if there is any correlation between immunological-induced changes and treatment toxicity.
- To identify if there is any correlation between immunological-induced changes and treatment efficacy.

3. RESULTS

3.1. VCN-01 TREATMENT INDUCES SIGNIFICANT CHANGES IN SOLUBLE IMMUNE MARKERS IN SERUM.

Serum samples were obtained from treated patients at different timepoints: Pre-treatment, day 1 (6h post-treatment), day 2 (24h post-treatment), day 3 (48h post-treatment), day 8, day 15, day 28, and end of treatment (EoT). They were analyzed for a panel of 34 soluble immune markers from the patients treated in P-VCNA-001:I or P-VCNA-001:II. We studied P-VCNA-001:I patients to profile serum changes exclusively induced by VCN-01 treatment as monotherapy, independently of the dose. In parallel, to identify the effect of concomitant chemotherapy in the soluble immune markers, patients from P-VCNA-001:II were analyzed (independently of the dose). Each analyte was normalized over the different time points by Z-score. The Z-score for each patient in every analyte and timepoint was calculated by substracting to each value the mean of the analyte concentration from all timepoints, and dividing for the correspondent standard deviation. The Z-score informs if the value of raw score is above or bleow the mean, and it was represented in a heatmap.

The monotherapy arm patients heatmap (P-VCNA-001:I, **Figure 17-A**) showed raised levels of several soluble immune markers at Days 1 to 3 and then other markers at Day 8 post-treatment, that can be viewed as an early and delayed immune waves. In the early wave, VCN-01 increased the levels of IL-6 immediately (6hours on Day 1). IL-6 is a pro-inflammatory mediator induced by innate immune sensing, previously detected in other Ad clinical trials. Following this inflammation signal, cytokines related to immune activity peaked at 24 hours (Day 2) such: IFNγ (marker of Th1 response) associated with anti-viral response and NK and T cell activity, and IL-2, which induces T cell proliferation. Furthermore, sLAG-3 released after T-cell activation was increased at the same timepoints (Day 2 and 3).

Other Th1 markers and IFNγ-induced proteins were detected in the serum, including IP-10, a monocyte and T cell chemoattractant, was induced 24 hours post-treatment.

Similarly, IDO1 enzyme, induced by IFNγ and related to anti-viral response, peaked on day 3 (48h) post-treatment. IL-10 and sE-selectin serum levels raised on day 2 and 3 as markers of homeostatic immune regulation secreted to counteract a strong inflammation. The changes were statistically relevant compared to the pre-treatment for IP-10, sLAG-3, and IDO1. The late immune wave induction was detected on day 8 in the rest of the analytes, with significant increases from basal levels for IL-8, IL-18, and sTIM-3. Particularly, these three markers were initially induced on day 2, and their serum concentration peaked on day 8 in a delayed or mid-late response. IL-8 is a neutrophil, basophil, and T cell chemoattractant. IL-18 augments the NK activity and IFNγ production by T cells, and sTIM-3 is also released after T cell activation.

On the other hand, the patients treated with the combination of VCN-01 and Gemcitabine/Abraxane (P-VCNA-001:II, **Figure 17-B**) presented a different response pattern compared to patients from the P-VCNA-001:I. The two induced-waves pattern seemed to be altered by GE/Abx. At early timepoints, a peak in serum concentration was detected for IL-6, IL-2, IFNγ, IP-10, sE-Selectin, IL-10, IL-8, IL-9, IL-12p70, sGITR, sLAG-3, and IDO1. A set of interleukins (IL-8, IL-12p70, IL-9) presented an earlier induction on day 2 compared to monotherapy. The late wave induced IL-18, IL-13, IL-17A, TNFα, sBTLA, sCD152, sCD28, sPD-L1, sCD27, sPD-L2 and sTIM-3. Compared to the P-VCNA-001:I patients, no increase on day 8 was observed in IL-23, IL-27, IL-21, and IL1β. It is worth to mention that IL-23 and IL-27 were detected in only one patient in P-VCNA-001:I and also in one patient in P-VCNA-001:II, indicating that VCN-01 treatment, independently of chemotherapy, hardly induced these interleukins systemically. Furthermore, IL-22 and sPD-1 serum levels decreased from the pre-treatment or early timepoints, showing opposite kinetics compared to monotherapy.

The significant increases observed in IP-10, IL-18, sLAG-3, IDO1, and sTIM-3 (but not IL-8) in VCN-01 monotherapy were also significantly increased in the patients treated with the combination of VCN-01 with Gemcitabine/Abraxane. Conversely, the detection of IFNγ, IL-17A, and sCD27 was statistically higher compared to the pre-treatment values in the patients of the second arm. IL-17A is a pro-inflammatory cytokine related to

epithelial and mucosal defense. The CD27 is shed in a soluble isoform after T cell activation in a positive stimulation loop. Finally, GM-CSF was hardly detected in both arms; only 1 patient per arm, suggesting that VCN-01 did not trigger a systemic increase of GM-CSF.

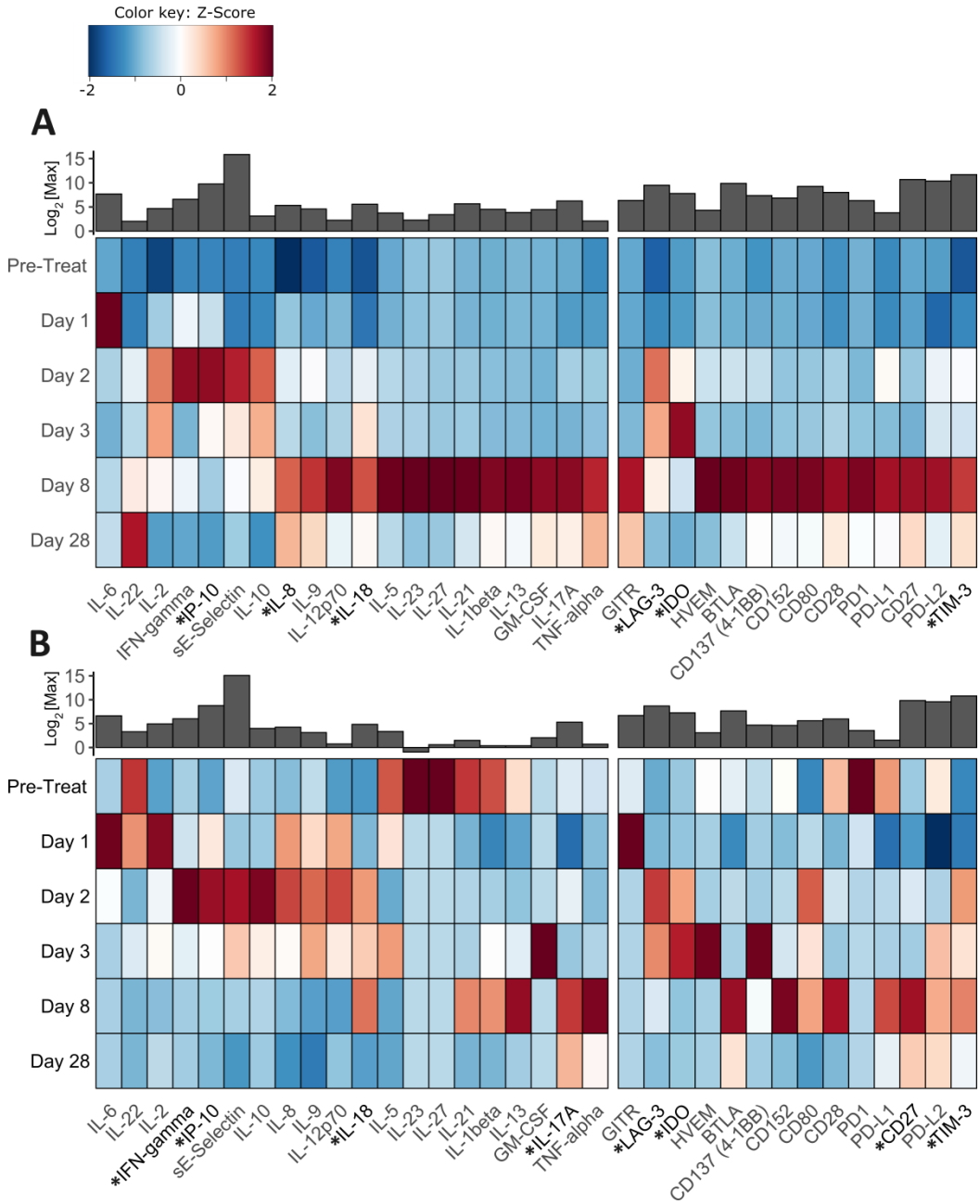

Figure 17. Soluble immune markers variation after VCN-01 treatment alone (A) P-VCNA-001:I or in combination with Gemicatabine/Abraxane (B) P-VCNA-001:II. The log2 of the maximum concentration mean detected per analyte is represented on the top of the graph by grey bars. The Z-score within each analyte is represented in the heatmap. Analytes that significantly variate compared to the pre-treatment values are highlighted with and asterisk in the column name (*p<0.05 by paired-Wilcoxon test). At the left part of heatmaps cytokines are represented and the right part the soluble immune markers or enzymes. **(A)** Serums from patients treated with VCN-01 as monotherapy (P-VCNA-001:I, n=8). **(B)** Serums from patients treated with VCN-01 combined with Gemcitabine and Abraxane (P-VCNA-001:II, n= 10).

In a second experiment, patients from P-VCNA-001:III, that were treated with delayed chemotherapy regime, were analyzed together with P-VCNA-001:II patients (already tested in the first Luminex). No direct comparison between data from different Luminex assays has been performed to avoid interference from interassay variations. The heatmap of P-VCNA-001:III treatment (**Figure 18**) presented the same two wave-pattern of P-VCNA-001:I as until day 8 both sets of patients were treated identically (non-chemotherapy regime, **Figure 15**). As previously described, early induction of IL-6, IFNγ, IP-10, IL-10, sLAG-3, and IDO1 was observed. The IP-10, IL-18, sLAG-3, and IDO1 levels were significantly higher compared to pre-treatment. Although shared tendencies, significant changes in IL-10 and IL-17A were detected only in P-VCNA-001:III patients but not in monotherapy treated patients. We did not detect relevant levels of CD152, CD28, and PD-L1 in this experiment, contrary to previous Luminex. In parallel, reanalyzed samples of P-VCNA-001:II matched with the results described in the first Luminex experiment (**Supplementary Figure 1 and 2**, Annex**-**).

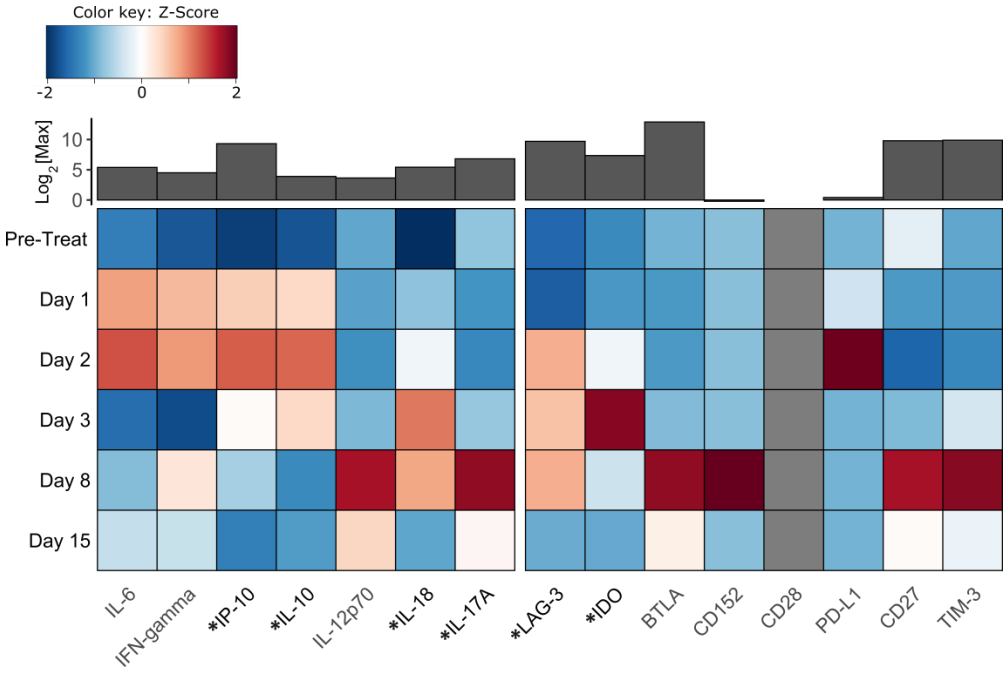

Figure 18 Soluble immune markers variation after treatment with VCN-01 and delayed Gemictabine/Abraxane (P-VCNA-001:III). Serums from patients treated with VCN-01 and at Day 8 with the first cycle of chemotherapeutic regime (P-VCNA-001:III, n=12) were analyzed. The log2 of the maximum concentration mean per analyte is represented on the top of the graph by grey bars. The Z-score within each analyte is represented in the heatmap. Analytes that significantly variate compared to the pre-treatment values are highlighted with and asterisk in the column name.*p<0.05 by paired-Wilcoxon test vs pre-Treatment.

To further profile the changes prompted by VCN-01, we analyzed the detailed kinetics of the significant analytes for each patient. In the early immune response, the IFNγ was markedly increased immediately after treatment. The highest levels were reached at 24-48 hours post-injection (Day 2-3) in both arms. However, it was statistically significant on day 3 (48h) only in the patients treated with the combination of VCN-01 and chemotherapy (**Figure 19-A**). Nonetheless, the monotherapy arm also presented a strong IFNγ induction with an almost significant p-value of 0.07, probably due to the lower number of patients (n=8). Then, we observed a subsequent and strong induction of the chemoattractant IP-10 after treatment in both clinical trial arms (**Figure 19-B**). Despite these shared kinetics, the patients treated with chemotherapy combination showed lower levels of IP-10. IDO1 enzyme was increased in the patient's serum from the beginning of the treatments and peaking at 48 hours (Day 3) in both arms (**Figure 19-C**). Both IP-10 and IDO1 are inducible by IFNγ, which is a marker of immune cell activation. sLAG-3 is also a surrogate marker of TCR triggering, and it was detected in this early immune wave significantly peaking at 24-48 hours post-treatment in patients from arms I and II (**Figure 19-D**).

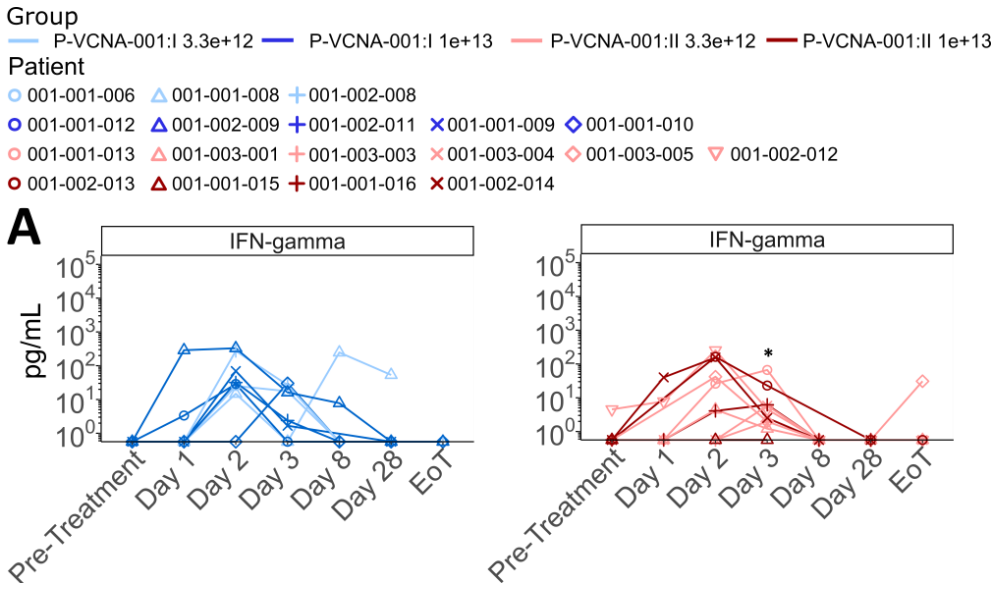

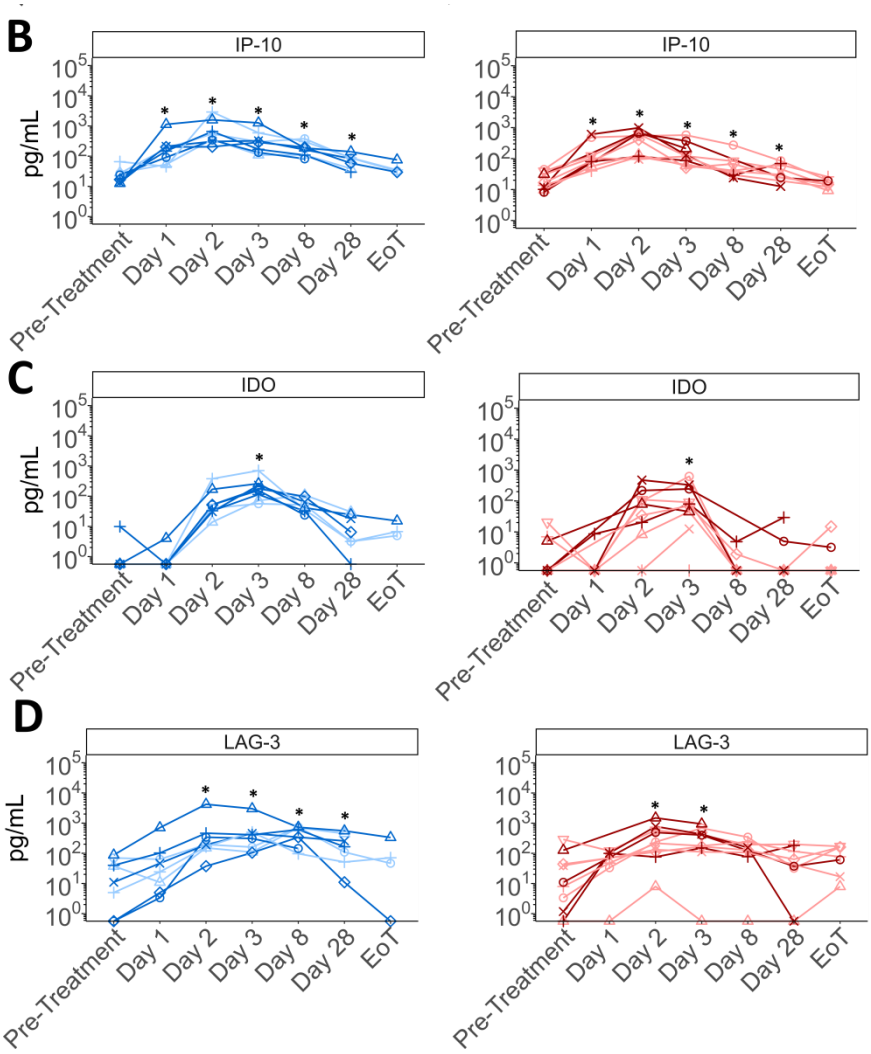

Figure 19. Early immune wave kinetics: IFNγ, IP-10, IDO1 and sLAG-3. The serum levels of **(A)** IFNγ, **(B)** IP-10, **(C)** IDO1 and **(D)** sLAG-3 over the time were analyzed in patients treated with VCN-01 as monotherapy (left, n=8), with two different doses 3.3e12 viral particles (vps, light blue) or 1e13vps (dark blue). And also in patients treated with VCN-01 in concomitant combination with chemotherapy (right, n=10) at 3.3e12vps (pink) or 1e13vps (dark red) were analyzed. *p<0.05 by paired-Wilcoxon test vs Pre-Treatment.

After the early immune wave, a rise in serum levels of IL-8, IL-18, and sTIM-3 was detected from early timepoints until day 8 or 28, in a considered mid-late or delayed immune wave. The chemokine IL-8 presented slight increases in both arms but was statistically significant in those patients treated only with VCN-01 after 24 hours of

administration until day 8 (**Figure 20-A**). The serum levels of IL-18 increased 6 hours until day 28 post-VCN-01 injection, peaking in most cases on day 8 in the monotherapy arm (P-VCNA-001:I). A similar pattern was observed in the combination arm samples (P-VCNA-001:II), but the changes were only significant after 24 hours of treatment (Day 2, **Figure 20-B**). Similarly, the levels of sTIM-3 were higher than pre-treatment on day 3 in patients with monotherapy of VCN-01, and on day 8 in patients with combined treatment (**Figure 20-C**).

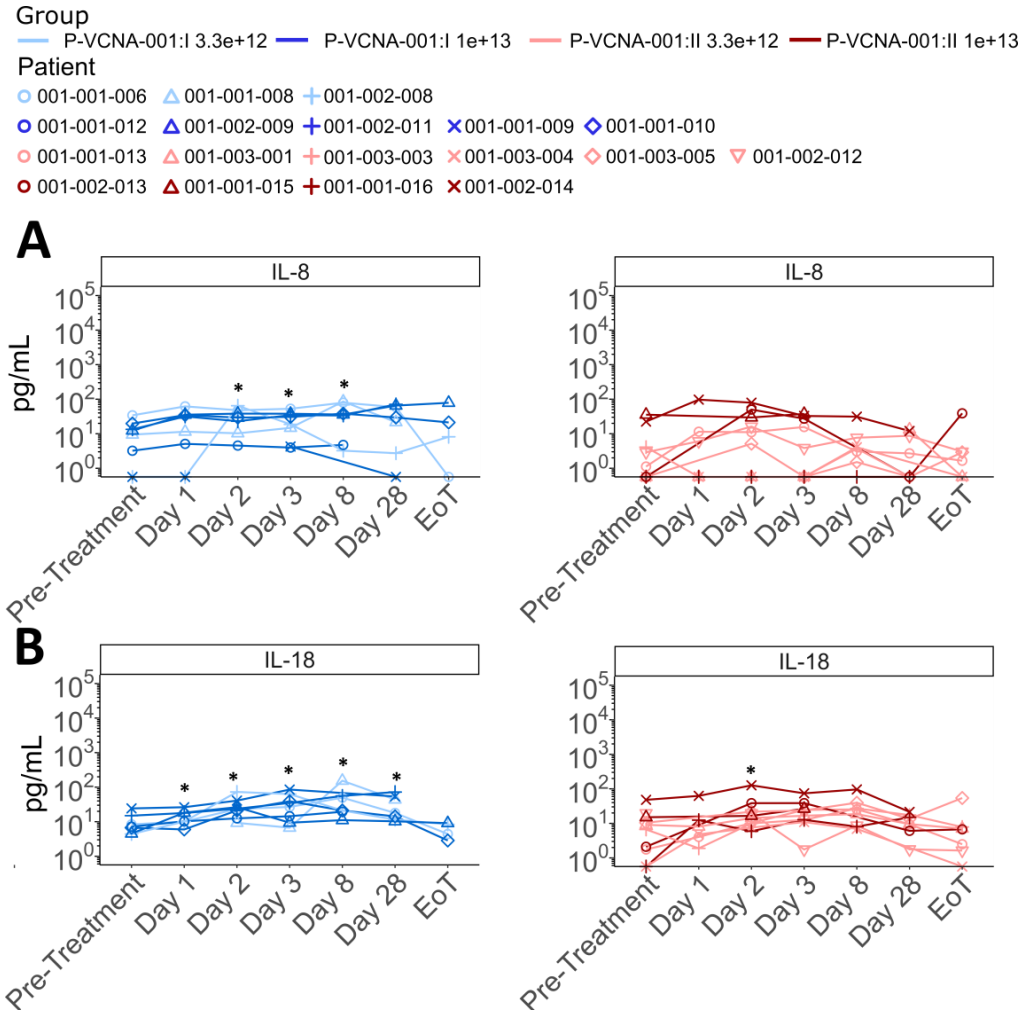

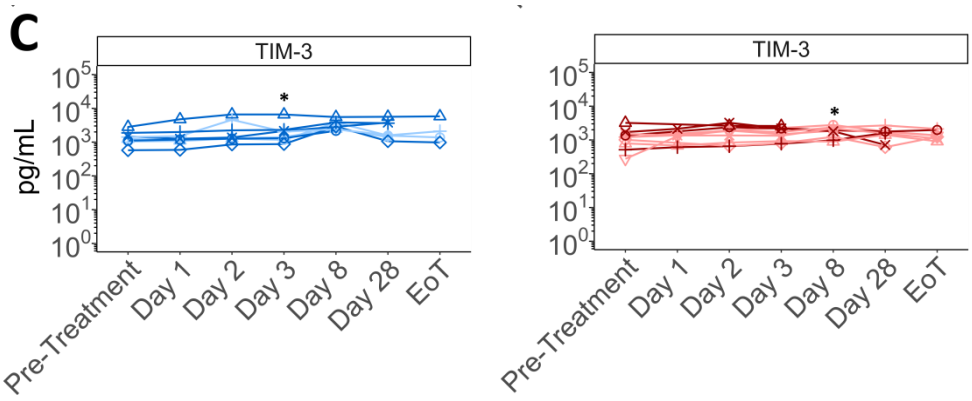

Figure 20. Delayed-immune wave kinetics: IL-8, IL-18, and sTIM-3. The serum levels of **(A)** IL-8, **(B)** IL-18, and **(C)** sTIM-3 over the time were analyzed in patients treated with VCN-01 as monotherapy (left, n=8), with two different doses 3.3e12 viral particles (vps, light blue) or 1e13vps (dark blue). And also in patients treated with VCN-01 in concomitant combination with chemotherapy (right, n=10) at 3.3e12vps (pink) or 1e13vps (dark red) were analyzed. *p<0.05 by paired-Wilcoxon test vs pre-Treatment.

Finally, an increase of serum concentration at late timepoints was observed in IL-17A and sCD27 markers. IL-17A was slightly induced at a late phase (day 8) in both arms, but only patients treated with chemotherapy had statistical significance (**Figure 21-A**). It is worth to mention that for IL-17A the p-value for monotherapy arm was near to 0,05 on day 8 and 28 (p-value around 0,07). The released CD27 (sCD27) was slightly raised in patients of P-VCNA-001:II on day 8 (**Figure 21-B**), and it was almost significant in monotherapy patients (Day 8, p-value = 0,072). The increases of these markers on day 8 might be considered a late immune response, although further analyses are needed to confirm their relevance. The rest of the analytes' kinetics are presented in the annex of this thesis (**Supplementary Figure 3 and 4**, Annex). The kinetics of P-VCNA-001:III patients were similar to P-VCNA-001:I within the first 8 days, are presented in **Supplementary Figure 5.**

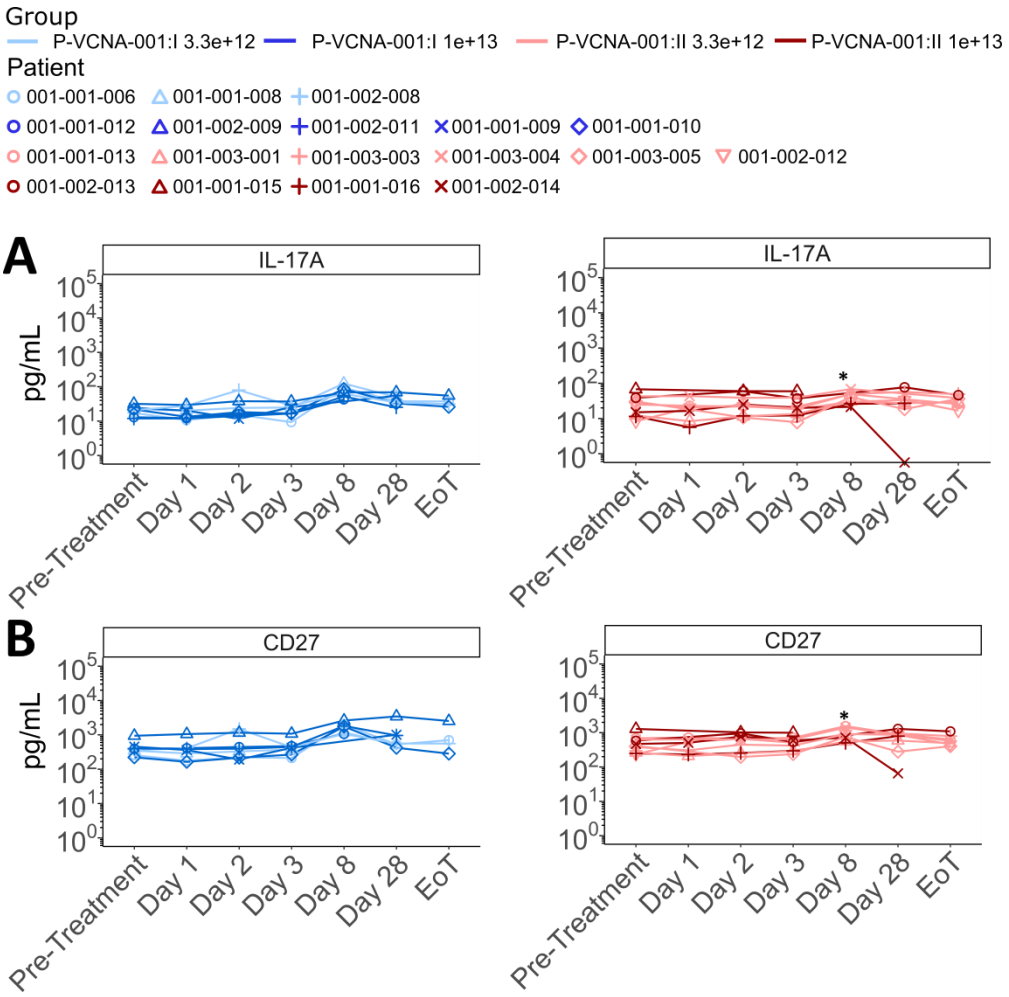

Figure 21. Late immune wave kinetics: IL-17A and sCD27. The serum levels of **(A)** IL-17A,and **(B)** sCD27 over the time were analyzed in patients treated with VCN-01 as monotherapy (left, n=8), with two different doses 3.3e12 viral particles (vps, light blue) or 1e13vps (dark blue). And also in patients treated with VCN-01 in combination with chemotherapy (right, n=10) at 3.3e12vps (pink) or 1e13vps (dark red) were analyzed. *p<0.05 by paired-Wilcoxon test vs pre-Treatment.

3.2. THE EFFECT OF VIRAL DOSE AND GEMICITABINE/ABRAXANE IN SERUM LEVELS OF SOLUBLE IMMUNE MARKERS.

Aiming to understand the impact of the different viral doses (3,3e12 or 1e13 vp/patient) or the concomitant combination of VCN-01 with GE/Abx, we compared the levels of each marker in every time point. To discern dose effects, statistic comparisons

were performed within the same treatment and different doses. No significant differences have been detected regarding dosage. To elucidate the effect of chemotherapy, comparisons between the same dose but different treatments were assessed. We observed significantly higher IDO1 levels on day 8 in patients treated with the low dose of VCN-01 monotherapy compared to the patients treated with the low dose of VCN-01 combined with GE/Abx. A similar trend was observed between the highest doses (**Figure 22-A**). In the case of sCD27, patients treated in monotherapy with 1e13vp reached higher levels on day 8 than those who received the combination with chemotherapy (**Figure 22-B**). Despite the low number of patients, we could speculate that in both cases, the depletion of growing cells by chemotherapy affects these markers in serum one week after administration.

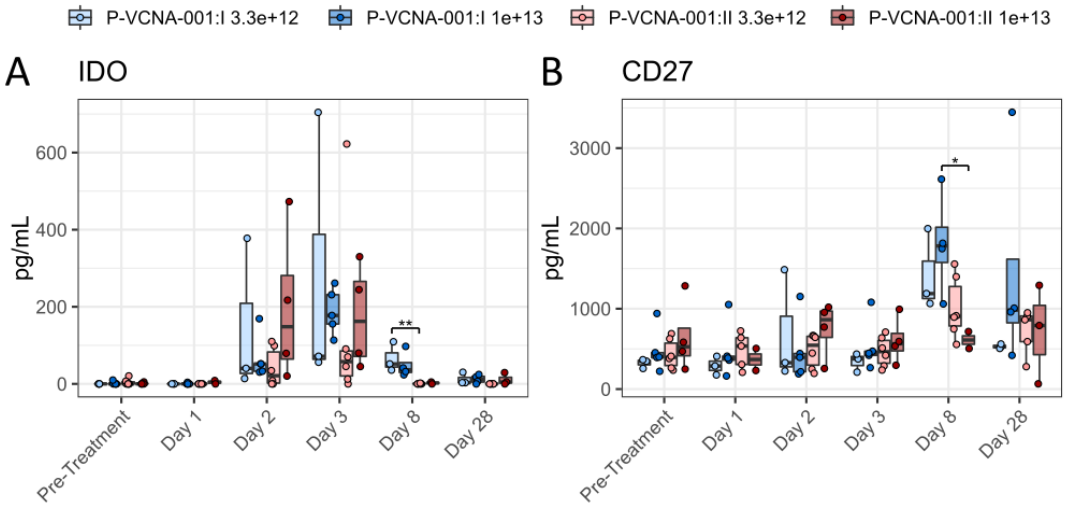

Figure 22. The concomitant chemotherapy affects the serum levels IDO1 and sCD27. Patients' sera from P-VCNA-001:I and P-VCNA-001:II were analyzed for the (A) IDO1 levels and (B) soluble CD27 levels. *p<0.05, **p<0.01 by Kruskal Wallis and Dunn's posthoc test with Holm's correction.

3.3. VCN-01- INDUCED ELEVATIONS OF SOLUBLE IMMUNE MARKERS ARE RELATED.

Despite the induced changes in soluble immune markers by VCN-01 treatments, the anti-adenovirus serotype 5 neutralizing antibodies (NAbs) were also monitored during

the clinical trial, reporting an increase in all patients over the treatment (data not shown, analyzed by Virotherapy and Immunotherapy Group at LRT-1).

To address the relevance of induced-immune changes by VCN-01 treatments, we assessed the relationship between analytes and NAbs. To do that, we worked with all patients from arms 1 and 2 together. The highest differences against basal levels for each soluble immune marker and NAbs increase (Diff NAbs) were correlated and plotted in a correlation map (**Figure 23**).

We observed four differentiated clusters (dark squares in the figure), the first one correlated the IL-18 to IL-23 positively indicating that those patients with low or high levels of IL-18 on day 8 also presented low or high levels of IL-27, sHVEM, and IL-23 on day 8. Although the statistical significance, further studies have to be performed for reliable conclusions about this putative cluster. IL-23, IL-27, and sHVEM were detected in a minority of patients (3/18, 2/18, and 4/18, respectively). According to the analysis, the patients with higher IL-18 induced quantifiable levels of IL-23, IL-27, and sHVEM.

Next, a cluster formed by soluble immune markers that peaked on day 8 (late immune wave) correlated in a positive manner. The correlated increases highlight a coordinated immune response induction. Interestingly, the levels of soluble PD-L1 on day 8 negatively correlated with the NAbs increase on day 8, and the trends were observed for NAbs increase on day 15 and day 28. It might imply that patients with higher serum levels of PD-L1 presented a lower antibody response against the VCN-01.

A relevant cluster with IL-10, IFNγ, IP-10, IDO, and sE-selectin was found. We already have mentioned their robust induction between arms at immediate-early timepoints (Day 2), and we note here a positive correlation. This could be explained by shared immune-response pathways, pointing at key-factors among analytes in the early anti-viral immune response. As expected, the levels of IP-10 and IDO1 were strongly correlated with their inductor IFNγ. IL-10 was correlated with the increase in anti-adenoviral NAbs on day 15 and day 28 post-treatment. However, no correlation with the other clusters was reported. Notably, no significant correlations with the previously

mentioned clusters were found, suggesting no relationship between the two immune waves induced by VCN-01.

Finally, a cluster was identified of CD137, IL1β, IL-5, and TNFα, but cautious conclusions should be done due to low detected levels of IL1β and TNFα.

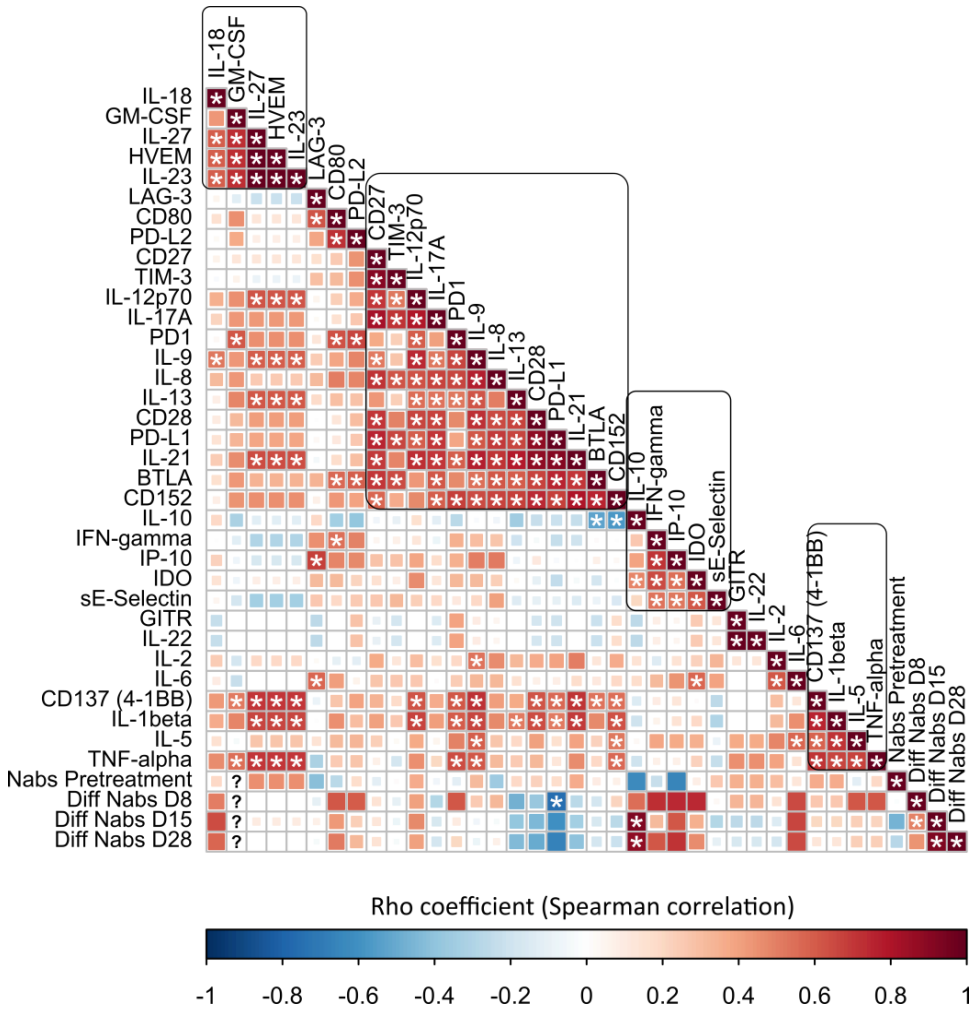

Figure 23. Correlation map of serum changes in P-VCNA-001:I and II patients.. The differences against pre-treatment values for each analyzed cytokine/immune marker were computed. Then, corresponding differences of the day with the highest mean were correlated between different analytes. *p<0.05 by Spearman correlation. The Rho coefficient indicates the sense of correlation (red positive, blue negative correlation). 4 clusters were detected and highlighted by black squares. Question mark indicates no correlation could be performed due to lack of values. Patients analyzed from P-VCNA-001:I and II (n= 18)

3.4. THE LEVELS OF IL-6 AND IL-10 DIRECTLY CORRELATE WITH TOXICITY.

As VCN-01 treatments induced remarkably changes at serum levels, we studied their biological impact in patients. First, we assessed the toxicity differences between the three arms of P-VCNA-001. The maximum toxicity grade per patient within the first 15 days was compared between treatments. Although no statistical differences were observed, more grade 4 toxicities were recorded in the concomitant chemotherapy arm (P-VCNA-001:II) compared to the others (**Figure 24**). Furthermore, the only grade 5 toxicity was detected during the concomitant treatment of VCN-01 and GE/Abx.

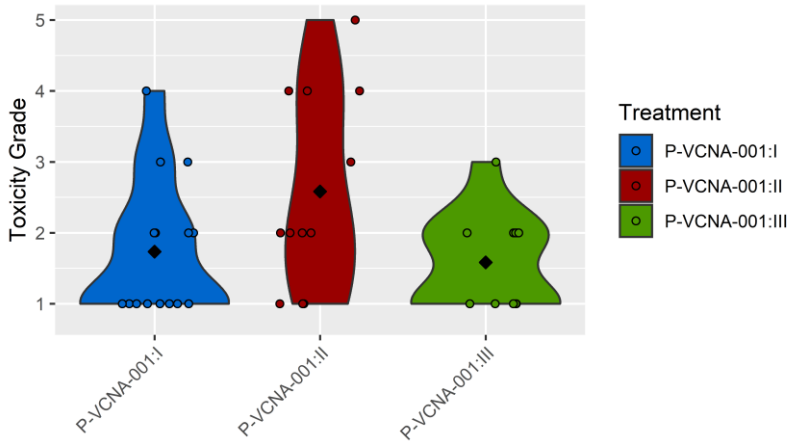

Figure 24. P-VCNA-001 maximum toxicity grades. The maximum toxicity grade of each patient within the first 15 days post-treatment is plotted in the violin plot. The mean of each treatment is represented as a black rhombus). No significant differences were detected between treatments by Kluskal-wallis and Dunn's post-hoc test .

The correlation between the levels of the mentioned 34 cytokine/immune markers and the maximum recorded toxicity grade was assessed. Correlations were performed for every analyte and every timepoint presented in the correlation map (Figure 25-**A**). We detected significant negative correlations between the pre-treatment levels of IL-13 and toxicity. Thus, higher IL-13 concentration in sera before treatment implies lower-

grade toxicity events. Moreover, the level of IFNγ on day 1; and BTLA, CD152 and CD80 IL-1β and IL-13 on day 2 also negatively correlated with the toxicity grades. However, these correlations should be further evaluated for reliable conclusions because most patients' analytes were undetectable (**Supplementary Figure 6,** Annex). On the other hand, a positive correlation between the levels of IL-10 on day 3 and the toxicity grade was observed (Figure 25-**B**). The IL-10 serum concentration from patients that suffered grade 4 toxicity was significantly higher than those with grade 1 or 2 toxicities on day 3 (**Figure 25-C**).

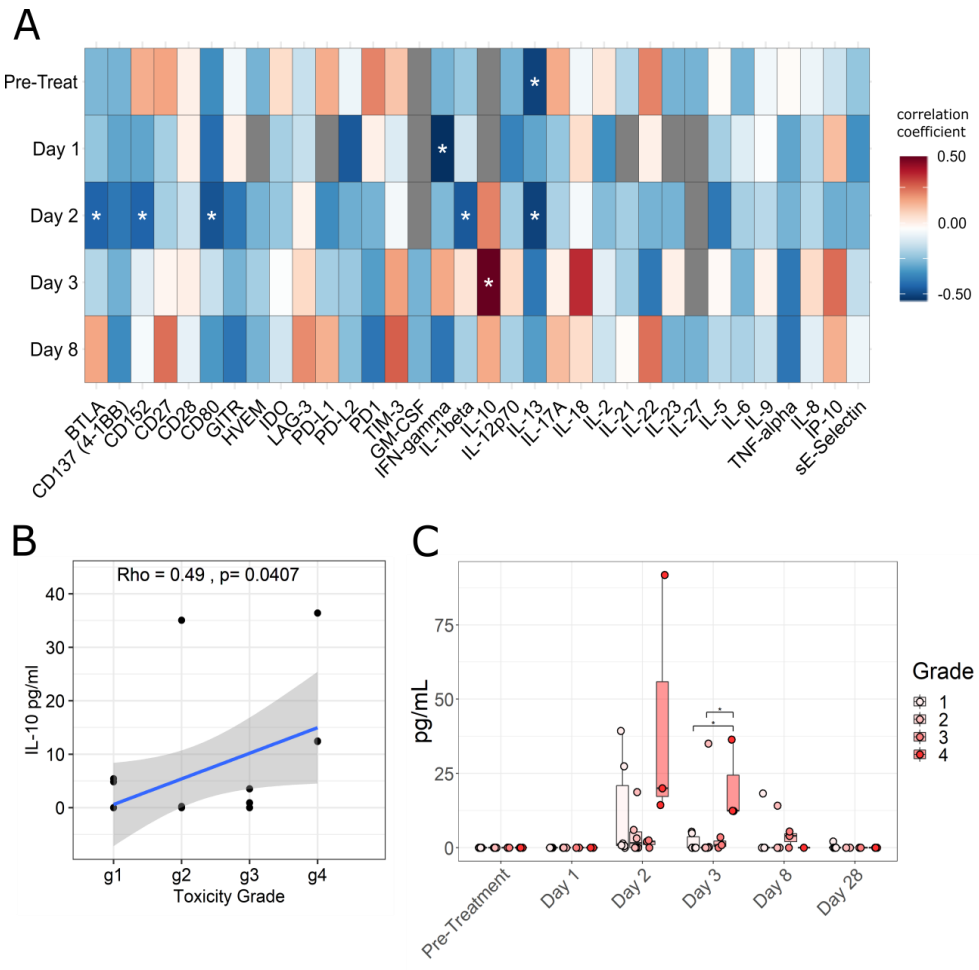

Figure 25. IL-10 correlates with toxicity grade. (A) Correlation map is presented. Spearman correlation between the analyte levels and the maximum toxicity grade was performed for every timepoint.*p<0.05 by Spearman correlation. Correlation coefficient is represented according to the legend (1 red, -1 blue). **(B)** Detail of IL-10 positive correlation at day 3 with the corresponding toxicity grade. **(C)** Detected levels of IL-10 in patients from P-VCNA-001: I and II grouped by toxicity grade.*p<0.05

To confirm the observed results in P-VCNA-001:I and II patients, we extended the analysis to all subjects from P-VCNA-001 with a more sensitive technique (ELISA). Apart from IL-10, IL-6 was also tested as it was published to be related to toxicity after adenovirus injection [267]. Moreover, the platelet-activating factor (PAF), reported as toxic in our preclinical models, was also evaluated.

The levels of IL-6 by ELISA were remarkably higher (30-fold higher on average) than the Luminex assay, as expected. We observed the highest levels 6 hours after VCN-01 injection (Day 1), followed by a reduction of serum levels for most of the patients, confirming the presented kinetics with the Luminex results. However, patients with a maximum toxicity grade 4 or 5 did not decrease the IL-6 serum concentration on days 2 or 3 (**Figure 26-A**). There was a statistical correlation between the grade of toxicity and the IL-6 levels on day 3 (**Figure 26-B**), probably due to those patients that had grade 4 and 5 did not show a reduction of IL-6 at this timepoint. Similarly, IL-10 was also assessed, finding a delayed peak in serum concentration (on day 2) compared to IL-6 (**Figure 26-C**), and also had a significant correlation with the toxicity grade and IL-10 serum levels on day 3 (**Figure 26-D**). Thus, VCN-01 intravenous injection induced an early burst of IL-6 at 6h followed by IL-10 at 24h, and their serum concentrations on day 3 directly correlated with the toxicity in the patients. Conversely, PAF increase at 6h was not detected in all patients and did not correlate with the toxicity grade (**Figure 26-E,F**).

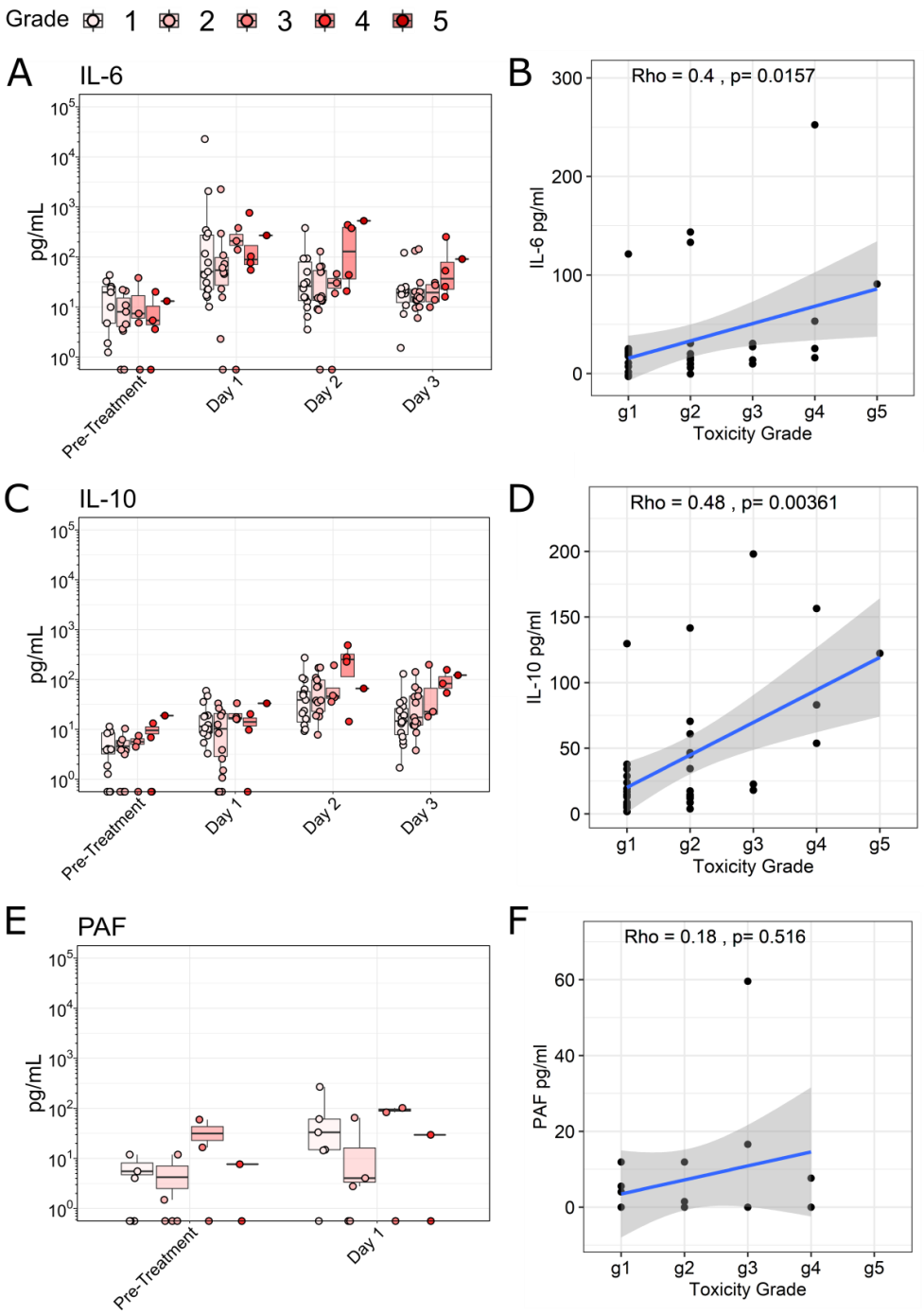

Figure 26. IL-6 and IL-10 serum levels correlate with toxicity grade. The serum of all P-VCNA-001 patients were analyzed by ELISA detecting **(A)** IL-6, **(C)** IL-10 and **(E)** Platelet activating factor (PAF). The levels on day 3 of **(B)** IL-6 and **(D)** IL-10 positively correlate with the maximum toxicity grade within the first 15 days of treatment. However, **(F)** PAF levels at pre-treatment nor day 1 (presented in the graph) showed any correlation with toxicity**.** Spearman Correlation was performed, stats are presented in the graphs.

3.5. INFLUENCE OF VCN-01 INDUCED IMMUNE CHANGES IN TUMOR EFFICACY.

As VCN-01 treatment prompted immune-related changes, we screened the influence of the soluble immune markers serum levels in the antitumor response. Patients from the monotherapy arm (P-VCNA-001:I) could not be evaluated for treatment efficacy and, therefore, not included in this analysis. From the first Luminex, we tested P-VCNA-001:II patients that were monitored for their tumor lesions (n=9). The analyte concentration in each timepoint was correlated with the maximum change in the tumor lesions.

We presented a correlation map with significant negative relations between IFNγ, IP-10, sE-selectin, IL-8, IL-18, IL-1β, IDO1, CD80, and tumor change (**Figure 27-A**). Higher levels of mentioned analytes corresponded to a lower percentage of tumor change (higher tumor reduction; the more negative value in "Maximum change in tumor size (%)", the more tumor reduction (%)).

Similarly to the toxicity analysis, some correlations should be further analyzed for a reliable conclusion, due to few responding patients and the low analyte levels (near to the Luminex detection limit), for instance: IL-8, IL-18, IL-1β, and CD80 presented in the annex of this thesis (Sup.Figure 6). In contrast, the rise of IFNγ, IP-10, sE-selectin, and IDO1 was statistically significant and relevant in the responding patients. These four markers have been related with the early immune-induced wave by VCN-01, and probably involved in an anti-viral immune response. Interestingly, the patients with higher levels of IFNγ on day 2 (**Figure 27-B**), IP-10 on day 8 (**Figure 27-C**), IDO1 on day 2 and 3 (Day 2, **Figure 27-D**) and sE-selectin on day 8 (**Figure 27-E**) presented a better outcome in terms of tumor size reduction.

The results surprisingly suggested that higher induction of these analytes in serum during the first week of treatment, especially within the first 48 hours, correlates with antitumor efficacy, suggesting that the anti-viral induced immune response might help to elicit antitumor activity.

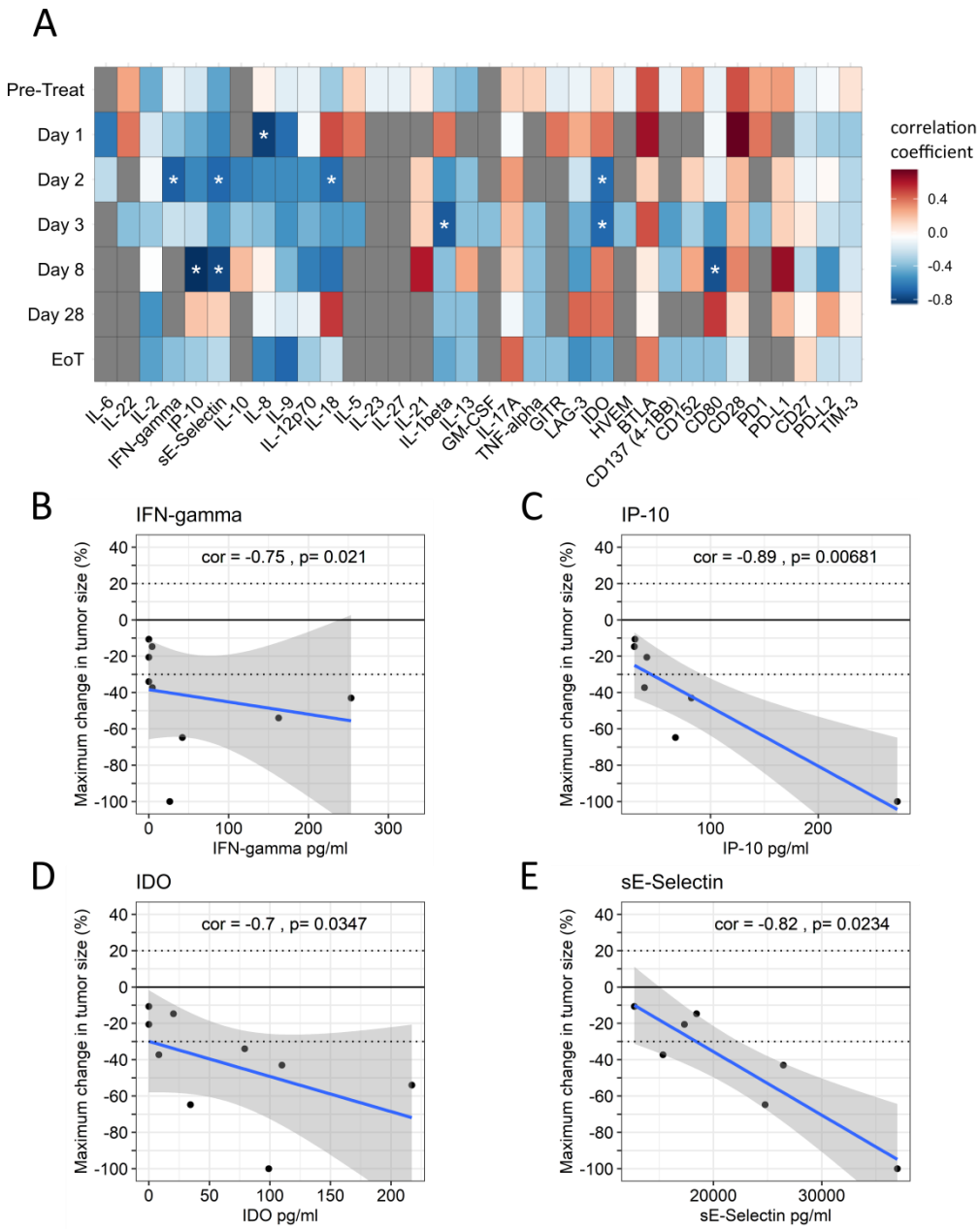

Figure 27. Correlation between anti-tumor response and soluble immune markers concentration in serum of P-VCNA-II patients. (A) A correlation map for the patients of P-VCNA-001:II is presented.*p<0.05 by Spearman correlation, the correlation coefficient (rho) is indicated by the color legend. The detailed correlations for **(B)** IFNγ on day 2, **(C)** IP-10 on day 8, **(D)** IDO1 on day 2 and **(E)** sE-selectin on day 8 are presented.

We extended the analysis to the patients from P-VCNA:III, that were also monitored for tumor volume changes. We performed the second Luminex assay with a less extensive panel of analytes and re-analyzing the P-VCNA-001:II patients. However, due to technical limitations, sE-selectin was not screened in this experiment. IL-8, IL-1β, and CD80 were not included in the new panel.

A similar approach was done with the data obtained from the second Luminex. To ensure the evaluation of the treatment's effect, the fold change versus pre-treatment for P-VCNA-001:II (n=7) and P-VCNA-001:III (n=12) patients were assessed by correlations. Less significant correlations were observed (**Supplementary Figure 7**, Annex). The relevant correlation between early IFNγ induction and the overall tumor change was still statistically significant (**Figure 28-A**). However, half of the patients (9/19) were under the Luminex quantification limit, and 0 value was arbitrarily attributed. This might mislead to artificial correlation. In order to explore the relevance of the correlation, we split the highest patient's IFNγ fold change for a low IFNγ increase (fold change below the median) and high IFNγ increase (fold change over the median). We observed that patients without IFNγ induction (low IFNγ) were 50% non-responders (Maximum change in tumor size > -30%) and 50% responders (Maximum change in tumor size ≤-30%). Conversely, patients with high induction of IFNγ were enriched with responders (88,9%, **Figure 28-B**), suggesting that there is an association between IFNγ and probability of response.

A similar approach was done for the rest of the analytes; IP-10 seemed to be not as relevant as observed in the first Luminex analysis on day 8 (**Figure 28-C**). A slight difference was observed in the percentage of responders between low IP-10 and high IP-10 increase populations (**Figure 28-D**), confirming the lack of correlation. IDO1 increases on day 3 again showed a negative correlation trend with maximum tumor change, but not significant (**Figure 28-E**). Furthermore, there were no differences between the percentage of responders and non-responders, comparing IDO1 increases (**Figure 28-F**).

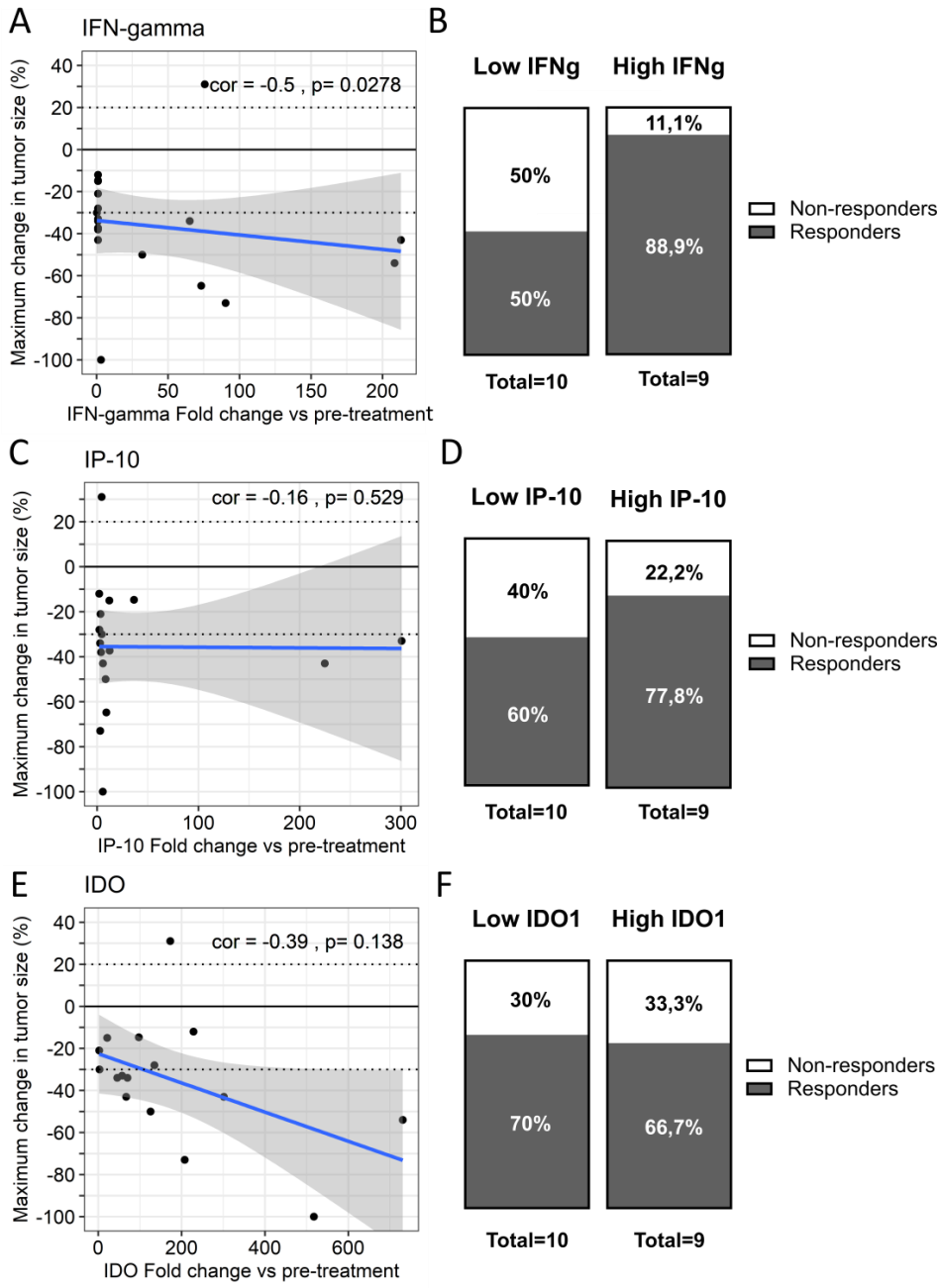

Figure 28. Correlation between anti-tumor response and serum levels of IFNγ, IP-10, and IDO1. The increases in serum levels of P-VCNA-001:II and III patients are presented. The fold change from pre-treatment was assessed by Spearman's correlation. The correlation coefficient (cor) and the p-value are in the graph. The patients have been divided according to their highest fold-change (between days 1 to 15) in low (below the median) or high (over the median). The percentage of non-responders (white) and responders (grey) have been plotted. **(A)** The detailed correlation of IFNγ on day 2, and **(B)** percentages for IFNγ (median=3,7). **(C)** Correlation of IP-10 on day 8 and **(D)** IP-10 percentages (median=14,06). **(E)** Correlation of IDO1 on day 3, and **(F)** IDO1 percentages (median=121,85). For non-quantifiable samples a fold change of 1 was arbitrary attributed.

Importantly, in this second Luminex, the increase of sLAG-3 induced after VCN-01 treatments, significantly correlated on day 3 with maximum percentages of tumor change (**Figure 29-A**). Although low sLAG-3 increases presented 50% of responders and non-responders, a high induction of this marker was associated with an 88,9% of responders (**Figure 29-B**), suggesting an implication of treatment outcome.

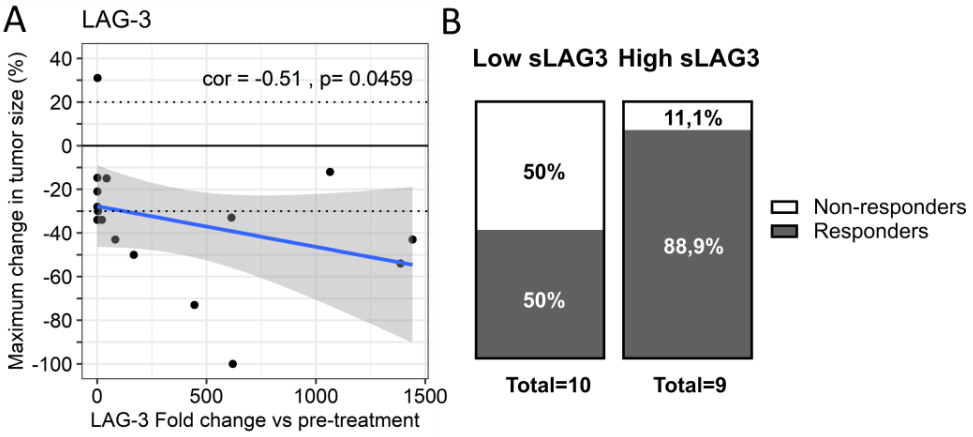

Figure 29. Correlation between the sLAG-3 increases and the maximum tumor volume change. (A) The correlation between maximum change in tumor size from the baseline and the fold change in sLAG-3 on day 3 is presented. Spearman correlation was performed. The correlation coefficient (rho, cor in the graph) and p-value are presented in the graph. **(B)** The greatest fold change (between day 1 and day 15) were split in low sLAG-3 (below median<391,27) and high sLAG-3 (over median>391,27) and percentage of non-responders (white) or responders (grey) are depicted in the graph.

All these results should be further evaluated to confirm conclusions. In consequence, we suggest that analyzing the levels of IFNγ, IP-10, sE-selectin, IL-8, IDO1, and sLAG-3 in the case of phase II clinical trial might be interesting. IFNγ is produced by activated T cells and NK cells. Similarly, sLAG-3 is released upon TCR signaling from T cells indicating immune activity. Thus, we speculate that an early immune activation (IFNγ and sLAG-3 on day 3), probably against the virus, could influence the overall efficacy of the treatment.

Following the mentioned rationale, the correlation between the specific immune response against the virus by the neutralizing antibodies (NAbs) titers in serum and the antitumor efficacy was assessed. The basal levels of NAbs (NAbs pre-treatment) did not

correlate with the maximum change in tumor size (**Figure 30-A**). However, low NAbs titer previous to treatment was enriched with patients that respond to treatment (71,4%) compared to non-responders (28,6%). Furthermore, high levels of NAbs before treatment were enriched with non-responders (62,5%) compared to responders (32%) (**Figure 30-B**). More revealing was the highest increase of NAbs titer during the treatment (Highest NAbs fold change). It significantly correlates with tumor reduction (**Figure 30-C**), and high anti-viral titer increase resulted in a high antitumor response (High NAbs increase, 72,7% of responders, **Figure 30-D**). These results converge with the reported results where higher anti-viral immune response (IFNγ and sLAG-3) implied higher tumor reduction.

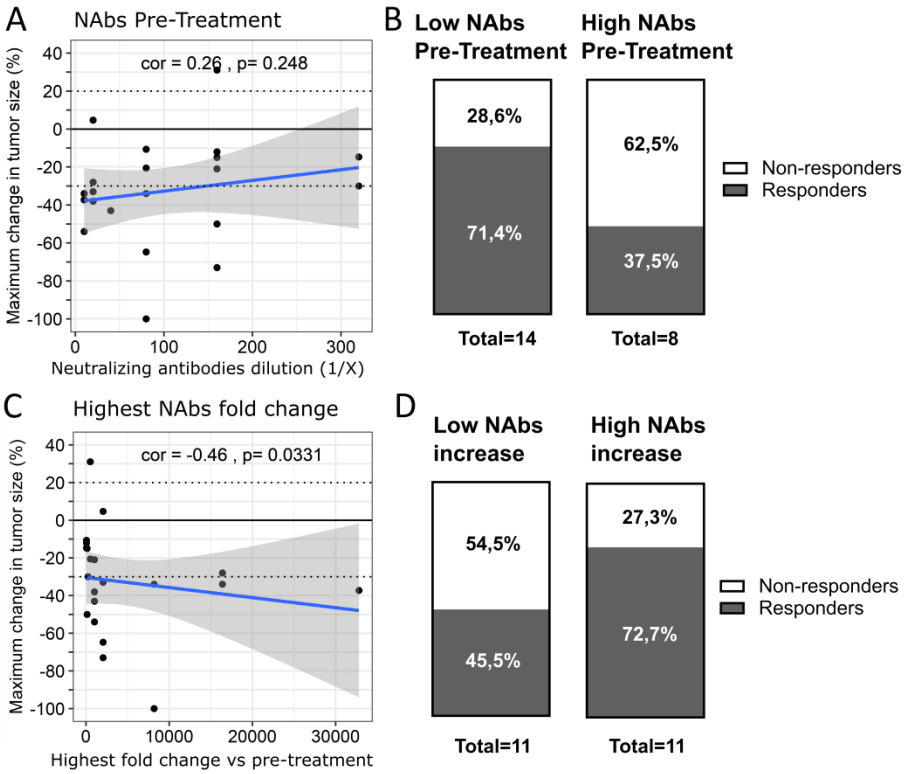

Figure 30. Correlation between the NAbs titer and tumor reduction. (A) Correlation between NAbs titer before treatment and the maximum change in tumor size. **(B)** Percentage of responders (grey) or non-responders (white) in patients with low NAbs pre-treatment titer (below the median<80, Low NAbs) or high titer (over the median>80, High NAbs). **(C)** Correlation between the highest fold change in NAbs titer and tumor change. **(D)** Percentages of responders and non-responders according to

NAbs increase (highest fold change, median=1024,5). Spearman correlations were performed. The correlation coefficient (rho, cor in the graph) and p-value are presented.

3.6. IDO ACTIVITY INCREASES AS A CONSEQUENCE OF ONCOLYTIC ADENOVIRUS TREATMENT

We have described the IDO1 induction by VCN-01 treatment in the Luminex analyses. We wanted to confirm the IDO1 increase in serum levels by a high-sensitive technique. IDO1 is an enzyme that oxidizes tryptophan to kynurenine. ELISAs to detect the tryptophan and kynurenine levels in P-VCNA-001:I and II patients were performed. The ratio of kynurenine to tryptophan, also known as KTR, was used to extrapolate the IDO activity. It must be considered that enzymes such as IDO2 or TDO could also act in an analog way.

Kynurenine and tryptophan were detected, and KTR was calculated for each patient. We confirmed the same tendencies observed in the Luminex analyses. A 10-fold increase on day 3 compared to pre-treatment levels in a high dose of VCN-01 and almost half in the low dose. We also observed lower IDO1 activity in P-VCNA-001:II concomitant group compared to monotherapy on day 8, confirming the Luminex observation. Despite this, no statistical changes were identified due to few numbers of subjects (**Figure 31-A**). Furthermore, we assessed samples from ICOVIR5 clinical trial in patients with advanced melanoma uveal (NCT01864759). We wanted to elucidate if IDO changes were related to oncolytic adenovirus treatment, or they were specifically associated with VCN-01 treatment (hyaluronidase expression). The intravenous injection of ICOVIR5 also triggered an increase of KTR fold change on day 3, similar to that observed for VCN-01 (**Figure 31-B**). In consequence, we could assume that IDO1 activity enhancement is produced by intravenous injection of oncolytic adenoviruses. It probably corresponds to an anti-viral triggered immune response.

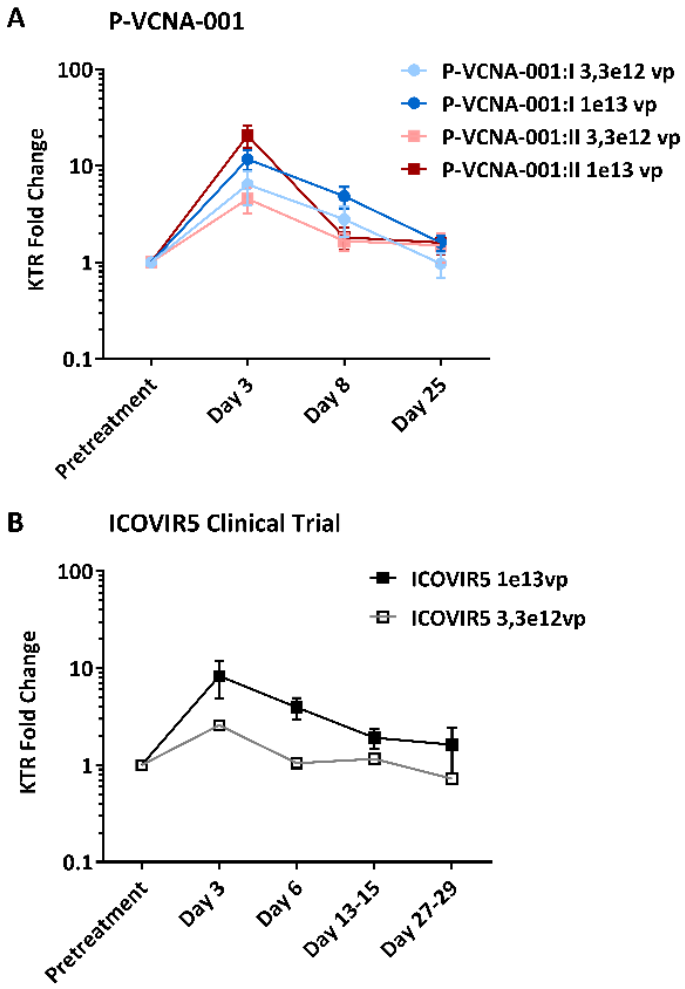

Figure 31.Oncolytic adenovirus increase the kyneurenine to tryptophan ratio. (A) Patients from P-VCNA-001:I (3,3e12vp n=4; 1e13vp n=6) and P-VCNA-001:II (3,3e12vp n=6; 1e13vp n=4) were assessed for kyneurenine to tryptophan ration (KTR) fold change over the time ± SEM. **(B)** Patients from ICOVIR5 clinical trial treated at 3.3e12vp (n=1) or 1e13vp (n=6) were also assessed for the KTR fold change ± SEM. No significant differences were detected between groups neither between timepoints by multiple Wilcoxon tests between groups, and paired-Wilcoxon test between timepoints.

3.6.1. IDO1 increase in tumors

We demonstrated the burst of IDO1 levels in patient's serums after intravenous injection of an oncolytic adenovirus. We speculate that this increase might impact on antitumor efficacy. Thus, we screened the presence of this protein in tumor tissues at different time points. Due to technical difficulties in obtaining patient samples, it was not possible to obtain paired tumor tissues from the same metastasis sites for all patients. Nevertheless, the induction of IDO1 expression was observed by IHQ on day 8 post-treatment compared to basal levels (**Figure 32-A, B**). Given that both analyzed patients are from P-VCNA-001:III (delayed chemotherapy schedule), and the analysis was performed on day 8 (before chemotherapy administration). All changes observed were due to viral treatment only. In consequence, we can conclude that VCN-01 enhances the IDO1 levels also in tumors on day 8.

Moreover, IDO1 positive staining was observed in day 28 biopsies from patients treated in combination with chemotherapy. However, the stained area and intensity of IDO1 were remarkably smaller than detected in day 8 biopsies (**Figure 32–C, D**). As we did not have the same patient samples on days 0, 8, and 28, profiling of IDO1 kinetics in the tumor could not be done. Despite that, stainings suggest an increase in IDO1 expression, with a peak on day 8 provoked by VCN-01. We can conclude that VCN-01 treatment altered the IDO1 expression at tumor and serum. No tumor samples on day 3 could be obtained. Thus, we were not able to associate the serum concentration directly with the tumor presence. However, taking all data together, we can hypothesize that following VCN-01 IV administration IDO1 is activated as an anti-viral immune response systemically and was also induced within the tumor, thereby changing the immune-status of the tumor microenvironment.

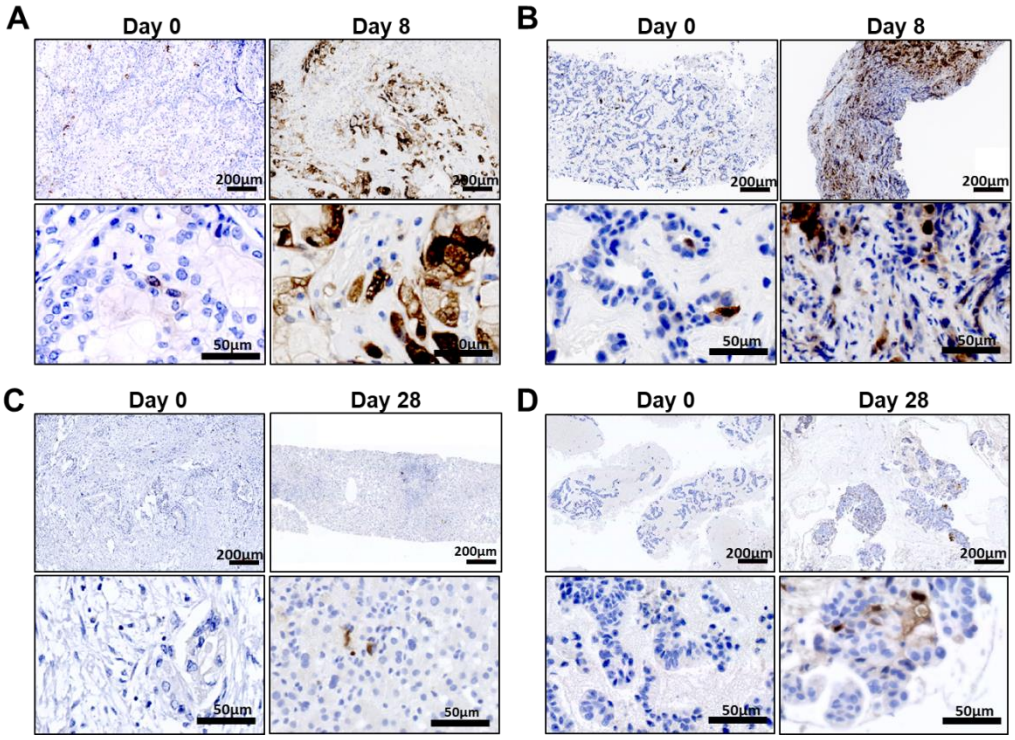

Figure 32. Treated tumors are positive for IDO Immunohistochemistry staining. (A) Patient 001-004-001 lymph node biopsies on day 0 and day 8 post-treatment (P-VCNA-001:III). **(B)** Patient 001-005-002 hepatic biopsies on day 0 and day 8 post-treatment (P-VCNA-001:III). **(C)** Patient 001-002-013 pancreatic biopsy on day 0 and day 28 post-treatment (P-VCNA-001:II). **(D)** Patient 001-003-002 pancreatic biopsies on day 0 and 28 post-treatment (P-VCNA-001:II).

4. DISCUSSION

The mechanisms that mediate the antitumor activity of oncolytic viruses have been under the focus in the last years, as a consequence of raising knowledge of tumor immunology. The principal hypothesis is that OVs efficacy depends on the triggered antitumor immune response. The hypothesis is supported by the long-lasting clinical responses observed in VCN-01 treated patients that cannot be attributed to chemotherapy neither viral replication.

Aiming to understand the relevance of the induced-immune changes after viral treatment, we performed an extensive serum analysis with a panel of immune markers, for the first time including soluble immune checkpoints, after systemic injection of VCN-01, as monotherapy (P-VCNA-001:I) or combined with Gemcitabine/Abraxane (P-VCNA-001: I and II). All patients showed an increase in several soluble immune markers in serum that can be viewed as early and delayed immune waves.

In the early wave, VCN-01 immediately (6hours, Day1) increased the levels of pro-inflammatory mediators (i.e. IL-6). The activation of NF-κB by innate sensors (mainly in Kupffer cells and splenic macrophages) promotes the synthesis and secretion of IL-6, which plays a critical activity for anti-viral response recruiting lymphocytes [311–313], and it was detected in previous clinical trials with OAds [99,107]. Following this inflammation signal, cytokines related to immune activity peaked at 24-48 hours (Day 2-3), including IFNγ and sLAG-3. The IFNγ is secreted upon T lymphocytes activation (and NK cells) [277,314–316], having anti-viral effect and a pivotal role of Th1 responses impeding other Th types maturation. The detected IFNγ increase converges with the data of Enadenotucirev clinical trial [99]. Conversly, we described for the first time an increase of LAG-3 release (sLAG-3) after OAd treatment. In line with the IFNγ burst, the sLAG-3 is a clear marker of proper T cell activation and its sera increase has been correlated with Th1 responses, stimulating the APCs through MHC-II signaling, and leading to an increased antigen-specific T-cell response *in vivo* [317].

IFNγ-induced proteins were also detected in the serum, mainly IP-10 and IDO1 enzyme. IP-10 is a chemoattractant for activated immune cells (expressing CXCR3 receptor) associated with viral infections the subsequent inflammatory process, and biased Th1 responses. IP-10 generates a positive feedback loop recruiting IFNγ-producing Th1 cells which increase the IP-10 production [291], as we detected after VCN-01 treatment with a significant induction of IP-10 since the early time points (as IFNγ peaks) until day 28.

IFNγ also interferes directly with viral replication, including adenoviruses [318], hindering the viral life-cycle at different levels: avoiding the entry (i.e., downregulation of CAR receptor [319]), inhibiting the replication or gene expression, activating the immunoproteasome [320], and starving the virus [321]. Regarding the latter, we describe for the first time induction of IDO1 serum levels after systemic OAd administration, induced by IFNγ (coinciding peaks). IDO1 metabolizes tryptophan (Trp) to kynurenine (Kyn), and plays dichotomous roles: anti-viral activity and immune-suppressive regulator. Viruses are sensible to Trp-depletion [322–325], due to most of viral capsids' core proteins are rich in Trp [326] (i.e., adenovirus hexon [327]). Moreover, IDO1 contributes to T-cell anergy and Treg differentiation to reduce excessive inflammation [328,329]. Taking all in account, the transient increase of IDO1 activity after VCN-01 treatment contributes to clear the virus and induce anergy in the infected tissue (such as tumor). Another marker of homeostatic immune regulation is the IL-10, increased at 24h post VCN-01, secreted to counteract the strong inflammation.

We can conclude that VCN-01 induces an early immune activation within the first 48hours. The levels of IL-6, IL-10, IFNγ, IP-10, IDO1, and sLAG-3 were robustly increased in most of the patients independent of treatment. According to the bibliography, these are markers of a Th1 response and are biologically related in common pathways of inflammation an anti-viral response. Furthermore, we confirmed a correlation between the levels of IFNγ, IP-10, and IDO1 in VCN-01 treated patients. We reported for the first time the burst of IP-10, IDO1, and sLAG-3 serum concentration after intravenous injection of an OAd.

Then the levels of IL-8, IL-18, and sTIM-3 were initially induced after 24hours of treatment until day 8, in a delayed immune wave. However, it was not significantly demonstrated in patients from different clinical trial arms, and the differences can not be associated with the effect of treatment (discussed in the next section). Furthermore, the small increase compared to the pre-treatment levels suggests that more analyses have to be done for solid conclusions. Similarly, the relevance of IL-17A and sCD27 concentration peaks on day 8 in some patients need to be carefully validated to infer a biological effect. All immune changes (early and late) normalize by day 15-28 post-treatment.

The reported immunological response induced by the intravenous administration of VCN-01 in cancer patients is consistent with cytokines and interleukins analyzed previously in animal models using VCN-01 [1] and also in cancer patients receiving other oncolytic adenoviruses systemically [2], but also provide new data regarding a wider characterization of other immune markers.

4.1. THE EFFECT OF DOSE AND GEMICTABINE/ABRAXANE IN VCN-01 IMMUNE ACTIVATION

We evaluated the impact of the dose and concomitant chemotherapy in the serum levels of markers. We did not find statistical differences between doses from each arm. This may be due to low number of patients analyzed when subdividing into groups which impairs the statitcal significance: P-VCNA-001:I low dose (n=3)/high dose (n=5) and P-VCNA-001:II low dose (n=6)/high dose (n=4). A clear example is the ELISA of IDO activity; the trends showed greater KTR fold change in high doses than low doses, suggesting a dose effect on IDO induction that can not be confirmed statistically.

However, we reported a significant effect of GE/Abx in levels of sCD27 and IDO1 on day 8 (before 2nd dose of GE/Abx), reducing the serum concentration. To the authors' knowledge, no reports evaluating immune activation after GE/Abx treatment in patients neither pre-clinical models have been published. We speculate that the killing of dividing cells, consequence of chemotherapy, might affect the immune populations

related to the secretion of IDO1 and sCD27. Lower IDO1 levels on day 8 in the chemotherapy arm were confirmed by ELISAs, yet without statistical significance.

On the other hand, the early immune induction was similar between the three arms of the clinical trial. Thus, immune induction can be associated with viral injection rather than chemotherapy. Moreover, it implies that concomitant chemotherapy did not hamper the VCN-01 "immune kick" in early timepoints.

4.2. BIOLOGICAL CONSEQUENCES OF VCN-01 INDUCED IMMUNE CHANGES

4.2.1. Treatment toxicity

The intravenous injection of VCN-01 caused some toxic effects. The most common adverse effects were flu-like symptoms, thrombocytopenia, neutropenia, and transaminases increases, as previously reported in OAds, and gene therapy vectors intravenously administrated [90,99,267]. The adverse effects of GE/Abx treatment are neutropenia, leukopenia, thrombocytopenia, receipt of growth factors, fatigue, peripheral neuropathy, and diarrhea [330]. The intensity of toxicity can be defined in grades. No statistical differences in toxicity grades were reported between P-VCNA-001 trial arms, but grades 4 and 5 were more common in concomitant chemotherapy treatment (Part II) than others. An overlapping of treatment toxicities was considered to occur in Part II of the trial and lead to test the delayed arm of the clinical trial (Part III).

IL-6 and IL-10 have been intrinsically related to viral toxicity since Gelsinger's case [267]. We described for the first time a positive correlation between the serum concentration of IL-6 or IL-10 and the toxicity grade in patients. Conversely, platelet-activating factor (PAF) is implicated in the shock induction after intravenous injection of adenovirus in pre-clinical models [331], which was observed with VCN-01 injection with the eventual death of treated mice. However, no impact of PAF induction in adverse

effect grade was observed, suggesting that the toxicity effects of VCN-01 in mice might not be reproduced in humans.

4.2.2. Treatment efficacy

Clinical trials with OAds have been done and reported objective tumor reduction in intratumoral treated patients, such as ONYX-015 [332] and H101[333], DNX-2401 [99], and ONCOS-102 [107]. However, to the authors' knowledge, no clinical responses have been observed after systemic OAd treatment. VCN-01 is the first OAd that shows clinical responses after intravenous delivery. Furthermore, the only reported systemic treatment with an oncolytic virus in clinical trials with pancreatic cancer is the Reolysin which has shown disease control rate (stable disease+partial responses) for 17 of 34 patients in combination with gemcitabine [334].

P-VCNA-001 tested the VCN-01 efficacy in combination with the standard of care for pancreatic cancer, Gemcitabine plus Abraxane (GE/Abx). The GE/Abx progression-free survival (PFS) in a phase III was 5,5 months, and the overall response rate (ORR, complete response (CR) + partial response (PR)) was 23%. Interestingly, 1 CR out of 431 patients was described [330]. P-VCNA-001:II PFS was 9,9 months and ORR 50%, with a complete responder. P-VCNA-001:III PFS was 6,7 months and ORR 50%. A direct comparison between the control group (GE/Abx) and VCN-01 treatment has to be done in the phase II clinical trial. Despite this, the promising outcomes in phase I suggest that the addition of VCN-01 to the standard of care might improve the pancreatic cancer treatment. Furthermore, the results appear to be better than Reolysin.

We evaluated the implications of VCN-01-induced changes in the treatment efficacy. Considering the low number of patients, we used the percentage of maximum change from baseline of targeted tumor lesions as a marker of response for the two evaluated arms (P-VCNA-001:II and III, **Figure 33**).

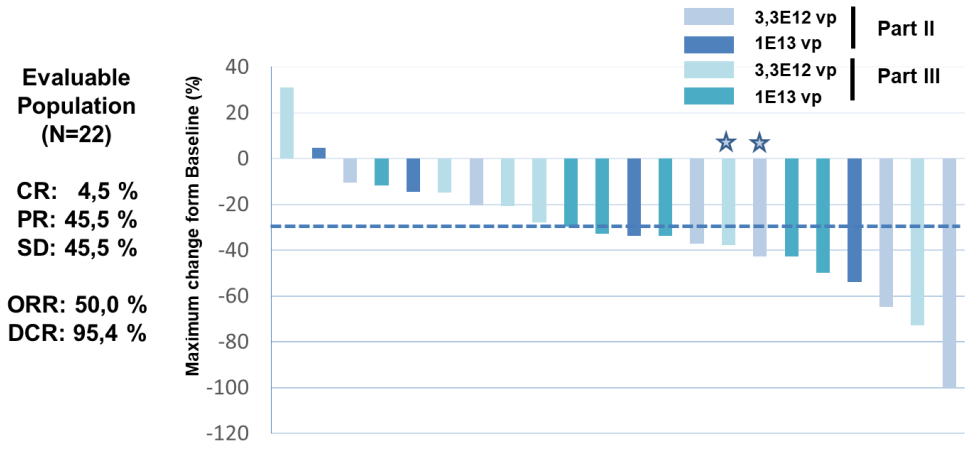

Figure 33. The best response rate in P-VCNA-001:II and III. The P-VCNA-001:I patients (Part III, n=10) and P-VCNA-001:II patients (Part II, n=12) are plotted based on the best percentage of change in the sum of target tumor lesions (%Maximum change from baseline). The total evaluated population is n=22 with one complete response (CR), 45,5% of partial responses (PR) and 45,5% of stable disease (SD). The overall response rate (ORR) is 50%, and the disease control rate (DCR) is 95,4%. Stars in the graph pointed clinical or biochemical progression.

The IFNγ and sLAG-3 increases during the VCN-01-induced early immune wave correlated with the therapy outcome. The patients with higher serum concentration increase of IFNγ 24 hours post-VCN-01 injection presented higher tumor reduction. A point to consider is that Luminex assay did not detect serum IFNγ peaks for some patients, which could lead to an unreliable correlation significance. In consequence, we described that IFNγ peak was associated with a high percentage of responders. Only 1 out 19 patient presented an IFNγ induction and did not respond to treatment. IFNγ expression by an adenoviral vector was also directly related to efficacy in cutaneous lymphomas [335]. In contrast, DNX-2401 was combined with IFNγ intratumoral injection (on day 14) without any improvement of the therapy [336], suggesting that IFNγ is not the only mediator of antitumor response, and the coexistence of different immune-triggers is required.

The sLAG-3 serum increase significantly correlated with tumor reduction, and it was confirmed by the association tests. Patients with great sLAG-3 fold change responded

in 88,9% of the cases. The serum detection of free LAG-3 has been recently used as a predictive biomarker in breast cancer [337] and gastric cancer [338]. This suggests that direct NK and T-cell activation markers IFNγ and sLAG-3 are correlated with antitumor responses, giving predictive information about the outcome of the therapy. Related markers (IP-10 or IDO1) presented some trends but they have to be further evaluated. The correlation with induced-immune response and efficacy was published in clinical trials with ONCOS-102, where the higher tumor infiltration of immune cells higher overall survival of the patient [107]. We described a correlation between humoral response against Ad5 (NAbs) and the tumor lesions reduction. The NAbs increase positively correlated with IL-10 serum increase and presented positive trends for all other early induced immune markers (IFNγ, IL-6, IP-10, IDO1), suggesting that the immune changes are related to the anti-viral response. In consequence, we propose that anti-viral response influence positively the antitumor efficacy, as suggested preclinically [129,130] and in ONCOS-102 patients [181]

We detected the IDO1 induction in tumors by IHQ which was higher on day 8 than day 28 post-treatment, confirming the transient expression detected in serum. We could use the IDO1 detection as a marker of viral presence, as confirmed by serial IHQ, which detected the simultaneous presence of virus (E1a) and immune induction (CD8 and IDO1, **Figure 34**). IDO1 was not evaluated in most of the OAds clinical trials except for DNX-2401 that did not report IDO1 induction in the tumor by IHC [93]. Importantly, the different timepoint analysis might influence in this disparity of results, as it is transiently expressed.

We hypothesize that VCN-01 in the bloodstream is rapidly sequestered in tissue-resident macrophages, triggering a strong anti-viral immune response after 24hours of injection (IFNγ, sLAG-3, IP-10). Eventually, viruses reach the tumor and replicate inducing an immune response in tumor. As higher anti-viral systemic response higher impact on tumor reduction. The VCN-01 is able to revert tumor immunosuppression converting “cold” tumors into “hot”. These immune-adjuvant-like properties might not be specific for VCN-01, as previously postulated [339].

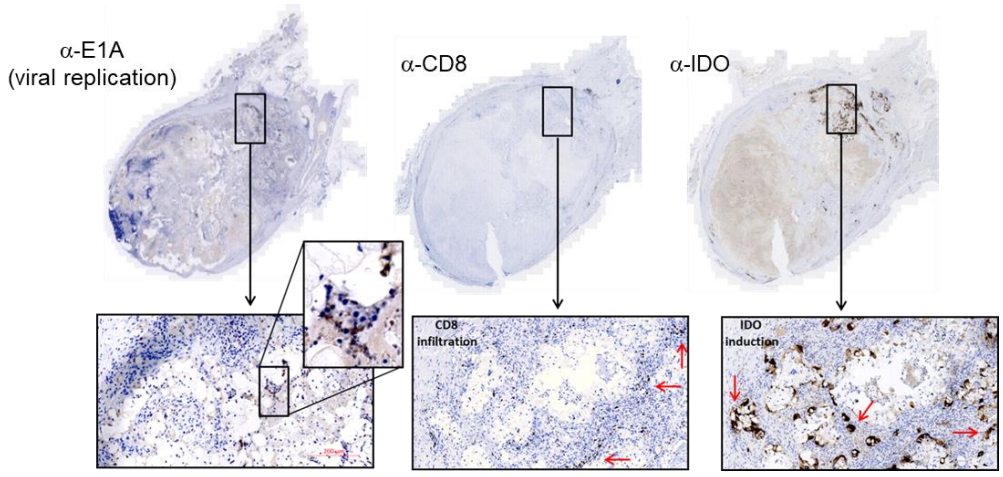

Figure 34. VCN-01 viral replication colocalizes with CD8$^+$ infiltration and IDO1 induction. Serial stainings of lymph node metastases from a P-VCNA-001:III patient on day 8 post-treatment (before GE/Abx injection). E1A expression colocalizes with CD8$^+$ and IDO1. Red arrows indicate positive staining.

4.3. STUDY LIMITATIONS AND FUTURE PERSPECTIVES

Two main limitations have to be considered with the present study. The low number of patients affects the reliability of conclusions. The subsetting of patients in the corresponding groups impair the statistical significance due to the poor n and inter-patient variability. Moreover, the Luminex assay is suitable for high-throughput and exploratory analysis, but its sensitivity is low compared to other techniques such as ELISA.

Regarding a phase II clinical trial, the immune-phenotyping presented in this thesis provided a panel of relevant immune markers (IFNγ, IP-10, sLAG-3, IDO1, IL-8, IL-18, sTIM-3, sCD27, IL-17A, sE-Selectin and NAbs) that may be valuable as predictive biomarkers of the therapy efficacy. The subsetting of phase-II patients after treatment, according to these markers, could identify responders. Moreover, pre-clinical studies might be planned to enhance the probability of producing the required immune-phenotype to ensure treatment response.

The immune-adjuvant effect reported in this thesis and previous studies, support the OAd combination with immunotherapies. The scheduling of combination is one of the issues that have to be addressed in the field. The disparity in clinical approaches exemplifies the need for data regarding this. VCN-01, ONCOS-102, and DNX-2401 are being tested in clinics with anti-PD-L1 at different timings (concomitant, 7 days-delay, 14 days-delay, and others). We described that VCN-01 intravenous injection, and probably other OVs, increased the soluble PD-L1 levels on day 8 after treatment, yet not significantly. PD-L1 negatively correlated with the NAbs increase. As far as we demonstrated that patients with higher NAbs titer increase presented best responses, we suggest that day 8 might be a suitable timepoint for anti-PD-L1 combination, blocking the activity of detected sPD-L1.

Similarly, the extensive immune-phenotype gives relevant data for other combinations. We could speculate that induced IDO1 in the tumor hinders viral replications and is one of the re-tolerizing mediators after viral "immune-kick". Eventhough, IDO1 inhibitors failed to demonstrated clinical responses in metastatic melanoma[340] and pancreatic cancers [341], the combination of VCN-01 and IDO1 inhibitors should be assessed at least pre-clincally. Given that IDO1 starts raising as early as 6h in some patients and peaks at day 3, it seems that a co-administration on the same day is a suitable timepoint for combining both players and possibly top-up on day 3 where maximum levels are observed.

As well as efficacy, the Luminex results might supply data for overlapped toxicities in combinations. Agents that induce IL-6 and IL-10 should be avoided or administrated after 7-days of virus treatment. The CAR-T cell therapy produces cytokine syndrome release as adverse effects including the induction of IL-6. In consequence, the viral administration has to be carefully studied to avoid simultaneous toxicities. On the other hand, the strong induction of Th1 mediators by VCN-01 offers a promising immune-profile for combining the virus with CAR-T cells and other immunotherapies.

5. CONCLUSIONS

- VCN-01 intravenous injection triggered a systemic immune response that was detected in serum concentration increases of immune markers in the three parts of the Clinical Trial P-VCNA-001.

- An early rise of IL-6, IL-10, IFNγ, IDO1, IP-10, and sLAG-3 serum concentrations were detected within the first 48 hours post-treatment, independently of chemotherapy.

- IL-10, IFNγ, IDO1, and IP-10 are markers of induced Th1 response and their serum increases were correlated.

- The concomitant combination with Gemcitabine and Abraxane reduced the serum concentration of IDO1 and sCD27 on day 8 after treatment.

- Most of serum immune markers induced normalize by days 15-28. Only the IP-10 levels remain slightly elevated by day 28.

- IDO1 is induced in tumors, and colocalizes with E1A viral protein and CD8 infiltration.

- IL-6 and IL-10 serum levels within the first 48hours after VCN-01 administration, positively correlated with the toxicity grade of adverse treatment effects. PAF induction did not correlate with treatment toxicity.

- The increase of IFNγ, sLAG-3, and neutralizing antibodies anti-Adenovirus 5 (NAbs) is associated with better antitumor efficacy.

CHAPTER B

ONCOLYTIC ADENOVIRUSES EXPRESSING TUMOR NEOEPITOPES AS VACCINES

1. INTRODUCTION

1.1. NEOEPITOPE CANCER VACCINES

Specific mutations in cancer cells could generate tumor-specific neoepitopes. A vaccine capable of inducing an immune response against the cancer neoepitopes has been a goal in the vaccination field. The strategy relies on the identification of non-synonymous mutations by tumor whole-exome sequencing (WES) or RNA sequencing (RNAseq), the prioritization of vaccine candidates, and the manufacture of the vaccine platform (RNA, DNA, SLP, or DC-based vaccine).

One of the first preclinical reports and relevant for this thesis is the work of Castle et al. They reported a neoepitope screening in the murine melanoma B16-F10 model, and antitumor efficacy by neoepitope peptide vaccines *in vivo* [342]. Then, preclinical data proved the neoantigen vaccination on murine tumor models of melanoma, colon carcinoma, sarcoma, glioma, and others [343–345]. The preclinical data led to test different settings of neoepitope vaccination in clinical trials.

The first trials in melanoma patients with neoepitope-loaded DCs demonstrated feasibility, tolerable toxicity, and specific-immune induction [346]. Following this, RNA and SLP vaccines were tested in advanced melanoma. Despite inducing vaccine-specific T cell responses (even *de novo*), they reported limited clinical activity as monotherapy; few regressions were achieved only in combination with anti-PD1 therapy [347,348]. More recently, two clinical studies with personalized neoantigen vaccines in patients with resected glioblastoma reported that, although the vaccine-triggered strong systemic T-cell responses, the majority of patients presented tumor recurrence [349,350].

The clinical trials provided a proof of concept that neoepitope vaccination can enhance the frequency of pre-existing or *de novo* neoantigen responses following immunization. Nevertheless, this induction of T cell response is rarely translated into clinical benefit. The observed responses in combination with checkpoint inhibitors, open an

opportunity of combinatorial approach; meanwhile, significant challenges have to be overcome.

1.1.1. Neoepitope vaccine limitations

There is evidence from the available studies that a small fraction of non-synonymous mutations identified by WES are processed, presented, and recognized by T cells [27,351,352]. In some cases, although selected neoantigens induced T-cell responses, they were not able to reject tumors in murine models [342,353,354] or target patients autologous melanoma cell lines [347]. These preclinical data explain the limited efficacy in clinical trials, suggesting that the identification and selection of relevant neoantigens is the main limitation of the vaccination approach.

Since the first clinical trials, several technological improvements have been made in the field. However, the neoantigen identification is still technically challenging, and all the steps involved can impact on the outcome. The actual pipeline for neoantigen identification is depicted in **Figure 35**. The WES from tumor and matched normal DNA are used to identify cancer-specific non-synonymous variations. RNAseq is used (when available) to confirm mutation expression. Then, candidates could be filtered by two strategies: *in silico* prediction of the likelihood to be immunogenic or direct elution of mutated peptides from tumor MHCs by immunopeptidomics. Finally, a variety of novel high-throughput immunological screening methods could be used to screen candidate neoepitopes that induce T cell responses.

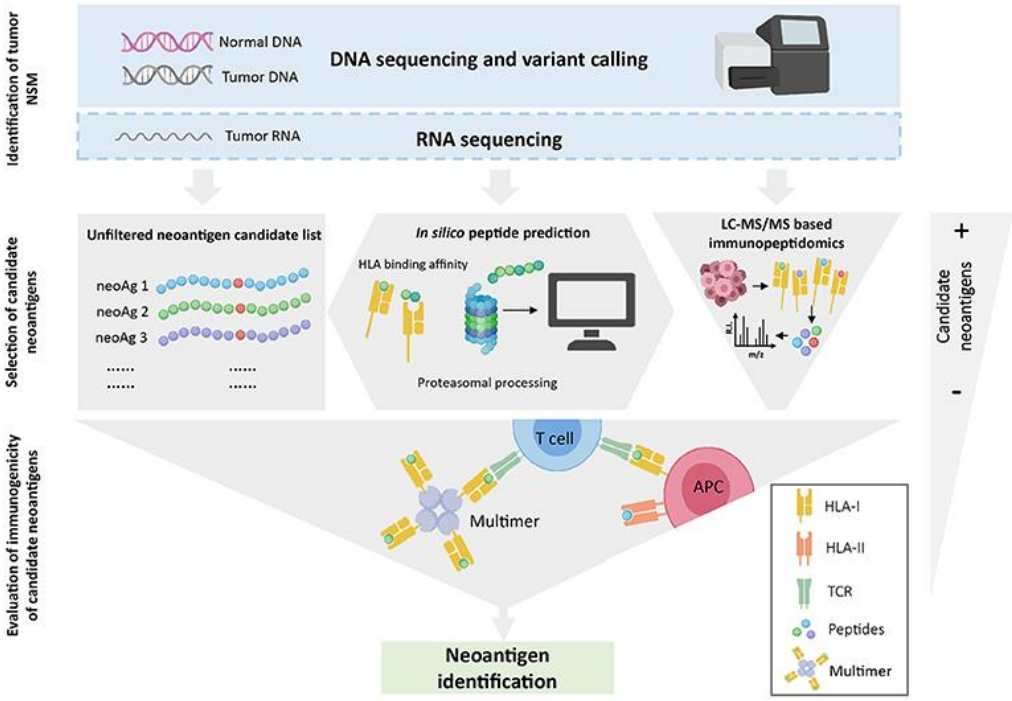

Figure 35. Overview of neoantigen identification. WES is performed on tumor and normal DNA to identify tumor-specific NSM. When available, RNAseq is used to select mutations that are expressed. Once NSMs are identified, three strategies can be used to select the list of candidate neoantigens that will be assessed for immunogenicity. The grey-filled shapes depict how each selection strategy will dictate the final number of candidate peptides to be evaluated. Note that *in silico* prediction initially increases the number of potential candidates but, after a ranking-based selection of peptides, this number decreases substantially. Finally, the immunogenicity of the selected candidate peptides is evaluated with different immunological screening assays. Image from [27]

The first step is the identification of tumor-specific mutations. Initially, only non-synonymous mutations were considered, but the improvements in the variant-calling algorithms also allowed to detect gene fusions and insertions or deletions (indels) variants. The indel mutations generate a remarkable percentage of immunogenic neoepitopes [355]. However, different algorithms considerably differ in their accuracy and sensitivity to detect somatic variants [356]. Consequently, a multiple and parallel mutations filtration is required to reduce the false positives, but reducing the potential to detect putative neoantigens (if they are not detected for all algorithms) [357–359].

The RNAseq is currently used to filter those neoantigens that are expressed in the tumor. It is the only method to identify putative neoantigens generated by alternative splicing, gene fusions, and post-transcriptional modifications. Moreover, recent findings demonstrated that many genomic regions previously annotated as non-protein-coding contain small open reading frames that are transcribed and translated into conserved microproteins. They are potentially processed and presented in the MHC as a new source of neoantigens, called cryptic neoantigens. In consequence, the RNAseq would be the only way to detect them as they have not been annotated in the human exome [360].

Furthermore, the tumor biopsy could influence in the neoepitope detection, as tumors are highly heterogenic. Depending on the biopsy, subclonal neoantigens might be detected, although they are irrelevant for the rest of the tumor. Thus, clonal mutations shared for as many cancer cells as possible have more therapeutic potential than subclonal mutations.

Once, putative neoantigens have been selected, a prioritization according to their immunogenicity is needed. The first approach is the *in silico* prediction with multiple algorithms available [361]. Algorithms capable of predicting peptide binding to MHC are the most widely used. Despite advances, these tools are still unreliable to predict which of peptides will be immunogenic. Only a few hundreds of candidates are immunogenic despite binding to MHC, reflecting that this is a limiting step in neoantigen screening.

The MHC binding prediction is a strong correlate of immunogenicity. However, accumulating data suggested a bias of *in silico* prediction toward strong binders overlooked immunogenic peptides with lower binding affinity. The first evidence was an algorithm based on the improved binding to MHC of neoantigen compared to the *wild-type* counterpart. The immunogenic peptides, predicted with this algorithm, presented MHC binding affinities higher than the threshold set by most of the MHC-binding predictors (<500nM) [353].

Furthermore, the patients from melanoma and glioblastoma trials appeared to favor $CD4^+$ over $CD8^+$ T-cell responses against immunizing peptides, even though these were predicted using HLA-I binding algorithms [347–349]. Altogether suggest that improved MHC-I and MHC-II binding algorithms need to be developed to predict immunogenicity. Nevertheless, the immunogenicity of given neoantigens does not necessarily translate into tumor rejection, thereby algorithms or screening tools capable of identifying neoantigens with the tumor-rejection ability might be crucial for the efficacy of cancer vaccination.

The tumor MHC immunopeptidome is used to prioritize candidate neoantigens, overcoming the prediction limitations. Immunopeptidomics (IS) is based on the elution of peptides from tumor MHCs and their identification by liquid chromatography and mass spectrometry [362,363]. IS substantially reduces the number of candidates and is the only unbiased method that directly interrogates the naturally presented MHC-bound peptides [364]. Moreover, MHC-eluted neoantigens could also derive from non-canonical or cryptic peptides [365]. As a caveat, IS requires large amounts of starting tumor material; in fact, the tumor biopsy size seems to be associated with the number of mutated peptides detected. Furthermore, depending on the amino acid composition, a fraction of peptides that are naturally presented could not be detected due to technical limitations [27].

Finally, immunogenicity testing has been a crucial step to detect neoantigens that trigger an immune response. Testing all candidates without filtration is another non-biased approach, meanwhile selecting the candidates from *in silico* prediction or immunopeptidomics is associated with mentioned limitations for each method. A variety of immunological high-throughput screening methods have been published [27]. Neoantigens encoded in minigenes concatenated conforming a tandem, or the use of peptide pools are the most common strategies to test the immunological response of candidates. However, their feasibility is restricted to tumors with a limited number of mutations, given the corresponding costs and efforts. If the tumor contains a high TMB, a prioritization step would be required.

Besides all the technical issues, the vaccine would face the historical immunoediting evolution of the tumor. During the immunosurveillance process, the tumor is under immune system pressure, and cancer cells constantly evolve to overcome the immune attack. This would also impair the vaccination because, as the neoantigen is immunogenic, the tumor probably has been developed mechanisms to bypass the response. For instance, lung cancers use different mechanisms to bypass neoantigen-specific T cells: a copy-number loss of previously clonal immunogenic neoantigens, the loss of heterozygosity of MHC, depletion of neoantigen expression by promoter hypermethylation of the gene [366].

In consequence, tumor vaccination might be useful to prime or boost specific antitumor T cells. However, a detailed study of tumor immune-evading mechanisms is imperative for a clinical benefit. Their combination with other therapies appears to be an obliged approach for the clinics.

1.2. ONCOLYTIC VACCINES

Although OVs can mediate the release of TAAs and TSAs through virus-mediated oncolysis and act as *in situ* cancer vaccine, few clinical complete responses have been reported. One approach to enhance the vaccination efficacy of OVs is to encode TAAs into their genome, to guide the triggered immune response towards the antigen, known as an oncolytic vaccine.

Various viral platforms have been armed with TAAs. A vaccinia virus codifying for an HER2/neu TAA controlled the tumor growth of an aggressive orthotopic model [367]. Genetically modified Maraba viruses (MG1) encoding for different TAAs were validated preclinically [368]. MG1 oncolytic vaccine for human melanoma-associated antigen-A3 (MAGE-A3) is being tested in clinics after priming with an Ad-MAGE-A3 vector (NCT02285816), known as a heterologous prime-boost setup. Our group has used ICOVIR15 to express TAAs fused to E3-19K, enhancing the presentation of exogenous epitopes in TAP-deficient cancer cells *in vitro* and the generation of higher specific immune responses *in vivo* [369].

Another strategy to enhance OV-induced tumor-specific T cell responses is the coating viral capsids with TAAs. Capasso et al. coated the OAd capsid with melanoma TAAs triggering $CD8^+$ specific populations and eradicating established melanoma tumors in mice [370]. Similarly, intratumorally injections of HSV-1 and vaccinia viruses coated with modified tumor epitope peptides increased intratumoral and systemic peptide-specific T cell responses [371].

1.2.1. Viral immunodominance

Oncolytic vaccines could direct immune responses to a TAA. However, one of the main concerns after oncolytic virus treatment is that anti-viral immune responses are much more efficient than antitumor triggered responses. The virus is cleared as soon as 1-2 weeks after administration; meanwhile, the tumor prevails in most cases. Multiple factors characterize the biased immune response. Although pre-immunity against OAd and also tumor (tumor immunosurveillance) exist, the anti-viral immunity did not suffer tolerogenic conditioning in contrast to antitumor CTLs (escape phase). Moreover, tumor neoepitopes might differ in one amino acid from the wild-type peptide for which lymphocytes have been educated in the thymus during the central tolerance process. Conversely, the viral epitopes are highly immunogenic (no central tolerance education).

Furthermore, T cells are known to compete with each other during their genesis and maturation to a complex antigenic challenge leading to epitope dominance and epitope interference [372,373], known as immunodominance. The adenoviral epitopes have been reported to mask immune responses to exogenous epitopes in vaccination. The immunodominance is more intense if patients have been pre-exposed to the epitope, as Ad5 in humans. Adenoviral immunodominance could bias the immune response towards the virus instead of the tumor. This dominance has not been clearly reported in cancer; on the contrary, Woller et al. suggested that OAd infection boosts the antitumor CTL repertoire [374].

It has been postulated that at early timepoint post-OV administration, the viral antigens are more abundant than tumor epitopes in the dying/phagocytosed infected

cells. The host machinery is sequestered to produce viral proteins shutting off of the cell protein production. Consequently, the infected cells mainly express and present viral antigens. The tumor:viral antigen ratio might increase along the time when the virus is eliminated [178]. This might explain the lack of epitope interference, although it needs further evaluation. In any case, the viral immunodominance and biased tumor:viral ratio explain the intense anti-viral immune response over the antitumoral.

Studies that distinguish the antiviral and the antitumoral immune response in the clinics are crucial but seldom done. Anti-viral immunity has been proposed as a limiting factor for OV success in patients. Conversely, reports suggesting that anti-viral responses can enhance the OV-therapy have been published [129,130]. Furthermore, we have reported in chapter A that VCN-01 treatment induced an immune response in patients. Although further analyses have to be performed for clear conclusions, taking observations and bibliography together, we suggest that these responses were mainly against the virus. However, they correlated with VCN-01 efficacy in patients.

Despite controversial issues about anti-viral immunity, a more balanced immune response between the virus and the tumor might be beneficial for the therapy. In this chapter, we propose the novel use of an oncolytic adenovirus as a “personalized oncolytic vaccine”.

2. OBJECTIVES

The main objective of this chapter is to generate oncoltic adenoviruses encoding for tumor neoepitopes.

Hypothesis: An oncolytic adenovirus expressing tumor neoepitopes enhances the immune response towards the tumor and, improves the efficacy of the treatment.

Specific objectives:

- To identify tumor neoepitopes in the B16-F10 and CMT64.6 murine models.
- To generate oncolytic adenoviruses encoding tumor neoepitopes of B16-F10 or CMT64.6.
- To evaluate neoepitope expression by oncolytic adenoviruses and their presentation *in vitro*.
- To determine the immune responses against the tumor neoepitopes upon mice immunization.
- To evaluate the antitumor efficacy of oncolytic adenoviruses expressing tumor neoepitopes *in vivo*.

3. RESULTS

3.1. IMMUNE CHARACTERIZATION AND NEOEPITOPE PREDICTION OF B16-F10

The B16-F10 cell line from a murine melanoma of C57BL/6 mouse strain has been used as a model for several immunotherapy regimes, with a highly resistant phenotype. Nonetheless, antitumor activity was reported in this model with RNA neoepitope vaccination. In consequence, we considered B16-F10 to test our hypothesis. First, we assessed the expression of the MHC-I alleles: H2-Kb and H2-Db by flow cytometry. Few B16-F10 cells exposed H2-Kb (31%) and Db (2%) on their surface, but these percentages significantly increased to almost 100% of cells after murine IFNγ incubation (Figure 36-**A, B**).

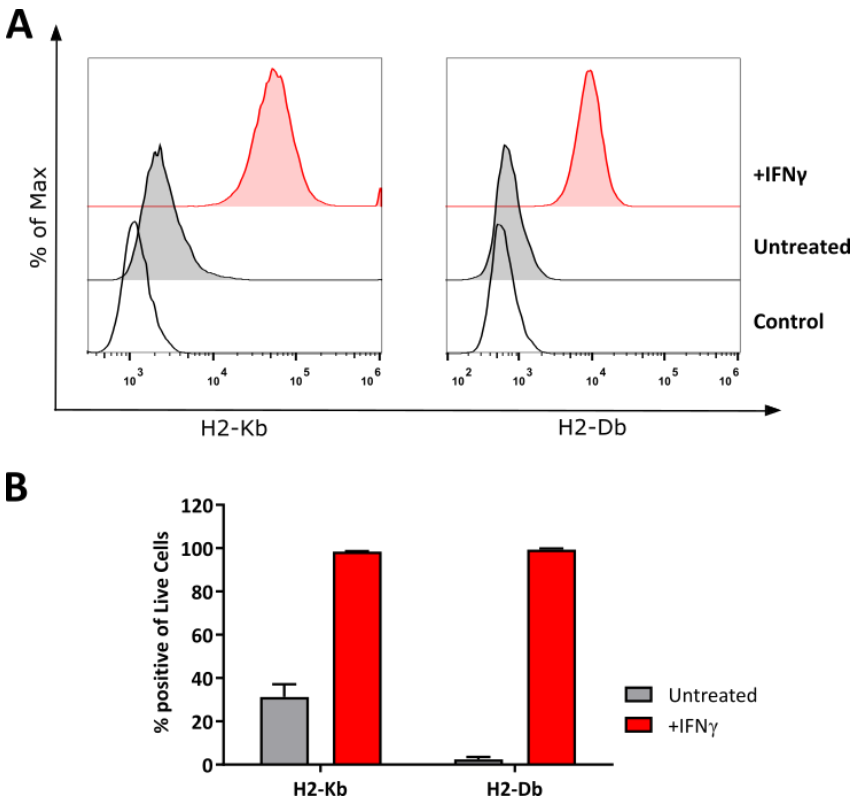

Figure 36. MHC-I levels of B16-F10 cell line. (A) Flow cytometry histograms representing the H2-Kb (left) and H2-Db (right) positive cells from the total live cells. **(B)** Percentage of positive live cells for murine MHC-I alleles after murine IFNγ treatment (400U/mL, O/N aprox. 12-16hours).

RNA from B16-F10 was extracted and purified. After checking the quality of RNA, it was sequenced at "Centre Nacional d'Anàlisi Genòmica" (CNAG) as explained (see 787.6.1, Materials and Methods). Reads from RNA sequencing (RNAseq) were mapped into a reference genome of C57BL/6 (mm10) to identify mutated transcripts. These transcripts were filtered for those that generated a missense or non-synonymous mutation, discarding insertions, deletions, codon stop gain/loss, and synonymous mutations. Only non-synonymous mutated transcripts with a corresponding fully sequenced protein in the Uniprot database were considered for epitope prediction purposes. Moreover, in the case that neoepitope was shared for different protein isoforms only the isoform-A was chosen, obtaining a total of 529 unique neoepitopes. Next, for each of these unique neoepitopes, we generated a 19 amino acid sequence centered in the mutation and also the corresponding *wild-type* peptide.

The 19mers were analyzed by NetMHCpan v2.8 server to infer putative 8 or 9mers immunogenic peptides for H2-Kb or H2-Db alleles. According to the software, a strong binder to MHC-I was defined for IC_{50}<50nM or rank<2%. Those sequences that contained a strong mutated binder into its sequence and a corresponding non-binder wild-type peptide were considered for the oncolytic vaccine. Moreover, the candidate neoepitopes should have a minimum of RNAseq coverage (number of reads), a high percentage of mutated reads (to discard subclones). Finally, those neoepitopes that at this cribbage stage were also published in the work of Castle et al.[375] were also included.

After to this prioritzation (**Figure 37**), minigenes with cDNA coding for 27mer centred in the selected neoepitope were generated. The Mut17, Mut25, Mut 44 were selected because they were already published. The β3galt6, Herc2, Nckipsd, and Rfwd3 were chosen as mutated peptides were predicted as binders in contrast as their *wild*-type counterparts (**Supplementary Table 4**, Annex). Furthermore, two peptides from ovalbumin: Ova257 and Ova323 were used as positive controls (**Supplementary Table 3,** Annex). They were reported as immunogenic in C57BL/6 mice. All selected minigenes (**Table 16**) were assembled in tandem.

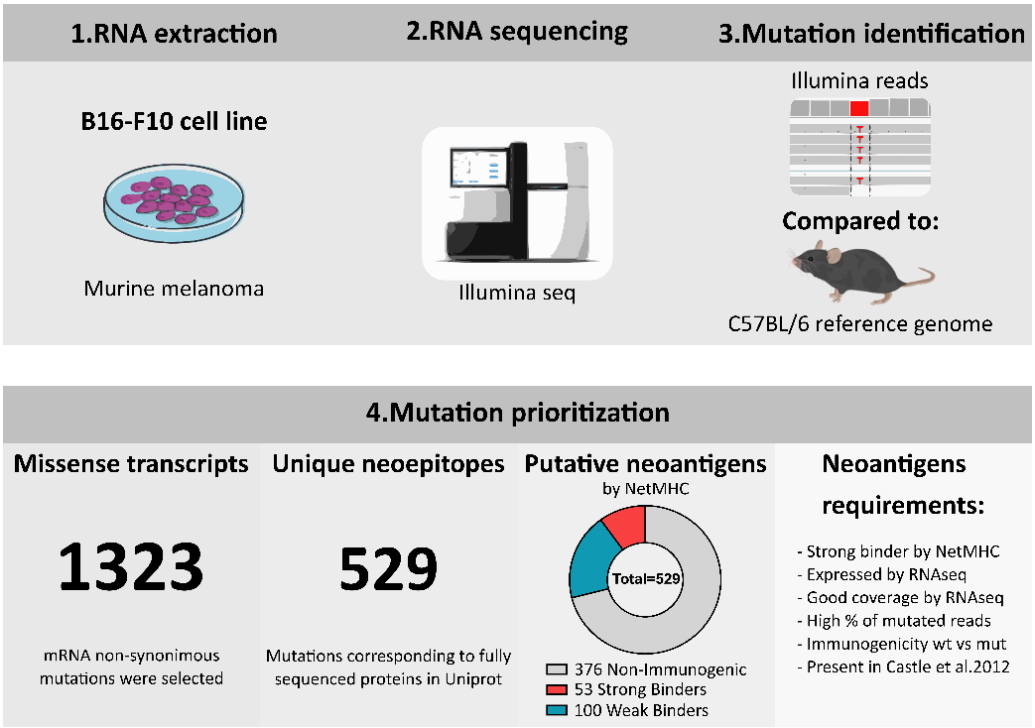

Figure 37. Pipeline of neoepitope identification and prioritization in B16-F10 cell line.

Table 16. Selected neoepitopes to generate B16-F10 Tandem Minigenes (TMG). Pos: position in TMG, Mut: mutation (*wild-type* amino acid-amino acid position-mutated amino acid), PK3:protein kinase-3, Ox: oxoglutarate

Pos.	Minigene	Gene	Protein name	Mut.	Minigene sequence (mutated AA)
1	OVA257	*Serpinb14*	Ovalbumin	#257-265	SIINFEKL
2	Mut44	*Cpsf3l*	Integrator complex subunit 11 (INT11)	D314N	EFKHIKAFDRTFA**N**NPGPMVVFATPGM
3	β3galt6	*B3galt6*	β-1,3-galactosyltransferase 6	R228L	VLSADLVHYLRLS**L**EYLRAWHSEDVSL
4	Herc2	*Herc2*	E3 ubiquitin-protein ligase HERC2	A4219D	CGSQFSVALTKSG**D**VYTWGKGDYHRLG
6	Nckipsd	*Nckipsd*	NCK-interacting protein with SH3 domain	K492N	LARDMQTDTQDHQ**N**LCYSALVLAMVFS
7	Mut25	*Plod2*	Procollagen-lysine,2-Ox. 5-dioxygenase 2	F530V	STANYNTSHLNND**V**WQIFENPVDWKEK
8	Rfwd3	*Rfwd3*	E3 ubiquitin-protein ligase RFWD3	G28V	SEMDHEVIYSHLQ**V**PLEGTIEPATPTE
9	Mut17	*Tnpo3*	Transportin-3	G504A	VVDRNPQFLDPVL**A**YLMKGLCEKPLAS
10	OVA323	*Serpinb14*	Ovalbumin	#323-340	ISQAVHAAHAEINEAGR

3.2. AN ONCOLYTIC ADENOVIRUS ENCODING B16-F10 TUMOR NEOEPITOPES

We have previously reported the generation of the oncolytic adenovirus ICOVIR15 (ICO15). It is an E1a-Δ24-based Ad which incorporates palindromic E2F binding sites in *E1a* promoter and contains an RGD motif in HI-loop of the adenovirus' fibre[376]. The 6.7K and 19K proteins from adenovirus' *Early 3* gene retain MHC-I in the endoplasmic reticulum avoiding the epitope presentation on the infected cell surface. In the context of this thesis, these genes were deleted to obtain ICO15d6.7/19K (**Figure 38-A**), which was used as a platform to incorporate the Tandem minigene (TMG) under a constitutive CMV promoter (**Figure 38-B**). As it was described, late genes are not translated in murine cell lines [377,378], so working in murine C57BL/6 model implied the use of CMV promoter for transgene expression in this model.

Selected neoepitopes from B16-F10 were designed as a cDNA encoding the epitope as a 27mer aminoacid centered in the mutation, also known as minigenes. The minigenes were concatenated one after the other, generating a tandem-minigene (TMG). The transgene also included a 5' β-globin untranslated region (UTR) upstream TMG and 3' β-globin UTR downstream to confer RNA stability to the transcript, as described [379]. Moreover, the signal peptide from MHC-I and its MHC class I trafficking signal (MITD) were included immediately upstream and downstream TMG respectively to enhance neoepitope presentation, as it was previously published [375,380,381] (**Figure 38-C**).

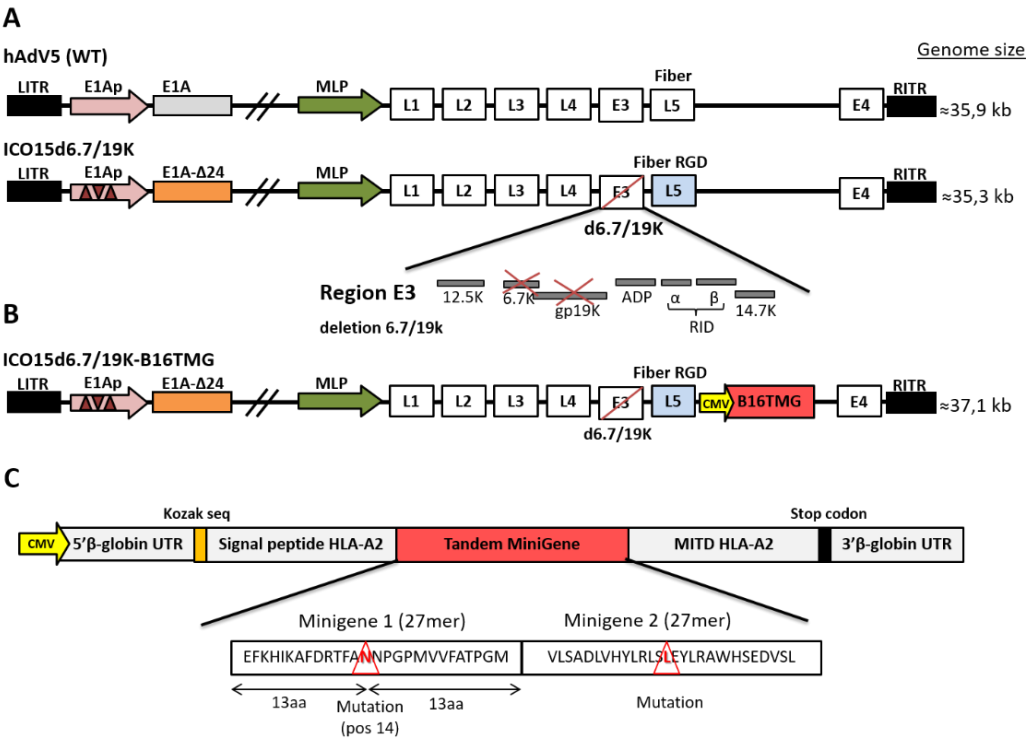

Figure 38. Schematic representation of OAds used in this thesis. (A) ICO15d6.7/19K genome characterised for: E2f boxes in E1a promoter (brown triangles), a deletion in E1a gene (Δ24), a deletion of 6.7K and 19K genes and an RGD motif in the HI-loop of the adenovirus fibre. **(B)** This modified virus was used as a platform to introduce the B16-F10 Tandem minigene (B16TMG) under CMV promoter (CMVp) control, generating the ICO15d6.7/19K-B16TMG. **(C)** Detail of B16TMG structure. UTR: untranslated region, MITD: MHC-I trafficking signal.

3.2.1. Generation and characterisation of ICO15d6.7/19K-B16TMG

The newly generated virus ICO15d6.7/19K-B16TMG and the parental virus were successfully rescued, plaque isolated and purified. Then, their oncolytic properties were tested by dose-response cytotoxicity assays with human A549 (**Figure 39-A**) and murine B16-F10 (**Figure 39-B**) tumor cell lines. We observed a 2-fold loss of cytotoxicity of ICO15d6.7/19K-B16TMG compared to the parental virus in A549 and B16-F10. Furthermore, if we compare the IC_{50} values between cell lines, we could confirm that, as expected, the B16-F10 is resistant to viral replication with an IC_{50} more than 600 times higher than a permissive cell line such as A549 (**Figure** 39-**C**).

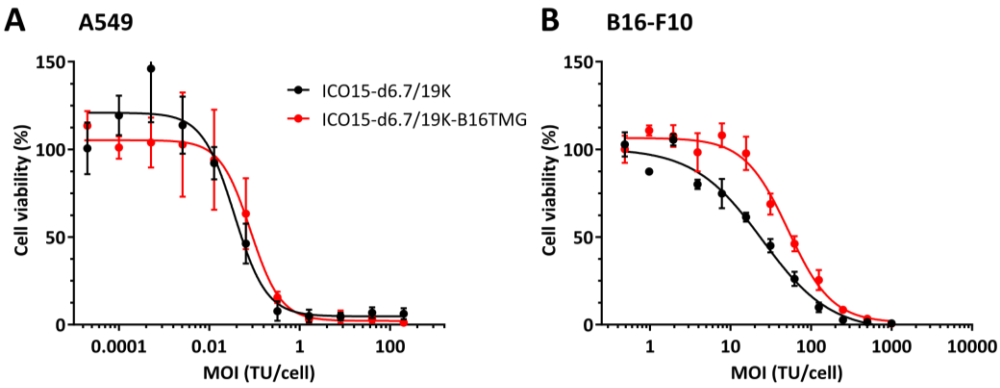

C

Cell line	IC_{50} ICO15d6.7/19K	IC_{50} ICO15d6.7/19K-B16TMG	Fold decrease vs ICO15d6.7/19K
A549	0.036 ± 0.013	0.081 ± 0.028	2.25x
B16-F10	24.78 ± 4.91	52.16 ± 7.99	2.1x

Figure 39. Oncolytic properties of ICO15d6.7/19K-B16TMG *in vitro*. (A) A549 cells were infected with serial 1:3 dilutions from 200 transfecting units per cell (TU/cell). After four days post-infection the cell viability was assessed by bicinchoninic acid assay (BCA). **(B)** B16-F10 cells were infected with serial 1:2 dilutions from 1000 TU/cell. After four days, cell viability was tested by BCA. **(C)** Summary table with the multiplicity of infection (MOI) to obtain 50% of cell viability, also known as 50% inhibition concentration (IC_{50}). The values represent the mean of triplicates ± SD. The fold decrease (IC_{50} TMG virus:IC_{50} parental virus) is represented at the fourth column.

3.2.2. Cells infected with ICO15d6.7/19K-B16TMG express and present the OVA257 epitope from the Tandem Minigene

To confirm transcription, translation and eventually presentation of epitopes from the Tandem Minigene (TMG), a dendritic murine cell line (JAWs-II) was pulsed with Ova257 peptide (SIINFEKL) or infected with ICO15d6.7/19K-B16TMG, which encodes for this peptide within the TMG. We had available an antibody to detect the SIINFEKL peptide bound to the H2-Kb molecule. Then 24hour post-pulsing or infection, the H2-Kb allele presenting the peptide was assessed by flow cytometry staining. Virus-infected cells and peptide-pulsed cells showed similar percentages of live cells presenting Ova257 on the cell surface loaded in H2-Kb (**Figure 40**).

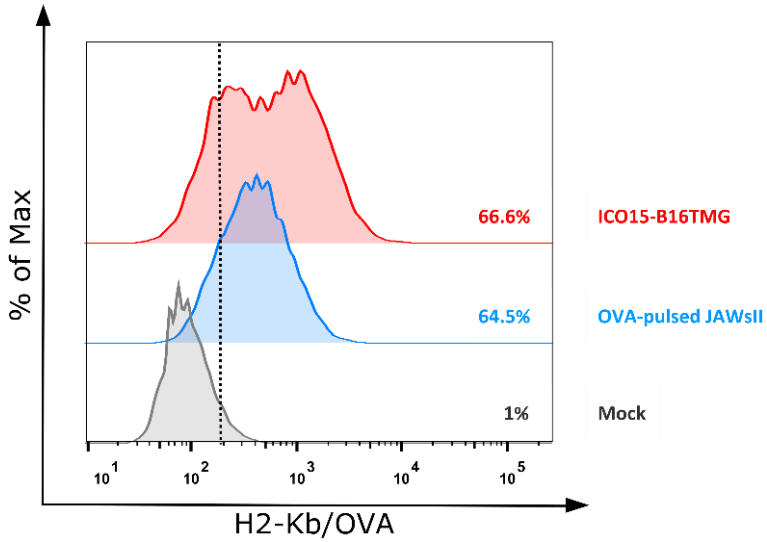

Figure 40. Ova257 peptide presentation on the JAWs-II cell surface via H2-Kb. JAWs II cells were infected with ICO15-B16TMG at 3000vp/cell or pulsed with 100µM of SIINFEKL peptide during 24hours. The histogram is representing the live cells with presented Ova257 by H2-Kb molecule on the cell surface of murine dendritic cells. It was detected by flow cytometry.

3.2.3. ICO15d6.7/19K-B16TMG induces an immune response *in vivo* against tumor neoepitope

Once minigene presentation was demonstrated *in vitro,* we wanted to address if it triggers an immune response *in vivo*. For this purpose, C57BL/6 mice were intravenously injected with 2e10vp/animal simulating a treatment with an oncolytic adenovirus. A week after treatment, their spleens were harvested and we performed an enzyme-linked immune absorbent spot assay (ELISPOT) to elucidate any IFN-γ immune response against TMG encoded neoepitopes. The expected immune response against viral E1b was observed exclusively in virus-treated animals. However, it was only statistically significant in the ICO15d6.7/19K group. As expected the immune response against the Ova257 epitope was elicited only in ICO15d6.7/19K-B16TMG group. Among the tumor neoepitopes, only a response against Mut17 was detected. This response was detected when the splenocytes were pulsed with 27mer peptide but not with the hypothetical most immunogenic 9mer by NetMHC prediction (**Figure 41**).

This highlighted that despite 27mer contained an immunogenic neoepitope, it was not the one predicted by NetMHC algorithm. The rest of neoepitopes were screened with 9mers or 27mers (data not shown) and no responses were observed. Similarly, OVA323 did not present any response (data not shown).

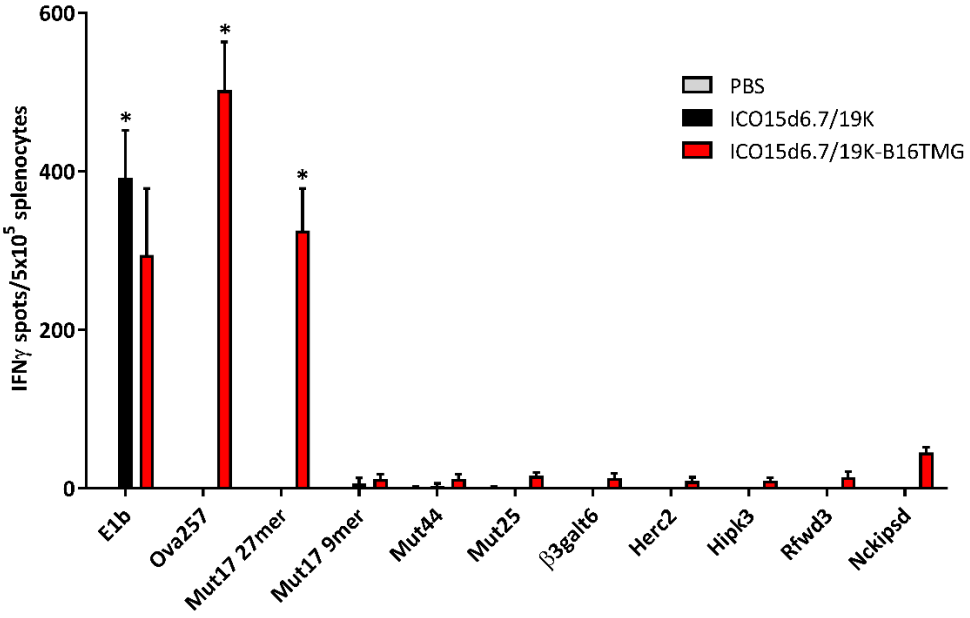

Figure 41. Immune response in vivo after ICO15d6.7/19K-B16TMG injection. C57BL/6 mice were injected with 2e10vp/animal of parental or B16TMG virus. One week after, the splenocytes were collected and screened by an IFNγ-ELISPOT. Splenocytes were incubated 48h with the corresponding stimulus: 27mer or predicted 9mer. The graph only represented the 27mer for Mut17, which was the only positive reaction. The rest were screened as well with 27mer or 9mer but did not induce spots. Thus only 9mer results are represented in the graph. *p<0.05 vs PBS by Kruskal-Wallis and Dunn's *post hoc* test, n=4 animals per group.

3.2.4. Linkers in TMG do not enhance the induction of an immune response against tumor neoepitopes

The results of **Figure 41** were somewhat surprising as, except for Mut17, the other previously published immunogenic neoepitopes did not trigger immune responses in our oncolytic vaccine setup. To further explore the immunogenicity of the oncolytic vaccine, we decided to reduce the number of neoepitopes encoded in TMG mimicking the poly-epitopes published by the same group that we based our TMG construction

[380]. Furthermore, we included the Mut30 neoepitope, which was one of the best candidates at Castle et al.[375], but did not pass our prioritization criteria in the neoepitope prediction. Additionally, we changed the minigene order within the tandem to discard that it conditioned the immunogenicity (**Table 17**), and we introduced linkers as spacers between minigenes, as published [1]. We generated two viruses encoding the same neoepitopes with or without linkers. The ICO15d6.7/19K-B16TMG2 and ICO15d6.7/19K-B16TMG2.L (with linkers) were successfully purified (**Figure 42**).

Table 17. Selected neoepitopes to generate B16-F10 TMG2. Pos: position in TMG, Mut: mutation (*wild-type* aminoacid-aminoacid position-mutated aminoacid), Ox: oxoglutarate.

Pos	Minigene	Gene	Protein name	Mut	Neoepitope sequence (mutated AA)
1	Mut25	*Plod2*	Procollagen-lysine,2-Ox. 5-dioxygenase 2	F530V	STANYNTSHLNND**V**WQIFENPVDWKEK
2	Mut44	*Cpsf3l*	Integrator complex subunit 11	D314N	EFKHIKAFDRTFA**N**NPGPMVVFATPGM
3	OVA257	*Serpinb14*	Ovalbumin	#257-265	SIINFEKL
4	Mut17	*Tnpo3*	Transportin-3	G504A	VVDRNPQFLDPVL**A**YLMKGLCEKPLAS
5	Mut30	*Kif18b*	Kinesin-like protein KIF18B	K739N	PSKPSFQEFVDWE**N**VSPELNSTDQPFL

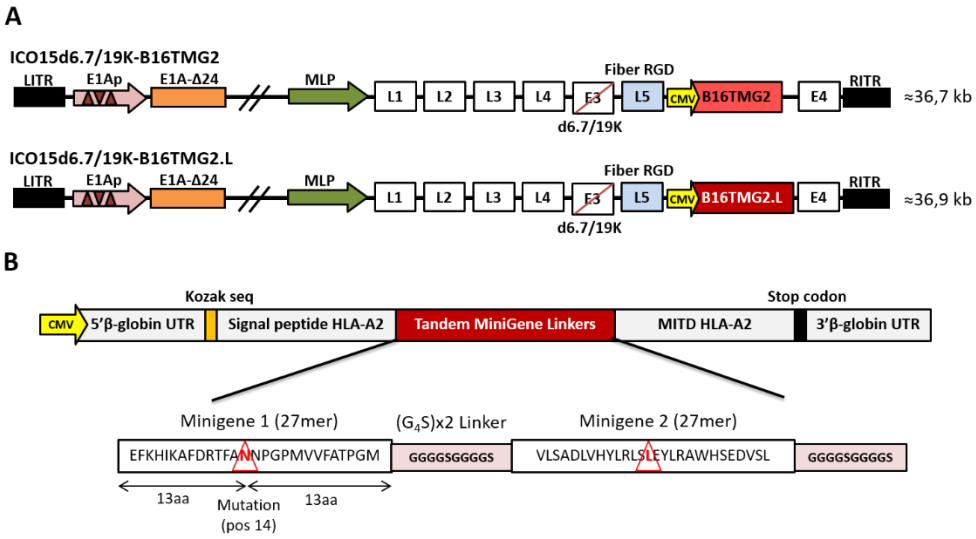

Figure 42. Schematic representation of B16-F10 TMG2 viruses. (A) Genome representation of ICO15d6.7/19K armed viruses with B16-F10 TMG2 without (top) or with linkers (down). **(B)** Detailed scheme of B16-F10 TMG2 with GS linkers (B16TMG2.L). UTR: untranslated region, MITD: MHC-I trafficking signal.

We tested these two new viruses *in vivo* in a similar experiment as before, where C57BL/6 mice were immunized intravenously with 2e10 vp/animal of the viruses and one week after treatment spleens were collected for an ELISPOT experiment. In this case, only 27mers were used for splenocyte analysis. IFNγ spots were significantly higher for E1b and OVA257 in virus treated groups compared to PBS, as expected. Nevertheless, no significant responses besides the Mut17, previously observed in **Figure 41**, were detected. Furthermore, Mut17 immune response was mostly lost when linkers were used in the TMG construction (ICO15d6.7/19K-B16TMG2.L, **Figure 43**).

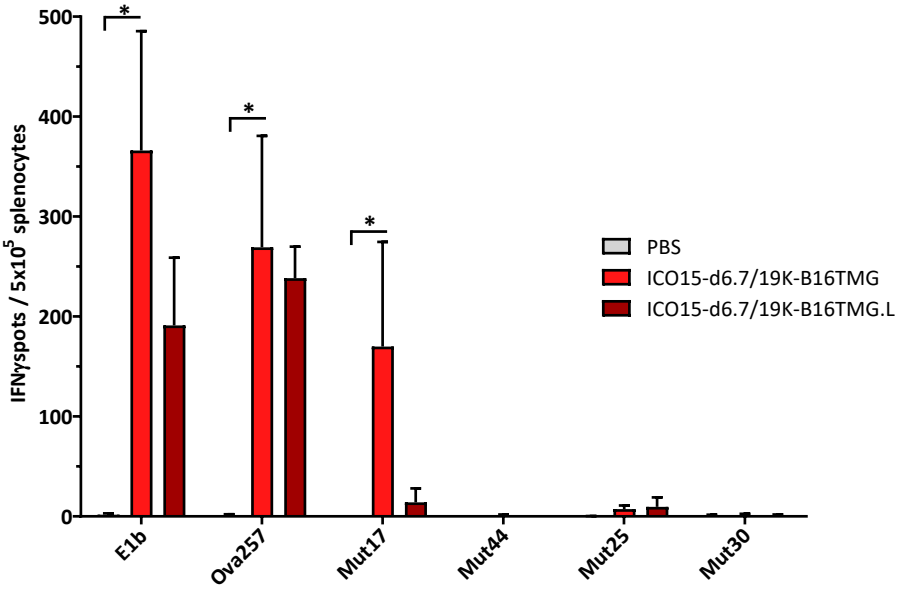

Figure 43. Evaluation of immune response *in vivo* against B16-F10 TMG with or without linkers. C57BL/6 mice were injected with 2e10vp/animal with different viruses. One week after, the splenocytes were collected and screened by an IFNγ-ELISPOT. Splenocytes were incubated 48h with corresponding 27mer stimulus**.** *p<0.05 vs PBS by Kruskal-Wallis and Dunn's *post hoc* test, n=3 animals per group.

3.3. IMMUNE CHARACTERIZATION AND ONCOLYTIC VACCINE FOR THE CMT64.6

To gain insight in the strategy we decided to use another immunocompetent murine model with different properties of B16-F10. Woller et al. have published a very relevant study on the immunogenicity of a pulmonary adenocarcinoma cell line from C57BL/6

called CMT64 [382]. They described CMT64 neoepitopes that were immunogenic after oncolytic adenovirus monotherapy treatment or in combination with anti-PD-1 immunotherapy. Besides, adenovirus replication is semi-permissive CMT64 and we have generated a subclone, the CMT64.6, with enhanced permissiveness [383].

To characterize the potential neoepitope presentation of CMT64.6 we assessed the H2-Kb and H2-Db levels with or without IFNγ pre-incubation. We observed moderate levels of H2-Kb (54%) and H2-Db (5%) at basal level compared to B16-F10 (31% and 2% respectively, see **Figure 36**). Also, they significantly increased after IFNγ stimulation exactly as we observed for B16-F10 model (**Figure 44**).

Taking these results together, we decided to sequence the RNA from this cell line to explore the possibility to generate an oncolytic vaccine codifying for CMT64.6 neoepitopes. A similar process as we did for B16-F10 cell line was performed. Briefly, the RNA was purified and sequenced at CNAG. Reads from RNAseq were filtered for coverage, missense mutations, and fully protein sequence in the Uniprot database until 469 unique neoepitopes were identified. For each of these unique neoepitopes, 19 amino acid sequences were selected centered in the mutation, for the *in silico* prediction. The 19mers were analyzed by NetMHC cons v1.0 server to infer putative 9mers immunogenic peptides for H2-Kb or H2-Db alleles. According to the software, a strong binder to MHC-I was defined for IC_{50} < 50nM or rank < 2%.

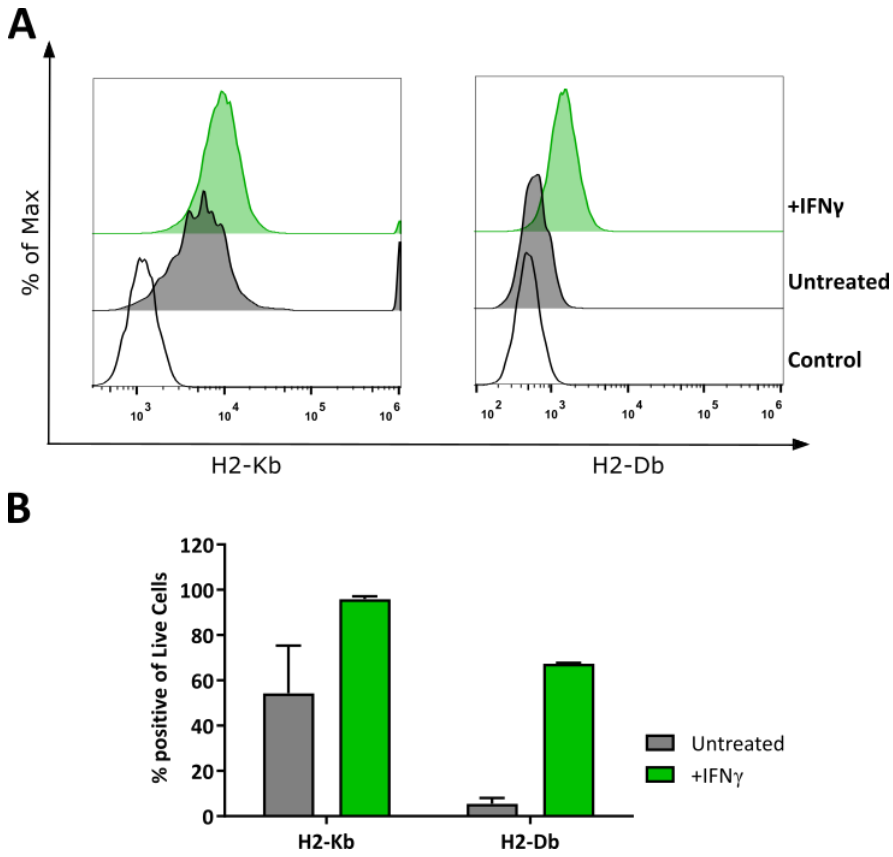

Figure 44. MHC-I levels of CMT64.6 cell line. (A) Flow cytometry histograms representing the H2-Kb (left) and H2-Db (right) positive cells from the total live cells. **(B)** Percentage of positive live cells for murine MHC-I alleles after murine IFNγ treatment (400U/mL O/N).

Surprisingly, only 60% of described neoepitopes in Woller et al. were present in our clone CMT64.6. Thus, every neoepitope reported as immunogenic in Woller et al and detected in our cell line was chosen for the oncolytic vaccine TMG independently of NetMHCcons prediction. Seven neoepitopes were selected according to this requirement. Then, we chose those sequences that contained a strong mutated binder by NetMHCcons without any consideration from the corresponding *wild-type* binding level. The candidate neoepitopes should have a minimum of RNA seq coverage (number of reads), a high percentage of mutated reads (to discard subclones).

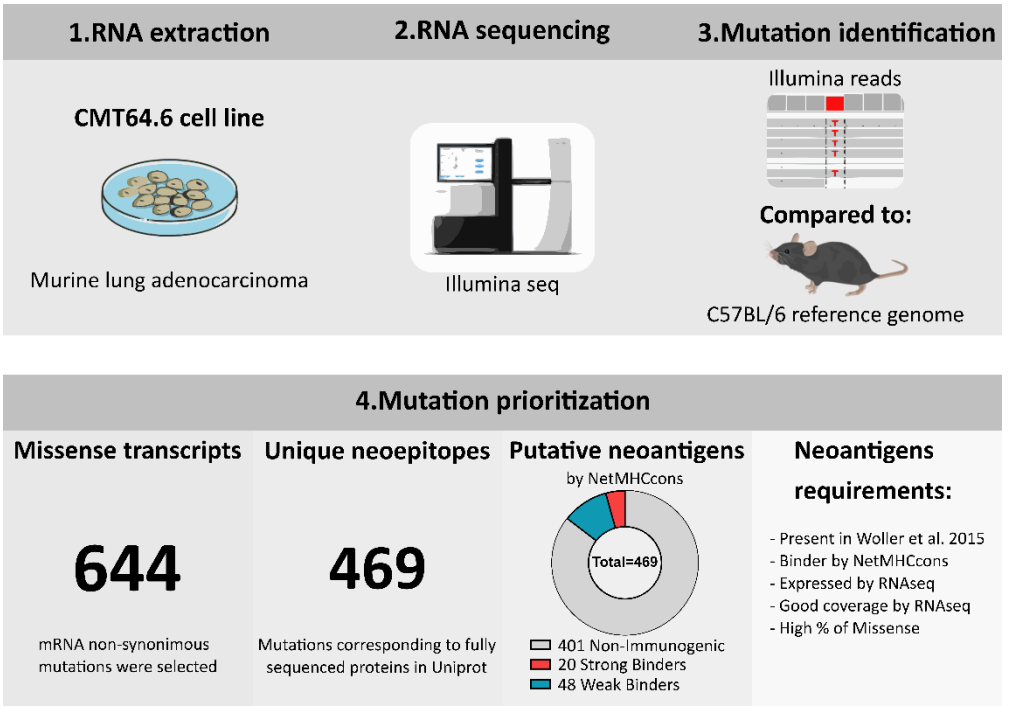

Figure 45. Pipeline of neoepitope identification and prioritization in CMT64.6 cell line.

With selected neoepitopes, a minigene was generated containing the cDNA sequence of a 27mer centered in the neoantigen (**Table 18**). The Pkhd1 and Itgav minigenes were chosen based on prediction (**Supplmentary Table** 5, Annex), the rest of minigenes were chosen as they were immunogenic in Woller et al [374]. Further, as for B16-F10 TMGs, the immunogenic peptide in C57BL/6 mice from ovalbumin, OVA257, was used as a positive control for immunogenicity. All selected minigenes were assembled in tandem.

Table 18. Selected neoepitopes to generate CMT64.6 TMG. Pos: position in TMG, Mut: mutation (*wild-type* aminoacid-aminoacid position-mutated aminoacid). * encoded by mitochondria; † isoform a

Pos	Minigene	Gene	Protein name	Mut	Neoepitope sequence (mutated AA)
1	Cep192A	*Cep192*	Centrosomal protein of 192 KDa	I2138T	AKTGCFQIINNSV**T**LLKFELYWPAHCL
2	Ndufs1	*Ndufs1*	NADH-ubiquinone oxidoreductase 75 kDa*	V491A	SSALQRDDGAAIL**A**AVSNMVQKIRVTT
3	Pkhd1	*Pkhd1*	Fibrocystin-L	L3813V	TRDGYVTFSRLAV**V**ISGSNWHLFFTVI
4	Nes	*Nes*	Nestin	S570L	PGKENCNSSIEEN**L**GTVKSPEKEKQTP
5	OVA257	*Serpinb14*	Ovalbumin	#257-265	AAASIINFEKLAAA
6	Arhgef10a.1	*Arhgef10*	Rho guanine nucleotide exchange factor 10†	M207I	LARWAADPANTAW**I**ENPEEAIYDDVPR

7	Arhgef10a.2	*Arhgef10*	Rho guanine nucleotide exchange factor 10[†]	G348R	DGLEKTKAAVKRG**R**SFIRTRSLVSQDH
8	Naip2	*Naip2*	Baculoviral IAP repeat-containing protein 1b	Y540N	IAFLWASGCCPLL**N**RFQLVFYLSLSSI
9	Itgav	*Itgav*	Integrin alpha-V	A921S	ITCQVGRLDRGKS**S**ILYVKSLLWTETF
10	Rab13	*Rab13*	Ras-related protein Rab-13	K196N	KPSSTGLKTSDKK**N**NKCLLG (13mer)

3.4. AN ONCOLYTIC ADENOVIRUS ENCODING CMT64.6 TUMOR NEOEPITOPES

The same strategy adopted for the viruses in B16-F10 model (detailed in 3.2.1) was followed to construct the ICO15d6.7/19K-CMT64.6TMG (**Figure 46-A,B**). An E1a-Δ24-based Ad which incorporates: palindromic E2F binding sites in *E1a* promoter, contains an RGD motif in HI-loop of the adenovirus' fiber and 6.7K and 19K deletion from *Early 3* gene was used as a platform to incorporate a transgene encoding the CMT64.6 neoepitopes after fiber under CMV promoter. The selected neoepitopes from CMT64.6 were designed as cDNA sequences encoding 27mer aminoacid centred in the mutation, also known as minigenes. The minigenes were concatenated one after the other, generating a tandem-minigene (TMG). The transgene also included a 5' β-globin untranslated region (UTR) upstream TMG and 3' β-globin UTR downstream to confer RNA stability to the transcript. Moreover, the signal peptide from MHC-I and MHC class I trafficking signal (MITD) were included immediately upstream and downstream TMG respectively, to enhance neoepitope presentation as published [375,380,381].

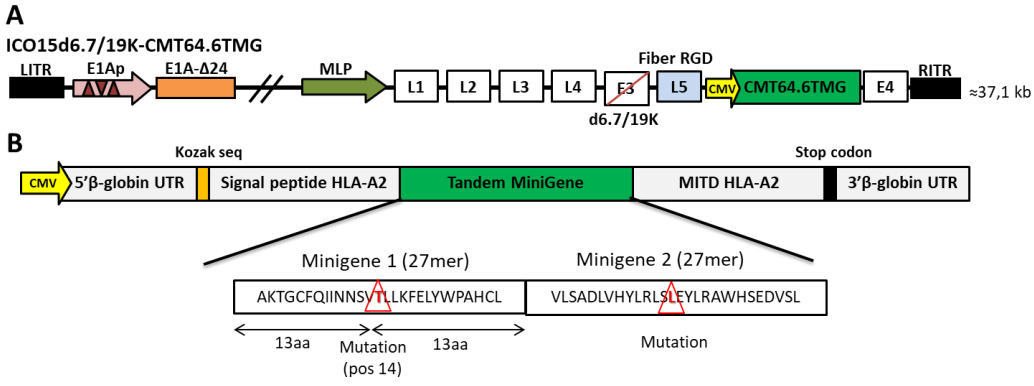

Figure 46 Schematic representation of ICO15d6.7/19K-CMT64.6TMG. (A) Genome representation of ICO15d6.7/19K armed viruses with CMT64.6 TMG. **(B)** Detailed scheme of CMT64.6 TMG. UTR: untranslated region, MITD: MHC-I trafficking signal.

3.4.1. Generation and characterization of ICO15d6.7/19K-CMT64.6TMG

ICO15d6.7/19K-CMT64.6 was successfully rescued, plaque isolated and purified. The oncolytic properties of the modified virus were assessed by dose-response cytotoxicity assays in human A549 and murine CMT64.6 cell lines after 4 days of infection. A loss of cytotoxicity of the TMG-virus was observed in A549 cells and CMT64.6 compared to the parental virus (**Figure 47-A, B**), ICO15d6.7/19K-CMT64.6TMG had an IC_{50} of 6 and 4 times higher than ICO15d6.7/19K respectively (**Figure 47-C**). However, the obtained IC_{50} value of ICO15d6.7/19K in CMT64.6 cell line (2,66 TU/cell) was 10-fold lower than B16-F10 cell line (24,78 TU/cell, see **Figure 39-C**). This confirmed that the CMT64.6 clone is more permissive to adenovirus replication or oncolytic effect than B16-F10.

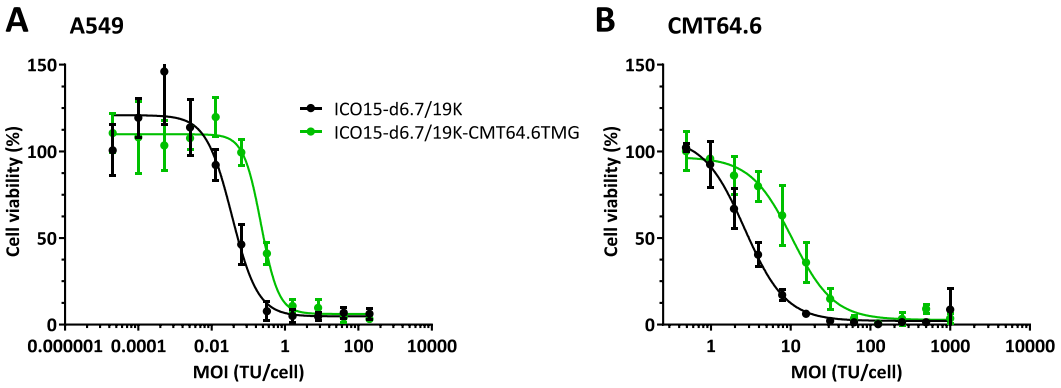

C

Cell line	IC_{50} ICO15d6.7/19K	IC_{50} ICO15d6.7/19K-CMT64.6TMG	Fold decrease vs ICO15d6.7/19K
A549	0.036 ± 0.013	0.221 ± 0.051	6x
CMT64.6	2.66 ± 0.45	10.45 ± 1.86	3.93x

Figure 47. Cell cytotoxicity of ICO15d6.7/19K-CMT64.6TMG *in vitro.* (A) A549 cells were infected with serial 1:3 dilutions from 200 transfecting units per cell (TU/cell). After four days post-infection the cell viability was assessed by bicinchoninic acid assay (BCA). **(B)** CMT64.6 cells were infected with serial 1:2 dilutions from 1000 TU/cell. After four days, cell viability was tested by BCA. **(C)** Summary table with the multiplicity of infection (MOI) to obtain 50% of cell viability, also known as 50%

inhibition concentration (IC_{50}). The values represent the mean of triplicates ± SD. The fold decrease (IC_{50} TMG virus: IC_{50} parental virus) is represented at the fourth column.

3.4.2. ICO15d6.7/19K-CMT64.6TMG induces an immune response *in vivo* against tumor neoepitope

To assess the immunogenicity of the tumor neoepitopes encoded in ICO15d6.7/19K-CMT64.6TMG, C57BL/6 mice were immunized and seven days later splenocytes were interrogated for IFNγ-immune response by an ELISPOT, similarly, as we did with B16-F10 model. The expected significant responses against the E1b virus epitope and against a mix of virus hexon epitopes were detected in virus-treated animals. The response against Ova257 was triggered only in ICO15d6.7/19K-CMT64.6TMG immunized animals, as a positive control of TMG. Most relevant, significant TMG neoepitope-induced immune responses were only detected for Ndufs1 from all screened neoepitopes, including the ones previously published [382] (**Figure 48**).

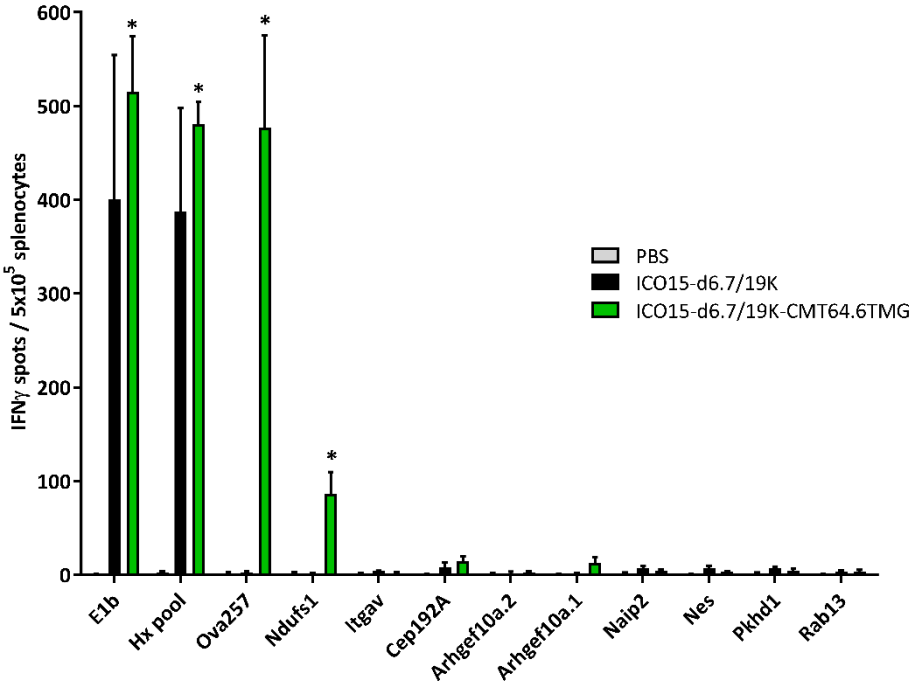

Figure 48 Immune response *in vivo* after ICO15d6.7/19K-CMT64.6TMG injection. C57BL/6 mice were injected with 2e10vp/animal of the different viruses. One week after, the splenocytes were collected and screened by an IFNγ-ELISPOT. Splenocytes were incubated 24h with the corresponding 9mer

peptides as the stimulus. Hx pool: adenoviral hexon protein pool. *p<0.05 vs PBS by Kruskal-Wallis and Dunn's *post hoc* test, n=4 animals per group**.**

3.4.3. ICO15d6.7/19K-CMT64.6TMG does not control tumor growth *in vivo* despite inducing anti-neoepitope responses.

Despite just one tumor neoepitope from the TMG induced an immune response, we decided to evaluate the antitumor efficacy of ICO15d6.7/19K-CMT64.6TMG. To this end, C57BL/6 mice bearing CMT64.6 tumors were treated in a two-arm experiment. A group of animals were intravenously injected with 3e10vp/animal when tumors reached 85mm^3 and tumor volume was monitored every two days. After 25 days, no tumor growth control was observed in viral treated groups compared to PBS (**Figure 49-A**).

In a parallel second arm, another set of animals were intratumorally treated with 3e10vp/tumor only in the right tumors, and their growth was monitored every 2 days and contralateral non-treated tumors were also monitored. At the endpoint, no differences were observed in non-treated tumors between PBS, ICO15d6.7/19K and ICO15d6.7/19K-CMT64.6TMG (data not shown). A slightly significant reduction in tumor growth was observed only at day 20 in ICO15d.6.7/19K injected tumors compared to the other two groups. However, antitumor activity cannot be concluded from this data (**Figure 49-C**).

3.4.3.1. ICO15d6.7/19K-CMT64.6TMG induces an immune response against tumor neoepitope *in vivo*

At the endpoint of the experiment, immune responses in intravenously (IV) and intratumorally (IT) treated mice were screened by an ELISPOT. Spleens were harvested and processed to obtain splenocytes and test them for IFNγ production after stimulation with CMT64.6 neoepitopes encoded by TMG.

The set of animals that were injected intravenously presented an evident activation of the immune system against the virus epitope E1b. The detected anti-E1b IFNγ-response

in ICO15d6.7/19K group was 2-fold higher in spots-count compared to ICO15d6.7/19K-CMT64.6TMG. The immunogenicity against Ova257 was also confirmed specifically for the animals that were treated with the TMG virus. Notably, a significantly strong immune response against neoepitope Ndufs1 was triggered only by ICO15d6.7/19K-CMT64.6TMG. In this group, the spots-count of Ndufs1 (mean=431 spots) was even higher than E1b (mean=148). Despite this strong immune activation against Ndufs1, there was no evidence of antitumor efficacy (**Figure 49-B**).

On the other hand, the intratumoral arm of this experiment was studied for the same immunty. Virus-treated groups were positive for E1b immunity, as expected, with comparable numbers as intravenously injected groups. Similar results were also obtained in Ova257 epitope; only the splenocytes from animals injected with ICO15d6.7/19K-CMT64.6TMG responded. However, no significant responses were observed for any of the CMT64.6 screened neoepitopes. Few spots-count were detected for Ndufs1 in the TMG treated group, 2-fold higher compared to PBS and parental group, but this weak response was not statistically significant (**Figure 49-D**).

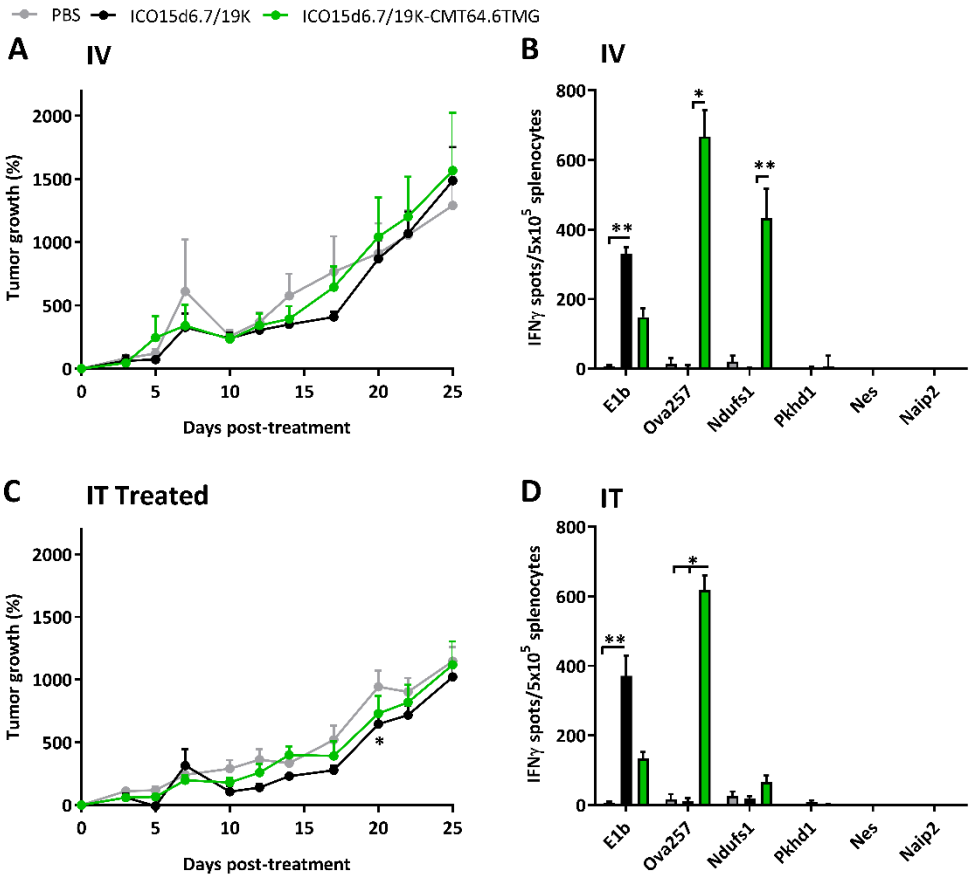

Figure 49. Antitumor efficacy and immune responses of ICO15d6.7/19K-CMT64.6TMG treatment (E016/18). C57/BL6 mice were implanted with CMT64.6 tumors when they reached a mean of 88mm3 were treated (A) with 3e10vp/animal intravenously and the tumor growth was monitored until day 25 (n = 5). (B) At the endpoint, animals were sacrificed and splenocytes were screened for immune responses by IFNγ-ELISPOT (n=5). *p<0.05, **p<0.01 significant by Kruskal-Wallis and Dunn's *post hoc* test. (C) In parallel, a set of animals were treated in the right tumor with 3e10vp/animal and their tumor growth was monitored until day 25, treated tumors are represented (contralateral non-treated tumors, data not shown).*p<0.05 vs PBS by Two-way ANOVA and Tukey's *post hoc* test. (D) At the endpoint, animals were screened for immune response by an ELISPOT against IFNγ (n=5). *p<0.05, **p<0.01 significant by Kruskal-Wallis and Dunn's *post hoc* test.

As the intravenous and intratumoral arms were performed in parallel, and splenocytes were screened in the same ELISPOT experiment, we were able to compare the immune induction of the same dose of virus intravenously or intratumorally. Checking the number of E1b IFNγ-spots induced in virus treated animals, we could not distinguish

significant differences between the route of administration. However, the ICO15d6.7/19K groups (both IV and IT) presented statistically significant higher anti-E1b immune responses than the ICO15d6.7/19K-CMT64.6TMG IT group and a tendency against the IV group. Regarding the anti-Ova257 immunity, it was found only in the TMG-virus treated animals as expected. Similarly, Ndufs1 responses were detected only in ICO15d6.7/19K-CMT64.6TMG treated mice. For this epitope, the IV route gave the highest spot-counts with differences statistically significant the IT route of administration (**Figure 50**).

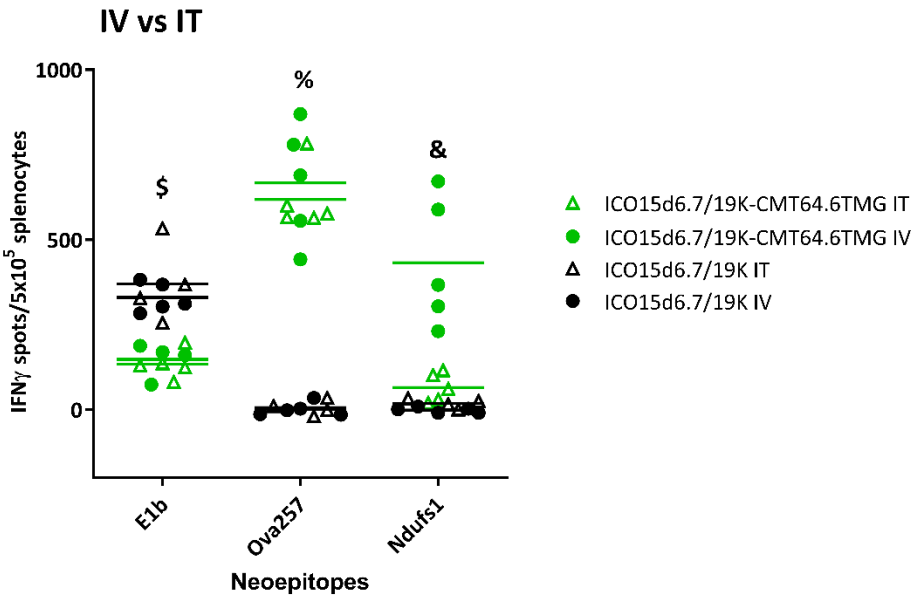

Figure 50. Immune response comparison after intratumoral or intravenous ICO15d6.7/19K-CMT64.6TMG treatment. The IFNγ spots-counts of each animal are represented. $ $p<0.05$ ICO15d6.7/19K IV and IT vs ICO15d6.7/19K-CMT64.6TMG IT. % $p<0.05$ ICO15d6.7/19K-CMT64.6TMG IT/IV vs ICO15d6.7/19K IV. & $p<0.001$ ICO15d6.7/19K-CMT64.6TMG IV vs ICO15d6.7/19K IV by Kruskal-Wallis and Dunn's *post hoc* test.

4. DISCUSSION

Cancer vaccines based on adenoviruses have been described with promising results [370], and RNA vaccines against murine melanoma's (B16-F10) neoepitopes have shown high antitumor efficacy preclinically [342,343], but limited responses in patients [347,348]. In consequence, there is a need to increase the efficacy of the therapy. We envisioned oncolytic adenoviruses expressing tumor neoepitopes as a "personalized oncolytic vaccine". The strong CTL/Th1 immune induction mediated by oncolytic adenovirus could enhance the efficacy of neoepitope vaccination in immunosuppressed environments, such as tumors. Moreover, the tumor neoepitopes might bias the anti-viral response towards cancer cells, a "win-win" strategy to bypass challenges for both therapies. We generated OAds encoding for neoepitopes of B16-F10 and murine lung adenocarcinoma (CMT64.6), as the first proof of concept for the feasibility of neoepitope oncolytic vaccine.

4.1. IMMUNOGENIC NEOEPITOPE IDENTIFICATION

Significant efforts have been focused on identifying immunogenic tumor neoepitopes. Different strategies are currently used to identify and prioritize tumor mutations in order to induce an immune response. During the course of this thesis, remarkable progress has been made in mutation prioritization steps (i.e., immunopeptidomics, improved *in silico* prediction algorithms). Nevertheless, to find an immunogenic neoepitope is still the bottleneck of these strategies.

We tried two different *in silico* prediction strategies. However, we primarily selected published immunogenic neoepitopes to reduce the prediction failure. In the B16-F10 model, we selected three candidates that passed our prioritization and were previously published as immunogenic in Castle et al. [342]: Mut17 (*Tnpo3*), Mut25 (*Plod2*), and Mut44 (*Cpsf3l)*. Notably, their *wild-type* counterparts also elicited some immune responses with less intensity. Then we chose 5 non-published neoepitopes with a high predicted MHC affinity (NetMHCpan software) for the mutated peptide and low MHC affinity for the correspondent *wild-type* peptide, as it was published to increase the

finding of immunogenic peptides [353]. The *ß3galt6*, *Herc2*, *Hipk3*, *Nckipsd*, and *Rfwd3* were selected.

Woller et al. tested the neoepitope immune response in the CMT64 murine model treated with an OAd, anti-PD-1, and the combination of both therapies. Interestingly, they reported a broader spectrum of immunogenic neoepitopes in the combination [374]. Our group isolated a clone from the CMT64 model with an enhanced permissiveness to adenoviral replication, the CMT64.6 [383]. Only 60% of published mutations in the parental cell line were present in our clone, thus those that were immunogenic in Woller et al. were directly selected as candidates for the oncolytic vaccine, as far as they were expressed (checked in RNAseq). Seven neoepitopes were included based on this criterion: *Ndufs1*, *Cep192*, *Nes*, *Arhgef10a.1*, *Arhgef10a.2*, *Naip2*, and *Rab13*. Then we predicted *in silico* (NetMHCcons software) two extra candidates: *Pkhd1* and *Itgav* independently of their peer *wild-type* peptide affinity.

4.2. ONCOLYTIC VACCINATION

Different strategies have been used to express tumor epitopes from oncolytic viruses as vaccines. Particularly in OAds, Capasso et al. coated the adenovirus capsid with TAA peptides, called PeptiCRAd [370]. However, this design allows one-round immunization; the viral progeny is not coated. Our group published an oncolytic adenovirus encoding for B16-OVA TAA in the HI-loop of the fiber or upstream of the *E3-19K* gene [369]. Adenoviruses stably accommodate 2kb of additional DNA beyond the size of the normal genome [384], thus this strategy did not allow large transgenes insertion (such TMGs ~2kb), and acted as a vaccine only when the viral cycle is completed (E3 expression, only in tumor cells).

No oncolytic virus expressing tumor neoepitopes as a vaccine was published when this project was conceived. We used the ICOVIR15 as a platform to encode the selected TMGs. Aiming to vaccinate as much as possible, we decided to express the TMG from every infected cell with a constitutive promoter (CMVp). The CMV-TMG cassette was higher than 2kb; consequently, adenoviral gene deletions were required to generate

viable viruses. The E3-6.7K and 19K are related with the evasion of immune system [385] [385–387]. Ad5 viruses with 6.7K/19K deletion had a reduced persistence in immunocompetent animals, suggesting that these two proteins are involved for the immune-escape, even in non-natural hosts [388]. We used a 6.7K/19K deleted virus (ICO15d6.7/19K) with the CMV-TMG cassette, expecting higher immunizing stimuli than previously described approaches.

We successfully generated OAds encoding for tumor neoepitopes. One virus for each model was produced: ICO15d6.7/19K-B16TMG and ICO15d6.7/19K-CMT64.6TMG. The TMG-expressing viruses showed some loss of cytotoxicity compared to the parental virus, probably due to a higher genome than parental. We also confirmed that B16-F10 cell line was not permissive to viral replication, and CMT64.6 clone had slightly more permissiveness. We demonstrated *in vitro* that TMG is successfully translated and loaded in MHC-I, by the Ova257 presentation in the H2-Kb molecule. Both viruses were tested in naïve immunocompetent mice by intravenous injection, simulating the ideal administration to treat a patient. Responses against the virus (E1b) and the Ova257 were detected in both cases one week after treatment, confirming the proper immunization. No significant differences in the anti-viral response were observed between TMG-viruses and parental.

The ICO15d6.7/19K-B16TMG elicited responses for only one tumor neoepitope out of eight. The Mut17 was induced at similar levels as published with long synthetic peptide (SLP) vaccine (300 IFNγspots/5e5 splenocytes) [342]. Unexpectedly, none of the other tumor neoepitopes induced IFNγ response. The splenocytes from immunized mice were screened with 9mers (based on the best NetMHC prediction) or 27mers, which include all putative neoantigens containing the mutation. Curiously, for Mut17 only the 27mer induced IFNγ secretion in splenocytes, but not the theoretical immunogenic 9mer. This result suggests that the epitope driving the immunogenicity is not the one with the highest MHC-I affinity, or that prediction is non-reliable, supporting that a failure in prediction may explain the lack of immunogenicity for the 5 neoepitopes selected based on our *in silico* prediction [389].

Most of the immunogenic responses against neoepitopes after vaccination in pre-clinical and clinical studies are $CD4^+$ responses [343,347–349], despite being predicted as MHC-I binders. A way to improve our results may be to predict the MHC-II binding, which enhances the finding of immunogenic peptides, as published [343]. Moreover, given that MHC binding is not necessarily translated into immunogenicity, algorithms predicting the immunogenicity are a requirement for the *in silico* prioritization viability.

In contrast, wrong-prediction does not explain the lack of reactivity of Mut25 and Mut44, as they were reported as immunogenic, as Mut17. Notably, the anti-Mut17 response was more intense than the anti-Mut25 or Mut44 [342]. We can hypothesize that only highly immunogenic peptides induce immune responses in the oncolytic vaccine setup, such as Ova257 or Mut17. It is worth to mention that there were differences between our screening method and the one by Castle et al. based on bone marrow dendritic cells pulsed with peptides or transfected with RNA encoding the minigenes as APCs in the ELISPOT, which may increase the sensitivity of the technique. In contrast, we directly assessed the splenocytes (variable number of APCs) stimulated with the minigene peptide (27mer), which may impact on the discrepant results.

To further explore our strategy, we decided to test only published B16-F10 neoepitopes. Taking advantage of a publication from the Sahin's group [343], we used their best neoepitope candidate, Mut 30 (discarded in our prediction, non-binder). We mimicked in the OAd the RNA poly-epitope that they used for vaccination, with only 5 neoepitopes: Mut17, Mut25, Mut 30, and Mut 44, with or without linkers in the TMG. According to our results, reducing the number of encoded neoepitopes, the order within TMG, and the presence of linkers between minigenes did not impact the immunogenicity. The only reactivity was again the anti-Mut17 and was hindered by the presence of linkers. Interestingly, Mut17 had been reported as immunogenic only after RNA vaccination but not with SLPs [343], whereas Mut25, Mut30, and Mut44 were immunogenic with both types of vaccines. Differential processing between exogenous peptides or endogenous peptides (RNA vaccine) could impact on these distinct

immunogenicities. However, further studies are needed to understand if it has real implications for an oncolytic vaccine.

The immunization of naïve mice with ICO15d6.7/19K-CMT64.6TMG, induced immune response against only one of 9 tumor neoepitopes. The predicted *Pkhd1* and *Itgav* did not induce an immune response; again, a non-accurate prediction might be the explanation. Among the published immunogenic neoepitopes, only anti-Ndufs1 IFNγ reactivity was detected. In Woller et al., lymphocytes reacting against Ndufs1 were robustly stimulated after viral treatment and anti-PD1 combination [374]. Furthermore, the Ndufs1 immunity was the highest among the neoepitopes that we tested. In this experiment, the splenocytes were stimulated with the same 9mers used in Woller et al.; thus, no technique differences sustain the divergences between our results and the published ones.

The result of *Ndufs1* converges with the reported in Mut17. The highest immunogenic neoepitopes in the previous publication are the only ones that triggered responses in our strategy. We postulate that competition between viral and TMG epitopes might mask the reactivity of less immunogenic TMG neoepitopes. The immune response biased towards viral epitopes is known as viral immunodominance, and it has been widely studied [390]. The adenovirus epitopes have been published to impair the immune response against encoded transgenes [391–393], in our case the TMG. We speculate that viral immunodominance affects only the simultaneous presentation of epitopes. Woller et al. published that OAd treatment enhances the epitope spreading [374], suggesting that previous immune responses against tumor neoepitopes were reactivated with virus injection without competition. Furthermore, an alternative combination of DNA vaccine and OAd treatment enhances the immune response against the vaccinated antigens, supporting this idea [394].

During the progress of this thesis, two publications related to our approach were published. D'Alise et al. used adenovirus derived from non-human great apes (GAd) as a genetic vaccine against CT26 and MC38 murine models. The authors selected 31 CT26

neoepitopes encoded in a TMG eliciting immune responses against 7 in naïve mice. For the MC38 model, they vaccinated with 6 out of 7 immunogenic neoepitopes [395]. Even more related, the EpicentRX company is clinically developing oncolytic adenovirus 5 encoding for tumor neoepitopes [396,397], as we intended in this thesis.

We demonstrated that oncolytic virus encoding for immunogenic tumor neoepitopes in a TMG triggers specific responses in naïve mice. We suggest that only those neoepitopes that induce high immunogenicity would be able to compete against viral epitopes during simultaneous immunization thereby would be suitable for an oncolytic vaccine. Thus we propose that a previous assessment of candidates' immunogenicity should be done in parallel with viral peptides to avoid prediction failures and ensure immune induction in coexistence with the virus. Moreover, a regime of a prime and boost with different viral agents, known as heterologous prime-boost, has reported to enhance specific immune responses from the encoded transgene over viral epitopes [398]. It has been tested in clinics [399] and could be interesting for the proposed therapy.

4.3. ANTITUMOR EFFICACY

We tested the therapeutic effect of oncolytic vaccination, despite only one neoepitope was immunogenic in our vaccines. We chose the CMT64.6 model as expressed higher basal levels of MHC-I, and it was more sensitive to adenoviral replication. Intravenously and intratumorally administrations of ICO15d6.7/19K-CMT64.6TMG were tested, but no antitumor activity was observed in established tumors. Although the induction of immune response against *Ndufs1* in IT or IV treated animals, it did not lead to tumor growth control. No reports of efficacy in established subcutaneous tumors were described after intratumoral treatment in Woller et al. Furthermore, the genetic vaccine from D'Alise et al. did not control tumor growth in established CT26 nor MC38 tumors. Only the combination with immune checkpoint blockade or a prophylactic setup presented tumor growth control activity [395]. Altogether suggests that established tumors cannot be controlled by triggered immune responses by oncolytic vaccines.

Ndufs1 could be an irrelevant immunogenic cancer neoepitope, which generates $CD8^+$ cells unable to recognize the tumor cell, due to insufficient presentation [354]. RNA expression is not a guarantee of sufficient MHC presentation; immunopeptidomics would bypass this limitation. Moreover, the syngeneic murine tumors come from a previously isolated tumor, which had been evolved to evade the immune system. This typically leads to a rapid escape phase and the outgrowth of the tumor models (as CMT64.6 or B16-F10). Their subcutaneous implantation induces local inflammation and putative immune detection of the injected cells (elimination, equilibrium phase), but rapidly ends into the escape phase (palpable tumors). In consequence, the effective window for immunotherapeutic vaccination is early and brief, and tumor control only occurs with early treated tumors [375,380], or prophylactic [395]. However, once the tumor has established, the vaccines need to overcome the immunosuppression (for instance, anti-PD-1/PD-L1).

According to the results, the virus is not enough to revert the immunosuppressing tumor microenvironment in this model (without proper replication). Despite no detected efficacy, our experiment provided some valuable data regarding the route of administration. The intensity of anti-Ndufs1 response was higher with intravenous injection than intratumoral. Viruses intravenously injected would reach multiple organs (mainly the liver), infect cells, and express the TMG, so induce anti-Ndufs1 reaction in multiple sites. In contrast, the intratumoral injection would be confined in the tumor, which after immunoediting, is an immunosuppressed environment. Thus our result put in value the relevance of intravenous injection for inducing immune responses against encoded epitopes.

4.4. STUDY LIMITATIONS AND FUTURE PERSPECTIVES

This chapter has several limitations. The selection of neoepitopes is crucial, and the common bottleneck for all neoepitope-targeted therapies. First, immunogenic neoepitopes have to be identified, and then they should be relevant for efficacy. The expression of appropriate neoepitopes from an oncolytic vaccine should have benefits (auto-amplifying vaccine) but presented some cons (viral immunodominance).

Assessing the immunogenicity of candidates in comparison with *wild-type* counterparts should be considered to confirm specific antitumor immune response induction. However, we were not able to test the complete significance of our approach due to human adenovirus does not replicate in murine cells, thereby auto-amplifying vaccination could not be evaluated. Moreover, syngeneic murine models usually are highly aggressive, and sometimes are not the best models for immunotherapeutic approaches [400].

In any case, our results are in line with the published, confirming that neoepitope vaccination from oncolytic adenoviruses does not control the tumor growth of established tumors. Prophylactic or combination with checkpoint inhibitors is needed for efficacy, which does not improve the previous pre-clinically or clinically data with RNA and SLP vaccines. Besides, the limited capacity of Ad5 to adquire transgenes larger than 2kb limits the vaccination capability. The great ape adenovirus can vaccinate against 31 neoepitopes compared to the 10 of Ad5, increasing the probability of encoding for immunogenic candidates. Nonetheless, the results of EpicentRX "AdAPT program" with oncolytic adenovirus 5 expressing patient's neoepitopes would provide critical data for the viability of the strategy.

5. CONCLUSIONS

- The oncolytic adenovirus ICO15d6.7/19K-B16TMG expressing B16-F10 neoepitopes from a TMG was successfully generated and showed similar oncolytic properties as the parental virus *in vitro.*

- The TMG of ICO15d6.7/19K-B16TMG is transcribed and translated inducing *in vitro* presentation of Ova257 in dendritic cells, and eliciting immune responses *in vivo* against Ova257 and Mut17.

- Linkers between minigenes do not enhance neoepitope immune response in an oncolytic vaccine setup.

- The order and number of minigenes of TMG do not affect the immunogenicity of minigenes in an oncolytic vaccine setup.

- The CMT64.6 cell line has 60% of non-synonymous genetic variations of CMT64 cell line.

- The oncolytic adenovirus ICO15d6.7/19K-CMT64.6TMG expressing CMT64.6 neoepitopes from a TMG was successfully generated.

- ICO15d6.7/19K-CMT64.6TMG elicited immune responses *in vivo* against Ova257 and Ndufs1 but did not control the tumor growth after intratumoral nor intravenously administration.

- The intravenous injection of ICO15d6.7/19K-CMT64.6TMG generates a more intense anti-Ndufs1 immune response than intratumoral administration.

CHAPTER C

ONCOLYTIC ADENOVIRUSES WITH ENHANCED HYALURONIDASE ACTIVITY

1. INTRODUCTION

1.1. HYALURONIC ACID

The main extracellular matrix (ECM) component is the hyaluronic acid (HA), a high molecular weight glycosaminoglycan composed of repeating disaccharide units. The ECM and different types of cells form the tumor stroma. High HA levels in tumor stroma have been associated with metastatic potential and poor overall survival (OS) [401,402]. Invasive fronts of growing tumors are rich in HA, suggesting that it is involved in cell proliferation and invasion [402,403]. Moreover, HA retains water molecules, increasing the tumoral interstitial pressure. It hampers the extravasation of therapeutic agents such as OAds, chemotherapeutics, or immunotherapeutics [404]. Thus HA plays an important role in acquired resistance to anticancer drugs [405]. The high-molecular-weight HA contributes to generating an immunosuppressive microenvironment, characteristic of worst-prognosis cancers, and resistance to immunotherapies [406,407]. The reduced access for monoclonal antibodies and NK cells into High-HA tumors have been reported in preclinical models [408]. As a consequence, many efforts have been made to degrade the HA in tumors to improve the therapies.

1.2. HYALURONIDASE

In 1942 Duran-Reynals published the first comprehensive review on the interplay of hyaluronidase and HA [409]. Since then, hyaluronidase enzymes degrading HA have been discovered in bacteria, insects, snakes, fish, and mammals. In humans, six different hyaluronidases, HYAL-1 to HYAL-4, HYAL-P1, and PH20, have been identified. Among them, the PH20 exerts the strongest biologic activity in physiological conditions. PH20 is found in high concentrations in testicles localized on the head and the acrosome of human spermatozoa as a transmembrane protein. Today, animal-derived bovine, ovine, and synthetic PH20, are clinically applied as an adjunct to increase the bioavailability of drugs, surgery, aesthetic medicine, and others [410].

In cancer therapy, the HA degradation by pegylated (PEG)-PH20 increases chemotherapy delivery and antitumor effects in preclinical models [411]. PEG-PH20 presented promising results in phase I and II clinical trials [412]. However, it failed to improve the overall survival compared to the standard of care in phase III [413].

Regarding the OAds, in high HA-containing melanoma and prostate xenograft models, the co-injection of OAd with hyaluronidase significantly improved virus spread and OS compared to animals treated with virus or hyaluronidase alone [127]. All together confirmed that the HA degradation improves the extravasation and spreading of drugs and OAds into the tumor, enhancing their antitumor efficacy (**Figure 51**). Our group generated the VCN-01 (detailed in General introduction, 5.5.1.1.1) with enhanced efficacy preclinically and currently tested in clinics. We analyzed in chapter A, the immune response induced in the VCN-01 pancreatic clinical trial.

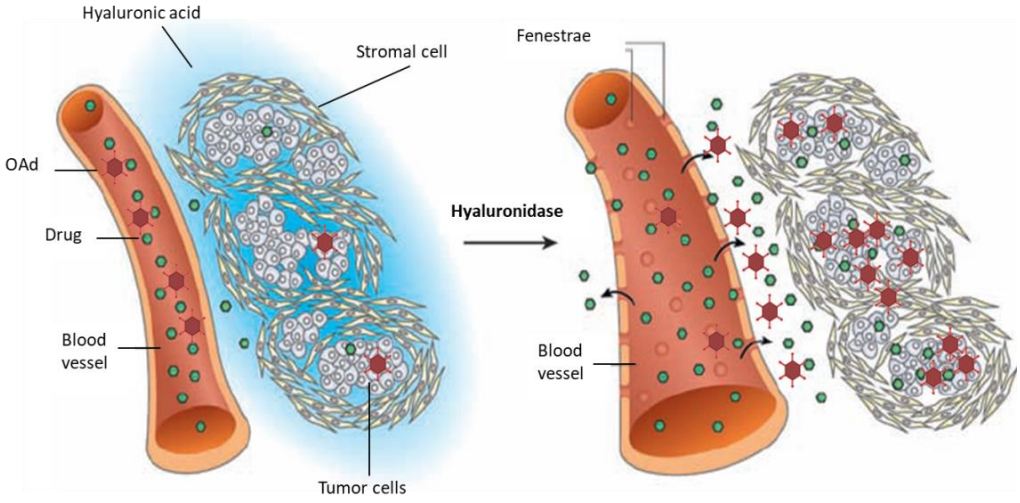

Figure 51. Effects of hyaluronidase on the tumor vasculature and interstitial fluid pressure in tumors. The hyaluronic acid (blue in the figure) retains water molecules increasing the interstitial pressure of the tumor, which compresses the blood vessel and reduces vascular permeability (lack of fenestrae) limiting the drug and OAds diffusion and extravasation. After hyaluronidase treatment, the HA is degraded and reduces the interstitial pressure, which decompresses the vessels and enhances the permeability and drug/OAd extravasation. Adapted from [414].

1.3. ARMING DESIGN

In this chapter, we aim to enhance the hyaluronidase activity of VCN-01. To do that, we exploited different arming strategies. Different issues need to be contemplated at the time to introduce exogenous DNA into the adenoviral genome. We recently reviewed different arming OAds strategies [415]. Briefly, we would focus on two relevant aspects for this chapter: the insertion site and the genetic element to control the transgene expression.

3.1.1. Transgene position

The strategy to insert additional genes stems from the historical use of adenoviruses as gene transfer vectors in the fields of gene therapy and vaccination. Recombinant adenoviruses will only stably accommodate approximately 2kb of additional DNA beyond the size of the normal genome [384]. Thus, gene deletions are needed to encode larger transgenes in their genome. Gene therapy vectors do not aim to replicate in the infected cells; in consequence, adenoviral essential transcription units *E1* or *E4* were deleted. Moreover, the *E3* has a higher genomic extension and encodes for immune-inhibitory proteins non-essential for viral replication *in vitro* [416–418]. Thus, the transcription units *E1, E3,* and *E4* were utilized as insertion sites for transgenes in the generation of recombinant Ad vectors [418–421].

In contrast, OAds replicate in cancer cells. Thus *E1* can not be deleted entirely. The partial deletion of E1B-55K was the first deletion, based on the rationale that the p53-blocking function of this protein is not needed in p53-deficient cells, usual in tumors [70]. The first armed-OAd contained an E1B-55K deletion and a transgene cassette, with a cytomegalovirus promoter (CMVp) and cytosine deaminase gene (CD) fused to the herpes virus thymidine kinase (TK). Similarly, the TK gene was inserted in an E1B-55K and E3-deleted adenovirus after the *E1* region [187]. Since then, entire or partial *E3* deletions were used to generate genomic space to insert expression cassettes containing an exogenous promoter, the transgene, and polyadenylation sequences in *E1*, *E3* or *E4* regions.

To bypass the need of exogenous promoters in OAds, the group led by Terry Hermiston at Onyx Therapeutics substituted *E3* genes with transgenes maintaining the endogenous promoters and polyadenylation sites, and endowing the transgene with the expression kinetics of the substituted *E3* gene [200–202]. They also developed transposon-based approaches to scan an E3-deleted adenoviral genome for new expression cassette insertion sites [422,423]. Based on the mentioned strategies, most armed-OAds have major deletions within the *E3* region. Notably, E3-deleted viruses were reported to be cleared much more rapidly than *wild-type* viruses and presented lower activity in immunocompetent *in vivo* models [388,424,425]. Therefore the E3 deletion may contribute to the fast clearance of adenoviruses in patients. Different strategies were designed to insert transgenes in a complete Ad backbone, despite the Ad's packaging limitation.

For non-E3-deleted OAds, the first reported insertion site was after fiber gene (*Late transcription unit 5* (*L5*)), previously defined also in E3-deleted backbones [423]. The green fluorescent protein (GFP) [426] or CD [188] were inserted under splice acceptor control as new transcription units into an Ad5 backbone. Alternatively, a new viable insertion site in the *L3* was also described achieving a high amount of transgene production at the late phase [427].

3.1.2. Transgene transcriptional control

The transcriptional control of the therapeutic transgene is one of the essential features when designing an OAd. There have been two main approaches in the field. First, transgenes are in expression cassettes containing an exogenous promoter and a polyadenylation signal. In this case, the transgene expression does not depend on virus replication. Second, transgenes are inserted into adenoviral transcription units, taking advantage of the viral gene expression machinery by internal ribosome entry sites (IRES), splice acceptor sites (SA) or protein fusions using 2A self-cleaving peptide linkers [428]. This strategy exploits the viral mechanisms of transcription and mimics the timing of transgene expression within the viral replication cycle. Therefore, transgenes linked to late phase genes depend on viral replication.

Alternatively, the use of microRNAs (miRNA) could regulate transgene expression. miRNAs have been validated to control and reduce the undesired transgene expression in Ad vectors [429–431]. Although to our knowledge it has not been published in OAds, we speculate that might be adapted to the field.

1.3.1.1. Exogenous promoters

The most used promoter is the human cytomegalovirus promoter (CMVp), a constitutive promoter trans-activated by early adenoviral proteins but easily silenced in mammalian systems. CMVp confers high levels of transgene transcription at early timepoints independent of viral replication. Transgenes are transcribed in every infected cell, even in normal tissues. Cellular promoters overactive in cancer cells have been used to achieve tumor-selective expression of transgenes. An example was an OAd encoding GFP controlled by a fusion promoter between human telomerase reverse transcriptase (hTERT) and a small fragment of the CMVp [432]. Aiming to control also the timing of transgene expression, an OAd was armed with a CD-TK fusion gene under heat shock protein 70 (hsp70) promoter, expressing the transgene only after induction of 41ºC during 1 hour [433].

The main limitation of exogenous promoters is that they require large DNA fragments. It increases the size of the transgene cassette, compromising the packaging limit of OAds.

1.3.1.2. Internal ribosome entry sites (IRES) and 2A sequences

The internal ribosome entry sites (IRESs) are highly structured viral sequences that facilitate biscistronic gene expression by internal translation initiation in addition to the cap-dependent translation at the 5’ of mRNAs. In consequence, the transgene is expressed with the same kinetics as the virus gene, which has been linked with the IRES. When the connection is with a late gene, transgene expression can be restricted to sites of viral replication, which is tumor-selective in the case of OAds [188,189,198,434,435]. Although IRES solved the transgene control related to viral replication, the size of the IRES-DNA sequences (approx. 600bp) was large and could

hinder viral replication in non-deleted adenoviral backbones. Shorter IRES have been described (elF4G – 339bp), but they are still far from the size economy of 2A sequences and splice acceptors.

The viral 2A sequences are short peptide sequences that facilitate multiprotein expression from one open reading frame by a process termed ribosomal skipping [436,437]. The 2A sequences from the *foot-and-mouth disease* virus F2A and the porcine *teschovirus-1* P2A were used to co-express GFP with adenoviral pIX [438]. Afterward, transgene selectivity and expression levels were compared between IRES or *thosea asigna* virus T2A sequence linked to the fiber gene, or cloned after E4 by an SA. It was reported that higher expression yields with IRES or SA than T2A [439]. A major concern was that 2A sequences reduced the replication of the respective OAds. Thus, other 2A sequences have to be considered, as we did in this thesis.

1.3.1.3. Splice acceptors

Alternative splicing was first described for adenovirus late mRNAs [440], and it can be used to create new transcripts in the adenovirus genome. The short sequence of SA, usually less than 50bps, is one of the main advantages for large insertions into the Ad genome.

The IIIa splicing unit and splice enhancer (3VDE) was the first one to be studied in detail [441]. We have used this SA in the group to express GFP, hyaluronidase, and bispecific T-cell engagers as transgenes after the fiber, as an extra late transcription unit [217,245,246,426]. The Ad41 long fiber SA was used to introduce the cytosine deaminase gene after Ad5 adenoviral fiber [188]. Alternatively, the SA from Ad40 long-fiber (40SA) produced at least 50-fold higher luciferase compared to a CMV-driven cassette at late time points [255]. An artificial splice acceptor site derived from the beta globulin gene (branch point and splice acceptor sequence, BPSA) has been used in the adenoviral context to express transgenes [423]. The 40SA produces higher transgene levels than BPSA [442]. However, parallel comparisons between these splice acceptors (IIIaSA, 40SA, 41SA, and BPSA) in terms of transgene production and viral fitness have

not been published. SA could be a suitable alternative, but the transgene sequence has to be analyzed for cryptic splice acceptors to prevent undesired or aberrant transgene products [439].

In this chapter, we armed OAds with hyaluronidase genes in different insertion sites (after E1A, after fiber, and after-E4) with different splice acceptors (IIIaSA and 40SA) or P2A sequences, aiming to generate a candidate with higher hyaluronidase activity than VCN-01.

2. OBJECTIVES

The main objective of this chapter is to improve the potency and efficacy of VCN-01.

Hypothesis: Increased hyaluronidase activity or expression improves VCN-01 oncolytic activity.

Specific objectives:

- To identify other hyaluronidases with higher activity than human PH20.
- To generate a panel of oncolytic adenoviruses expressing hyaluronidases in different genome locations under different transcription control systems.
- To identify hyaluronidase-expressing OAd candidate with higher hyaluronidase activity and preserved oncolytic properties.
- To characterize the efficacy profile of the candidate in immunodeficient and immunocompetent models.
- To explore the relevance of hyaluronidase in the T cell extravasation.

3. RESULTS

3.1. HYALURONIDASE FROM APIS MELLIFERA PRESENTS HIGHER ACTIVITY THAN HUMAN PH20.

We envisioned OAds with higher hyaluronidase activity than VCN-01. In order to find a hyaluronidase with higher activity than hPH20, we speculated that the hyaluronidase from *Apis Mellifera*'s venom (BHyal) could be a candidate. Expression plasmids (GT4082) codifying for His-tagged hPH20 or BHyal were successfully cloned (see 8.1 and 8.2, Materials and Methods) and then transfected in HEK293 cells. Five days post-transfection, supernatants were collected, and we assessed the presence and quantity of each enzyme by anti-HisTag Western blot. A commercial recombinant His-tagged PH20 was used as a positive control and to prepare a standard curve; it allowed us to quantify the supernatants (SN). The SN from hPH20 had higher concentration than BHyal (**Figure 52-A**). Then hyaluronidase activity was tested by a turbidimetric assay, BHyal presented a significantly enhanced activity compared to hPH20 (**Figure 52-B**).

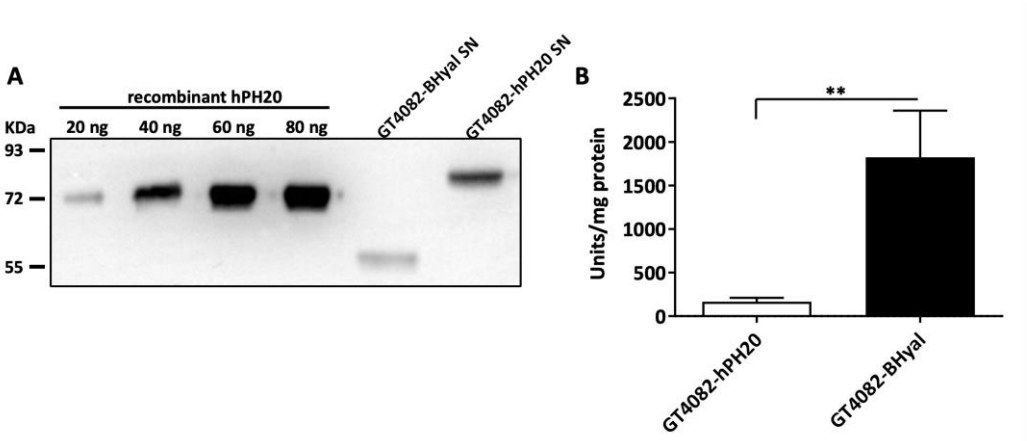

Figure 52. BHyal activity is higher than hPH20. (A) Equivolumes of supernatants from 5-days transfected HEK293 were assessed by anti-HisTag Western Blot. A commercial purified recombinant His-tagged hPH20 (Acro Biosystems, PH0-H5225) was used as a positive control and to perform a standard curve ranging from 20 to 80 ng in order to quantify the samples. **(B)** Hyaluronidase activity of the same samples was analyzed by turbidimetric assay and normalized according to the amount of protein detected in Western Blot. Representative results from one of three experiments are shown. Bars represent the mean±SD of triplicates. **p-value<0.01 by unpaired two-tailed T-test.

3.2. GENERATION OF HYALURONIDASE-EXPRESSING ONCOLYTIC ADENOVIRUSES.

We have previously reported the generation of the OAd ICO15K, an E1a-Δ24-based Ad which incorporates palindromic E2F binding sites in *E1a* promoter and contains an RGDK motif replacing KKTK heparan sulfate glycosaminoglycan-binding domain in the fibre shaft [79]. This virus has shown safer toxicity profiles and improved antitumor targeting *in vivo*. Therefore, it was chosen as a platform to incorporate a truncated soluble version of human hyaluronidase PH20 (*SPAM1*) as transgene after fiber (*Late 5*, L5), under the major late promoter (MLP) restriction using the endogenous splice acceptor from adenoviral IIIa gene, generating VCN-01 [268] (**Figure 53-A**).

To obtain a virus with higher hyaluronidase activity, six new viruses were designed and generated in the context of this thesis (**Figure 53-B**). A first strategy was to change the transgene splice acceptor IIIa for a previously reported strong splice acceptor from the long fiber gene of Adenovirus 40, known as 40SA splicing acceptor [255]. Thus, ICO15K genome was genetically engineered by homologous recombineering in bacteria to introduce hPH20 with the new splice acceptor resulting in ICO15K-40SAPH20. Then, to test different genomic positions, the transgene was placed downstream *E4* gene with these two splice acceptors obtaining ICO15K-E4.IIIaPH20 and ICO15K-E4.40SAPH20. Another strategy to obtain higher hyaluronidase activity was expressing hyaluronidase earlier in the virus life cycle. For this reason, hPH20 was fused to an early gene *E1a* by a viral self-cleavable peptide P2A [255] to get ICO15K-E1aP2APH20. Finally, hPH20 was replaced for BHyal which we demonstrated that have higher activity, generating ICO15K-IIIaBHyal and ICO15K-E4.IIIaBHyal. All these viruses were successfully rescued, plaque-isolated, and amplified obtaining cell extracts with similar titers.

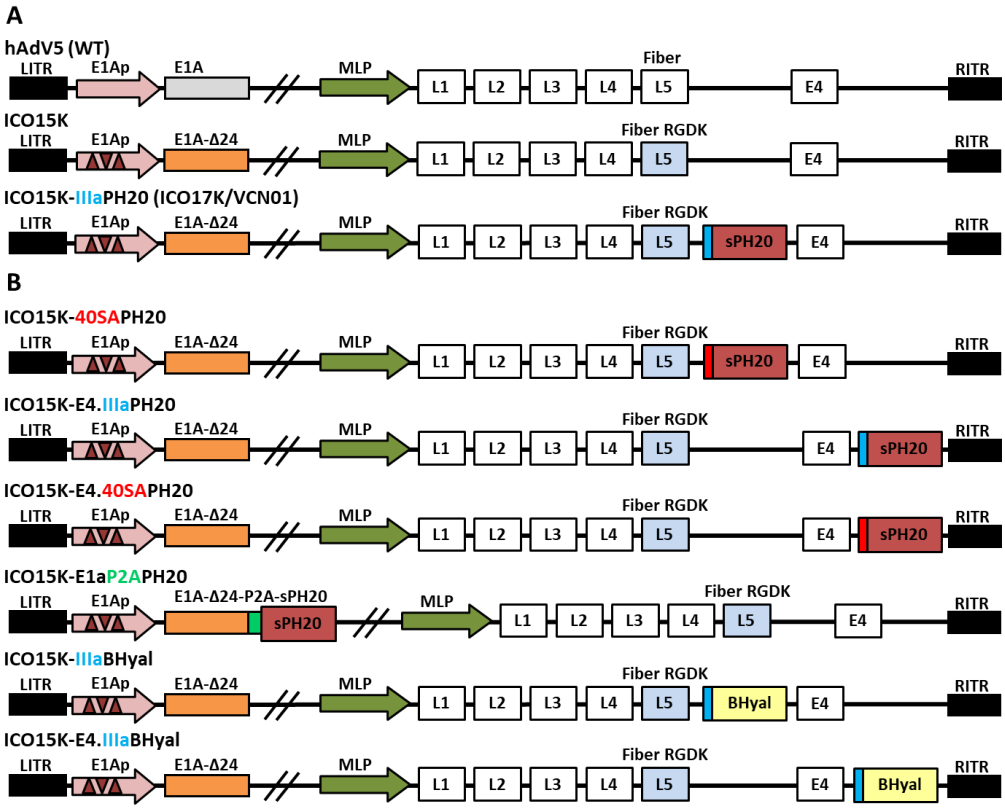

Figure 53. Schematic representation of Hyal-OAds genomes. (A) Compared to the hAdV5 *wild*-type the ICO15K carries the *E1a*Δ24 mutation and E2F binding sites in the promoter of the gene (represented as a brown triangles), and the RGDK motif in the fiber shaft also known as a RGDK fiber. ICO15K was used to introduce a soluble version of human PH20 (sPH20) after fiber (*Late 5* gene, *L5*) under IIIa splice acceptor (represented in blue) restricted to major late promoter (MLP) generating ICO17K or VCN-01. **(B)** ICO15K was engineered to generate all the hyaluronidase-expressing viruses developed in this thesis. sPH20 was inserted after fiber under 40SA (represented in red) splice acceptor control, or after *E4* gene with IIIa or 40SA splice acceptors and fused with P2A sequence (represented in green) to *E1a* gene. BHyal, represented in yellow, was used also as a transgene after fiber or *E4* under IIIa splice acceptor.

3.3. CANDIDATE SELECTION.

To test the role of higher Hyal expression we wanted viruses with similar cytotoxic properties as VCN-01 and enhanced hyaluronidase activity. We addressed the oncolytic potential by a dose-response cytotoxicity assay with A549 cell line (**Figure 54-A**). Although every candidate showed dose-dependent oncolytic properties *in vitro*, the IC_{50} (Transfecting Units/cell) values were significantly higher in ICO15K-BHyal compared to VCN-01 suggesting a loss of cytotoxicity.

On the other hand, to assess the hyaluronidase activity of these viruses A549 cells were infected at the multiplicity of infection (MOI) 20 TU/cell. 72hours post-infection the supernatants were harvested and concentrated 30-fold to perform a turbidimetric assay. ICO15K-BHyal presented a significant higher hyaluronidase activity than VCN-01. In addition, ICO15K-40SAPH20 had higher hyaluronidase activity, even though not statistically significant compared to VCN-01. ICO15K-E1aP2APH20 and ICO15K-E4.IIIaBHyal showed similar levels of activity as VCN-01 (**Figure 54-B**).

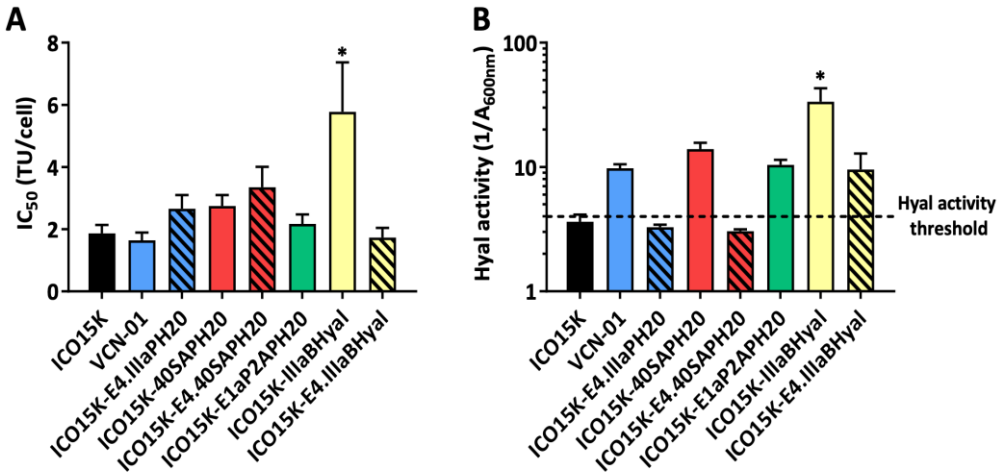

Figure 54. In vitro characterization of Hyal-OAds candidates. (A) A549 cell line was infected with the multiplicity of infections (MOIs) ranging from 200 to 0 TU/cell. Five days post-infection, cell viability was determined by BCA staining and the IC_{50} for each virus was calculated. The mean of IC_{50} triplicates per each virus ± SD is plotted. **p*<0.05 by Kruskal-Wallis with Dunn's *post hoc* test. **(B)** A549 cells were infected at MOI 20 and after 72hours supernatants were harvested, clarified by centrifugation and

concentrated 30-fold using 30KDa AMICON® tubes. After overnight incubation with hyaluronic acid, the activity of the supernatant is measured as the inverse of the absorbance at 600nm ($1/A_{600nm}$). Mean of triplicates ± SD is plotted. **p*<0.05 by Kruskal-Wallis with Dunn's *post hoc* test.

According to these results, we selected as candidates for this project the next viruses: ICO15K-40SAPH20, ICO15K-E1aPH20 and ICO15K-E4.IIIaBHyal as they maintain the oncolytic properties of VCN-01 and may have more hyaluronidase activity. They were successfully purified obtaining similar physical and functional titers as those of VCN-01.

3.4. HYAL-OADS PRESENT SIMILAR CYTOTOXIC PROPERTIES AND COMPARABLE PRODUCTION YIELDS AS VCN-01

To further evaluate the chosen candidates' viral replication, cytotoxic assays were performed in a panel of cancer cell lines after 5 days of controlled infection. The cytotoxicity was first evaluated in A549 as permissive cell line; no differences were observed among the selected candidates (**Figure 55-A**).

Then 6 other cancer cell lines were tested, only in MIA PaCa-02 cell line ICO15K-E4.IIIaBhyal presented a significantly lower IC_{50} value than VCN-01, indicating greater cytotoxicity in this model. The IC_{50} values suggest that at least the selected candidates maintain the oncolytic properties of VCN-01, even with lower IC_{50} suggesting a cytotoxic improvement in some models, such as HT-1080, MDA-MB-231 or Sk-mel-28 (**Figure 55-B**).

Having confirmed the oncolytic properties, we measured the viral production of our candidates. We infected A549 cells at MOI 20 and monitored the amount of transfecting units per cell (TU/cell) produced in cell extracts (**Figure 56-A**) and released in supernatants over time (**Figure 56-B**). Differences in total virus production in the culture cell extracts were not statistically significant despite the tendencies of higher production of VCN-01 compared to ICO15K-E1aPH20 after 72 hours (**Figure 56-C**). At the same time, the functional viral particles released to the supernatant were analyzed, and in this parameter, ICO15K showed significantly released more infection units

compared to ICO15K-E1aP2APH20 virus (**Figure 56-D**). Nevertheless, no significant differences in viral production were observed comparing VCN-01 to the new Hyal-expressing viruses.

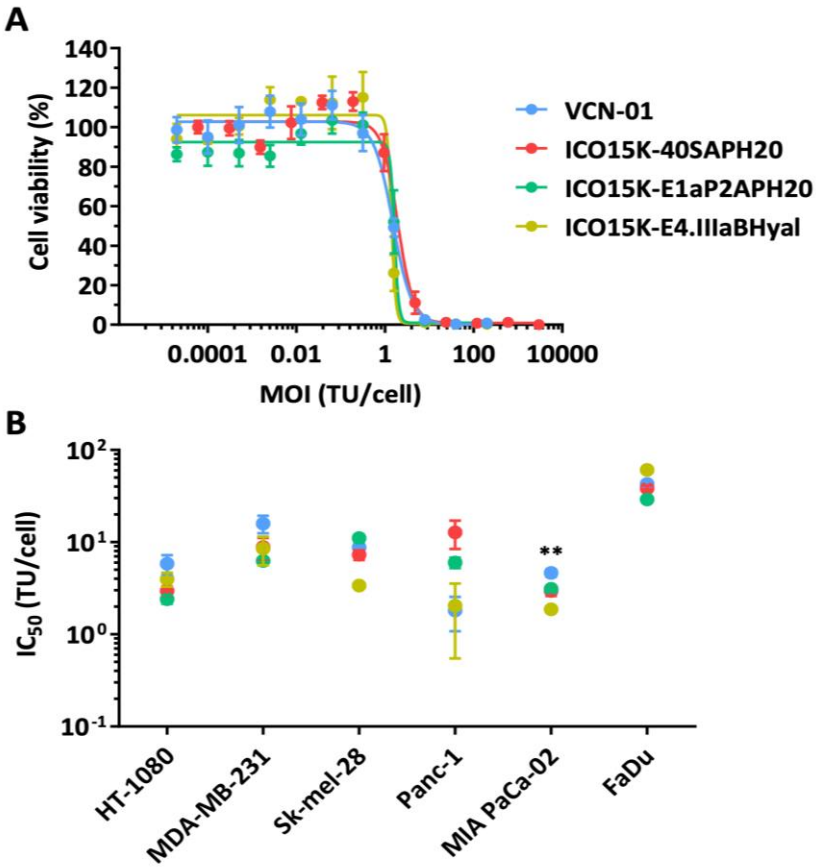

Figure 55. Hyal-OAds present similar cytotoxic properties as VCN-01 *in vitro*. (A) A dose-response cytotoxic assay was performed *in vitro* with A549 cell line. 4 days post-infection, cell viability was determined by BCA staining and the IC_{50} for each virus was calculated. **(B)** Similar experimental setting was used in a panel of human cancer cell lines: connective tissue fibrosarcoma (HT-1080), breast adenocarcinoma (MDA-MB-231), melanoma (Sk-mel-28), pancreas carcinoma (Panc-01 and MIA Paca-02) and pharynx squamous cell carcinoma (FaDu). The mean of IC_{50} triplicates ± SD is represented. **p<0.01 by Kruskal-Wallis with Dunn's post-hoc test.

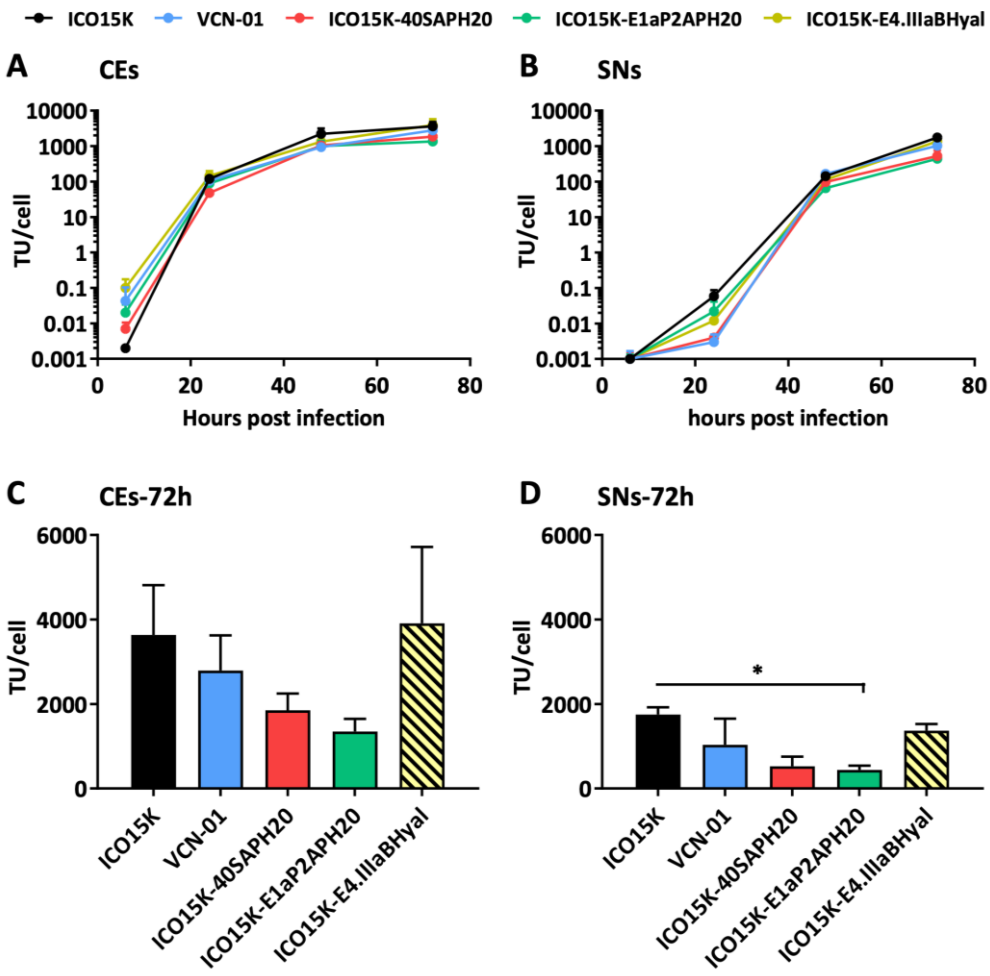

Figure 56. Hyal-OAds present comparable viral production yields as VCN-01. A549 cell line was infected at MOI 20 for 4 hours. Then, excess of viruses was washed and cells were incubated for 24, 48 or 72 hours. Total virus production in **(A)** culture cell extracts (CEs) or in **(B)** supernatants (SNs) was determined by anti-hexon staining method. Results are expressed as transducing units (TU) produced per cell. Mean ± SD of triplicates is shown. **(C and D)** Detailed analysis of 72 hours time point is represented. Mean±SD of triplicates is shown. *p<0.05 by Kruskal-Wallis with Dunn's post-hoc test.

3.5. HYAL-OADS PRESENT HIGHER HYALURONIDASE ACTIVITY THAN VCN-01 IN VITRO AND IN VIVO.

After determining the cytotoxic and virus production properties, we assessed the hyaluronidase activity of the Hyal-OAds candidates. A549 cells were infected at MOI 20 and supernatants were collected at 24h, 48h or 72h post-infection. The hPH20 protein levels of these supernatants were detected by anti-hPH20 Western Blot. The adenovirus fiber was used as a control protein to compare hPH20 levels. We observed higher amounts of hPH20 in ICO15K-40SAPH20 and ICO15K-E1aPH20 compared to VCN-01 and ICO15K (used as a negative control) (**Figure 57-A**). Unexpectedly, hPH20 protein was not detected in VCN-01. This is probably due to supernatant concentration is needed to detect the PH20. In fact, preliminary studies revealed that VCN-01 hyal activity was only detected in concentrated supernatants, as published [219].

The results of Western blot lead us to compare the hyaluronidase activity in non-concentrated supernatants. As expected, we observed a significantly enhanced hyaluronidase activity of ICO15K-40SAPH20 compared to VCN-01 after 48 and 72 hours post infection. Moreover, the ICO15K-E1aPH20 activity was higher than VCN-01, significantly 24hours post-infection. Additionally, although BHyal levels could not be detected in supernatants due to lack of a commercial antibody, we detected also a higher turbidimetric activity compared to VCN-01 but fewer than other candidates (**Figure 57-B**). A 20-fold concentration of supernatants was required to detect hyaluronidase activity of VCN-01, as previously published, confirming that the rest of candidates have considerably higher activity. However, the concentrated SNs of Hyal-candidates reached the upper limit of quantification (ULOQ) of the assay (all hyaluronic acid was degraded), impeding a reliable quantification (**Figure 57-C**). An optimization of the assay should be done to detect and quantify all supernatants in the same experiment.

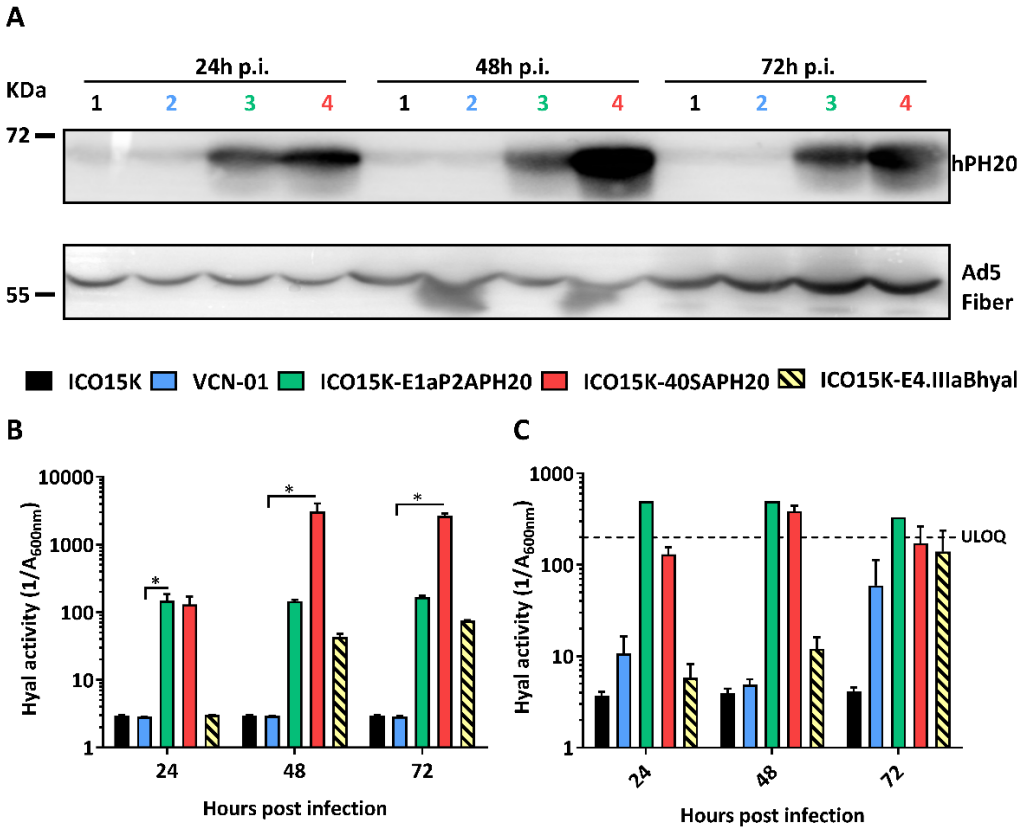

Figure 57. Hyal-OAds have higher hyaluronidase activity *in vitro* than VCN-01. (A) A549 cells were infected with different viruses at MOI 20. After 24, 48 or 72h hours supernatants were harvested, clarified and analyzed for the protein levels by Western Blot anti-hPH20 and anti-Ad5 fiber. Different viruses were compared: ICO15K (1), VCN-01 (2) ICO15K-E1aP2APH20 (3) and ICO15K-40SAPH20 (4). **(B)** Same supernatants were assessed for hyaluronidase activity by turbidimetric assay overnight. The hyaluronidase activity is represented as the inverse of the absorbance at 600nm ($1/A_{600nm}$). Mean±SEM of triplicates is shown. *p<0.05 by Kruskal-Wallis with Dunn's *post hoc* test. **(C)** Supernatants harvested after 24h, 48h, or 72h, post infection at MOI 20 of different viruses were 20-fold concentrated with AMICON tubes. Then the concentrated supernatants were tested in a turbidimetric assay overnight. Samples of ICO15K-E1aP2APH20 (24h, 48h, and 72h), ICO15K-40SAPH20 (24h, 48h, and 72h), and ICO15K-E4.IIIaBHyal (72h) were not quantifiable as they were over the upper limit of quantification (ULOQ) of the assay (all hyaluronic acid was degraded). The hyaluronidase activity is represented as the inverse of the absorbance at 600nm ($1/A_{600nm}$). Mean±SEM of triplicates is shown. No statistical changes were noted by Kruskal-Wallis with Dunn's *post hoc* test.

To confirm virus and hyaluronidase expression *in vivo*, a pilot experiment was performed in nude athymic mice bearing subcutaneously implanted Sk-mel-28 tumors. When they reached 150mm^3 were treated intratumorally with 1x10^8 TUs of ICO15K, VCN-01 or ICO15K-40SAPH20 to ensure the viral presence in tumors. Then, tumors were monitored for 40 days and collected and stained by immunohistochemistry for viral E1a protein and hyaluronic acid (HA). All tumor were E1a positive and we analyzed in a consecutive slide the presence of HA in the surrounding areas of E1a positivity (represented in black arrows in **Figure 58**). We observed that ICO15K had strong positive HA staining compared to VCN-01 or ICO15K-40SAPH20 treated tumors, implying that the later viruses presented hyaluronidase activity *in vivo*. Furthermore, ICO15K-40SAPH20 treated tumors seemed to present less intense positive HA areas surrounding E1a focus than VCN-01, suggesting an enhanced hyaluronidase activity. Nonetheless, further experiments should be performed to confirm a higher hyaluronidase activity *in vivo* by ICO15K-40SAPH20.

3.6. ASSESSMENT OF ANTITUMOR EFFICACY IN VIVO.

Having demonstrated that ICO15K-40SAPH20 and ICO15K-E1aP2APH20 have similar oncolytic properties as VCN-01 and higher hyaluronidase, we decided to evaluate their antitumor efficacy in different models, to validate our hypothesis that more hyaluronidase translates into more efficacy. The ICO15K-E4.BHyal was discarded for the *in vivo* tests due to lower hyaluronidase activity *in vitro* compared to the other two candidates.

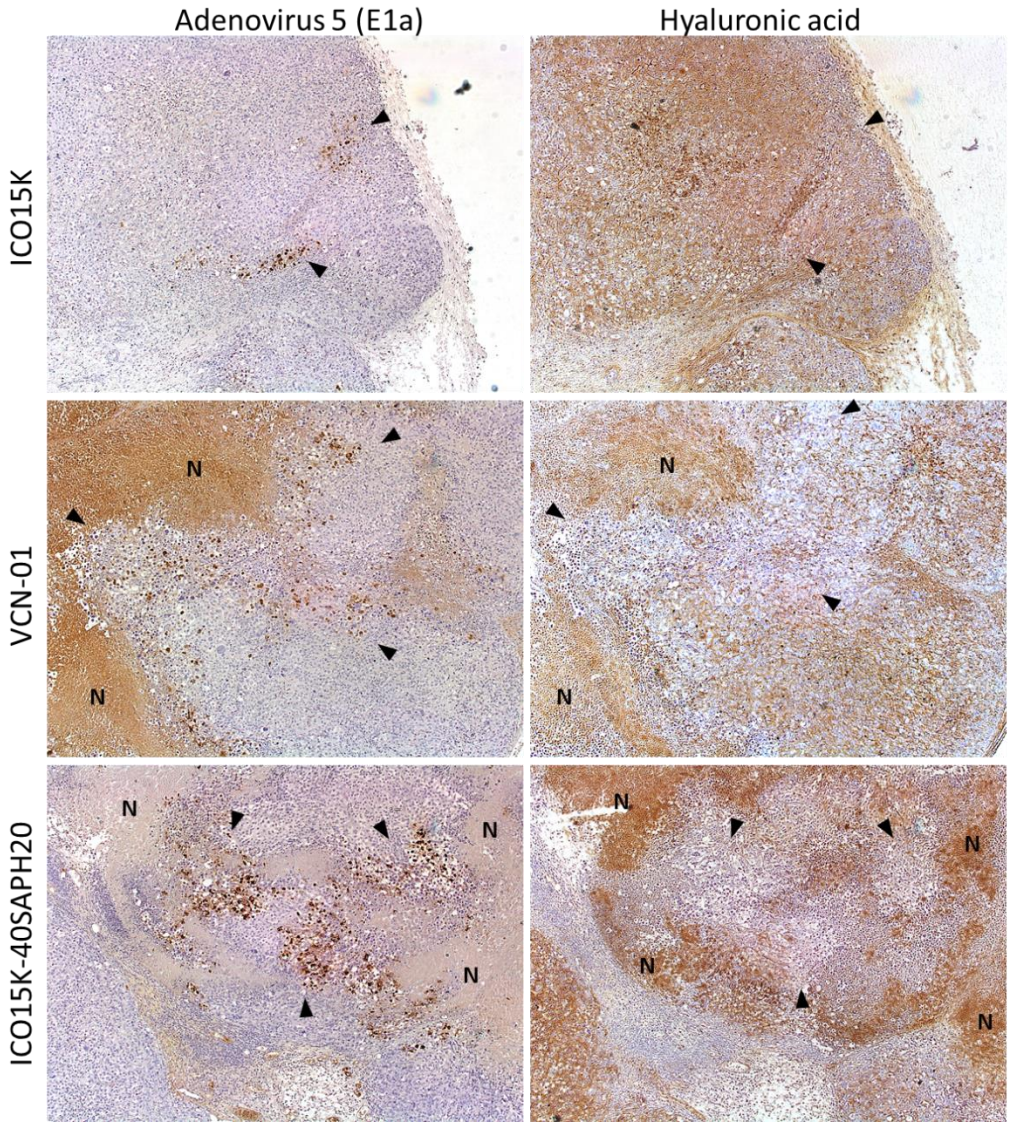

Figure 58. Hyaluronidase activity *in vivo* (E078/19). Immunohistochemical staining of E1a viral protein (left column) and hyaluronic acid (right column) were performed in Sk-mel-28 tumortumors after 40 days post-treatment with $1x10^8$ TUs of ICO15K (first row), VCN-01 (second row), and ICO15K-40SAPH20 (third row). Representative images at 40x were presented with black arrows indicating viral replication focus. Necrotic zones were unspecifically stained, so should not be considerate positive in the IHQ evaluation (marked with an N in the images).

3.6.1. Higher hyaluronidase activity enhances antitumor efficacy in a human melanoma model (Sk-mel-28).

It was reported that the combination of soluble hyaluronidase and oncolytic adenoviruses presented potent tumor efficacy in the Sk-mel-28 model [127]. Moreover, VCN-01 was previously tested in this model demonstrating efficient tumor growth control [268]. Thus, the Sk-mel-28 model is sensitive to hyaluronidase-expressing viruses.

We decided to compare VCN-01, which was very effective in this model, with the selected Hyal-OAds. We implanted NSG mice subcutaneously with Sk-mel-28 tumors and when tumors reached 180mm^3 mice were treated intravenously with 2x10^{10} vp per animal. Tumor volume of every detected tumor nodule was monitored during 81 days, and the tumor growth is depicted in **Figure 59**-**A**. We observed a significant efficacy of all viruses compared to the PBS since day 25. Focusing only in treated groups, we detected a statistically higher efficacy in ICO15K-40SAPH20 and ICO15K-E1aP2APH20 compared to VCN-01 since day 35. In detail, we observed that 40SAPH20-virus and E1aPH20-virus groups regressed almost to the initial tumor volumes (tumor growth 15% and 8% at the endpoint, respectively), whereas VCN-01 group maintained a slow, sustained tumor growth. It was translated in a lower percentage of disease control rate (DCR, sum of complete responders (CR), partial responders (PR) and stable disease (SD)) according to clinical criteria. The VCN-01 group had 14% of DCR (1 out 7, **Figure 59-C**), whereas ICO15K-E1aPH20 had a 66% of DCR and ICO15K-40SAPH20 a 54% of DCR (**Figure 59-D and E**).

At the endpoint, macroscopical observations indicated that some tumors were mainly necrotic and fibrotic areas, and some tumors presented viable growing tumor nodules. Particularly, VCN-01-treated tumors presented more viable nodules (circled in **Figure 60**) than other groups, suggesting that these nodules were not controlled by virus replication and lead the higher tumor growth.

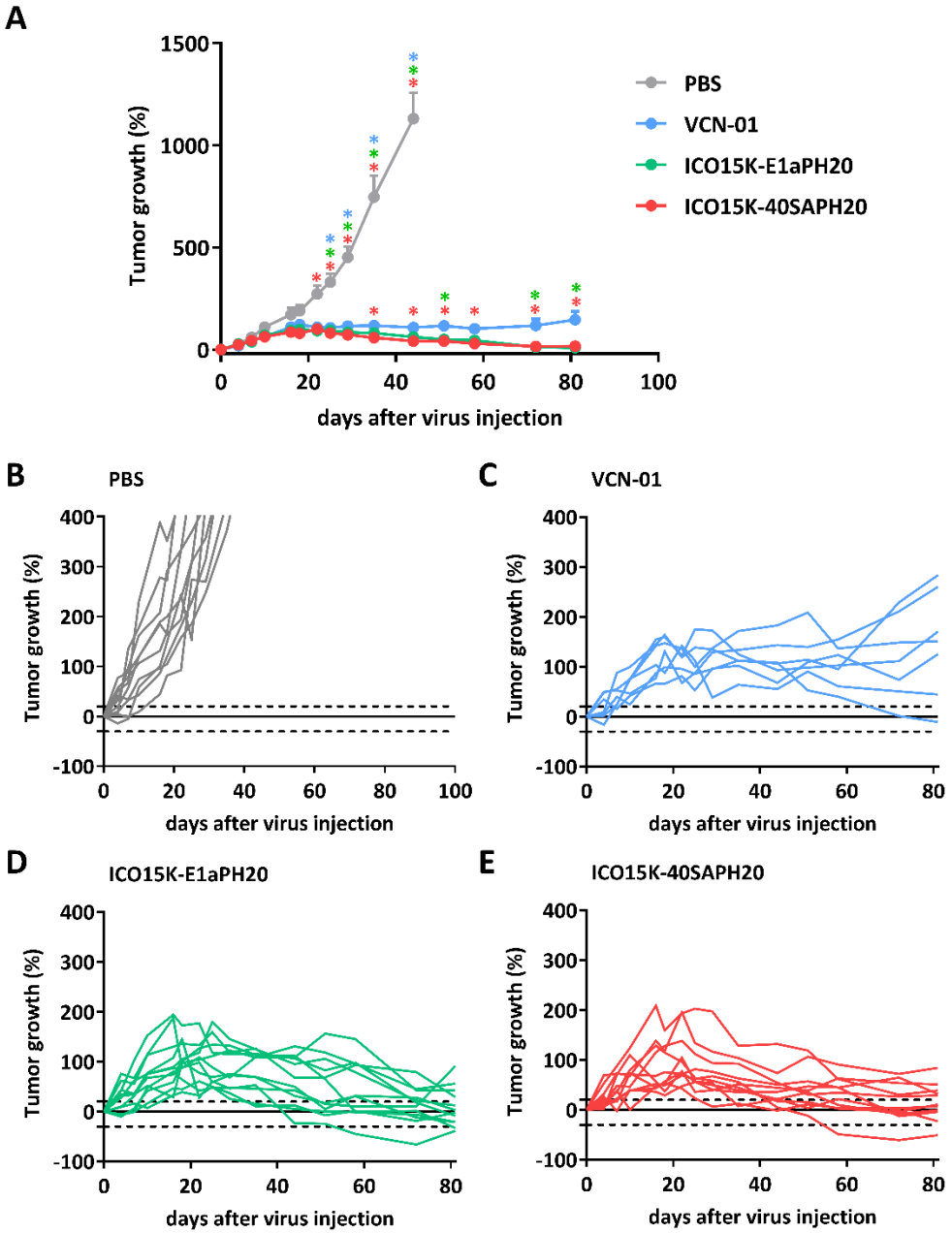

Figure 59. Antitumor efficacy of Hyal-OAds in Sk-mel-28 in vivo (NSG2). (A) Sk-mel-28 tumors implanted in NSG mice were monitored after treatment (2e10 vp/animal intravenously) during 81 days. Tumor growth is represented. *p<0.05 significant vs corresponding group (color) by Two-way ANOVA and Tukey *post hoc* test. **(B-E)** Detailed tumor growth of treated tumors of the same experiment. Dotted lines in axis Y at 20% and -30% indicate the criteria for clinical status. Progression disease ≥20%, Stable disease <20% to >-30%, Partial response ≤-30%, Complete response=-100%.

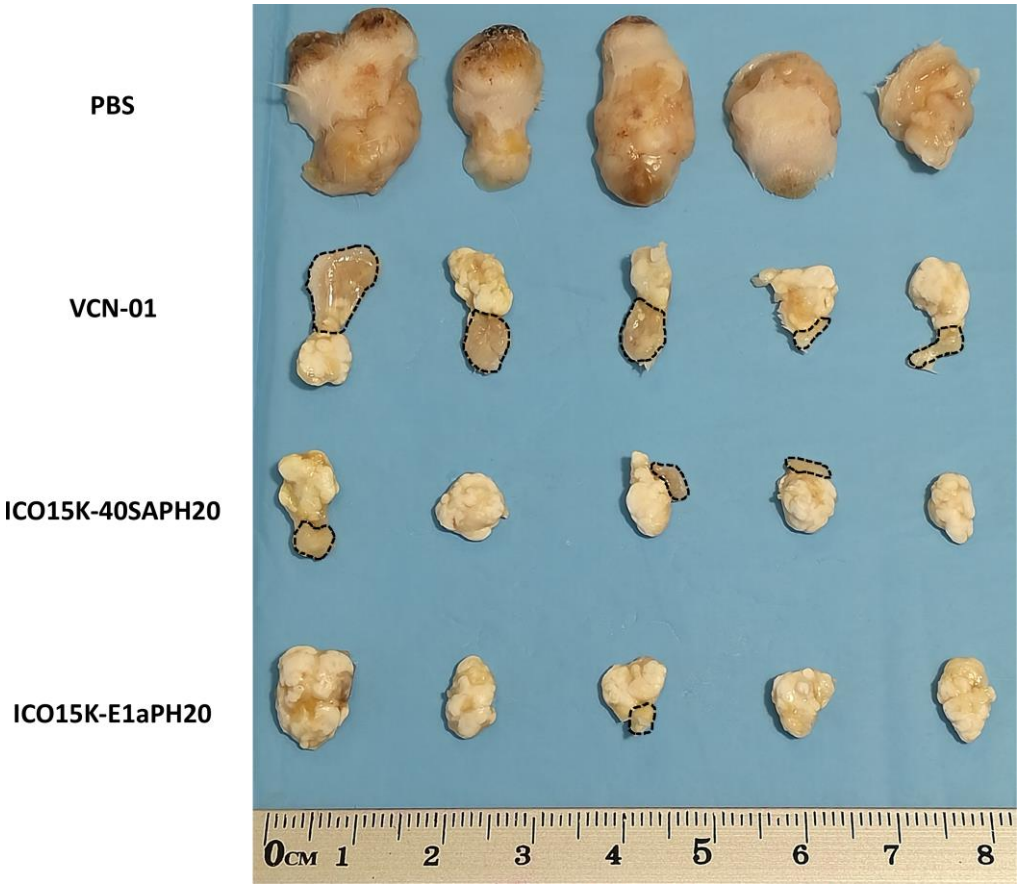

Figure 60. Macroscopic images of Sk-mel-28 tumors treated with Hyal-OAds (NSG2). NSG mice bearing Sk-mel-28 tumors were treated intravenously with different viruses. Control group (PBS) was sacrificed according to ethical criteria on day 44 after treatment. The endpoint for the VCN-01, ICO15K-40SAPH20, and ICO15K-E1aPH20 was on day 81 post-treatment. Viable growing nodules were detected macroscopically and highlighted in the image with dotted black line. Most of tumors ICO15K-40SAPH20 and ICO15K-E1aPH20 were highly necrotic.

3.6.2. ICO15K-40SAPH20 and VCN-01 significantly control tumor growth in a human lung adenocarcinoma model (A549).

Having proved an increased efficacy of our candidates compared to VCN-01 in a favorable model such as Sk-mel-28. We tested them in the A549 model, which has been reported to be more resistant to the VCN-01 treatment [182].

Nude athymic mice were implanted with A549 tumors subcutaneously, and when they reached 120mm^3 mice were treated intravenously with the Hyal-OAds viruses at 4x10^{10} vp/animal. Tumor growth was monitored during 112 days. We observed significant antitumor efficacy of Hyal-OAds compared to the PBS from 51 days post-treatment to 79, when ICO15K-E1aPH20–treated tumors grew losing any significant activity versus PBS. In contrast, VCN-01 and ICO15K-40SAPH20 controlled the tumor growth until the end of the experiment, with significant reduced tumor growth compared to PBS and ICO15K-E1aPH20 (**Figure 61-A**).

No differences were observed between ICO15K-40SAPH20 and VCN-01 tumor growth means. Applying the clinical criteria in every single treated tumor, VCN-01-treated group contained 2/10 CR (-100% tumor growth), 2/10 PR (tumor growth ≤ -30%) and 6/10 non-responders (progression disease, PD; tumor growth ≥20%). The ICO15K-40SAPH20 group presented a slightly higher percentage of responders than VCN-01, 3/12 complete responders, 1/12 partial responses, and 2 SD (tumor growth <20% to >-30%). Thus, the disease control rate (CR+PR+SD) of VCN-01 tumors is 40% of the cases (4/10) and 50% (6/12) for ICO15K-40SAPH20 (**Figure 61-B,C,D,E**).

Apparently the long-term efficacy was not related to hyaluronidase, as suspected, because ICO15K-E1aPH20 (with higher hyal-activity than VCN-01) presented a poor disease control rate (20%) compared with VCN-01. Conversely, the ICO15K-40SAPH20 showed similar antitumor activity as VCN-01, suggesting that may be a good candidate for further studies.

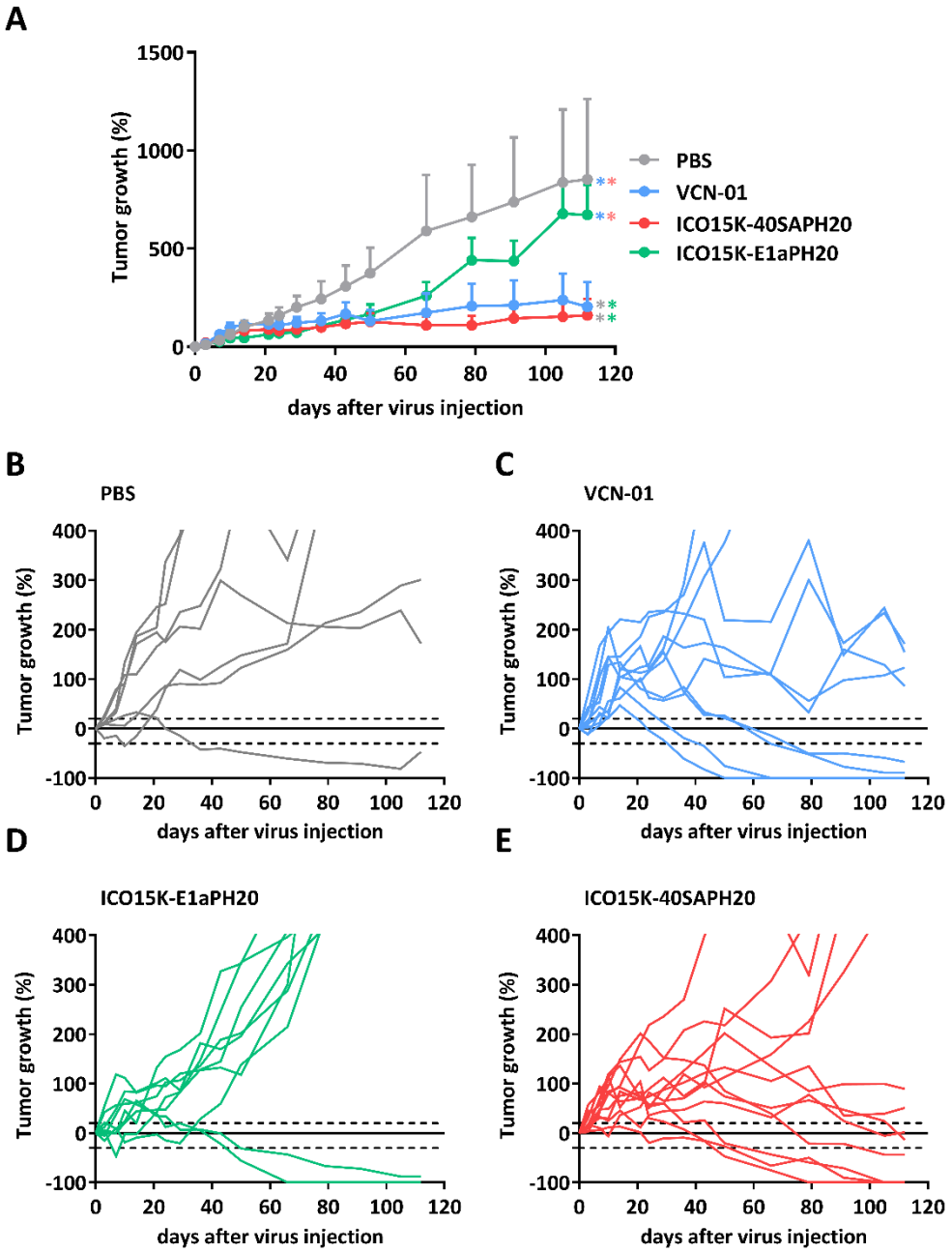

Figure 61. Antitumor efficacy of Hyal-OAds in A549 in vivo (E002/20). (A) NSG mice bearing A549 tumors were monitored after treatment (2e10 vp/animal intravenously) during 112 days. Tumor growth is represented. *p<0.05 significant vs corresponding group (color) by Two-way ANOVA and Tukey *post hoc* test. **(B-E)** Detailed tumor growth of treated tumors of the same experiment. Dotted lines in axis Y at 20% and -30% indicate the criteria for clinical status. Progression disease ≥20%, Stable disease <20% to >-30%, Partial response ≤-30%, Complete response=-100%.

3.6.3. Hyaluronidase expression linked to E1a by oncolytic adenovirus controls tumor growth in the CMT64.6 model in an immunocompetent setting.

Hyal-OAds had significant long-term control of xenograft models in immunodeficient mice. Aiming to assess the relevance of the hyaluronidase expression for the immune response against the tumor in a most physiological setup, we decided to use an immunocompetent mouse model. However, human adenoviruses do not replicate in most murine cell lines [377]. In fact, they do not translate late genes, neither transgenes in late [378]. Taking this into account, we evaluated the capability of viral production in the semi-permissive clonal mouse cell line CMT64.6, which had been generated in our group [383].

We observed as expected, that the total viral production per cell after 72hours of infection was around 4 transfecting units without significant differences between viruses (**F**igure 62-**A, B**). It could be considered almost no replication, taking into account the results previously obtained in A549 human cell line (500-fold higher TU/cell, **Figure 56**). Then we checked the oncolytic properties of the candidates in this cell line performing a dose-response cytotoxic assay. We obtained IC_{50} values ranging from 75 TU/cell in the case of VCN-01 to 41TU/cell for ICO15K-E4.IIIaBHyal (**F**igure 62-**C**). The combination of viral production and IC_{50} values confirmed the difficulties for a complete viral replication in this model.

We tested the hyaluronidase expression of the different candidates; the only reported activity was in ICO15K-E1aPH20 supernatants. It was expected as early genes are expressed in murine cells. As in this candidate the PH20 expression was linked to the early gene *E1a* we detected a statistically significant higher hyal activity than VCN-01 (**F**igure 62-**D**).

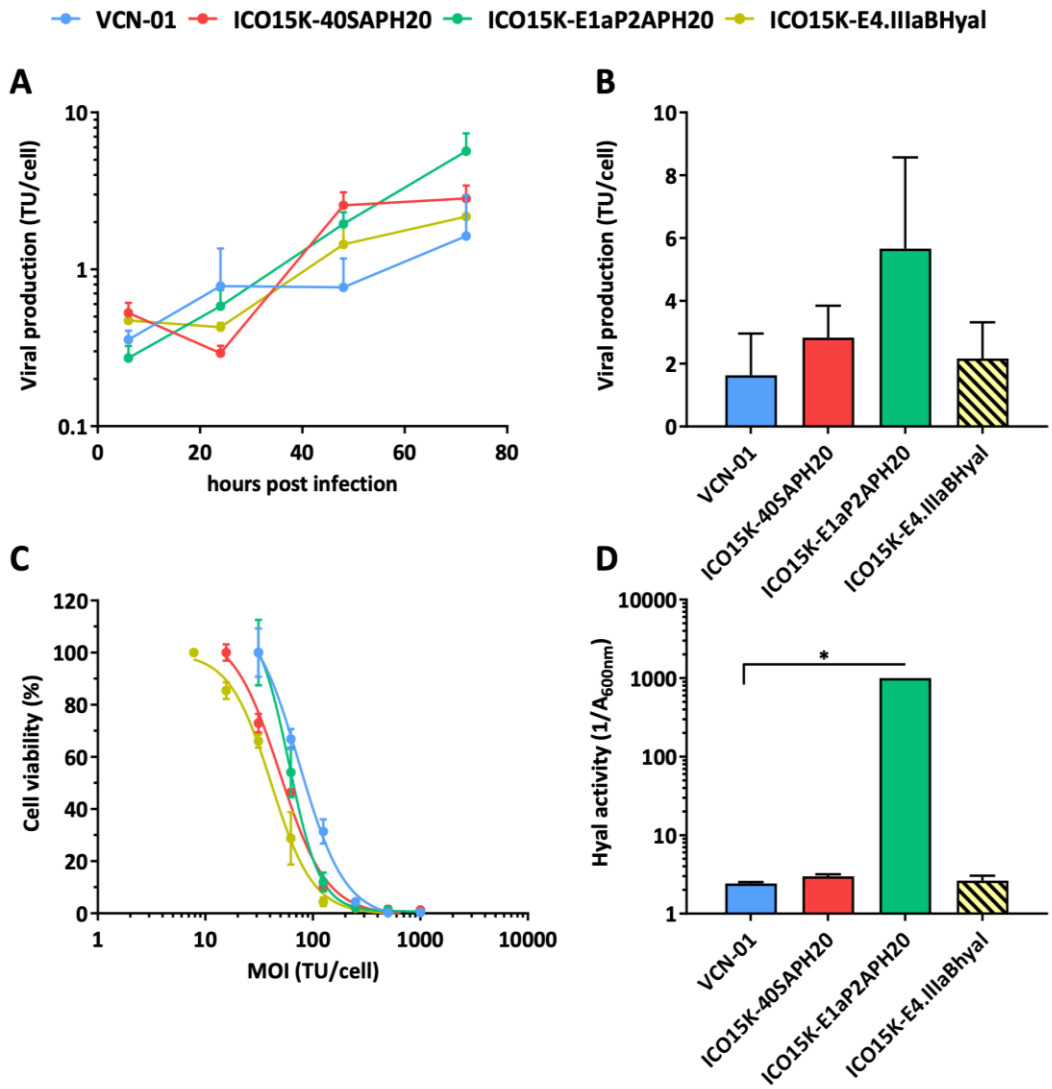

Figure 62. In vitro characterization of Hyal-OAds in CMT64.6 murine model. (A) CMT64.6 cell line was infected at MOI 400 for 4 hours. Then, excess of viruses was washed, and transfecting units production was assessed at 24h, 48h and 72h. **(B)** The last timepoint is detailed. Total virus production in culture cell extracts was determined by anti-hexon staining method. Results are expressed as transducing units (TU) produced per cell. Mean ± SD of triplicates is shown. No significant differences (ns) were observed by Kruskal-Wallis with Dunn's *post hoc* test. **(C)** CMT64.6 cells were infected, ranging from 1000 TU/cell to 0 TU/cell and 5 days post-infection cell viability was determined by BCA staining. The IC50 for each virus was calculated. **(D)** A turbidimetric assay was performed with supernatants harvested at 72hours post-infection of CMT64.6 cells at MOI 400. The hyaluronidase activity is represented as the inverse of the absorbance at 600nm (1/A600nm). Mean±SD of triplicates is plotted. *p<0.05 by Kruskal-Wallis with Dunn's *post hoc* test.

According to *in vitro* results, the only virus that had hyaluronidase activity in this model was ICO15K-E1aP2APH20. Despite the poor replication, we decided to test this virus *in vivo* treating C57BL/6 mice bearing CMT64.6 tumors. Animals were intratumorally injected with $1x10^9$ TUs of VCN-01 or ICO15K-E1aP2APH20 when tumor reached a mean of $100mm^3$. The intratumoral treatment was chosen in this case to ensure the viral presence in the tumors, thereby the hyaluronidase activity in the case of ICO15K-E1aPH20. It presented a statistically significant antitumor efficacy from day 13, compared to PBS and VCN-01 (**Figure 63-A**). At the end of the experiment, spleens were harvested and an ELISPOT was performed to analyze the immune responses elicited against 4 different described tumor neoepitopes (*Ndufs1, Itgav, Arghef10a.2,* and *Cep192A*) and also against one viral protein (E1b). Although no statistically significant, we detected evident responses against *Itgav* neoepitope in VCN-01 and ICO15K-E1aP2APH20 treated groups. As expected, it was also observed immune responses against E1b exclusively in virus-treated groups (**Figure 63-B**).

No differences in anti-Itgav responses were observed between VCN-01 and ICO15K-E1aPH20-treated animals. In consequence, we studied the treated animals of both groups together for correlation analyses. Interestingly, there was a significant positive correlation between the number of IFNγ spots against E1b and Itgav (**Figure 63-C**). To discard an experimental artifact of better activated spleens, the correlation between the ELISPOT's positive control (PMA and Ionomycin, PMA) and IFNγ spots of E1b or Itgav were evaluated without significant relationship (**Supplementary Figure-8**, Annex). The immune response against Itgav did not correlate with the tumor growth (**Figure 63-D**), suggesting that the treatment efficacy is not mediated by anti-Itgav immune response. Considering that the only difference between treatments was the hyaluronidase activity, it suggests that hyaluronidase expression lead to the antitumor efficacy.

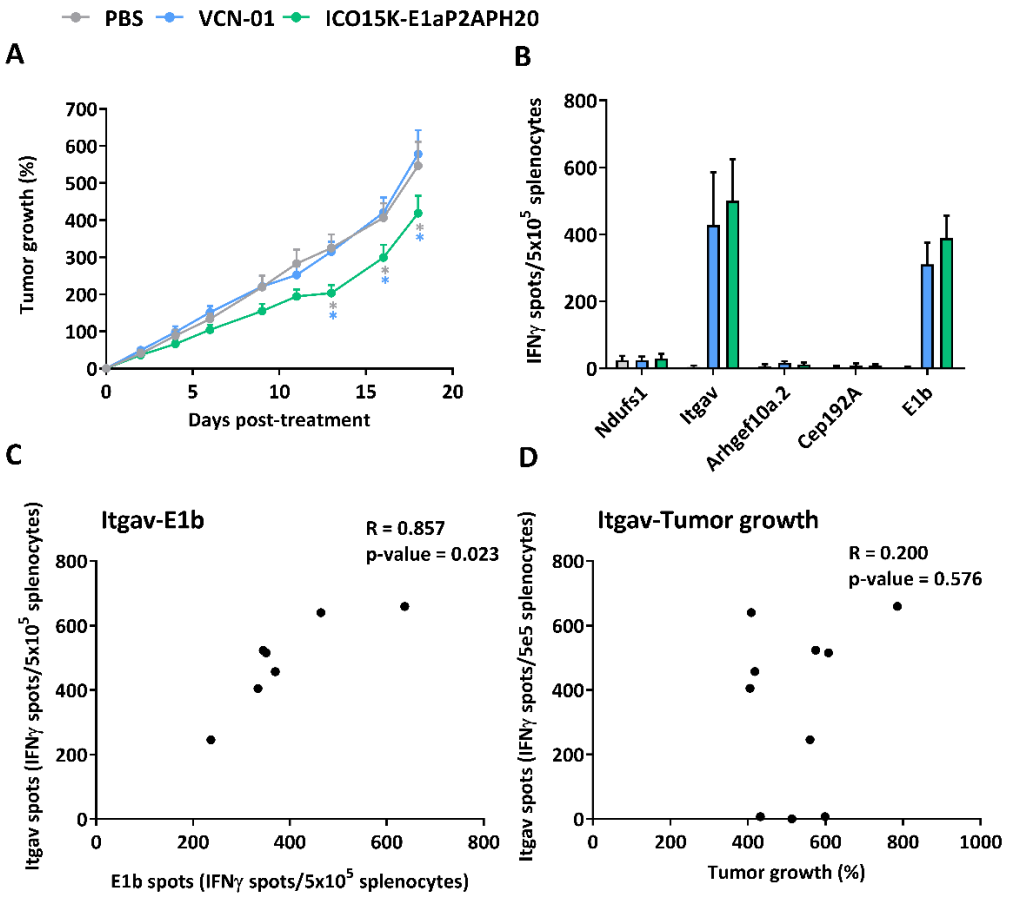

Figure 63. Hyaluronidase expression is crucial for in vivo efficacy against CMT64.6 tumors (E138/18). **(A)** Tumor growth of CMT64.6 tumors was monitored every 3-4 days until the end of the study (each group had n=10-12 tumors). The mean +SEM is plotted. *p<0.05 vs other groups (colors) by Two-way ANOVA and Tukey's *post hoc* test. **(B)** Spleens were collected (n≥3/group) to perform an ELISPOT against 4 CMT64.6 neoepitopes and E1b viral epitope. Mean+SD of IFNγ spots with the background subtraction is plotted. **(C)** Spearman correlation between Itgav spots and E1b spots in VCN-01 and ICO15K-E1aPH20 groups together (n=7). **(D)** There was no correlation between Itgav spots and the % of tumor growth at the endpoint (n=10). The mean of duplicate with background value subtracted is shown per each animal in every correlation.

3.6.4. Hyaluronidase activity in the tumor enhances the T cell accumulation.

Having demonstrated in an immunocompetent model that hyaluronidase expression enhanced the antitumor efficacy, it was still unclear the mechanism of this efficacy. To further analyze the relevance of hyaluronidase expression within the tumor in the presence of the immune system, we looked for a more controlled experimental system. Our group published that the use of an adenovirus which expresses a Bi-specific T-cell engager (ICO15K-cBiTE). The cBiTE is formed by a single chain against the human CD3 present in T cells fused to another against scFv against human EGFR (present in tumor cells). ICO15K-cBiTE could recruit passively injected human T cells to EGFR positive tumors implanted in NSG immunodeficient mice [245].

We wanted to evaluate the relevance of hyaluronic acid in tumor as a barrier for T-cell penetration, and the role of hyaluronidase activity as a therapeutic element to allow T-cell recruitment and accumulation. To achieve this, NSG mice bearing A549 (EGFR positive) subcutaneous tumors were intratumorally treated with ICO15K-cBiTE as monotherapy or combined with recombinant human hyaluronidase (50U/tumor). Three days after treatment, tumors were injected with PBS (virus monotherapy) or a second dose of hyaluronidase (virus/hyal combination). Seven days after the first treatment, luciferase-expressing T cells were intravenously injected and monitored for 4 days for the homing to the tumor by in vivo imaging system (IVIS). One animal treated with PBS was used as a negative control for IVIS imaging.

At the endpoint (day 11), the tumor volume of the virus/hyal combination group was significantly lower than the monotherapy (**Figure 64-A**). The number of adenovirus genomes in the tumors treated with hyaluronidase was higher than the ones treated only with ICO15K-cBiTE (**Figure 64-B**).

The injected luciferase-expressing T cells were detected by luminescence emission in the tumors. Luminescence increased substantially in both treated groups during 4 days post T cell administration. However, tumors of animals receiving the ICO15K-cBiTE

combined with hyaluronidase presented higher luminescence at the endpoint than the monotherapy group. These results suggest that the recombinant hyaluronidase enhanced T cell recruitment (**Figure 64-C**).

There was no direct correlation between the tumor efficacy and the T cell recruitment (or luminescence in the tumor, **Figure 64-D**). We assessed if tumor size correlated with the amount of ICO15K-cBiTE virus that could be responsible for attracting more T cells independently of the injected hyaluronidase. The number of adenovirus copies within the tumor did not correlate with antitumor efficacy (**Figure 64-E**). Most relevant, there was no correlation between the number of Ad copies and the detected luminescence (**Figure 64-F**). This point to the role of hyaluronidase and suggests that hyaluronic acid may impair T cell accumulation in the tumor, and hyaluronidase activity might be important to enhance T cell recruitment.

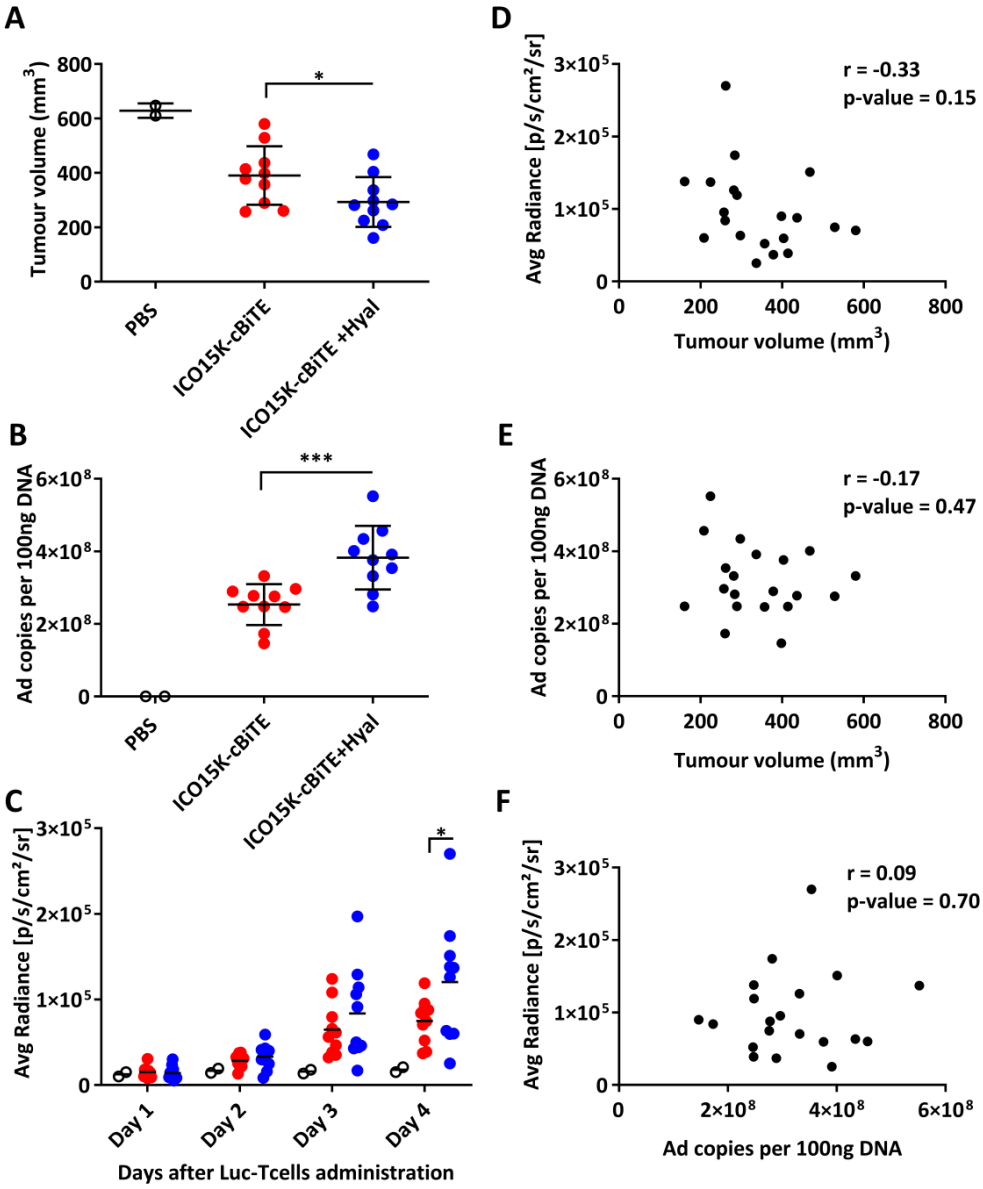

Figure 64. Hyaluronidase could enhance the T-cell accumulation in tumors (NSG 1). NSG mice bearing human A549 were treated intratumorally with 2e9 vp/tumor with ICO15K-cBiTE (n=10) or ICO15K-cBiTE and 50U of human recombinant Hyaluronidase (n=10), then at day 3 post-treatment Hyal group was treated again with 50U hyaluronidase. **(A)** Tumor volume at endpoint (day 11).*p<0.05 by Unpaired T-test. **(B)** The qPCR against E1a gene form tumor DNA. ***p<0.001 by Unpaired T-test. **(C)** 4 days post last hyaluronidase injection (Day 7) 5e6 luciferase expressing-T cells were injected. The bioluminescence *in vivo* was monitored during 4 days by In-vivo Imaging System (IVIS).*p<0.05 by Two-way ANOVA and Tukey's post-hoc test. **(D)** No correlation was detected between the amount of viral genomes and tumor volume. **(E)** There was not a correlation between the radiance of tumors and their tumor volume. **(F)** No correlation was observed between Radiance emitted by tumor and the amount of viral genomes in this tumor. Pearson correlations were performed.

4. DISCUSSION

Solid tumors are complex organ-like structures that consist not only cancer cells but also, vasculature, extracellular matrix (ECM), stromal, and immune cells. Hyaluronic acid (HA) accumulates in the ECM of many solid tumors, including pancreatic ductal adenocarcinomas (PDACs, are particularly rich in HA [443]), breast, colon, and prostate cancer [444], among others. HA is associated with poor prognosis and metastatic potential [401,402], and increases tumoral interstisial pressure playing an important role in resistance to anti-cancer therapies, including OAds [404,405].

The use of hyaluronidase as a therapeutic approach has been considered [445–447]. In the oncolytic virotherapy field, Ganesh et al. proved that hyaluronidase and oncolytic adenovirus combination enhanced the antitumor efficacy [127]. Our group, further develop the strategy generating the VCN-01, a hyaluronidase-expressing OAd [219]. Despite the promising results of VCN-01 in clinics, we aimed to optimize the therapy, looking for candidates with maintained cytotoxic properties and higher hyaluronidase activity.

4.1. CANDIDATES SELECTION

To generate an adenovirus with higher hyaluronidase, we envisioned different strategies: OAds producing higher amounts of PH20 than VCN-01, or OAds expressing hyaluronidases with higher activity than PH20. A soluble hyaluronidase in the *Apis Mellifera* (BHyal) venom was identified [448,449], and homology to mammals PH20 was demonstrated [450]. High activity of BHyal was suggested in previous publications [451]. However, we compared for the first time the BHyal activity against the soluble PH20 (the same encoded in VCN-01), confirming considerably higher BHyal activity than PH20.

In order to generate Hyal-OAds candidates, we armed the ICOVIR15K with the mentioned BHyal or PH20 in different arming strategies. ICO15K genome only exceeds the wild-type Ad5 genome in 151 bp, so it still allows the incorporation of up to ~2 Kb

of foreign DNA. The insertion of a soluble version of PH20 (without transmembrane region, 1,7Kb) did not hamper the viral viability in VCN-01. Therefore, we presumed that BHyal (1,4Kb) would not require adenoviral gene deletions.

The reported insertion sites in non-E3 deleted viruses are downstream of L3 [427] and downstream of L5 (After-fiber), generating a new transcription unit [188,426]. Previous studies in our group revealed the viability of inserting transgenes between *E4* gene and RITR (After-E4), which has been only described in E3 deleted viruses [423,442]. In this chapter, we compared the After-fiber insertion site against the After-E4 insertion site. Furthermore, the insertion of PH20 linked to *E1a* was also tested to try to obtain a virus with earlier hyaluronidase activity than VCN-01.

Apart from the insertion site, the transgene transcriptional control is a key-element when arming OAds. Autonomous transgenes cassettes with exogenous promoters or linking the transgene expression to a viral gene are two main strategies. We belive that the use of splice acceptor (SA) is the most suitable approach to insert a transgene in late. Four different SA have been described in the literature [188,255,423,441]. The IIIa (also named 3VDE) endogenous splicing acceptor from the IIIa protein of the Ad5 is the splicing acceptor currently used in our group, such as in VCN-01 [217,245,246]. No direct comparisons between SA expression levels have been published. Nonetheless, the SA from Ad40 long fiber (40SA) was reported as a strong SA [255,442]. Preliminary data from our group confirmed that 40SA is stronger than IIIaSA, but could hinder the viral fitness. Moreover, BHyal was suspected to impact also in viral fitness. For these reasons, the combination of 40SA and BHyal was not tested in any insertion site. The BHyal was inserted in two different locations under the IIIaSA, whereas PH20 was cloned After-fiber or After-E4 under the IIIaSA or 40SA.

However, the SA could not drive the expression in early, as they depend on the major late promoter. Linking the expression to an early gene without deleting any adenoviral gene, requires an IRES or 2A peptide. IRES are large sequences (around 500bp) bringing the Ad genome to the packaging limit. The reported 2A viral peptide linkers (20-50 bp)

used to insert transgenes in OAds reduced the viral replication yields [438,439]. We decided to use a different 2A sequence [256] to link the PH20 to E1a, generating the ICO15K-E1aPH20.

After comparing the hyaluronidase activity and oncolytic properties *in vitro* of the new viruses and VCN-01, the BHyal viruses had higher hyaluronidase activity than the corresponding PH20 virus, as expected. At the same time, the ICO15K-IIIaBHyal presented reduced cytotoxic properties than VCN-01 (ICO15K-IIIaPH20), thus we did not consider this virus for further development. The ICO15K-IIIaBHyal results suggested that high hyaluronidase activity or the BHyal itself hinders the viral replication. It was published that adenovirus genes can be clustered according to their particular set of codons, known as codon usage [452]. The codon usage of transgenes expressed in late affects viral fitness. Transgenes with a codon usage similar to human compete with adenoviral late genes (human-like codon usage, except fiber) for the same ttRNAs, reducing the oncolytic activity. According to this, the BHyal codon usage explains the cytotoxicity loss [453], and our group confirmed this hypothesis with other transgenes. The testis codon usage differs from the rest of the human tissues [454]; thereby, the PH20 has non-human codon usage and does not compete with late genes.

The after-E4 insertion site reported less transgene production than after-fiber, as previously suggested [442]. The viruses expressing PH20 after-E4 were discarded as no hyaluronidase activity was detected. The ICO15K-E4.BHyal had lower activity than ICO15K-BHyal, but still similar or higher activity than VCN-01, maintaining the oncolytic properties compared to VCN-01. The fewer number of transcripts after-E4 insertion site reduces the transgene competition with late genes, avoiding the viral replication impairment observed in the ICO15K-BHyal. Results in line with this hypothesis were obtained in our group with luciferase transgene.

4.2. HYAL-OADS CHARACTERIZATION

The ICO15K-E1aPH20, ICO15K-40SAPH20, and ICO15K-E4.Bhyal were selected as Hyal-OAds candidates, successfully purified, and their cell cytotoxicity was compared in a

panel of cell lines *in vitro*. No loss of oncolytic properties compared to VCN-01 was detected, except in a pancreatic cell line Panc-1 in which ICO15K-40SA.PH20 and ICO15K-E1aPH20 presented higher IC_{50} values than VCN-01. The obtained values for VCN-01 were higher than previous data in all cell lines [73]; consequence of assessing the cytotoxicity at different timepoints. The VCN-01 and ICO15K-E4.BHyal produced similar yields of TUs, whereas ICO15K-40SAPH20 and ICO15K-E1aPH20 surprisingly presented fewer viral production and release in the supernatant, yet no significant. The slight reduced viral production did not hinder the oncolytic properties in permissive cells according to previous results from the cytotoxic assay. Further studies would be necessary to confirm the loss of production yields of these two viruses.

The PH20 secretion was assessed by Western blot of clarified supernatants from infected cells. Surprisingly, we detected the PH20 only in ICO15K-E1aPH20 and ICO15K-40SAPH20 supernatants. The VCN-01 supernatants did not present detectable levels of PH20, as the negative control ICO15K. Comparable fiber expression confirmed the presence and replication of all viruses. We observed a higher transgene expression of 40SA than the E1aP2A virus, corroborated by the turbidometry of these supernatants. Moreover, the activity of ICO15K-E4.BHyal was also detected. No hyal activity was observed in VCN-01, as expected from Western results. According to previous data, the concentration of VCN-01 supernatants is required to detect hyaluronidase activity[219], suggesting that IIIaSA produces low transgene levels, as we demonstrated in other transgenes. This need for concentration explains the lack of PH20 detection in VCN-01 supernatants, and confirms that the new Hyal-OAds have higher hyaluronidase activity than VCN-01.

The higher activity of hyal-OAds was not detected in the first turbidimetric assay (**Figure 54**). It is worth mentioning that the experimental setup was considerably different. Cell extracts were used to generate the supernatants in the first experiment, whereas the second was infected with purified viruses. The turbidimetric assay is not a sensitive assay with high inter-experiment and intra-experiment variability. Moreover, the supernatant concentration adds another source of variability into the experiments.

We assumed that these two factors explain the divergences, and the Western Blot was used to confirm and support the differential PH20 expression. More sensitive techniques were used to quantify the PH20 presence or activity (ELISA), but cell culture media interference hindered the obtention of reliable conclusions.

Finally, it should take into account that the peak of E1a expression is earlier than 24hours; thus PH20 levels and activity of ICO15K-E1aPH20 should be evaluated earlier. A plateau in the detection and turbidometry experiments could support this hypothesis. Taking all together, we moved to *in vivo* experiments with ICO15K-40SAPH20 and ICO15K-E1aPH20.

4.3. IN VIVO ASSESSMENT OF ENHANCED HYALURONIDASE EXPRESSION IN TUMORS

Sk-mel-28 cells synthesize high HA, and the tumors they form have been identified as sensitive to hyaluronidase activity in combination with oncolytic adenovirus [127,217,219]. We corroborated that Sk-mel-28 tumors have hyaluronic acid, and the VCN-01 and ICO15K-40SAPH20 degrade hyaluronic acid *in vivo*. Then, the antitumor efficacy was assessed after a single intravenous injection, mimicking the clinical treatment of VCN-01. The viruses showed outstanding tumor growth control in long-term responses compared to the untreated tumors, as expected [219].

Interestingly, ICO15K-40SAPH20 and ICO15K-E1aPH20 improved the efficacy of VCN-01 significantly. Based on clinical criteria, the new viruses treatments presented more responders than VCN-01, which was translated in around a 4-fold increase in the disease rate control (DCR, ICO15K-40SAPH20 54%, ICO15K-E1aPH20 66% vs. VCN-01 14%). At the end of the experiment, most of the treated tumors presented a necrotic aspect, suggesting viral efficacy. However, VCN-01 treated tumors showed growing nodules of viable tumor, whereas the other two viruses had less and smaller growing tumor nodules. Further analyses have to be done to confirm these macroscopical observations, but we speculate that higher hyaluronidase activity enhances the viral biodistribution in a rich-HA ECM, which leads to control of all growing tumor nodules.

The new Hyal-OAds were tested in a less sensitive tumor model, such as A549. A549 cells produce low levels of HA [217], and A549 tumors have been resistant to VCN-01 treatment [182]. Surprisingly, we observed tumor growth control by all viruses until day 60, then only the ICO15K-40SAPH20 and VCN-01 presented long-term efficacy compared to untreated control. No significant differences were seen between VCN-01 and ICO15K-40SAPH20, but the latter presented a small increase in the disease control rate. The ICO15K-E1aPH20 did not have antitumor activity from day 60, confirming that hyaluronidase is not mediating the efficacy.

We previously published that VCN-01 (ICO17K) did not have activity in A549 tumors, only a virus with enhanced infectivity (ICO17K-iRGD) significantly showed antitumor efficacy [182]. These results support the idea that hyaluronidase is not essential in this model. However, our results showed a statistically long-term efficacy of VCN-01. We treated the tumors when reached 120mm^3, whereas reported experiment without VCN-01 activity treated tumors at 200mm^3. It might impact on the divergent results. Moreover, the interexperimental variation also could have an influence.

Aiming to evaluate the relationship between hyaluronidase expression from the virus and the immune system, we tested the Hyal-OAds in an immunocompetent model. We confirmed *in vitro* that CMT64.6 model hardly allows viral replication. Moreover, the murine cells do not translate late genes from human adenoviruses [378], as confirmed by hyal activity in CMT64.6. However, ICO15K-E1aPH20 expresses the PH20 linked to E1a having functional PH20 in murine cells. We compared the *in vivo* efficacy of VCN-01 and ICO15K-E1aPH20 in intratumorally treated tumors. The intratumoral injection was used to ensure the viral presence in tumors. The VCN-01 did not show antitumor activity, as previously published [182]. Surprisingly, the ICO15K-E1aPH20 presented a delayed tumor growth compared to the other groups. We detected immune response against the virus (*E1b*) and one CMT64.6 neoepitope (*Itgav*). Higher responses against the virus correlated with a higher anti-*Itgav* response. This may converge with results obtained in Chapter A, where a high anti-viral immune response is associated with

antitumor activity. However, only the virus expressing PH20 showed efficacy. Several hypotheses could explain the differences.

It should be pointed out that the immune analysis is not complete, and responses against other neoepitopes (that we did not analyze) might drive the efficacy. Different neoepitopes responses between viruses driving the differential activity seem unreasonable, as capsid and most of the genes are identical. Nonetheless, the PH20 expression is the only variation between viruses, thus it should be contemplated that expressing a human protein within the murine tumor might induce some extra immune-response. However, the virus itself generates a strong immune induction, and the hPH20 has 60% of homology with mPH20; therefore an extra-immune response against hPH20 mediating the tumor efficacy is unlikely.

Perhaps more reasonable is to highlight the role of PH20 activity. It has been published that pericellular hyaluronic acid might impede the lymphocyte-mediated cytolysis, the NK recognition, and the binding of therapeutic antibodies to their targets [408,455,456]. We speculate that ICO15K-E1aPH20 confers tumor growth control due to PH20 activity. Treated tumors were assessed for viral replication, hyaluronidase activity, and lymphocyte infiltration (data not shown(, without detection of virus, hyal activity, nor lymphocyte accumulation. At the endpoint of the experiment (18 days post-treatment), the virus had been cleared, therefore further experiments must be done evaluating early timepoints to elucidate the role of PH20 activity in the immune cell infiltration in this model.

Looking for a more controlled experimental system, we used a previous experimental setting published in our group. The ICO15K-cBiTE secretes the cBiTE, which binds to CD3 and human EGFR, attracting T cells to EGFR positive tumors (such as A549) [245]. Then, NSG mice implanted with A549 mice were treated intratumorally with ICO15K-cBITE in monotherapy or in combination with recombinant PH20. Two intratumoral rPH20 injections were done, as PH20 has a short lifetime (3min in the blood, [457]) and trying to mimic a hyaluronidase-expressed from a Hyal-OAd. Although not being the

scope of the experiment, we obtained an enhanced tumor efficacy in combination with hyaluronidase, as expected [127]. More viral genomes were detected in tumors combined with hyaluronidase and increased tumor luminescence (T cell accumulation). Remarkably, luminescence did not correlate with viral genomes (thus cBiTE), suggesting that hyaluronidase activity played a role in the T cell accumulation.

4.4. STUDY LIMITATIONS AND FUTURE PERSPECTIVES

The present study showed some limitations. The first virus screening was done according two experiments in the same cell line (A549). Evaluating more cell lines could have been important, as our collaborators demonstrated latter that ICO15K-BHyal do not lose cytotoxicity in other cell lines [453]. Moreover, a sensitive technique to detect and quantify the hyaluronidase activity of all viruses at the same time might be interesting. If not, the optimization of turbidimetric assay must be done. Corroborate the restricted replication and expression of hyaluronidase from a non-tumoral human cell might be interesting. Finally, the lack of an immunocompetent model with human adenovirus replication impairs the assessment of the relationship between hyaluronidase-expressing adenovirus and the immune system.

The next steps for this project should be evaluating the antitumor efficacy in other models. We suggest expanding the panel of High-HA and low-HA human tumors to confirm our results. Orthotopic models might be interesting, as they represent a more physiological situation than subcutaneous xenografts. Regarding this, using a semi-replicative immunocompetent model, such golden Syrian hamter, could bypass complex experimental systems to find out the role of hyaluronidase and immune response. Moreover, repeating the passive immunization of NSG mice treated with ICO15K-cBiTE with adjusted settings may be valuable. The use of a replicative virus and recombinant PH20 should be replaced by tumor cells expressing cBiTE or chemoattractants and the treatment with a hyaluronidase-expressing virus. Also, a mix of non-replicative adenovirus secreting cBiTE and Hyal-OAd could be an option. Finally, extravasation studies with chemotherapy and immunotherapeutics should be done to

understand the relevance of expressing higher hyaluronidase from viruses in putative combinations.

Despite this, we demonstrated that ICO15K-40SAPH20 has better hyaluronidase expression than VCN-01, improving the therapeutic efficacy in a high-HA model and maintaining the oncolytic properties in a low-HA model. Although further characterization is required, we suggest that 40SA-PH20 technology might be incorporated into new company candidates. We also have insights that hyaluronidase activity in the tumor might be valuable for immune cells' extravasation and activity.

Some promising immunotherapies such CAR T cells, adoptive cell transfer, immune checkpoint inhibitors showed limited efficacy in “cold” solid tumors. We propose based on our results and previous publications, that a virus with a high-hyaluronidase activity could be a suitable agent for combinations. The immunogenicity of the virus has demonstrated to revert, at least temporarily, the tumor immunosuppression and the hyaluronidase activity showed to enhance T cell accumulation and allow antibody, T cell, and NK recognition.

5. CONCLUSIONS

- The hyaluronidase from *Apis Mellifera* (BHyal) has higher activity than soluble version of PH20. The BHyal codon usage hampers the adenoviral replication.

- The After-Fiber insertion site and transgene linked to E1a with P2A confers higher transgene production than After-E4 location.

- The 40SA produces more transcripts than IIIaSA.

- ICO15K-40SAPH20, ICO15K-E1aPH20 and ICO15K-E4.IIIaBHyal have higher hyaluronidase activity than VCN-01, and maintained oncolytic properties.

- The ICO15K-40SAPH20 and ICO15K-E1aPH20 improved the antitumor efficacy of VCN-01 in a high-HA melanoma model (Sk-mel-28).

- The ICO15K-40SAPH20 have similar antitumor activity as VCN-01 in a model of less sensitivity to hyaluronidase activity (A549).

- The hyaluronidase expression by ICO15K-E1aPH20 controls the tumor growth in an immunocompetent model (CMT64.6) with restricted viral replication.

- The hyaluronidase activity within the tumor enhances the viral replication of ICO15K-cBITE and the T-cell accumulation in tumors.

BIBLIOGRAPHY

1. Tian, T.; Olson, S.; Whitacre, J.M.; Harding, A. The origins of cancer robustness and evolvability. *Integrative Biology* **2011**, *3*, 17–30, doi:10.1039/c0ib00046a.
2. Burnet, F.M. The concept of immunological surveillance. *Prog Exp Tumor Res* **1970**, *13*, 1–27, doi:10.1159/000386035.
3. Waldhauer, I.; Steinle, A. NK cells and cancer immunosurveillance. *Oncogene* **2008**, *27*, 5932–5943, doi:10.1038/onc.2008.267.
4. Zou, C.; Zhao, P.; Xiao, Z.; Han, X.; Fu, F.; Fu, L. γδ T cells in cancer immunotherapy. *Oncotarget* **2017**, *8*, 8900–8909, doi:10.18632/oncotarget.13051.
5. de Graaf, J.F.; de Vor, L.; Fouchier, R. a. M.; van den Hoogen, B.G. Armed oncolytic viruses: A kick-start for anti-tumor immunity. *Cytokine Growth Factor Rev.* **2018**, *41*, 28–39, doi:10.1016/j.cytogfr.2018.03.006.
6. Kapsenberg, M.L. Dendritic-cell control of pathogen-driven T-cell polarization. *Nat. Rev. Immunol.* **2003**, *3*, 984–993, doi:10.1038/nri1246.
7. Chen, D.S.; Mellman, I. Oncology Meets Immunology: The Cancer-Immunity Cycle. *Immunity* **2013**, *39*, 1–10, doi:10.1016/j.immuni.2013.07.012.
8. Motz, G.T.; Coukos, G. Deciphering and Reversing Tumor Immune Suppression. *Immunity* **2013**, *39*, 61–73, doi:10.1016/j.immuni.2013.07.005.
9. Boon, T.; Cerottini, J.-C.; Van Den Eynde, B.; Van Der Bruggen, P.; Pel, A. Van Tumor antigens recognized by T lymphocytes. *Annu. Rev. Immunol* **1994**, *12*, 337–65, doi:10.1146/annurev.iy.12.040194.002005.
10. Lennerz, V.; Fatho, M.; Gentilini, C.; Frye, R.A.; Lifke, A.; Ferel, D.; Wölfel, C.; Huber, C.; Wölfel, T. The response of autologous T cells to a human melanoma is dominated by mutated neoantigens. *Proc. Natl. Acad. Sci. U.S.A.* **2005**, *102*, 16013–16018, doi:10.1073/pnas.0500090102.
11. Sharonov, G.V.; Serebrovskaya, E.O.; Yuzhakova, D.V.; Britanova, O.V.; Chudakov, D.M. B cells, plasma cells and antibody repertoires in the tumour microenvironment. *Nat Rev Immunol* **2020**, *20*, 294–307, doi:10.1038/s41577-019-0257-x.
12. Bruno, T.C.; Ebner, P.J.; Moore, B.L.; Squalls, O.G.; Waugh, K.A.; Eruslanov, E.B.; Singhal, S.; Mitchell, J.D.; Franklin, W.A.; Merrick, D.T.; et al. Antigen-Presenting Intratumoral B Cells Affect CD4+ TIL Phenotypes in Non-Small Cell Lung Cancer Patients. *Cancer Immunol Res* **2017**, *5*, 898–907, doi:10.1158/2326-6066.CIR-17-0075.
13. Rossetti, R.A.M.; Lorenzi, N.P.C.; Yokochi, K.; Rosa, M.B.S. de F.; Benevides, L.; Margarido, P.F.R.; Baracat, E.C.; Carvalho, J.P.; Villa, L.L.; Lepique, A.P. B lymphocytes can be activated to act as antigen presenting cells to promote anti-tumor responses. *PLoS ONE* **2018**, *13*, e0199034, doi:10.1371/journal.pone.0199034.
14. Schreiber, R.D.; Old, L.J.; Smyth, M.J. Cancer immunoediting: integrating immunity's roles in cancer suppression and promotion. *Science* **2011**, *331*, 1565–1570, doi:10.1126/science.1203486.
15. van der Burg, S.H.; Arens, R.; Ossendorp, F.; van Hall, T.; Melief, C.J.M. Vaccines for established cancer: overcoming the challenges posed by immune evasion. *Nat. Rev. Cancer* **2016**, *16*, 219–233, doi:10.1038/nrc.2016.16.

16. Yu, J.; Du, W.; Yan, F.; Wang, Y.; Li, H.; Cao, S.; Yu, W.; Shen, C.; Liu, J.; Ren, X. Myeloid-derived suppressor cells suppress antitumor immune responses through IDO expression and correlate with lymph node metastasis in patients with breast cancer. *J. Immunol.* **2013**, *190*, 3783–3797, doi:10.4049/jimmunol.1201449.
17. Bronte, V.; Serafini, P.; Mazzoni, A.; Segal, D.M.; Zanovello, P. L-arginine metabolism in myeloid cells controls T-lymphocyte functions. *Trends Immunol.* **2003**, *24*, 302–306, doi:10.1016/s1471-4906(03)00132-7.
18. Pitt, J.M.; Marabelle, A.; Eggermont, A.; Soria, J.-C.; Kroemer, G.; Zitvogel, L. Targeting the tumor microenvironment: removing obstruction to anticancer immune responses and immunotherapy. *Annals of Oncology* **2016**, *27*, 1482–1492, doi:10.1093/annonc/mdw168.
19. Carretero, R.; Romero, J.M.; Ruiz-Cabello, F.; Maleno, I.; Rodriguez, F.; Camacho, F.M.; Real, L.M.; Garrido, F.; Cabrera, T. Analysis of HLA class I expression in progressing and regressing metastatic melanoma lesions after immunotherapy. *Immunogenetics* **2008**, *60*, 439–447, doi:10.1007/s00251-008-0303-5.
20. Drake, C.G.; Jaffee, E.; Pardoll, D.M. Mechanisms of immune evasion by tumors. *Adv. Immunol.* **2006**, *90*, 51–81, doi:10.1016/S0065-2776(06)90002-9.
21. Galluzzi, L.; Buqué, A.; Kepp, O.; Zitvogel, L.; Kroemer, G. Immunogenic cell death in cancer and infectious disease. *Nat. Rev. Immunol.* **2017**, *17*, 97–111, doi:10.1038/nri.2016.107.
22. Knocke, S.; Fleischmann-Mundt, B.; Saborowski, M.; Manns, M.P.; Kühnel, F.; Wirth, T.C.; Woller, N. Tailored Tumor Immunogenicity Reveals Regulation of CD4 and CD8 T Cell Responses against Cancer. *Cell Reports* **2016**, *17*, 2234–2246, doi:10.1016/j.celrep.2016.10.086.
23. Fridman, W.H.; Pagès, F.; Sautès-Fridman, C.; Galon, J. The immune contexture in human tumours: impact on clinical outcome. *Nat. Rev. Cancer* **2012**, *12*, 298–306, doi:10.1038/nrc3245.
24. Vaddepally, R.K.; Kharel, P.; Pandey, R.; Garje, R.; Chandra, A.B. Review of Indications of FDA-Approved Immune Checkpoint Inhibitors per NCCN Guidelines with the Level of Evidence. *Cancers (Basel)* **2020**, *12*, doi:10.3390/cancers12030738.
25. Bonaventura, P.; Shekarian, T.; Alcazer, V.; Valladeau-Guilemond, J.; Valsesia-Wittmann, S.; Amigorena, S.; Caux, C.; Depil, S. Cold Tumors: A Therapeutic Challenge for Immunotherapy. *Front Immunol* **2019**, *10*, doi:10.3389/fimmu.2019.00168.
26. Ribas, A.; Wolchok, J.D. Cancer immunotherapy using checkpoint blockade. *Science* **2018**, *359*, 1350–1355, doi:10.1126/science.aar4060.
27. Garcia-Garijo, A.; Fajardo, C.A.; Gros, A. Determinants for Neoantigen Identification. *Front Immunol* **2019**, *10*, doi:10.3389/fimmu.2019.01392.
28. Commissioner, O. of the FDA approves CAR-T cell therapy to treat adults with certain types of large B-cell lymphoma Available online: https://www.fda.gov/news-events/press-announcements/fda-approves-car-t-cell-therapy-treat-adults-certain-types-large-b-cell-lymphoma (accessed on May 13, 2020).

29. Commissioner, O. of the FDA approval brings first gene therapy to the United States Available online: https://www.fda.gov/news-events/press-announcements/fda-approval-brings-first-gene-therapy-united-states (accessed on May 13, 2020).
30. Guedan, S.; Ruella, M.; June, C.H. Emerging Cellular Therapies for Cancer. *Annual Review of Immunology* **2019**, *37*, 145–171, doi:10.1146/annurev-immunol-042718-041407.
31. Guedan, S.; Calderon, H.; Posey, A.D.; Maus, M.V. Engineering and Design of Chimeric Antigen Receptors. *Mol Ther Methods Clin Dev* **2019**, *12*, 145–156, doi:10.1016/j.omtm.2018.12.009.
32. Goebeler, M.-E.; Bargou, R.C. T cell-engaging therapies — BiTEs and beyond. *Nat Rev Clin Oncol* **2020**, doi:10.1038/s41571-020-0347-5.
33. Mahoney, K.M.; Rennert, P.D.; Freeman, G.J. Combination cancer immunotherapy and new immunomodulatory targets. *Nature Reviews Drug Discovery* **2015**, *14*, 561–584, doi:10.1038/nrd4591.
34. Jiang, T.; Shi, T.; Zhang, H.; Hu, J.; Song, Y.; Wei, J.; Ren, S.; Zhou, C. Tumor neoantigens: from basic research to clinical applications. *Journal of Hematology & Oncology* **2019**, *12*, 93, doi:10.1186/s13045-019-0787-5.
35. Coulie, P.G.; Van den Eynde, B.J.; van der Bruggen, P.; Boon, T. Tumour antigens recognized by T lymphocytes: at the core of cancer immunotherapy. *Nat. Rev. Cancer* **2014**, *14*, 135–146, doi:10.1038/nrc3670.
36. Welters, M.J.P.; Kenter, G.G.; Steenwijk, P.J. de V. van; Löwik, M.J.G.; Meer, D.M.A.B. der; Essahsah, F.; Stynenbosch, L.F.M.; Vloon, A.P.G.; Ramwadhdoebe, T.H.; Piersma, S.J.; et al. Success or failure of vaccination for HPV16-positive vulvar lesions correlates with kinetics and phenotype of induced T-cell responses. *PNAS* **2010**, *107*, 11895–11899, doi:10.1073/pnas.1006500107.
37. Trimble, C.L.; Morrow, M.P.; Kraynyak, K.A.; Shen, X.; Dallas, M.; Yan, J.; Edwards, L.; Parker, R.L.; Denny, L.; Giffear, M.; et al. Safety, efficacy, and immunogenicity of VGX-3100, a therapeutic synthetic DNA vaccine targeting human papillomavirus 16 and 18 E6 and E7 proteins for cervical intraepithelial neoplasia 2/3: a randomised, double-blind, placebo-controlled phase 2b trial. *Lancet* **2015**, *386*, 2078–2088, doi:10.1016/S0140-6736(15)00239-1.
38. Monie, A.; Hung, C.-F.; Roden, R.; Wu, T.-C. Cervarix^{TM}: a vaccine for the prevention of HPV 16, 18-associated cervical cancer. *Biologics* **2008**, *2*, 107–113.
39. Rosenberg, S.A.; Sherry, R.M.; Morton, K.E.; Scharfman, W.J.; Yang, J.C.; Topalian, S.L.; Royal, R.E.; Kammula, U.; Restifo, N.P.; Hughes, M.S.; et al. Tumor Progression Can Occur despite the Induction of Very High Levels of Self/Tumor Antigen-Specific CD8+ T Cells in Patients with Melanoma. *The Journal of Immunology* **2005**, *175*, 6169–6176, doi:10.4049/jimmunol.175.9.6169.
40. Hedley, S.J.; Chen, J.; Mountz, J.D.; Li, J.; Curiel, D.T.; Korokhov, N.; Kovesdi, I. Targeted and shielded adenovectors for cancer therapy. *Cancer Immunol Immunother* **2006**, *55*, 1412–1419, doi:10.1007/s00262-006-0158-2 [doi].
41. Russell, S.J.; Peng, K.W.; Bell, J.C. Oncolytic virotherapy. *Nat Biotechnol* **2012**, *30*, 658–670.

42. Kaufman, H.L.; Kohlhapp, F.J.; Zloza, A. Oncolytic viruses: a new class of immunotherapy drugs. *Nat Rev Drug Discov* **2015**, *14*, 642–662, doi:10.1038/nrd4663.
43. Garber, K. China Approves World's First Oncolytic Virus Therapy For Cancer Treatment. *J Natl Cancer Inst* **2006**, *98*, 298–300, doi:10.1093/jnci/djj111.
44. Doniņą, S.; Strele, I.; Proboka, G.; Auziņš, J.; Alberts, P.; Jonsson, B.; Venskus, D.; Muceniece, A. Adapted ECHO-7 virus Rigvir immunotherapy (oncolytic virotherapy) prolongs survival in melanoma patients after surgical excision of the tumour in a retrospective study. *Melanoma Research* **2015**, *25*, 421–426, doi:10.1097/CMR.0000000000000180.
45. Coffin, R. Interview with Robert Coffin, inventor of T-VEC: The first oncolytic immunotherapy approved for the treatment of cancer. *Immunotherapy* **2016**, *8*, 103–106, doi:10.2217/imt.15.116.
46. Cody, J.J.; Douglas, J.T. Armed replicating adenoviruses for cancer virotherapy. *Cancer Gene Ther* **2009**, *16*, 473–488, doi:cgt20093 [pii]10.1038/cgt.2009.3 [doi].
47. Ungerechts, G.; Bossow, S.; Leuchs, B.; Holm, P.S.; Rommelaere, J.; Coffey, M.; Coffin, R.; Bell, J.; Nettelbeck, D.M. Moving oncolytic viruses into the clinic: clinical-grade production, purification, and characterization of diverse oncolytic viruses. *Mol Ther Methods Clin Dev* **2016**, *3*, 16018, doi:10.1038/mtm.2016.18 [doi]S2329-0501(16)30159-0 [pii].
48. Howley, P.M.; Livingston, D.M. Small DNA tumor viruses: Large contributors to biomedical sciences. *Virology* **2009**, *384*, 256–259, doi:10.1016/j.virol.2008.12.006.
49. Berk, A.J. Recent lessons in gene expression, cell cycle control, and cell biology from adenovirus. *Oncogene* **2005**, *24*, 7673–7685, doi:10.1038/sj.onc.1209040.
50. Hall, K.; Blair Zajdel, M.E.; Blair, G.E. Unity and diversity in the human adenoviruses: exploiting alternative entry pathways for gene therapy. *Biochemical Journal* **2010**, *431*, 321–336, doi:10.1042/BJ20100766.
51. Ison, M.G. Emerging Infections: Adenovirus Infections in Transplant Recipients. *Clinical Infectious Diseases* **2006**, *43*, 331–339, doi:10.1086/505498.
52. Evans, J.D.; Hearing, P. Chapter 3 - Adenovirus Replication. In *Adenoviral Vectors for Gene Therapy*; Curiel, D.T., Douglas, J.T., Eds.; Academic Press: San Diego, 2002; pp. 39–70 ISBN 978-0-12-199504-1.
53. Russell, W.C. Adenoviruses: update on structure and function. *J Gen Virol* **2009**, *90*, 1–20, doi:90/1/1 [pii]10.1099/vir.0.003087-0 [doi].
54. Zhang, Y.; Bergelson, J.M. Adenovirus receptors. *J Virol* **2005**, *79*, 12125–12131, doi:79/19/12125 [pii]10.1128/JVI.79.19.12125-12131.2005 [doi].
55. Verma, I.M.; Weitzman, M.D. GENE THERAPY: Twenty-First Century Medicine. *Annual Review of Biochemistry* **2005**, *74*, 711–738, doi:10.1146/annurev.biochem.74.050304.091637.
56. Hall, K.; Blair Zajdel, M.E.; Blair, G.E. Unity and diversity in the human adenoviruses: exploiting alternative entry pathways for gene therapy. *Biochemical Journal* **2010**, *431*, 321–336, doi:10.1042/BJ20100766.

57. Bewley, M.C. Structural Analysis of the Mechanism of Adenovirus Binding to Its Human Cellular Receptor, CAR. *Science* **1999**, *286*, 1579–1583, doi:10.1126/science.286.5444.1579.
58. Nemerow, G.R. Cell receptors involved in adenovirus entry. *Virology* **2000**, *274*, 1–4, doi:10.1006/viro.2000.0468.
59. Kelkar, S.A.; Pfister, K.K.; Crystal, R.G.; Leopold, P.L. Cytoplasmic Dynein Mediates Adenovirus Binding to Microtubules. *Journal of Virology* **2004**, *78*, 10122–10132, doi:10.1128/JVI.78.18.10122.
60. Wiethoff, C.M.; Wodrich, H.; Gerace, L.; Nemerow, G.R. Adenovirus Protein VI Mediates Membrane Disruption following Capsid Disassembly. *Journal of Virology* **2005**, *79*, 1992–2000, doi:10.1128/JVI.79.4.1992-2000.2005.
61. Parreno, M.; Garriga, J.; Limon, A.; Albrecht, J.H.; Grana, X. E1A modulates phosphorylation of p130 and p107 by differentially regulating the activity of G1/S cyclin/CDK complexes. *Oncogene* **2001**, *20*, 4793–4806, doi:10.1038/sj.onc.1204644 [doi].
62. Sester, M.; Ruszics, Z.; Mackley, E.; Burgert, H.-G. The transmembrane domain of the adenovirus E3/19K protein acts as an endoplasmic reticulum retention signal and contributes to intracellular sequestration of major histocompatibility complex class I molecules. *J. Virol.* **2013**, *87*, 6104–6117, doi:10.1128/JVI.03391-12.
63. McSharry, B.P.; Burgert, H.-G.; Owen, D.P.; Stanton, R.J.; Prod'homme, V.; Sester, M.; Koebernick, K.; Groh, V.; Spies, T.; Cox, S.; et al. Adenovirus E3/19K Promotes Evasion of NK Cell Recognition by Intracellular Sequestration of the NKG2D Ligands Major Histocompatibility Complex Class I Chain-Related Proteins A and B. *Journal of Virology* **2008**, *82*, 4585–4594, doi:10.1128/JVI.02251-07.
64. Flint, J.; Racaniello, V.R.; Rall, G.F.; Skalka, A.M. *Principles of Virology Volume I: Molecular Biology*; 2015; ISBN 9781555819514.
65. Cripe, T.P.; Dunphy, E.J.; Holub, A.D.; Saini, A.; Vasi, N.H.; Mahller, Y.Y.; Collins, M.H.; Snyder, J.D.; Krasnykh, V.; Curiel, D.T.; et al. Fiber knob modifications overcome low, heterogeneous expression of the coxsackievirus-adenovirus receptor that limits adenovirus gene transfer and oncolysis for human rhabdomyosarcoma cells. *Cancer Research* **2001**, *61*, 2953–2960.
66. Dmitriev, I.; Krasnykh, V.; Miller, C.R.; Wang, M.; Kashentseva, E.; Mikheeva, G.; Belousova, N.; Curiel, D.T. An adenovirus vector with genetically modified fibers demonstrates expanded tropism via utilization of a coxsackievirus and adenovirus receptor-independent cell entry mechanism. *Journal of virology* **1998**, *72*, 9706–13.
67. Bauerschmitz, G.J.; Lam, J.T.; Kanerva, A.; Suzuki, K.; Nettelbeck, D.M.; Dmitriev, I.; Krasnykh, V.; Mikheeva, G. V; Barnes, M.N.; Alvarez, R.D.; et al. Treatment of ovarian cancer with a tropism modified oncolytic adenovirus. *Cancer Res* **2002**, *62*, 1266–1270.
68. Hanahan, D.; Weinberg, R.A. The Hallmarks of Cancer. *Cell* **2000**, *100*, 57–70, doi:10.1016/S0092-8674(00)81683-9.
69. Fueyo, J.; Gomez-Manzano, C.; Alemany, R.; Lee, P.S.Y.; McDonnell, T.J.; Mitlianga, P.; Shi, Y.X.; Levin, V.A.; Yung, W.K.A.; Kyritsis, A.P. A mutant oncolytic

adenovirus targeting the Rb pathway produces anti-glioma effect in vivo. *Oncogene* **2000**, *19*, 2–12, doi:10.1038/sj.onc.1203251.

70. Bischoff, J.R.; Kirn, D.H.; Williams, A.; Heise, C.; Horn, S.; Muna, M.; Ng, L.; Nye, J.A.; Sampson-Johannes, A.; Fattaey, A.; et al. An adenovirus mutant that replicates selectively in p53-deficient human tumor cells. *Science* **1996**, *274*, 373–376, doi:10.1126/science.274.5286.373.
71. Cascalló, M.; Capellà, G.; Mazo, A.; Alemany, R. Ras-dependent Oncolysis with an Adenovirus VAI Mutant. *Cancer Res* **2003**, *63*, 5544–5550.
72. Heise, C.; Hermiston, T.; Johnson, L.; Brooks, G.; Sampson-Johannes, A.; Williams, A.; Hawkins, L.; Kirn, D. An adenovirus E1A mutant that demonstrates potent and selective systemic anti-tumoral efficacy. *Nat. Med.* **2000**, *6*, 1134–1139, doi:10.1038/80474.
73. Rodríguez García, A. Enhancing the antitumor activity of oncolytic adenoviruses by combining tumor targeting with hyaluronidase expression or by increasing the immunogenicity of exogenous epitopes. *Doctoral thesis* **2015**.
74. Ylösmäki, E.; Hakkarainen, T.; Hemminki, A.; Visakorpi, T.; Andino, R.; Saksela, K. Generation of a Conditionally Replicating Adenovirus Based on Targeted Destruction of E1A mRNA by a Cell Type-Specific MicroRNA. *J Virol* **2008**, *82*, 11009–11015, doi:10.1128/JVI.01608-08.
75. Cawood, R.; Chen, H.H.; Carroll, F.; Bazan-Peregrino, M.; van Rooijen, N.; Seymour, L.W. Use of tissue-specific microRNA to control pathology of wild-type adenovirus without attenuation of its ability to kill cancer cells. *PLoS Pathog.* **2009**, *5*, e1000440, doi:10.1371/journal.ppat.1000440.
76. Geisler, A.; Fechner, H. MicroRNA-regulated viral vectors for gene therapy. *World J Exp Med* **2016**, *6*, 37–54, doi:10.5493/wjem.v6.i2.37.
77. Kumar, M.S.; Lu, J.; Mercer, K.L.; Golub, T.R.; Jacks, T. Impaired microRNA processing enhances cellular transformation and tumorigenesis. *Nat. Genet.* **2007**, *39*, 673–677, doi:10.1038/ng2003.
78. Rojas, J.J.; Guedan, S.; Searle, P.F.; Martinez-Quintanilla, J.; Gil-Hoyos, R.; Alcayaga-Miranda, F.; Cascallo, M.; Alemany, R. Minimal RB-responsive E1A Promoter Modification to Attain Potency, Selectivity, and Transgene-arming Capacity in Oncolytic Adenoviruses. *Mol Ther* **2010**, *18*, 1960–1971.
79. Rojas, J.J.; Gimenez-Alejandre, M.; Gil-Hoyos, R.; Cascallo, M.; Alemany, R. Improved systemic antitumor therapy with oncolytic adenoviruses by replacing the fiber shaft HSG-binding domain with RGD. *Gene Ther* **2012**, *19*, 453–457, doi:gt2011106 [pii]10.1038/gt.2011.106 [doi].
80. Rojas, J.J.; Guedan, S.; Searle, P.F.; Martinez-Quintanilla, J.; Gil-Hoyos, R.; Alcayaga-Miranda, F.; Cascallo, M.; Alemany, R. Minimal RB-responsive E1A promoter modification to attain potency, selectivity, and transgene-arming capacity in oncolytic adenoviruses. *Molecular Therapy* **2010**, *18*, 1960–1971, doi:10.1038/mt.2010.173.
81. Karlseder, J.; Rotheneder, H.; Wintersberger, E. Interaction of Sp1 with the growth- and cell cycle-regulated transcription factor E2F. *Mol Cell Biol* **1996**, *16*, 1659–1667.

82. Suzuki, K.; Fueyo, J.; Krasnykh, V.; Reynolds, P.N.; Curiel, D.T.; Alemany, R. A conditionally replicative adenovirus with enhanced infectivity shows improved oncolytic potency. *Clin Cancer Res* **2001**, *7*, 120–126.
83. Bayo-Puxan, N.; Gimenez-Alejandre, M.; Lavilla-Alonso, S.; Gros, A.; Cascallo, M.; Hemminki, A.; Alemany, R. Replacement of adenovirus type 5 fiber shaft heparan sulfate proteoglycan-binding domain with RGD for improved tumor infectivity and targeting. *Hum Gene Ther* **2009**, *20*, 1214–1221, doi:10.1089/hum.2009.038 [doi].
84. Rojas Expósito, L.A. Blood barriers for oncolytic adenovirus efficacy: study of binding to erythrocytes via CAR and albumin-mediated evasion of neutralizing antibodies. *Doctoral thesis* **2017**.
85. Kirn, D. Clinical research results with dl1520 (Onyx-015), a replication-selective adenovirus for the treatment of cancer: what have we learned? *Gene Ther.* **2001**, *8*, 89–98, doi:10.1038/sj.gt.3301377.
86. Nemunaitis, J.; Khuri, F.; Ganly, I.; Arseneau, J.; Posner, M.; Vokes, E.; Kuhn, J.; McCarty, T.; Landers, S.; Blackburn, A.; et al. Phase II Trial of Intratumoral Administration of ONYX-015, a Replication-Selective Adenovirus, in Patients With Refractory Head and Neck Cancer. *JCO* **2001**, *19*, 289–298, doi:10.1200/JCO.2001.19.2.289.
87. Kirn, D.H. The End of the Beginning: OncolyticVirotherapy Achieves Clinical Proof-of-Concept. *Molecular Therapy* **2006**, *13*, 237–238, doi:10.1016/j.ymthe.2005.12.005.
88. O'Shea, C.C.; Johnson, L.; Bagus, B.; Choi, S.; Nicholas, C.; Shen, A.; Boyle, L.; Pandey, K.; Soria, C.; Kunich, J.; et al. Late viral RNA export, rather than p53 inactivation, determines ONYX-015 tumor selectivity. *Cancer Cell* **2004**, *6*, 611–623, doi:10.1016/j.ccr.2004.11.012.
89. Cascallo, M.; Alonso, M.M.; Rojas, J.J.; Perez-Gimenez, A.; Fueyo, J.; Alemany, R. Systemic toxicity-efficacy profile of ICOVIR-5, a potent and selective oncolytic adenovirus based on the pRB pathway. *Mol. Ther.* **2007**, *15*, 1607–1615, doi:10.1038/sj.mt.6300239.
90. García, M.; Moreno, R.; Gil-Martin, M.; Cascallò, M.; de Olza, M.O.; Cuadra, C.; Piulats, J.M.; Navarro, V.; Domenech, M.; Alemany, R.; et al. A Phase 1 Trial of Oncolytic Adenovirus ICOVIR-5 Administered Intravenously to Cutaneous and Uveal Melanoma Patients. *Human Gene Therapy* **2018**, *30*, 352–364, doi:10.1089/hum.2018.107.
91. Fueyo, J.; Alemany, R.; Gomez-Manzano, C.; Fuller, G.N.; Khan, A.; Conrad, C.A.; Liu, T.-J.; Jiang, H.; Lemoine, M.G.; Suzuki, K.; et al. Preclinical Characterization of the Antiglioma Activity of a Tropism-Enhanced Adenovirus Targeted to the Retinoblastoma Pathway. *J Natl Cancer Inst* **2003**, *95*, 652–660, doi:10.1093/jnci/95.9.652.
92. Kimball, K.J.; Preuss, M.A.; Barnes, M.N.; Wang, M.; Siegal, G.P.; Wan, W.; Kuo, H.; Saddekni, S.; Stockard, C.R.; Grizzle, W.E.; et al. A phase I study of a tropism-modified conditionally replicative adenovirus for recurrent malignant gynecologic diseases. *Clinical Cancer Research* **2010**, *16*, 5277–5287, doi:10.1158/1078-0432.CCR-10-0791.

93. Lang, F.F.; Conrad, C.; Gomez-Manzano, C.; Yung, W.K.A.; Sawaya, R.; Weinberg, J.S.; Prabhu, S.S.; Rao, G.; Fuller, G.N.; Aldape, K.D.; et al. Phase I Study of DNX-2401 (Delta-24-RGD) Oncolytic Adenovirus: Replication and Immunotherapeutic Effects in Recurrent Malignant Glioma. *J. Clin. Oncol.* **2018**, *36*, 1419–1427, doi:10.1200/JCO.2017.75.8219.
94. DNX-2401 (Tasadenoturev) | DNAtrix Available online: https://www.dnatrix.com/technology/DNX-2401-platform/ (accessed on May 4, 2020).
95. Yu, D.C.; Chen, Y.; Seng, M.; Dilley, J.; Henderson, D.R. The addition of adenovirus type 5 region E3 enables calydon virus 787 to eliminate distant prostate tumor xenografts. *Cancer Res* **1999**, *59*, 4200–4203.
96. Small, E.J.; Carducci, M.A.; Burke, J.M.; Rodriguez, R.; Fong, L.; van Ummersen, L.; Yu, D.C.; Aimi, J.; Ando, D.; Working, P.; et al. A phase I trial of intravenous CG7870, a replication-selective, prostate-specific antigen-targeted oncolytic adenovirus, for the treatment of hormone-refractory, metastatic prostate cancer. *Mol Ther* **2006**, *14*, 107–117, doi:S1525-0016(06)00075-X [pii]10.1016/j.ymthe.2006.02.011 [doi].
97. Kuhn, I.; Harden, P.; Bauzon, M.; Chartier, C.; Nye, J.; Thorne, S.; Reid, T.; Ni, S.; Lieber, A.; Fisher, K.; et al. Directed evolution generates a novel oncolytic virus for the treatment of colon cancer. *PLoS One* **2008**, *3*, e2409, doi:10.1371/journal.pone.0002409 [doi].
98. Garcia-Carbonero, R.; Salazar, R.; Duran, I.; Osman-Garcia, I.; Paz-Ares, L.; Bozada, J.M.; Boni, V.; Blanc, C.; Seymour, L.; Beadle, J.; et al. Phase 1 study of intravenous administration of the chimeric adenovirus enadenotucirev in patients undergoing primary tumor resection. *J Immunother Cancer* **2017**, *5*, doi:10.1186/s40425-017-0277-7.
99. Machiels, J.-P.; Salazar, R.; Rottey, S.; Duran, I.; Dirix, L.; Geboes, K.; Wilkinson-Blanc, C.; Pover, G.; Alvis, S.; Champion, B.; et al. A phase 1 dose escalation study of the oncolytic adenovirus enadenotucirev, administered intravenously to patients with epithelial solid tumors (EVOLVE). *Journal for ImmunoTherapy of Cancer* **2019**, *7*, 20, doi:10.1186/s40425-019-0510-7.
100. Tejada, S.; Alonso, M.; Patiño, A.; Fueyo, J.; Gomez-Manzano, C.; Diez-Valle, R. Phase I Trial of DNX-2401 for Diffuse Intrinsic Pontine Glioma Newly Diagnosed in Pediatric Patients. *Neurosurgery* **2018**, *83*, 1050–1056, doi:10.1093/neuros/nyx507.
101. Ramirez, M.; Ruano, D.; Moreno, L.; Lassaletta, Á.; Sirvent, F.J.B.; Andión, M.; Hernández, C.; González-Murillo, Á.; Melen, G.; Alemany, R.; et al. First-in-child trial of celyvir (autologous mesenchymal stem cells carrying the oncolytic virus ICOVIR-5) in patients with relapsed and refractory pediatric solid tumors. *JCO* **2018**, *36*, 10543–10543, doi:10.1200/JCO.2018.36.15_suppl.10543.
102. Small, E.J.; Carducci, M.A.; Burke, J.M.; Rodriguez, R.; Fong, L.; van Ummersen, L.; Yu, D.C.; Aimi, J.; Ando, D.; Working, P.; et al. A phase I trial of intravenous CG7870, a replication-selective, prostate-specific antigen-targeted oncolytic adenovirus, for the treatment of hormone-refractory, metastatic prostate cancer. *Mol. Ther.* **2006**, *14*, 107–117, doi:10.1016/j.ymthe.2006.02.011.

103. Burke, J.M.; Lamm, D.L.; Meng, M.V.; Nemunaitis, J.J.; Stephenson, J.J.; Arseneau, J.C.; Aimi, J.; Lerner, S.; Yeung, A.W.; Kazarian, T.; et al. A first in human phase 1 study of CG0070, a GM-CSF expressing oncolytic adenovirus, for the treatment of nonmuscle invasive bladder cancer. *J. Urol.* **2012**, *188*, 2391–2397, doi:10.1016/j.juro.2012.07.097.
104. Packiam, V.T.; Lamm, D.L.; Barocas, D.A.; Trainer, A.; Fand, B.; Davis, R.L.; Clark, W.; Kroeger, M.; Dumbadze, I.; Chamie, K.; et al. An open label, single-arm, phase II multicenter study of the safety and efficacy of CG0070 oncolytic vector regimen in patients with BCG-unresponsive non-muscle-invasive bladder cancer: Interim results. *Urol. Oncol.* **2018**, *36*, 440–447, doi:10.1016/j.urolonc.2017.07.005.
105. Vassilev, L.; Ranki, T.; Joensuu, T.; Jäger, E.; Karbach, J.; Wahle, C.; Partanen, K.; Kairemo, K.; Alanko, T.; Turkki, R.; et al. Repeated intratumoral administration of ONCOS-102 leads to systemic antitumor CD8 $^{+}$ T-cell response and robust cellular and transcriptional immune activation at tumor site in a patient with ovarian cancer. *OncoImmunology* **2015**, *4*, e1017702, doi:10.1080/2162402X.2015.1017702.
106. Ranki, T.; Joensuu, T.; Jäger, E.; Karbach, J.; Wahle, C.; Kairemo, K.; Alanko, T.; Partanen, K.; Turkki, R.; Linder, N.; et al. Local treatment of a pleural mesothelioma tumor with ONCOS-102 induces a systemic antitumor CD8 $^{+}$ T-cell response, prominent infiltration of CD8 $^{+}$ lymphocytes and Th1 type polarization. *OncoImmunology* **2014**, *3*, e958937, doi:10.4161/21624011.2014.958937.
107. Ranki, T.; Pesonen, S.; Hemminki, A.; Partanen, K.; Kairemo, K.; Alanko, T.; Lundin, J.; Linder, N.; Turkki, R.; Ristimäki, A.; et al. Phase I study with ONCOS-102 for the treatment of solid tumors – an evaluation of clinical response and exploratory analyses of immune markers. *J Immunother Cancer* **2016**, *4*, doi:10.1186/s40425-016-0121-5.
108. Marchini, A.; Scott, E.M.; Rommelaere, J. Overcoming barriers in oncolytic virotherapy with HDAC inhibitors and immune checkpoint blockade. *Viruses* 2016, *8*.
109. Yamamoto, M.; Curiel, D.T. Current Issues and Future Directions of Oncolytic Adenoviruses. *Mol Ther* **2010**, *18*, 243–250, doi:10.1038/mt.2009.266.
110. Alemany, R.; Suzuki, K.; Curiel, D.T. Blood clearance rates of adenovirus type 5 in mice. *J Gen Virol* **2000**, *81*, 2605–2609, doi:10.1099/0022-1317-81-11-2605 [doi].
111. Hamid, O.; Varterasian, M.L.; Wadler, S.; Hecht, J.R.; Benson 3rd, A.; Galanis, E.; Uprichard, M.; Omer, C.; Bycott, P.; Hackman, R.C.; et al. Phase II trial of intravenous CI-1042 in patients with metastatic colorectal cancer. *J Clin Oncol* **2003**, *21*, 1498–1504, doi:10.1200/JCO.2003.09.114 [doi]JCO.2003.09.114 [pii].
112. Bradley, R.R.; Maxfield, L.F.; Lynch, D.M.; Iampietro, M.J.; Borducchi, E.N.; Barouch, D.H. Adenovirus Serotype 5-Specific Neutralizing Antibodies Target Multiple Hexon Hypervariable Regions. *Journal of Virology* **2012**, *86*, 1267–1272, doi:10.1128/JVI.06165-11.
113. Fausther-Bovendo, H.; Kobinger, G.P. Pre-existing immunity against Ad vectors: Humoral, cellular, and innate response, what's important? *Human Vaccines and Immunotherapeutics* 2014, *10*, 2875–2884.

114. Smith, J.S.; Xu, Z.; Tian, J.; Stevenson, S.C.; Byrnes, A.P. Interaction of systemically delivered adenovirus vectors with Kupffer cells in mouse liver. *Hum Gene Ther* **2008**, *19*, 547–554, doi:10.1089/hum.2008.004 [doi].
115. Khare, R.; Hillestad, M.L.; Xu, Z.; Byrnes, A.P.; Barry, M.A. Circulating antibodies and macrophages as modulators of adenovirus pharmacology. *J Virol* **2013**, *87*, 3678–3686, doi:JVI.01392-12 [pii]10.1128/JVI.01392-12 [doi].
116. Shayakhmetov, D.M.; Gaggar, A.; Ni, S.; Li, Z.Y.; Lieber, A. Adenovirus binding to blood factors results in liver cell infection and hepatotoxicity. *J Virol* **2005**, *79*, 7478–7491, doi:79/12/7478 [pii]10.1128/JVI.79.12.7478-7491.2005 [doi].
117. Parker, A.L.; Waddington, S.N.; Nicol, C.G.; Shayakhmetov, D.M.; Buckley, S.M.; Denby, L.; Kemball-Cook, G.; Ni, S.; Lieber, A.; McVey, J.H.; et al. Multiple vitamin K-dependent coagulation zymogens promote adenovirus-mediated gene delivery to hepatocytes. *Blood* **2006**, *108*, 2554–2561, doi:blood-2006-04-008532 [pii]10.1182/blood-2006-04-008532 [doi].
118. Rojas, L.A.; Moreno, R.; Calderón, H.; Alemany, R. Adenovirus coxsackie adenovirus receptor-mediated binding to human erythrocytes does not preclude systemic transduction. *Cancer Gene Ther.* **2016**, *23*, 411–414, doi:10.1038/cgt.2016.50.
119. Carlisle, R.C.; Di, Y.; Cerny, A.M.; Sonnen, A.F.-P.; Sim, R.B.; Green, N.K.; Subr, V.; Ulbrich, K.; Gilbert, R.J.C.; Fisher, K.D.; et al. Human erythrocytes bind and inactivate type 5 adenovirus by presenting Coxsackie virus-adenovirus receptor and complement receptor 1. *Blood* **2009**, *113*, 1909–1918, doi:10.1182/blood-2008-09-178459.
120. Smith, E.; Breznik, J.; Lichty, B.D. Strategies to enhance viral penetration of solid tumors. *Hum. Gene Ther.* **2011**, *22*, 1053–1060, doi:10.1089/hum.2010.227.
121. Fisher, K.D.; Stallwood, Y.; Green, N.K.; Ulbrich, K.; Mautner, V.; Seymour, L.W. Polymer-coated adenovirus permits efficient retargeting and evades neutralising antibodies. *Gene Ther.* **2001**, *8*, 341–348, doi:10.1038/sj.gt.3301389.
122. Kasala, D.; Yun, C.-O. 29 - Polymer-Anchored Adenovirus as a Therapeutic Agent for Cancer Gene Therapy. In *Adenoviral Vectors for Gene Therapy (Second Edition)*; Curiel, D.T., Ed.; Academic Press: San Diego, 2016; pp. 707–737 ISBN 978-0-12-800276-6.
123. Rojas, L.A.; Condezo, G.N.; Olié, R.M.; Fajardo, C.A.; Arias-Badia, M.; San Martín, C.; Alemany, R. Albumin-binding adenoviruses circumvent pre-existing neutralizing antibodies upon systemic delivery. *Journal of Controlled Release* **2016**, *237*, 78–88, doi:10.1016/j.jconrel.2016.07.004.
124. Bradley, R.R.; Maxfield, L.F.; Lynch, D.M.; Iampietro, M.J.; Borducchi, E.N.; Barouch, D.H. Adenovirus serotype 5-specific neutralizing antibodies target multiple hexon hypervariable regions. *J. Virol.* **2012**, *86*, 1267–1272, doi:10.1128/JVI.06165-11.
125. Swanner, J.; Meisen, W.H.; McCormack, R.M.; Lewis, C.T.; Hong, B.; Kaur, B. Current Challenges and Applications of Oncolytic Viruses in Overcoming the Development of Resistance to Therapies in Cancer. In *Current Applications for Overcoming Resistance to Targeted Therapies*; Szewczuk, M.R., Qorri, B., Sambi,

M., Eds.; Resistance to Targeted Anti-Cancer Therapeutics; Springer International Publishing: Cham, 2019; pp. 63–96 ISBN 978-3-030-21477-7.
126. Smith, E.; Breznik, J.; Lichty, B.D. Strategies to Enhance Viral Penetration of Solid Tumors. *Human Gene Therapy* **2011**, *22*, 1053–1060, doi:10.1089/hum.2010.227.
127. Ganesh, S.; Gonzalez-Edick, M.; Gibbons, D.; Van Roey, M.; Jooss, K. Intratumoral coadministration of hyaluronidase enzyme and oncolytic adenoviruses enhances virus potency in metastatic tumor models. *Clin. Cancer Res.* **2008**, *14*, 3933–3941, doi:10.1158/1078-0432.CCR-07-4732.
128. Kelly, E.; Russell, S.J. History of oncolytic viruses: genesis to genetic engineering. *Mol Ther* **2007**, *15*, 651–659, doi:S1525-0016(16)31331-4 [pii]10.1038/sj.mt.6300108 [doi].
129. Conrad, D.P.; Tsang, J.; Maclean, M.; Diallo, J.-S.; Le Boeuf, F.; Lemay, C.G.; Falls, T.J.; Parato, K.A.; Bell, J.C.; Atkins, H.L. Leukemia cell-rhabdovirus vaccine: personalized immunotherapy for acute lymphoblastic leukemia. *Clin. Cancer Res.* **2013**, *19*, 3832–3843, doi:10.1158/1078-0432.CCR-12-3199.
130. Ricca, J.M.; Oseledchyk, A.; Walther, T.; Liu, C.; Mangarin, L.; Merghoub, T.; Wolchok, J.D.; Zamarin, D. Pre-existing Immunity to Oncolytic Virus Potentiates Its Immunotherapeutic Efficacy. *Mol. Ther.* **2018**, *26*, 1008–1019, doi:10.1016/j.ymthe.2018.01.019.
131. Forsyth, P.A.; Abate-Daga, D. Oncolytic Virotherapy for Malignant Gliomas. *Journal of Clinical Oncology* **2018**, doi:10.1200/JCO.2017.77.3192.
132. Fejer, G.; Freudenberg, M.; Greber, U.F.; Gyory, I. Adenovirus-triggered innate signalling pathways. *Eur J Microbiol Immunol (Bp)* **2011**, *1*, 279–288, doi:10.1556/EuJMI.1.2011.4.3.
133. Reid, T.; Galanis, E.; Abbruzzese, J.; Sze, D.; Andrews, J.; Romel, L.; Hatfield, M.; Rubin, J.; Kirn, D. Intra-arterial administration of a replication-selective adenovirus (dl1520) in patients with colorectal carcinoma metastatic to the liver: a phase I trial. *Gene Ther.* **2001**, *8*, 1618–1626, doi:10.1038/sj.gt.3301512.
134. Crystal, R.G.; Harvey, B.-G.; Wisnivesky, J.P.; O'Donoghue, K.A.; Chu, K.W.; Maroni, J.; Muscat, J.C.; Pippo, A.L.; Wright, C.E.; Kaner, R.J.; et al. Analysis of risk factors for local delivery of low- and intermediate-dose adenovirus gene transfer vectors to individuals with a spectrum of comorbid conditions. *Hum. Gene Ther.* **2002**, *13*, 65–100, doi:10.1089/10430340152712647.
135. Muruve, D.A.; Barnes, M.J.; Stillman, I.E.; Libermann, T.A. Adenoviral gene therapy leads to rapid induction of multiple chemokines and acute neutrophil-dependent hepatic injury in vivo. *Hum. Gene Ther.* **1999**, *10*, 965–976, doi:10.1089/10430349950018364.
136. McCoy, R.D.; Davidson, B.L.; Roessler, B.J.; Huffnagle, G.B.; Janich, S.L.; Laing, T.J.; Simon, R.H. Pulmonary inflammation induced by incomplete or inactivated adenoviral particles. *Hum. Gene Ther.* **1995**, *6*, 1553–1560, doi:10.1089/hum.1995.6.12-1553.
137. Doronin, K.; Flatt, J.W.; Di Paolo, N.C.; Khare, R.; Kalyuzhniy, O.; Acchione, M.; Sumida, J.P.; Ohto, U.; Shimizu, T.; Akashi-Takamura, S.; et al. Coagulation factor X activates innate immunity to human species C adenovirus. *Science* **2012**, *338*, 795–798, doi:10.1126/science.1226625.

138. Eichholz, K.; Mennechet, F.J.D.; Kremer, E.J. Human coagulation factor X-adenovirus type 5 complexes poorly stimulate an innate immune response in human mononuclear phagocytes. *J. Virol.* **2015**, *89*, 2884–2891, doi:10.1128/JVI.03576-14.
139. Lyons, M.; Onion, D.; Green, N.K.; Aslan, K.; Rajaratnam, R.; Bazan-Peregrino, M.; Phipps, S.; Hale, S.; Mautner, V.; Seymour, L.W.; et al. Adenovirus type 5 interactions with human blood cells may compromise systemic delivery. *Mol Ther* **2006**, *14*, 118–128, doi:S1525-0016(06)00018-9 [pii]10.1016/j.ymthe.2006.01.003 [doi].
140. Shirley, J.L.; de Jong, Y.P.; Terhorst, C.; Herzog, R.W. Immune Responses to Viral Gene Therapy Vectors. *Molecular Therapy* **2020**, *28*, 709–722, doi:10.1016/j.ymthe.2020.01.001.
141. Atasheva, S.; Shayakhmetov, D. Adenovirus sensing by the immune system. *Curr Opin Virol* **2016**, *21*, 109–113, doi:10.1016/j.coviro.2016.08.017.
142. He, J.Q.; Katschke, K.J.; Gribling, P.; Suto, E.; Lee, W.P.; Diehl, L.; Eastham-Anderson, J.; Ponakala, A.; Komuves, L.; Egen, J.G.; et al. CRIg mediates early Kupffer cell responses to adenovirus. *Journal of Leukocyte Biology* **2013**, *93*, 301–306, doi:10.1189/jlb.0612311.
143. Hj, H.; M, B.; Am, B.; Bw, van der S.; Dt, C.; A, P.; S, G.; Ar, B. Scavenger Receptor A: A New Route for Adenovirus 5 Available online: https://pubmed.ncbi.nlm.nih.gov/19227971/ (accessed on May 20, 2020).
144. Cotter, M.J.; Zaiss, A.K.; Muruve, D.A. Neutrophils interact with adenovirus vectors via Fc receptors and complement receptor 1. *Journal of virology* **2005**, *79*, 14622–31, doi:10.1128/JVI.79.23.14622-14631.2005.
145. Paolo, N.C.D.; Baldwin, L.K.; Irons, E.E.; Papayannopoulou, T.; Tomlinson, S.; Shayakhmetov, D.M. IL-1α and Complement Cooperate in Triggering Local Neutrophilic Inflammation in Response to Adenovirus and Eliminating Virus-Containing Cells. *PLOS Pathogens* **2014**, *10*, e1004035, doi:10.1371/journal.ppat.1004035.
146. Kawai, T.; Takahashi, K.; Sato, S.; Coban, C.; Kumar, H.; Kato, H.; Ishii, K.J.; Takeuchi, O.; Akira, S. IPS-1, an adaptor triggering RIG-I- and Mda5-mediated type I interferon induction. *Nat. Immunol.* **2005**, *6*, 981–988, doi:10.1038/ni1243.
147. Honda, K.; Yanai, H.; Mizutani, T.; Negishi, H.; Shimada, N.; Suzuki, N.; Ohba, Y.; Takaoka, A.; Yeh, W.-C.; Taniguchi, T. Role of a transductional-transcriptional processor complex involving MyD88 and IRF-7 in Toll-like receptor signaling. *Proc. Natl. Acad. Sci. U.S.A.* **2004**, *101*, 15416–15421, doi:10.1073/pnas.0406933101.
148. Gregory, S.M.; Nazir, S.A.; Metcalf, J.P. Implications of the innate immune response to adenovirus and adenoviral vectors. *Future Virol* **2011**, *6*, 357–374, doi:10.2217/fvl.11.6.
149. Manickan, E.; Smith, J.S.; Tian, J.; Eggerman, T.L.; Lozier, J.N.; Muller, J.; Byrnes, A.P. Rapid Kupffer cell death after intravenous injection of adenovirus vectors. *Mol Ther* **2006**, *13*, 108–117, doi:S1525-0016(05)01559-5 [pii]10.1016/j.ymthe.2005.08.007 [doi].
150. Tao, N.; Gao, G.P.; Parr, M.; Johnston, J.; Baradet, T.; Wilson, J.M.; Barsoum, J.; Fawell, S.E. Sequestration of adenoviral vector by Kupffer cells leads to a

nonlinear dose response of transduction in liver. *Mol. Ther.* **2001**, *3*, 28–35, doi:10.1006/mthe.2000.0227.

151. Franchi, L.; Warner, N.; Viani, K.; Nuñez, G. Function of Nod-like receptors in microbial recognition and host defense. *Immunol. Rev.* **2009**, *227*, 106–128, doi:10.1111/j.1600-065X.2008.00734.x.
152. Martinon, F.; Burns, K.; Tschopp, J. The inflammasome: a molecular platform triggering activation of inflammatory caspases and processing of proIL-beta. *Mol. Cell* **2002**, *10*, 417–426, doi:10.1016/s1097-2765(02)00599-3.
153. van de Veerdonk, F.L.; Netea, M.G.; Dinarello, C.A.; Joosten, L.A.B. Inflammasome activation and IL-1β and IL-18 processing during infection. *Trends Immunol.* **2011**, *32*, 110–116, doi:10.1016/j.it.2011.01.003.
154. Steinstraesser, L.; Sorkin, M.; Jacobsen, F.; Al-Benna, S.; Kesting, M.R.; Niederbichler, A.D.; Otte, J.-M.; Hirsch, T.; Stupka, J.; Steinau, H.-U.; et al. Evaluation of signal transduction pathways after transient cutaneous adenoviral gene delivery. *BMC Immunol.* **2011**, *12*, 8, doi:10.1186/1471-2172-12-8.
155. Minamitani, T.; Iwakiri, D.; Takada, K. Adenovirus virus-associated RNAs induce type I interferon expression through a RIG-I-mediated pathway. *J. Virol.* **2011**, *85*, 4035–4040, doi:10.1128/JVI.02160-10.
156. Saito, T.; Gale, M. Differential recognition of double-stranded RNA by RIG-I–like receptors in antiviral immunity. *J Exp Med* **2008**, *205*, 1523–1527, doi:10.1084/jem.20081210.
157. Chiu, Y.-H.; Macmillan, J.B.; Chen, Z.J. RNA polymerase III detects cytosolic DNA and induces type I interferons through the RIG-I pathway. *Cell* **2009**, *138*, 576–591, doi:10.1016/j.cell.2009.06.015.
158. Appledorn, D.M.; Patial, S.; McBride, A.; Godbehere, S.; Rooijen, N.V.; Parameswaran, N.; Amalfitano, A. Adenovirus Vector-Induced Innate Inflammatory Mediators, MAPK Signaling, As Well As Adaptive Immune Responses Are Dependent upon Both TLR2 and TLR9 In Vivo. *The Journal of Immunology* **2008**, *181*, 2134–2144, doi:10.4049/jimmunol.181.3.2134.
159. Haveman, L.M.; Bierings, M.; Klein, M.R.; Beekman, J.M.; de Jager, W.; Kuis, W.; Albani, S.; Prakken, B.J. Selection of perforin expressing CD4+ adenovirus-specific T-cells with artificial antigen presenting cells. *Clin. Immunol.* **2013**, *146*, 228–239, doi:10.1016/j.clim.2013.01.002.
160. Atasheva, S.; Yao, J.; Shayakhmetov, D.M. Innate immunity to adenovirus: lessons from mice. *FEBS Letters* **2019**, *593*, 3461–3483, doi:10.1002/1873-3468.13696@10.1002/(ISSN)1873-3468.reviews.
161. Bruder, J.T.; Kovesdi, I. Adenovirus infection stimulates the Raf/MAPK signaling pathway and induces interleukin-8 expression. *J. Virol.* **1997**, *71*, 398–404.
162. M, S.; K, A.; V, S.; A, B.; A, L.; C, P.; F, P.; A, C.; M, N.; G, S.; et al. Toll Like Receptors and Pancreatic Diseases: From a Pathogenetic Mechanism to a Therapeutic Target Available online: http://pubmed.ncbi.nlm.nih.gov/26036357/ (accessed on May 21, 2020).
163. Meseure, D.; Vacher, S.; Drak Alsibai, K.; Trassard, M.; Nicolas, A.; Leclere, R.; Lerebours, F.; Guinebretiere, J.M.; Marangoni, E.; Lidereau, R.; et al. Biopathological Significance of TLR9 Expression in Cancer Cells and Tumor

Microenvironment Across Invasive Breast Carcinomas Subtypes. *Cancer Microenviron* **2016**, *9*, 107–118, doi:10.1007/s12307-016-0186-1.

164. Shaw, A.R.; Suzuki, M. Immunology of Adenoviral Vectors in Cancer Therapy. *Molecular Therapy - Methods & Clinical Development* **2019**, *15*, 418–429, doi:10.1016/j.omtm.2019.11.001.
165. Lam, E.; Falck-Pedersen, E. Unabated Adenovirus Replication following Activation of the cGAS/STING-Dependent Antiviral Response in Human Cells. *J Virol* **2014**, *88*, 14426–14439, doi:10.1128/JVI.02608-14.
166. Lemos de Matos, A.; Franco, L.S.; McFadden, G. Oncolytic Viruses and the Immune System: The Dynamic Duo. *Mol Ther Methods Clin Dev* **2020**, *17*, 349–358, doi:10.1016/j.omtm.2020.01.001.
167. Thaci, B.; Ulasov, I.V.; Wainwright, D.V.; Lesniak, M.S. The Challenge for Gene Therapy: Innate Immune Response to Adenoviruses. *Oncotarget* **2011**, *2*, 113–121, doi:10.18632/oncotarget.231.
168. Zitvogel, L.; Kepp, O.; Kroemer, G. Decoding Cell Death Signals in Inflammation and Immunity. *Cell* **2010**, *140*, 798–804, doi:10.1016/j.cell.2010.02.015.
169. H, I.; H, A.; F, K.; Y, K.; S, K.; T, W.; E, I.; A, I.; K, F.; Kr, H.; et al. Autophagic Cell Death of Malignant Glioma Cells Induced by a Conditionally Replicating Adenovirus Available online: http://pubmed.ncbi.nlm.nih.gov/16670388/?dopt=Abstract (accessed on May 21, 2020).
170. Ma, J.; Ramachandran, M.; Jin, C.; Quijano-Rubio, C.; Martikainen, M.; Yu, D.; Essand, M. Characterization of virus-mediated immunogenic cancer cell death and the consequences for oncolytic virus-based immunotherapy of cancer. *Cell Death & Disease* **2020**, *11*, 1–15, doi:10.1038/s41419-020-2236-3.
171. H, R.-R.; Jg, G.-G.; A, G.-G.; Xm, R.; L, C.; Km, M.; Hs, Z. Adenoviruses Induce Autophagy to Promote Virus Replication and Oncolysis Available online: http://pubmed.ncbi.nlm.nih.gov/21575980/?dopt=Abstract (accessed on May 21, 2020).
172. Endo, Y.; Sakai, R.; Ouchi, M.; Onimatsu, H.; Hioki, M.; Kagawa, S.; Uno, F.; Watanabe, Y.; Urata, Y.; Tanaka, N.; et al. Virus-mediated oncolysis induces danger signal and stimulates cytotoxic T-lymphocyte activity via proteasome activator upregulation. *Oncogene* **2008**, *27*, 2375–2381, doi:10.1038/sj.onc.1210884.
173. I, D.; V, C.; Ml, H.; S, E.; M, U.; Sk, P.; S, B.; S, P.; A, K.; As, L.; et al. Immune Response Is an Important Aspect of the Antitumor Effect Produced by a CD40L-encoding Oncolytic Adenovirus Available online: https://pubmed.ncbi.nlm.nih.gov/22396493/ (accessed on May 21, 2020).
174. Di Somma, S.; Iannuzzi, C.A.; Passaro, C.; Forte, I.M.; Iannone, R.; Gigantino, V.; Indovina, P.; Botti, G.; Giordano, A.; Formisano, P.; et al. The Oncolytic Virus dl922-947 Triggers Immunogenic Cell Death in Mesothelioma and Reduces Xenograft Growth. *Front. Oncol.* **2019**, *9*, doi:10.3389/fonc.2019.00564.
175. G, P.; G, A.; G, M.; J, H.; S, B.; A, M.; L, F. Phagocytosis of Cells Dying Through Autophagy Induces Inflammasome Activation and IL-1β Release in Human Macrophages Available online:

http://pubmed.ncbi.nlm.nih.gov/21217200/?dopt=Abstract (accessed on May 21, 2020).

176. Q, W.; R, I.; K, M.; H, K.; S, N.; T, S. Pyroptotic Cells Externalize Eat-Me and Release Find-Me Signals and Are Efficiently Engulfed by Macrophages Available online: http://pubmed.ncbi.nlm.nih.gov/23446850/?dopt=Abstract (accessed on May 21, 2020).
177. Marelli, G.; Howells, A.; Lemoine, N.R.; Wang, Y. Oncolytic viral therapy and the immune system: A double-edged sword against cancer. *Frontiers in Immunology* **2018**, *9*, 1–8, doi:10.3389/fimmu.2018.00866.
178. Russell, S.J.; Barber, G.N. Oncolytic Viruses as Antigen Agnostic Tumor Vaccines. *Cancer Cell* **2018**, *33*, 599–605, doi:10.1016/j.ccell.2018.03.011.
179. Yamano, T.; Kubo, S.; Fukumoto, M.; Yano, A.; Mawatari-Furukawa, Y.; Okamura, H.; Tomita, N. Whole cell vaccination using immunogenic cell death by an oncolytic adenovirus is effective against a colorectal cancer model. *Molecular Therapy - Oncolytics* **2016**, *3*, 16031, doi:10.1038/mto.2016.31.
180. Woller, N.; Gürlevik, E.; Fleischmann-Mundt, B.; Schumacher, A.; Knocke, S.; Kloos, A.M.; Saborowski, M.; Geffers, R.; Manns, M.P.; Wirth, T.C.; et al. Viral Infection of Tumors Overcomes Resistance to PD-1-immunotherapy by Broadening Neoantigenome-directed T-cell Responses. *Molecular Therapy* **2015**, *23*, 1630–1640, doi:10.1038/mt.2015.115.
181. Kanerva, A.; Nokisalmi, P.; Diaconu, I.; Koski, A.; Cerullo, V.; Liikanen, I.; Tähtinen, S.; Oksanen, M.; Heiskanen, R.; Pesonen, S.; et al. Antiviral and antitumor T-cell immunity in patients treated with GM-CSF-coding oncolytic adenovirus. *Clinical Cancer Research* **2013**, *19*, 2734–2744, doi:10.1158/1078-0432.CCR-12-2546.
182. Al-Zaher, A.A.; Moreno, R.; Fajardo, C.A.; Arias-Badia, M.; Farrera, M.; de Sostoa, J.; Rojas, L.A.; Alemany, R. Evidence of Anti-tumoral Efficacy in an Immune Competent Setting with an iRGD-Modified Hyaluronidase-Armed Oncolytic Adenovirus. *Molecular Therapy - Oncolytics* **2018**, *8*, 62–70, doi:10.1016/j.omto.2018.01.003.
183. Li, X.; Wang, P.; Li, H.; Du, X.; Liu, M.; Huang, Q.; Wang, Y.; Wang, S. The Efficacy of Oncolytic Adenovirus Is Mediated by T-cell Responses against Virus and Tumor in Syrian Hamster Model. *Clin. Cancer Res.* **2017**, *23*, 239–249, doi:10.1158/1078-0432.CCR-16-0477.
184. DeWeese, T.L.; van der Poel, H.; Li, S.; Mikhak, B.; Drew, R.; Goemann, M.; Hamper, U.; DeJong, R.; Detorie, N.; Rodriguez, R.; et al. A phase I trial of CV706, a replication-competent, PSA selective oncolytic adenovirus, for the treatment of locally recurrent prostate cancer following radiation therapy. *Cancer Res.* **2001**, *61*, 7464–7472.
185. Chen, Y.; DeWeese, T.; Dilley, J.; Zhang, Y.; Li, Y.; Ramesh, N.; Lee, J.; Pennathur-Das, R.; Radzyminski, J.; Wypych, J.; et al. CV706, a prostate cancer-specific adenovirus variant, in combination with radiotherapy produces synergistic antitumor efficacy without increasing toxicity. *Cancer Res.* **2001**, *61*, 5453–5460.
186. Hermiston, T.W.; Kuhn, I. Armed therapeutic viruses: Strategies and challenges to arming oncolytic viruses with therapeutic genes. *Cancer Gene Ther* **2002**, *9*, 1022–1035, doi:10.1038/sj.cgt.7700542.

187. Wildner, O.; Blaese, R.M.; Morris, J.C. Therapy of Colon Cancer with Oncolytic Adenovirus Is Enhanced by the Addition of Herpes Simplex Virus-thymidine kinase. 5.
188. Fuerer, C.; Iggo, R. 5-Fluorocytosine increases the toxicity of Wnt-targeting replicating adenoviruses that express cytosine deaminase as a late gene. *Gene Ther* **2004**, *11*, 142–151, doi:10.1038/sj.gt.3302148.
189. Lukashev, A.N.; Fuerer, C.; Chen, M.-J.; Searle, P.; Iggo, R. Late Expression of Nitroreductase in an Oncolytic Adenovirus Sensitizes Colon Cancer Cells to the Prodrug CB1954. 11.
190. Akbulut, H.; Zhang, L.; Tang, Y.; Deisseroth, A. Cytotoxic effect of replication-competent adenoviral vectors carrying L-plastin promoter regulated E1A and cytosine deaminase genes in cancers of the breast, ovary and colon. *Cancer Gene Therapy* **2003**, *10*, 388–395, doi:10.1038/sj.cgt.7700579.
191. Chen, M.-J.; Green, N.K.; Reynolds, G.M.; Flavell, J.R.; Mautner, V.; Kerr, D.J.; Young, L.S.; Searle, P.F. Enhanced efficacy of Escherichia coli nitroreductase/CB1954 prodrug activation gene therapy using an E1B-55K-deleted oncolytic adenovirus vector. *Gene Therapy* **2004**, *11*, 1126–1136, doi:10.1038/sj.gt.3302271.
192. Singleton, D.C.; Li, D.; Bai, S.Y.; Syddall, S.P.; Smaill, J.B.; Shen, Y.; Denny, W.A.; Wilson, W.R.; Patterson, A.V. The nitroreductase prodrug SN 28343 enhances the potency of systemically administered armed oncolytic adenovirus ONYX-411 NTR. *Cancer Gene Therapy* **2007**, *14*, 953–967, doi:10.1038/sj.cgt.7701088.
193. Stubdal, H.; Perin, N.; Lemmon, M.; Holman, P.; Bauzon, M.; Potter, P.M.; Danks, M.K.; Fattaey, A.; Dubensky, T.; Johnson, L. A Prodrug Strategy Using ONYX-015-Based Replicating Adenoviruses to Deliver Rabbit Carboxylesterase to Tumor Cells for Conversion of CPT-11 to SN-38. 10.
194. Schepelmann, S.; Hallenbeck, P.; Ogilvie, L.M.; Hedley, D.; Friedlos, F.; Martin, J.; Scanlon, I.; Hay, C.; Hawkins, L.K.; Marais, R.; et al. Systemic Gene-Directed Enzyme Prodrug Therapy of Hepatocellular Carcinoma Using a Targeted Adenovirus Armed with Carboxypeptidase G2. *Cancer Res* **2005**, *65*, 5003–5008, doi:10.1158/0008-5472.CAN-05-0393.
195. Qian, C.-Y.; Wang, K.-L.; Fang, F.-F.; Gu, W.; Huang, F.; Wang, F.-Z.; Li, B.; Wang, L.-N. Triple-controlled oncolytic adenovirus expressing melittin to exert inhibitory efficacy on hepatocellular carcinoma. *Int J Clin Exp Pathol* **2015**, *8*, 10403–10411.
196. Li, B.; Ling, C.; Zhang, C.; Gu, W.; Li, S.; Huang, X.; Zhang, Y.; Yu, C. [The induced apoptosis of recombinant adenovirus carrying melittin gene for hepatocellular carcinoma cell]. *Zhonghua Gan Zang Bing Za Zhi* **2004**, *12*, 453–455.
197. Mi, J.; Li, Z.-Y.; Ni, S.; Steinwaerder, D.; Lieber, A. Induced Apoptosis Supports Spread of Adenovirus Vectors in Tumors. *Human Gene Therapy* **2001**, *12*, 1343–1352, doi:10.1089/104303401750270995.
198. Sauthoff, H.; Pipiya, T.; Heitner, S.; Chen, S.; Norman, R.G.; Rom, W.N.; Hay, J.G. Late Expression of p53 from a Replicating Adenovirus Improves Tumor Cell Killing and Is More Tumor Cell Specific than Expression of the Adenoviral Death Protein. *Human Gene Therapy* **2002**, *13*, 1859–1871, doi:10.1089/104303402760372954.

199. Beusechem, V.W. van; Doel, P.B. van den; Grill, J.; Pinedo, H.M.; Gerritsen, W.R. Conditionally Replicative Adenovirus Expressing p53 Exhibits Enhanced Oncolytic Potency. *Cancer Res* **2002**, *62*, 6165–6171.
200. Hawkins, L.; Johnson, L.; Bauzon, M.; Nye, J.; Castro, D.; Kitzes, G.; Young, M.; Holt, J.; Trown, P.; Hermiston, T. Gene delivery from the E3 region of replicating human adenovirus: evaluation of the 6.7 K/gp19 K region. *Gene Ther* **2001**, *8*, 1123–1131, doi:10.1038/sj.gt.3301507.
201. Hawkins, L.; Hermiston, T. Gene delivery from the E3 region of replicating human adenovirus: evaluation of the ADP region. *Gene Ther* **2001**, *8*, 1132–1141, doi:10.1038/sj.gt.3301508.
202. Hawkins, L.; Hermiston, T. Gene delivery from the E3 region of replicating human adenovirus: evaluation of the E3B region. *Gene Ther* **2001**, *8*, 1142–1148, doi:10.1038/sj.gt.3301509.
203. Kurihara, T.; Brough, D.E.; Kovesdi, I.; Kufe, D.W. Selectivity of a replication-competent adenovirus for human breast carcinoma cells expressing the MUC1 antigen. *J. Clin. Invest.* **2000**, *106*, 763–771, doi:10.1172/JCI9180.
204. Zhang, R.; Zhang, X.; Ma, B.; Xiao, B.; Huang, F.; Huang, P.; Ying, C.; Liu, T.; Wang, Y. Enhanced antitumor effect of combining TRAIL and MnSOD mediated by CEA-controlled oncolytic adenovirus in lung cancer. *Cancer Gene Ther* **2016**, *23*, 168–177, doi:10.1038/cgt.2016.11.
205. Sova, P.; Ren, X.-W.; Ni, S.; Bernt, K.M.; Mi, J.; Kiviat, N.; Lieber, A. A Tumor-Targeted and Conditionally Replicating Oncolytic Adenovirus Vector Expressing TRAIL for Treatment of Liver Metastases. *Molecular Therapy* **2004**, *9*, 496–509, doi:10.1016/j.ymthe.2003.12.008.
206. Han, Z.; Lee, S.; Je, S.; Eom, C.-Y.; Choi, H.J.; Song, J.J.; Kim, J.-H. Survivin silencing and TRAIL expression using oncolytic adenovirus increase anti-tumorigenic activity in gemcitabine-resistant pancreatic cancer cells. *Apoptosis* **2016**, *21*, 351–364, doi:10.1007/s10495-015-1208-z.
207. Oh, E.; Hong, J.; Kwon, O.-J.; Yun, C.-O. A hypoxia- and telomerase-responsive oncolytic adenovirus expressing secretable trimeric TRAIL triggers tumour-specific apoptosis and promotes viral dispersion in TRAIL-resistant glioblastoma. *Sci Rep* **2018**, *8*, doi:10.1038/s41598-018-19300-6.
208. Zou, H.; Zheng, Y.-F.; Ge, W.; Wang, S.-B.; Mou, X.-Z. Synergistic Anti-tumour Effects of Quercetin and Oncolytic Adenovirus expressing TRAIL in Human Hepatocellular Carcinoma. *Sci Rep* **2018**, *8*, 2182, doi:10.1038/s41598-018-20213-7.
209. Gao, H.; Zhang, X.; Ding, Y.; Qiu, R.; Hong, Y.; Chen, W. Synergistic Suppression Effect on Tumor Growth of Colorectal Cancer by Combining Radiotherapy With a TRAIL-Armed Oncolytic Adenovirus. *Technol Cancer Res Treat* **2019**, *18*, 153303381985329, doi:10.1177/1533033819853290.
210. Fang, L.; Cheng, Q.; Liu, W.; Zhang, J.; Ge, Y.; Zhang, Q.; Li, L.; Liu, J.; Zheng, J. Selective effects of a fiber chimeric conditionally replicative adenovirus armed with hep27 gene on renal cancer cell. *Cancer Biol Ther* **2016**, *17*, 664–673, doi:10.1080/15384047.2016.1190485.

211. Xie, W.; Hao, J.; Zhang, K.; Fang, X.; Liu, X. Adenovirus armed with VGLL4 selectively kills hepatocellular carcinoma with G2/M phase arrest and apoptosis promotion. *Biochemical and Biophysical Research Communications* **2018**, *503*, 2758–2763, doi:10.1016/j.bbrc.2018.08.036.
212. Jiang, H.; Guo, S.; Xiao, D.; Bian, X.; Wang, J.; Wang, Y.; Zhou, H.; Cai, J.; Zheng, Z. Arginine deiminase expressed in vivo, driven by human telomerase reverse transcriptase promoter, displays high hepatoma targeting and oncolytic efficiency. *Oncotarget* **2017**, *8*, 37694–37704, doi:10.18632/oncotarget.17032.
213. Wang, S.-B.; Shu, J.; Chen, L.; Chen, X.; Zhao, J.; Li, S.; Mou, X.; Tong, X. Synergistic suppression effect on tumor growth of ovarian cancer by combining cisplatin with a manganese superoxide dismutase-armed oncolytic adenovirus. *OTT* **2016**, *Volume 9*, 6381–6388, doi:10.2147/OTT.S113014.
214. Kuriyama, N.; Kuriyama, H.; Julin, C.M.; Lamborn, K.; Israel, M.A. Pretreatment with protease is a useful experimental strategy for enhancing adenovirus-mediated cancer gene therapy. *Hum. Gene Ther.* **2000**, *11*, 2219–2230, doi:10.1089/104303400750035744.
215. Kim, J.-H.; Lee, Y.-S.; Kim, H.; Huang, J.-H.; Yoon, A.-R.; Yun, C.-O. Relaxin Expression From Tumor-Targeting Adenoviruses and Its Intratumoral Spread, Apoptosis Induction, and Efficacy. *J Natl Cancer Inst* **2006**, *98*, 1482–1493, doi:10.1093/jnci/djj397.
216. Ganesh, S.; Edick, M.G.; Idamakanti, N.; Abramova, M.; VanRoey, M.; Robinson, M.; Yun, C.-O.; Jooss, K. Relaxin-Expressing, Fiber Chimeric Oncolytic Adenovirus Prolongs Survival of Tumor-Bearing Mice. *Cancer Res* **2007**, *67*, 4399–4407, doi:10.1158/0008-5472.CAN-06-4260.
217. Guedan, S.; Rojas, J.J.; Gros, A.; Mercade, E.; Cascallo, M.; Alemany, R. Hyaluronidase Expression by an Oncolytic Adenovirus Enhances Its Intratumoral Spread and Suppresses Tumor Growth. *Molecular Therapy* **2010**, *18*, 1275–1283, doi:10.1038/mt.2010.79.
218. Tedcastle, A.; Illingworth, S.; Brown, A.; Seymour, L.W.; Fisher, K.D. Actin-resistant DNAse I Expression From Oncolytic Adenovirus Enadenotucirev Enhances Its Intratumoral Spread and Reduces Tumor Growth. *Mol Ther* **2016**, *24*, 796–804, doi:10.1038/mt.2015.233.
219. Rodríguez-García, A.; Giménez-Alejandre, M.; Rojas, J.J.; Moreno, R.; Bazan-Peregrino, M.; Cascalló, M.; Alemany, R. Safety and efficacy of VCN-01, an oncolytic adenovirus combining fiber HSG-binding domain replacement with RGD and hyaluronidase expression. *Clinical cancer research : an official journal of the American Association for Cancer Research* **2015**, *21*, 1406–18, doi:10.1158/1078-0432.CCR-14-2213.
220. Martínez-Vélez, N.; Xipell, E.; Vera, B.; Acanda de la Rocha, A.; Zalacain, M.; Marrodán, L.; Gonzalez-Huarriz, M.; Toledo, G.; Cascallo, M.; Alemany, R.; et al. The Oncolytic Adenovirus VCN-01 as Therapeutic Approach Against Pediatric Osteosarcoma. *Clinical cancer research : an official journal of the American Association for Cancer Research* **2016**, *22*, 2217–25, doi:10.1158/1078-0432.CCR-15-1899.

221. Pascual-Pasto, G.; Bazan-Peregrino, M.; Olaciregui, N.G.; Restrepo-Perdomo, C.A.; Mato-Berciano, A.; Ottaviani, D.; Weber, K.; Correa, G.; Paco, S.; Vila-Ubach, M.; et al. Therapeutic targeting of the RB1 pathway in retinoblastoma with the oncolytic adenovirus VCN-01. *Science Translational Medicine* **2019**, *11*, doi:10.1126/scitranslmed.aat9321.
222. Garcia-Moure, M.; Martinez-Velez, N.; Gonzalez-Huarriz, M.; Marrodán, L.; Cascallo, M.; Alemany, R.; Patiño-García, A.; Alonso, M.M. The oncolytic adenovirus VCN-01 promotes anti-tumor effect in primitive neuroectodermal tumor models. *Scientific Reports* **2019**, *9*, 1–10, doi:10.1038/s41598-019-51014-1.
223. Koski, A.; Kangasniemi, L.; Escutenaire, S.; Pesonen, S.; Cerullo, V.; Diaconu, I.; Nokisalmi, P.; Raki, M.; Rajecki, M.; Guse, K.; et al. Treatment of Cancer Patients With a Serotype 5/3 Chimeric Oncolytic Adenovirus Expressing GMCSF. *Molecular Therapy* **2010**, *18*, 1874–1884, doi:10.1038/mt.2010.161.
224. Ramesh, N.; Ge, Y.; Ennist, D.L.; Zhu, M.; Mina, M.; Ganesh, S.; Reddy, P.S.; Yu, D.-C. CG0070, a conditionally replicating granulocyte macrophage colony-stimulating factor--armed oncolytic adenovirus for the treatment of bladder cancer. *Clin. Cancer Res.* **2006**, *12*, 305–313, doi:10.1158/1078-0432.CCR-05-1059.
225. Ahn, H.M.; Hong, J.; Yun, C.-O. Oncolytic adenovirus coexpressing interleukin-12 and shVEGF restores antitumor immune function and enhances antitumor efficacy. *Oncotarget* **2016**, *7*, 84965–84980, doi:10.18632/oncotarget.13087.
226. Oh, E.; Choi, I.-K.; Hong, J.; Yun, C.-O. Oncolytic adenovirus coexpressing interleukin-12 and decorin overcomes Treg-mediated immunosuppression inducing potent antitumor effects in a weakly immunogenic tumor model. *Oncotarget* **2017**, *8*, 4730–4746, doi:10.18632/oncotarget.13972.
227. Huang, J.H.; Zhang, S.N.; Choi, K.J.; Choi, I.K.; Kim, J.H.; Lee, M.; Kim, H.; Yun, C.O. Therapeutic and tumor-specific immunity induced by combination of dendritic cells and oncolytic adenovirus expressing IL-12 and 4-1BBL. *Molecular therapy : the journal of the American Society of Gene Therapy* **2010**, *18*, 264–274, doi:10.1038/mt.2009.205.
228. Yan, Y.; Xu, H.; Wang, J.; Wu, X.; Wen, W.; Liang, Y.; Wang, L.; Liu, F.; Du, X. Inhibition of breast cancer cells by targeting E2F-1 gene and expressing IL15 oncolytic adenovirus. *Biosci Rep* **2019**, *39*, doi:10.1042/BSR20190384.
229. Ye, J.; Qi, W.; Liu, M.; Li, Y. The combination of NK and CD8+ T cells with CCL20/IL15-armed oncolytic adenoviruses enhances the growth suppression of TERT-positive tumor cells. *Cellular Immunology* **2017**, *318*, 35–41, doi:10.1016/j.cellimm.2017.06.002.
230. Li, Y.; Li, Y.; Si, C.; Zhu, Y.; Jin, Y.; Zhu, T.; Liu, M.; Liu, G. CCL21/IL21-armed oncolytic adenovirus enhances antitumor activity against TERT-positive tumor cells. *Virus Research* **2016**, *220*, 172–178, doi:10.1016/j.virusres.2016.05.002.
231. Sarkar, D.; Lebedeva, I.V.; Su, Z.; Park, E.-S.; Chatman, L.; Vozhilla, N.; Dent, P.; Curiel, D.T.; Fisher, P.B. Eradication of Therapy-Resistant Human Prostate Tumors Using a Cancer Terminator Virus. *Cancer Res* **2007**, *67*, 5434–5442, doi:10.1158/0008-5472.CAN-07-0195.

232. Ashshi, A.M.; El-Shemi, A.G.; Dmitriev, I.P.; Kashentseva, E.A.; Curiel, D.T. Combinatorial strategies based on CRAd-IL24 and CRAd-ING4 virotherapy with anti-angiogenesis treatment for ovarian cancer. *J Ovarian Res* **2016**, *9*, 38, doi:10.1186/s13048-016-0248-5.
233. Mao, L.; Ding, M.; Xu, K.; Pan, J.; Yu, H.; Yang, C. Oncolytic Adenovirus Harboring Interleukin-24 Improves Chemotherapy for Advanced Prostate Cancer. *J Cancer* **2018**, *9*, 4391–4397, doi:10.7150/jca.26437.
234. Yuan, S.; Fang, X.; Xu, Y.; Ni, A.; Liu, X.-Y.; Chu, L. An oncolytic adenovirus that expresses the HAb18 and interleukin 24 genes exhibits enhanced antitumor activity in hepatocellular carcinoma cells. *Oncotarget* **2016**, *7*, 60491–60502, doi:10.18632/oncotarget.11134.
235. Zhao, L.; Gu, J.; Dong, A.; Zhang, Y.; Zhong, L.; He, L.; Wang, Y.; Zhang, J.; Zhang, Z.; Huiwang, J.; et al. Potent Antitumor Activity of Oncolytic Adenovirus Expressing mda-7/IL-24 for Colorectal Cancer. 14.
236. Wei, X.; liu, L.; Wang, G.; Li, W.; Xu, K.; Hu, X.; Qian, C.; Shao, J. Targeting eradication of chronic myeloid leukemia using chimeric oncolytic adenovirus to drive IL-24 expression. *Int J Clin Exp Pathol* **2015**, *8*, 3775–3784.
237. Cervera-Carrascon, V.; Siurala, M.; Santos, J.M.; Havunen, R.; Tähtinen, S.; Karell, P.; Sorsa, S.; Kanerva, A.; Hemminki, A. TNFa and IL-2 armed adenoviruses enable complete responses by anti-PD-1 checkpoint blockade. *OncoImmunology* **2018**, *7*, e1412902, doi:10.1080/2162402X.2017.1412902.
238. Eriksson, E.; Milenova, I.; Wenthe, J.; Ståhle, M.; Leja-Jarblad, J.; Ullenhag, G.; Dimberg, A.; Moreno, R.; Alemany, R.; Loskog, A. Shaping the Tumor Stroma and Sparking Immune Activation by CD40 and 4-1BB Signaling Induced by an Armed Oncolytic Virus. *Clin Cancer Res* **2017**, *23*, 5846–5857, doi:10.1158/1078-0432.CCR-17-0285.
239. Dias, J.D.; Hemminki, O.; Diaconu, I.; Hirvinen, M.; Bonetti, A.; Guse, K.; Escutenaire, S.; Kanerva, A.; Pesonen, S.; Löskog, A.; et al. Targeted cancer immunotherapy with oncolytic adenovirus coding for a fully human monoclonal antibody specific for CTLA-4. *Gene Ther* **2012**, *19*, 988–998, doi:10.1038/gt.2011.176.
240. Jiang, H.; Rivera-Molina, Y.; Gomez-Manzano, C.; Clise-Dwyer, K.; Bover, L.; Vence, L.M.; Yuan, Y.; Lang, F.F.; Toniatti, C.; Hossain, M.B.; et al. Oncolytic adenovirus and tumor-targeting immune modulatory therapy improve autologous cancer vaccination. *Cancer Res* **2017**, *77*, 3894–3907, doi:10.1158/0008-5472.CAN-17-0468.
241. Rivera-Molina, Y.; Jiang, H.; Fueyo, J.; Nguyen, T.; Shin, D.H.; Youssef, G.; Fan, X.; Gumin, J.; Alonso, M.M.; Phadnis, S.; et al. GITRL-armed Delta-24-RGD oncolytic adenovirus prolongs survival and induces anti-glioma immune memory. *Neuro-Oncology Advances* **2019**, *1*, vdz009, doi:10.1093/noajnl/vdz009.
242. Zhang, Y.; Zhang, H.; Wei, M.; Mou, T.; Shi, T.; Ma, Y.; Cai, X.; Li, Y.; Dong, J.; Wei, J. Recombinant Adenovirus Expressing a Soluble Fusion Protein PD-1/CD137L Subverts the Suppression of CD8+ T Cells in HCC. *Molecular Therapy* **2019**, *27*, 1906–1918, doi:10.1016/j.ymthe.2019.07.019.

243. Yang, Y.; Xu, W.; Peng, D.; Wang, H.; Zhang, X.; Wang, H.; Xiao, F.; Zhu, Y.; Ji, Y.; Gulukota, K.; et al. An Oncolytic Adenovirus Targeting Transforming Growth Factor β Inhibits Protumorigenic Signals and Produces Immune Activation: A Novel Approach to Enhance Anti-PD-1 and Anti-CTLA-4 Therapy. *Human Gene Therapy* **2019**, *30*, 1117–1132, doi:10.1089/hum.2019.059.
244. Li, Y.; Xiao, F.; Zhang, A.; Zhang, D.; Nie, W.; Xu, T.; Han, B.; Seth, P.; Wang, H.; Yang, Y.; et al. Oncolytic adenovirus targeting TGF-β enhances anti-tumor responses of mesothelin-targeted chimeric antigen receptor T cell therapy against breast cancer. *Cell. Immunol.* **2020**, *348*, 104041, doi:10.1016/j.cellimm.2020.104041.
245. Fajardo, C.A.; Guedan, S.; Rojas, L.A.; Moreno, R.; Arias-Badia, M.; de Sostoa, J.; June, C.H.; Alemany, R. Oncolytic Adenoviral Delivery of an EGFR-Targeting T-cell Engager Improves Antitumor Efficacy. *Cancer Res* **2017**, *77*, 2052–2063, doi:10.1158/0008-5472.CAN-16-1708.
246. de Sostoa, J.; Fajardo, C.A.; Moreno, R.; Ramos, M.D.; Farrera-Sal, M.; Alemany, R. Targeting the tumor stroma with an oncolytic adenovirus secreting a fibroblast activation protein-targeted bispecific T-cell engager. *j. immunotherapy cancer* **2019**, *7*, 19, doi:10.1186/s40425-019-0505-4.
247. Bimboim, H.C.; Doly, J. A rapid alkaline extraction procedure for screening recombinant plasmid DNA. *Nucleic Acids Research* **1979**, *7*, 1513–1523, doi:10.1093/nar/7.6.1513.
248. Warming, S.; Costantino, N.; Court, D.L.; Jenkins, N.A.; Copeland, N.G. Simple and highly efficient BAC recombineering using galK selection. *Nucleic Acids Research* **2005**, *33*, 1–12, doi:10.1093/nar/gni035.
249. Stanton, R.J.; McSharry, B.P.; Armstrong, M.; Tomasec, P.; Wilkinson, G.W.G. Re-engineering adenovirus vector systems to enable high-throughput analyses of gene function. *BioTechniques* **2008**, *45*, 659–668, doi:10.2144/000112993.
250. Wang, S.; Zhao, Y.; Leiby, M.; Zhu, J. A new positive/negative selection scheme for precise BAC recombineering. *Molecular Biotechnology* **2009**, *42*, 110–116, doi:10.1007/s12033-009-9142-3.
251. Stavropoulos, T.A.; Strathdee, C.A. Synergy between tetA and rpsL provides high-stringency positive and negative selection in bacterial artificial chromosome vectors. *Genomics* **2001**, *72*, 99–104, doi:10.1006/geno.2000.6481.
252. Rincón, E.; Cejalvo, T.; Kanojia, D.; Alfranca, A.; Ángel Rodríguez-Milla, M.; Andrés, R.; Hoyos, G.; Han, Y.; Zhang, L.; Alemany, R.; et al. Mesenchymal stem cell carriers enhance antitumor efficacy of oncolytic adenoviruses in an immunocompetent mouse model. *Oncotarget* **2017**, *8*, 45415–45431, doi:10.18632/oncotarget.17557.
253. Guedan, S.; Rojas, J.J.; Gros, A.; Mercade, E.; Cascallo, M.; Alemany, R. Hyaluronidase Expression by an Oncolytic Adenovirus Enhances Its Intratumoral Spread and Suppresses Tumor Growth. *Molecular Therapy* **2010**, *18*, 1275–1283, doi:10.1038/mt.2010.79.
254. Rojas, J.J.; Gimenez-Alejandre, M.; Gil-Hoyos, R.; Cascallo, M.; Alemany, R. Improved systemic antitumor therapy with oncolytic adenoviruses by replacing

the fiber shaft HSG-binding domain with RGD. *Gene Therapy* **2012**, *19*, 453–457, doi:10.1038/gt.2011.106.

255. Carette, J.E.; Graat, H.C.A.; Schagen, F.H.E.; Abou El Hassan, M.A.I.; Gerritsen, W.R.; van Beusechem, V.W. Replication-dependent transgene expression from a conditionally replicating adenovirus via alternative splicing to a heterologous splice-acceptor site. *J. Gene Med.* **2005**, *7*, 1053–1062, doi:10.1002/jgm.754.
256. Kim, J.H.; Lee, S.-R.; Li, L.-H.; Park, H.-J.; Park, J.-H.; Lee, K.Y.; Kim, M.-K.; Shin, B.A.; Choi, S.-Y. High Cleavage Efficiency of a 2A Peptide Derived from Porcine Teschovirus-1 in Human Cell Lines, Zebrafish and Mice. *PLOS ONE* **2011**, *6*, e18556, doi:10.1371/journal.pone.0018556.
257. Levine, S.J. Molecular Mechanisms of Soluble Cytokine Receptor Generation. *J. Biol. Chem.* **2008**, *283*, 14177–14181, doi:10.1074/jbc.R700052200.
258. Mantovani, A.; Locati, M.; Vecchi, A.; Sozzani, S.; Allavena, P. Decoy receptors: a strategy to regulate inflammatory cytokines and chemokines. *Trends in Immunology* **2001**, *22*, 328–336, doi:10.1016/S1471-4906(01)01941-X.
259. Zonneveld, R.; Martinelli, R.; Shapiro, N.I.; Kuijpers, T.W.; Plötz, F.B.; Carman, C.V. Soluble adhesion molecules as markers for sepsis and the potential pathophysiological discrepancy in neonates, children and adults. *Crit Care* **2014**, *18*, 204, doi:10.1186/cc13733.
260. Kang, S.-A.; Blache, C.A.; Bajana, S.; Hasan, N.; Kamal, M.; Morita, Y.; Gupta, V.; Tsolmon, B.; Suh, S.K.; Gorenstein, D.G.; et al. The effect of soluble E-selectin on tumor progression and metastasis. *BMC Cancer* **2016**, *16*, doi:10.1186/s12885-016-2366-2.
261. Gu, D.; Ao, X.; Yang, Y.; Chen, Z.; Xu, X. Soluble immune checkpoints in cancer: production, function and biological significance. *J Immunother Cancer* **2018**, *6*, doi:10.1186/s40425-018-0449-0.
262. Clayton, K.; Douglas-Vail, M.; Rahman, A.; Medcalf, K.; Xie, I.; Chew, G.; Tandon, R.; Lanteri, M.; Norris, P.; Deeks, S.; et al. Soluble Tim-3 is shed from CD8+ T cells by the sheddase ADAM10, is increased in plasma during untreated HIV infection, and correlates with HIV disease progression (VIR6P.1165). *The Journal of Immunology* **2015**, *194*, 149.5-149.5.
263. Chang, B.; Huang, T.; Wei, H.; Shen, L.; Zhu, D.; He, W.; Chen, Q.; Zhang, H.; Li, Y.; Huang, R.; et al. The correlation and prognostic value of serum levels of soluble programmed death protein 1 (sPD-1) and soluble programmed death-ligand 1 (sPD-L1) in patients with hepatocellular carcinoma. *Cancer Immunol. Immunother.* **2019**, *68*, 353–363, doi:10.1007/s00262-018-2271-4.
264. Sorensen, S.F.; Demuth, C.; Weber, B.; Sorensen, B.S.; Meldgaard, P. Increase in soluble PD-1 is associated with prolonged survival in patients with advanced EGFR-mutated non-small cell lung cancer treated with erlotinib. *Lung Cancer* **2016**, *100*, 77–84, doi:10.1016/j.lungcan.2016.08.001.
265. Chatterjee, J.; Dai, W.; Aziz, N.H.A.; Teo, P.Y.; Wahba, J.; Phelps, D.L.; Maine, C.J.; Whilding, L.M.; Dina, R.; Trevisan, G.; et al. Clinical Use of Programmed Cell Death-1 and Its Ligand Expression as Discriminatory and Predictive Markers in Ovarian Cancer. *Clin. Cancer Res.* **2017**, *23*, 3453–3460, doi:10.1158/1078-0432.CCR-16-2366.

266. Zhu, X.; Lang, J. Soluble PD-1 and PD-L1: predictive and prognostic significance in cancer. *Oncotarget* **2017**, *8*, 97671–97682, doi:10.18632/oncotarget.18311.
267. Raper, S.E.; Chirmule, N.; Lee, F.S.; Wivel, N.A.; Bagg, A.; Gao, G.; Wilson, J.M.; Batshaw, M.L. Fatal systemic inflammatory response syndrome in a ornithine transcarbamylase deficient patient following adenoviral gene transfer. *Mol. Genet. Metab.* **2003**, *80*, 148–158, doi:10.1016/j.ymgme.2003.08.016.
268. Rodriguez-Garcia, A.; Gimenez-Alejandre, M.; Rojas, J.J.; Moreno, R.; Bazan-Peregrino, M.; Cascallo, M.; Alemany, R. Safety and Efficacy of VCN-01, an Oncolytic Adenovirus Combining Fiber HSG-Binding Domain Replacement with RGD and Hyaluronidase Expression. *Clinical Cancer Research* **2015**, *21*, 1406–1418, doi:10.1158/1078-0432.CCR-14-2213.
269. Tay, R.E.; Richardson, E.K.; Toh, H.C. Revisiting the role of CD4 + T cells in cancer immunotherapy—new insights into old paradigms. *Cancer Gene Therapy* **2020**, 1–13, doi:10.1038/s41417-020-0183-x.
270. Bhattacharya, P.; Budnick, I.; Singh, M.; Thiruppathi, M.; Alharshawi, K.; Elshabrawy, H.; Holterman, M.J.; Prabhakar, B.S. Dual Role of GM-CSF as a Pro-Inflammatory and a Regulatory Cytokine: Implications for Immune Therapy. *J Interferon Cytokine Res* **2015**, *35*, 585–599, doi:10.1089/jir.2014.0149.
271. Balkwill, F. Tumour necrosis factor and cancer. *Nature Reviews Cancer* **2009**, *9*, 361–371, doi:10.1038/nrc2628.
272. Dinarello, C.A. Overview of the IL-1 family in innate inflammation and acquired immunity. *Immunol Rev* **2018**, *281*, 8–27, doi:10.1111/imr.12621.
273. Tanaka, T.; Narazaki, M.; Kishimoto, T. Interleukin (IL-6) Immunotherapy. *Cold Spring Harb Perspect Biol* **2018**, *10*, doi:10.1101/cshperspect.a028456.
274. Scheller, J.; Chalaris, A.; Schmidt-Arras, D.; Rose-John, S. The pro- and anti-inflammatory properties of the cytokine interleukin-6. *Biochimica et Biophysica Acta (BBA) - Molecular Cell Research* **2011**, *1813*, 878–888, doi:10.1016/j.bbamcr.2011.01.034.
275. Saxena, A.; Khosraviani, S.; Noel, S.; Mohan, D.; Donner, T.; Hamad, A.R.A. Interleukin-10 paradox: A potent immunoregulatory cytokine that has been difficult to harness for immunotherapy. *Cytokine* **2015**, *74*, 27–34, doi:10.1016/j.cyto.2014.10.031.
276. Lasek, W.; Zagożdżon, R.; Jakobisiak, M. Interleukin 12: still a promising candidate for tumor immunotherapy? *Cancer Immunol. Immunother.* **2014**, *63*, 419–435, doi:10.1007/s00262-014-1523-1.
277. Schoenborn, J.R.; Wilson, C.B. Regulation of Interferon-γ During Innate and Adaptive Immune Responses. In *Advances in Immunology*; Academic Press, 2007; Vol. 96, pp. 41–101.
278. Castro, F.; Cardoso, A.P.; Gonçalves, R.M.; Serre, K.; Oliveira, M.J. Interferon-Gamma at the Crossroads of Tumor Immune Surveillance or Evasion. *Front. Immunol.* **2018**, *9*, doi:10.3389/fimmu.2018.00847.
279. Abbas, A.K.; Trotta, E.; R Simeonov, D.; Marson, A.; Bluestone, J.A. Revisiting IL-2: Biology and therapeutic prospects. *Sci Immunol* **2018**, *3*, doi:10.1126/sciimmunol.aat1482.

280. Malek, T.R. The biology of interleukin-2. *Annu. Rev. Immunol.* **2008**, *26*, 453–479, doi:10.1146/annurev.immunol.26.021607.090357.
281. Noelle, R.J.; Nowak, E.C. Cellular sources and immune functions of interleukin-9. *Nat Rev Immunol* **2010**, *10*, doi:10.1038/nri2848.
282. Greenfeder, S.; Umland, S.P.; Cuss, F.M.; Chapman, R.W.; Egan, R.W. Th2 cytokines and asthma — The role of interleukin-5 in allergic eosinophilic disease. *Respir Res* **2001**, *2*, 71–79, doi:10.1186/rr41.
283. Gorski, S.A.; Hahn, Y.S.; Braciale, T.J. Group 2 Innate Lymphoid Cell Production of IL-5 Is Regulated by NKT Cells during Influenza Virus Infection. *PLoS Pathog* **2013**, *9*, doi:10.1371/journal.ppat.1003615.
284. Mannon, P.; Reinisch, W. Interleukin 13 and its role in gut defence and inflammation. *Gut* **2012**, *61*, 1765–1773, doi:10.1136/gutjnl-2012-303461.
285. Monin, L.; Gaffen, S.L. Interleukin 17 Family Cytokines: Signaling Mechanisms, Biological Activities, and Therapeutic Implications. *Cold Spring Harb Perspect Biol* **2018**, *10*, doi:10.1101/cshperspect.a028522.
286. Yi, J.S.; Cox, M.A.; Zajac, A.J. Interleukin-21: A Multifunctional Regulator of Immunity to Infections. *Microbes Infect* **2010**, *12*, 1111–1119, doi:10.1016/j.micinf.2010.08.008.
287. Hernandez, P.; Gronke, K.; Diefenbach, A. A catch-22: Interleukin-22 and cancer. *European Journal of Immunology* **2018**, *48*, 15–31, doi:10.1002/eji.201747183.
288. Li, Y.; Wang, H.; Lu, H.; Hua, S. Regulation of Memory T Cells by Interleukin-23. *Int. Arch. Allergy Immunol.* **2016**, *169*, 157–162, doi:10.1159/000445834.
289. Tang, C.; Chen, S.; Qian, H.; Huang, W. Interleukin-23: as a drug target for autoimmune inflammatory diseases. *Immunology* **2012**, *135*, 112–124, doi:10.1111/j.1365-2567.2011.03522.x.
290. Xie, K. Interleukin-8 and human cancer biology. *Cytokine Growth Factor Rev.* **2001**, *12*, 375–391, doi:10.1016/s1359-6101(01)00016-8.
291. Liu, M.; Guo, S.; Hibbert, J.M.; Jain, V.; Singh, N.; Wilson, N.O.; Stiles, J.K. CXCL10/IP-10 in infectious diseases pathogenesis and potential therapeutic implications. *Cytokine Growth Factor Rev* **2011**, *22*, 121–130, doi:10.1016/j.cytogfr.2011.06.001.
292. Raffray, L.; Giry, C.; Thirapathi, Y.; Reboux, A.-H.; Jaffar-Bandjee, M.-C.; Gasque, P. Increased levels of soluble forms of E-selectin and ICAM-1 adhesion molecules during human leptospirosis. *PLoS One* **2017**, *12*, doi:10.1371/journal.pone.0180474.
293. Munn, D.H.; Mellor, A.L. IDO in the Tumor Microenvironment: Inflammation, Counter-Regulation, and Tolerance. *Trends in Immunology* **2016**, *37*, 193–207, doi:10.1016/j.it.2016.01.002.
294. Takeuchi, M.; Doi, T.; Obayashi, K.; Hirai, A.; Yoneda, K.; Tanaka, F.; Iwai, Y. Soluble PD-L1 with PD-1-binding capacity exists in the plasma of patients with non-small cell lung cancer. *Immunology Letters* **2018**, *196*, 155–160, doi:10.1016/j.imlet.2018.01.007.
295. Mahoney, K.M.; Shukla, S.A.; Patsoukis, N.; Chaudhri, A.; Browne, E.P.; Arazi, A.; Eisenhaure, T.M.; Pendergraft, W.F.; Hua, P.; Pham, H.C.; et al. A secreted PD-L1 splice variant that covalently dimerizes and mediates immunosuppression.

Cancer Immunol Immunother **2019**, *68*, 421–432, doi:10.1007/s00262-018-2282-1.

296. Dai, S.; Jia, R.; Zhang, X.; Fang, Q.; Huang, L. The PD-1/PD-Ls pathway and autoimmune diseases. *Cellular Immunology* **2014**, *290*, 72–79, doi:10.1016/j.cellimm.2014.05.006.
297. Mortensen, J.B.; Yoanna, V.; Hansen, I.M.; Bjerre, M.; d'Amore, F. Characterization of Soluble Immune Checkpoint Protein PD-1, PD-L1 and PD-L2 Levels in Different Types of Lymphoid Malignancies. *Blood* **2018**, *132*, 5306–5306, doi:10.1182/blood-2018-99-114509.
298. Buderath, P.; Schwich, E.; Jensen, C.; Horn, P.A.; Kimmig, R.; Kasimir-Bauer, S.; Rebmann, V. Soluble Programmed Death Receptor Ligands sPD-L1 and sPD-L2 as Liquid Biopsy Markers for Prognosis and Platinum Response in Epithelial Ovarian Cancer. *Front Oncol* **2019**, *9*, doi:10.3389/fonc.2019.01015.
299. Furtner, M.; Straub, R.H.; Krüger, S.; Schwarz, H. Levels of soluble CD137 are enhanced in sera of leukemia and lymphoma patients and are strongly associated with chronic lymphocytic leukemia. *Leukemia* **2005**, *19*, 883–885, doi:10.1038/sj.leu.2403675.
300. Brignone, C.; Grygar, C.; Marcu, M.; Perrin, G.; Triebel, F. IMP321 (sLAG-3), an immunopotentiator for T cell responses against a HBsAg antigen in healthy adults: a single blind randomised controlled phase I study. *J Immune Based Ther Vaccines* **2007**, *5*, 5, doi:10.1186/1476-8518-5-5.
301. Baltz, K.M.; Krusch, M.; Baessler, T.; Schmiedel, B.J.; Bringmann, A.; Brossart, P.; Salih, H.R. Neutralization of tumor-derived soluble glucocorticoid-induced TNFR-related protein ligand increases NK cell anti-tumor reactivity. *Blood* **2008**, *112*, 3735–3743, doi:10.1182/blood-2008-03-143016.
302. Dong, M.P.; Enomoto, M.; Thuy, L.T.T.; Hai, H.; Hieu, V.N.; Hoang, D.V.; Iida-Ueno, A.; Odagiri, N.; Amano-Teranishi, Y.; Hagihara, A.; et al. Clinical significance of circulating soluble immune checkpoint proteins in sorafenib-treated patients with advanced hepatocellular carcinoma. *Scientific Reports* **2020**, *10*, 3392, doi:10.1038/s41598-020-60440-5.
303. Lange, A.; Sundén-Cullberg, J.; Magnuson, A.; Hultgren, O. Soluble B and T Lymphocyte Attenuator Correlates to Disease Severity in Sepsis and High Levels Are Associated with an Increased Risk of Mortality. *PLOS ONE* **2017**, *12*, e0169176, doi:10.1371/journal.pone.0169176.
304. Heo, S.-K.; Ju, S.-A.; Kim, G.Y.; Park, S.-M.; Back, S.H.; Park, N.-H.; Min, Y.J.; An, W.G.; Nguyen, T.-H.T.; Kim, S.-M.; et al. The presence of high level soluble herpes virus entry mediator in sera of gastric cancer patients. *Experimental & Molecular Medicine* **2012**, *44*, 149–158, doi:10.3858/emm.2012.44.2.010.
305. Jung, H.W.; La, S.J.; Kim, J.Y.; Heo, S.K.; Kim, J.Y.; Wang, S.; Kim, K.K.; Lee, K.M.; Cho, H.R.; Lee, H.W.; et al. High levels of soluble herpes virus entry mediator in sera of patients with allergic and autoimmune diseases. *Exp. Mol. Med.* **2003**, *35*, 501–508, doi:10.1038/emm.2003.65.
306. Huang, J.; Jochems, C.; Anderson, A.M.; Talaie, T.; Jales, A.; Madan, R.A.; Hodge, J.W.; Tsang, K.Y.; Liewehr, D.J.; Steinberg, S.M.; et al. Soluble CD27-pool in

humans may contribute to T-cell activation and tumor immunity. *J Immunol* **2013**, *190*, 6250–6258, doi:10.4049/jimmunol.1300022.

307. HEBBAR, M.; JEANNIN, P.; MAGISTRELLI, G.; HATRON, P.-Y.; HACHULLA, E.; DEVULDER, B.; BONNEFOY, J.-Y.; DELNESTE, Y. Detection of circulating soluble CD28 in patients with systemic lupus erythematosus, primary Sjögren's syndrome and systemic sclerosis. *Clin Exp Immunol* **2004**, *136*, 388–392, doi:10.1111/j.1365-2249.2004.02427.x.
308. Sun, Z.; Yi, L.; Tao, H.; Huang, J.; Jin, Z.; Xiao, Y.; Feng, C.; Sun, J. Enhancement of soluble CD28 levels in the serum of Graves' disease. *Cent Eur J Immunol* **2014**, *39*, 216–222, doi:10.5114/ceji.2014.43726.
309. Horn, L.A.; Long, T.M.; Atkinson, R.; Clements, V.; Ostrand-Rosenberg, S. Soluble CD80 Protein Delays Tumor Growth and Promotes Tumor-Infiltrating Lymphocytes. *Cancer Immunol Res* **2018**, *6*, 59–68, doi:10.1158/2326-6066.CIR-17-0026.
310. Haile, S.T.; Dalal, S.P.; Clements, V.; Tamada, K.; Ostrand-Rosenberg, S. Soluble CD80 Restores T Cell Activation and Overcomes Tumor Cell Programmed Death Ligand 1–Mediated Immune Suppression. *The Journal of Immunology* **2013**, *191*, 2829–2836, doi:10.4049/jimmunol.1202777.
311. Kopf, M.; Baumann, H.; Freer, G.; Freudenberg, M.; Lamers, M.; Kishimoto, T.; Zinkernagel, R.; Bluethmann, H.; Köhler, G. Impaired immune and acute-phase responses in interleukin-6-deficient mice. *Nature* **1994**, *368*, 339–342, doi:10.1038/368339a0.
312. Lauder, S.N.; Jones, E.; Smart, K.; Bloom, A.; Williams, A.S.; Hindley, J.P.; Ondondo, B.; Taylor, P.R.; Clement, M.; Fielding, C.; et al. Interleukin-6 limits influenza-induced inflammation and protects against fatal lung pathology. *Eur. J. Immunol.* **2013**, *43*, 2613–2625, doi:10.1002/eji.201243018.
313. Yang, M.-L.; Wang, C.-T.; Yang, S.-J.; Leu, C.-H.; Chen, S.-H.; Wu, C.-L.; Shiau, A.-L. IL-6 ameliorates acute lung injury in influenza virus infection. *Scientific Reports* **2017**, *7*, 43829, doi:10.1038/srep43829.
314. McKenzie, A.N.J.; Spits, H.; Eberl, G. Innate lymphoid cells in inflammation and immunity. *Immunity* **2014**, *41*, 366–374, doi:10.1016/j.immuni.2014.09.006.
315. Billiau, A.; Matthys, P. Interferon-gamma: a historical perspective. *Cytokine Growth Factor Rev.* **2009**, *20*, 97–113, doi:10.1016/j.cytogfr.2009.02.004.
316. Artis, D.; Spits, H. The biology of innate lymphoid cells. *Nature* **2015**, *517*, 293–301, doi:10.1038/nature14189.
317. Casati, C.; Camisaschi, C.; Rini, F.; Arienti, F.; Rivoltini, L.; Triebel, F.; Parmiani, G.; Castelli, C. Soluble Human LAG-3 Molecule Amplifies the In vitro Generation of Type 1 Tumor-Specific Immunity. *Cancer Res* **2006**, *66*, 4450–4460, doi:10.1158/0008-5472.CAN-05-2728.
318. Mistchenko, A.S.; Diez, R.A.; Falcoff, R. Inhibitory effect of interferon-gamma on adenovirus replication and late transcription. *Biochem. Pharmacol.* **1989**, *38*, 1971–1978, doi:10.1016/0006-2952(89)90496-6.
319. Vincent, T.; Pettersson, R.F.; Crystal, R.G.; Leopold, P.L. Cytokine-mediated downregulation of coxsackievirus-adenovirus receptor in endothelial cells. *J. Virol.* **2004**, *78*, 8047–8058, doi:10.1128/JVI.78.15.8047-8058.2004.

320. Robek, M.D.; Garcia, M.L.; Boyd, B.S.; Chisari, F.V. Role of immunoproteasome catalytic subunits in the immune response to hepatitis B virus. *J. Virol.* **2007**, *81*, 483–491, doi:10.1128/JVI.01779-06.
321. Kang, S.; Brown, H.M.; Hwang, S. Direct Antiviral Mechanisms of Interferon-Gamma. *Immune Netw* **2018**, *18*, doi:10.4110/in.2018.18.e33.
322. Adams, O.; Besken, K.; Oberdörfer, C.; MacKenzie, C.R.; Rüssing, D.; Däubener, W. Inhibition of human herpes simplex virus type 2 by interferon gamma and tumor necrosis factor alpha is mediated by indoleamine 2,3-dioxygenase. *Microbes Infect.* **2004**, *6*, 806–812, doi:10.1016/j.micinf.2004.04.007.
323. Obojes, K.; Andres, O.; Kim, K.S.; Däubener, W.; Schneider-Schaulies, J. Indoleamine 2,3-dioxygenase mediates cell type-specific anti-measles virus activity of gamma interferon. *J. Virol.* **2005**, *79*, 7768–7776, doi:10.1128/JVI.79.12.7768-7776.2005.
324. Bodaghi, B.; Goureau, O.; Zipeto, D.; Laurent, L.; Virelizier, J.L.; Michelson, S. Role of IFN-gamma-induced indoleamine 2,3 dioxygenase and inducible nitric oxide synthase in the replication of human cytomegalovirus in retinal pigment epithelial cells. *J. Immunol.* **1999**, *162*, 957–964.
325. Terajima, M.; Leporati, A.M. Role of Indoleamine 2,3-Dioxygenase in Antiviral Activity of Interferon-gamma Against Vaccinia Virus. *Viral Immunol.* **2005**, *18*, 722–729, doi:10.1089/vim.2005.18.722.
326. Mao, R.; Zhang, J.; Jiang, D.; Cai, D.; Levy, J.M.; Cuconati, A.; Block, T.M.; Guo, J.-T.; Guo, H. Indoleamine 2,3-dioxygenase mediates the antiviral effect of gamma interferon against hepatitis B virus in human hepatocyte-derived cells. *J. Virol.* **2011**, *85*, 1048–1057, doi:10.1128/JVI.01998-10.
327. Wiethoff, C.M.; Wodrich, H.; Gerace, L.; Nemerow, G.R. Adenovirus Protein VI Mediates Membrane Disruption following Capsid Disassembly. *J Virol* **2005**, *79*, 1992–2000, doi:10.1128/JVI.79.4.1992-2000.2005.
328. Lahl, K.; Loddenkemper, C.; Drouin, C.; Freyer, J.; Arnason, J.; Eberl, G.; Hamann, A.; Wagner, H.; Huehn, J.; Sparwasser, T. Selective depletion of Foxp3+ regulatory T cells induces a scurfy-like disease. *J Exp Med* **2007**, *204*, 57–63, doi:10.1084/jem.20061852.
329. Pallotta, M.T.; Orabona, C.; Volpi, C.; Vacca, C.; Belladonna, M.L.; Bianchi, R.; Servillo, G.; Brunacci, C.; Calvitti, M.; Bicciato, S.; et al. Indoleamine 2,3-dioxygenase is a signaling protein in long-term tolerance by dendritic cells. *Nature Immunology* **2011**, *12*, 870–878, doi:10.1038/ni.2077.
330. Von Hoff, D.D.; Ervin, T.; Arena, F.P.; Chiorean, E.G.; Infante, J.; Moore, M.; Seay, T.; Tjulandin, S.A.; Ma, W.W.; Saleh, M.N.; et al. Increased Survival in Pancreatic Cancer with nab-Paclitaxel plus Gemcitabine. *New England Journal of Medicine* **2013**, *369*, 1691–1703, doi:10.1056/NEJMoa1304369.
331. Xu, Z.; Smith, J.S.; Tian, J.; Byrnes, A.P. Induction of Shock After Intravenous Injection of Adenovirus Vectors: A Critical Role for Platelet-activating Factor. *Molecular Therapy* **2010**, *18*, 609–616, doi:10.1038/mt.2009.279.
332. Hecht, J.R.; Bedford, R.; Abbruzzese, J.L.; Lahoti, S.; Reid, T.R.; Soetikno, R.M.; Kirn, D.H.; Freeman, S.M. A phase I/II trial of intratumoral endoscopic ultrasound

injection of ONYX-015 with intravenous gemcitabine in unresectable pancreatic carcinoma. *Clin. Cancer Res.* **2003**, *9*, 555–561.

333. Xia, Z.J.; Chang, J.H.; Zhang, L.; Jiang, W.Q.; Guan, Z.Z.; Liu, J.W.; Zhang, Y.; Hu, X.H.; Wu, G.H.; Wang, H.Q.; et al. Phase III randomized clinical trial of intratumoral injection of E1B gene-deleted adenovirus (H101) combined with cisplatin-based chemotherapy in treating squamous cell cancer of head and neck or esophagus. *Cancer communications (London, England)* **2004**, *23*, 1666–1670.
334. Mahalingam, D.; Goel, S.; Aparo, S.; Patel Arora, S.; Noronha, N.; Tran, H.; Chakrabarty, R.; Selvaggi, G.; Gutierrez, A.; Coffey, M.; et al. A Phase II Study of Pelareorep (REOLYSIN®) in Combination with Gemcitabine for Patients with Advanced Pancreatic Adenocarcinoma. *Cancers* **2018**, *10*, 160, doi:10.3390/cancers10060160.
335. Urosevic, M.; Fujii, K.; Calmels, B.; Laine, E.; Kobert, N.; Acres, B.; Dummer, R. Type I IFN innate immune response to adenovirus-mediated IFN-γ gene transfer contributes to the regression of cutaneous lymphomas. *J Clin Invest* **2007**, *117*, 2834–2846, doi:10.1172/JCI32077.
336. Lang, F.F.; Tran, N.D.; Puduvalli, V.K.; Elder, J.B.; Fink, K.L.; Conrad, C.A.; Yung, W.K.A.; Penas-Prado, M.; Gomez-Manzano, C.; Peterkin, J.; et al. Phase 1b open-label randomized study of the oncolytic adenovirus DNX-2401 administered with or without interferon gamma for recurrent glioblastoma. *JCO* **2017**, *35*, 2002–2002, doi:10.1200/JCO.2017.35.15_suppl.2002.
337. Triebel, F.; Hacene, K.; Pichon, M.-F. A soluble lymphocyte activation gene-3 (sLAG-3) protein as a prognostic factor in human breast cancer expressing estrogen or progesterone receptors. *Cancer Lett.* **2006**, *235*, 147–153, doi:10.1016/j.canlet.2005.04.015.
338. Li, N.; Jilisihan, B.; Wang, W.; Tang, Y.; Keyoumu, S. Soluble LAG3 acts as a potential prognostic marker of gastric cancer and its positive correlation with CD8+T cell frequency and secretion of IL-12 and INF-γ in peripheral blood. *Cancer Biomark* **2018**, *23*, 341–351, doi:10.3233/CBM-181278.
339. Gujar, S.; Pol, J.G.; Kim, Y.; Lee, P.W.; Kroemer, G. Antitumor Benefits of Antiviral Immunity: An Underappreciated Aspect of Oncolytic Virotherapies. *Trends in Immunology* **2018**, *39*, 209–221, doi:10.1016/j.it.2017.11.006.
340. Van den Eynde, B.J.; van Baren, N.; Baurain, J.-F. Is There a Clinical Future for IDO1 Inhibitors After the Failure of Epacadostat in Melanoma? *Annual Review of Cancer Biology* **2020**, *4*, 241–256, doi:10.1146/annurev-cancerbio-030419-033635.
341. Fox, E.; Oliver, T.; Rowe, M.; Thomas, S.; Zakharia, Y.; Gilman, P.B.; Muller, A.J.; Prendergast, G.C. Indoximod: An Immunometabolic Adjuvant That Empowers T Cell Activity in Cancer. *Front Oncol* **2018**, *8*, doi:10.3389/fonc.2018.00370.
342. Castle, J.C.; Kreiter, S.; Diekmann, J.; Löwer, M.; Roemer, N. van de; Graaf, J. de; Selmi, A.; Diken, M.; Boegel, S.; Paret, C.; et al. Exploiting the Mutanome for Tumor Vaccination. *Cancer Res* **2012**, *72*, 1081–1091, doi:10.1158/0008-5472.CAN-11-3722.
343. Kreiter, S.; Vormehr, M.; van de Roemer, N.; Diken, M.; Löwer, M.; Diekmann, J.; Boegel, S.; Schrörs, B.; Vascotto, F.; Castle, J.C.; et al. Mutant MHC class II

epitopes drive therapeutic immune responses to cancer. *Nature* **2015**, *520*, 692–696, doi:10.1038/nature14426.

344. Aurisicchio, L.; Salvatori, E.; Lione, L.; Bandini, S.; Pallocca, M.; Maggio, R.; Fanciulli, M.; De Nicola, F.; Goeman, F.; Ciliberto, G.; et al. Poly-specific neoantigen-targeted cancer vaccines delay patient derived tumor growth. *J. Exp. Clin. Cancer Res.* **2019**, *38*, 78, doi:10.1186/s13046-019-1084-4.
345. Schumacher, T.; Bunse, L.; Pusch, S.; Sahm, F.; Wiestler, B.; Quandt, J.; Menn, O.; Osswald, M.; Oezen, I.; Ott, M.; et al. A vaccine targeting mutant IDH1 induces antitumour immunity. *Nature* **2014**, *512*, 324–327, doi:10.1038/nature13387.
346. Carreno, B.M.; Magrini, V.; Becker-Hapak, M.; Kaabinejadian, S.; Hundal, J.; Petti, A.A.; Ly, A.; Lie, W.-R.; Hildebrand, W.H.; Mardis, E.R.; et al. Cancer immunotherapy. A dendritic cell vaccine increases the breadth and diversity of melanoma neoantigen-specific T cells. *Science* **2015**, *348*, 803–808, doi:10.1126/science.aaa3828.
347. Ott, P.A.; Hu, Z.; Keskin, D.B.; Shukla, S.A.; Sun, J.; Bozym, D.J.; Zhang, W.; Luoma, A.; Giobbie-Hurder, A.; Peter, L.; et al. An immunogenic personal neoantigen vaccine for patients with melanoma. *Nature* **2017**, *547*, 217–221, doi:10.1038/nature22991.
348. Sahin, U.; Derhovanessian, E.; Miller, M.; Kloke, B.-P.; Simon, P.; Löwer, M.; Bukur, V.; Tadmor, A.D.; Luxemburger, U.; Schrörs, B.; et al. Personalized RNA mutanome vaccines mobilize poly-specific therapeutic immunity against cancer. *Nature* **2017**, *547*, 222–226, doi:10.1038/nature23003.
349. Hilf, N.; Kuttruff-Coqui, S.; Frenzel, K.; Bukur, V.; Stevanović, S.; Gouttefangeas, C.; Platten, M.; Tabatabai, G.; Dutoit, V.; van der Burg, S.H.; et al. Actively personalized vaccination trial for newly diagnosed glioblastoma. *Nature* **2019**, *565*, 240–245, doi:10.1038/s41586-018-0810-y.
350. Keskin, D.B.; Anandappa, A.J.; Sun, J.; Tirosh, I.; Mathewson, N.D.; Li, S.; Oliveira, G.; Giobbie-Hurder, A.; Felt, K.; Gjini, E.; et al. Neoantigen vaccine generates intratumoral T cell responses in phase Ib glioblastoma trial. *Nature* **2019**, *565*, 234–239, doi:10.1038/s41586-018-0792-9.
351. Deniger, D.C.; Pasetto, A.; Robbins, P.F.; Gartner, J.J.; Prickett, T.D.; Paria, B.C.; Malekzadeh, P.; Jia, L.; Yossef, R.; Langhan, M.M.; et al. T-cell Responses to TP53 "Hotspot" Mutations and Unique Neoantigens Expressed by Human Ovarian Cancers. *Clin. Cancer Res.* **2018**, *24*, 5562–5573, doi:10.1158/1078-0432.CCR-18-0573.
352. Karpanen, T.; Olweus, J. The Potential of Donor T-Cell Repertoires in Neoantigen-Targeted Cancer Immunotherapy. *Front Immunol* **2017**, *8*, 1718, doi:10.3389/fimmu.2017.01718.
353. Duan, F.; Duitama, J.; Al Seesi, S.; Ayres, C.M.; Corcelli, S.A.; Pawashe, A.P.; Blanchard, T.; McMahon, D.; Sidney, J.; Sette, A.; et al. Genomic and bioinformatic profiling of mutational neoepitopes reveals new rules to predict anticancer immunogenicity. *J. Exp. Med.* **2014**, *211*, 2231–2248, doi:10.1084/jem.20141308.
354. Vormehr, M.; Reinhard, K.; Blatnik, R.; Josef, K.; Beck, J.D.; Salomon, N.; Suchan, M.; Selmi, A.; Vascotto, F.; Zerweck, J.; et al. A non-functional neoepitope specific

CD8+ T-cell response induced by tumor derived antigen exposure in vivo. *Oncoimmunology* **2019**, *8*, 1553478, doi:10.1080/2162402X.2018.1553478.

355. Hansen, U.K.; Ramskov, S.; Bjerregaard, A.-M.; Borch, A.; Andersen, R.; Draghi, A.; Donia, M.; Bentzen, A.K.; Marquard, A.M.; Szallasi, Z.; et al. Tumor-Infiltrating T Cells From Clear Cell Renal Cell Carcinoma Patients Recognize Neoepitopes Derived From Point and Frameshift Mutations. *Front Immunol* **2020**, *11*, 373, doi:10.3389/fimmu.2020.00373.
356. Xu, C. A review of somatic single nucleotide variant calling algorithms for next-generation sequencing data. *Comput Struct Biotechnol J* **2018**, *16*, 15–24, doi:10.1016/j.csbj.2018.01.003.
357. Hwang, S.; Kim, E.; Lee, I.; Marcotte, E.M. Systematic comparison of variant calling pipelines using gold standard personal exome variants. *Sci Rep* **2015**, *5*, 17875, doi:10.1038/srep17875.
358. O'Rawe, J.; Jiang, T.; Sun, G.; Wu, Y.; Wang, W.; Hu, J.; Bodily, P.; Tian, L.; Hakonarson, H.; Johnson, W.E.; et al. Low concordance of multiple variant-calling pipelines: practical implications for exome and genome sequencing. *Genome Medicine* **2013**, *5*, 28, doi:10.1186/gm432.
359. Liu, Z.-K.; Shang, Y.-K.; Chen, Z.-N.; Bian, H. A three-caller pipeline for variant analysis of cancer whole-exome sequencing data. *Mol Med Rep* **2017**, *15*, 2489–2494, doi:10.3892/mmr.2017.6336.
360. Merino-Valverde, I.; Greco, E.; Abad, M. The microproteome of cancer: From invisibility to relevance. *Exp. Cell Res.* **2020**, 111997, doi:10.1016/j.yexcr.2020.111997.
361. Boegel, S.; Castle, J.C.; Kodysh, J.; O'Donnell, T.; Rubinsteyn, A. Chapter Two - Bioinformatic methods for cancer neoantigen prediction. In *Progress in Molecular Biology and Translational Science*; Teplow, D.B., Ed.; Cancer Immunotherapy; Academic Press, 2019; Vol. 164, pp. 25–60.
362. Yadav, M.; Jhunjhunwala, S.; Phung, Q.T.; Lupardus, P.; Tanguay, J.; Bumbaca, S.; Franci, C.; Cheung, T.K.; Fritsche, J.; Weinschenk, T.; et al. Predicting immunogenic tumour mutations by combining mass spectrometry and exome sequencing. *Nature* **2014**, *515*, 572–576, doi:10.1038/nature14001.
363. Bassani-Sternberg, M. Mass Spectrometry Based Immunopeptidomics for the Discovery of Cancer Neoantigens. *Methods Mol. Biol.* **2018**, *1719*, 209–221, doi:10.1007/978-1-4939-7537-2_14.
364. Bassani-Sternberg, M.; Bräunlein, E.; Klar, R.; Engleitner, T.; Sinitcyn, P.; Audehm, S.; Straub, M.; Weber, J.; Slotta-Huspenina, J.; Specht, K.; et al. Direct identification of clinically relevant neoepitopes presented on native human melanoma tissue by mass spectrometry. *Nature Communications* **2016**, *7*, 13404, doi:10.1038/ncomms13404.
365. Chong, C.; Müller, M.; Pak, H.; Harnett, D.; Huber, F.; Grun, D.; Leleu, M.; Auger, A.; Arnaud, M.; Stevenson, B.J.; et al. Integrated Proteogenomic Deep Sequencing and Analytics Accurately Identify Non-Canonical Peptides in Tumor Immunopeptidomes. *bioRxiv* **2019**, 758680, doi:10.1101/758680.
366. Rosenthal, R.; Cadieux, E.L.; Salgado, R.; Bakir, M.A.; Moore, D.A.; Hiley, C.T.; Lund, T.; Tanić, M.; Reading, J.L.; Joshi, K.; et al. Neoantigen-directed immune

escape in lung cancer evolution. *Nature* **2019**, *567*, 479–485, doi:10.1038/s41586-019-1032-7.

367. de Vries, C.R.; Monken, C.E.; Lattime, E.C. The addition of recombinant vaccinia HER2/neu to oncolytic vaccinia-GMCSF given into the tumor microenvironment overcomes MDSC-mediated immune escape and systemic anergy. *Cancer Gene Therapy* **2015**, *22*, 154–162, doi:10.1038/cgt.2015.2.
368. Pol, J.G.; Atherton, M.J.; Bridle, B.W.; Stephenson, K.B.; Le Boeuf, F.; Hummel, J.L.; Martin, C.G.; Pomoransky, J.; Breitbach, C.J.; Diallo, J.-S.; et al. Development and applications of oncolytic Maraba virus vaccines. *Oncolytic Virother* **2018**, *7*, 117–128, doi:10.2147/OV.S154494.
369. Rodríguez-García, A.; Svensson, E.; Gil-Hoyos, R.; Fajardo, C.A.; Rojas, L.A.; Arias-Badia, M.; Loskog, A.S.I.; Alemany, R. Insertion of exogenous epitopes in the E3-19K of oncolytic adenoviruses to enhance TAP-independent presentation and immunogenicity. *Gene Therapy* **2015**, *22*, 596–601, doi:10.1038/gt.2015.41.
370. Capasso, C.; Hirvinen, M.; Garofalo, M.; Romaniuk, D.; Kuryk, L.; Sarvela, T.; Vitale, A.; Antopolsky, M.; Magarkar, A.; Viitala, T.; et al. Oncolytic adenoviruses coated with MHC-I tumor epitopes increase the antitumor immunity and efficacy against melanoma. *Oncoimmunology* **2015**, *5*, doi:10.1080/2162402X.2015.1105429.
371. Ylösmäki, E.; Malorzo, C.; Capasso, C.; Honkasalo, O.; Fusciello, M.; Martins, B.; Ylösmäki, L.; Louna, A.; Feola, S.; Paavilainen, H.; et al. Personalized Cancer Vaccine Platform for Clinically Relevant Oncolytic Enveloped Viruses. *Molecular Therapy* **2018**, *26*, 2315–2325, doi:10.1016/j.ymthe.2018.06.008.
372. Kedl, R.M.; Kappler, J.W.; Marrack, P. Epitope dominance, competition and T cell affinity maturation. *Curr. Opin. Immunol.* **2003**, *15*, 120–127, doi:10.1016/s0952-7915(02)00009-2.
373. Kedl, R.M.; Rees, W.A.; Hildeman, D.A.; Schaefer, B.; Mitchell, T.; Kappler, J.; Marrack, P. T cells compete for access to antigen-bearing antigen-presenting cells. *J. Exp. Med.* **2000**, *192*, 1105–1113, doi:10.1084/jem.192.8.1105.
374. Woller, N.; Gürlevik, E.; Fleischmann-Mundt, B.; Schumacher, A.; Knocke, S.; Kloos, A.M.; Saborowski, M.; Geffers, R.; Manns, M.P.; Wirth, T.C.; et al. Viral Infection of Tumors Overcomes Resistance to PD-1-immunotherapy by Broadening Neoantigenome-directed T-cell Responses. *Mol. Ther.* **2015**, *23*, 1630–1640, doi:10.1038/mt.2015.115.
375. Castle, J.C.; Kreiter, S.; Diekmann, J.; Lower, M.; van de Roemer, N.; de Graaf, J.; Selmi, A.; Diken, M.; Boegel, S.; Paret, C.; et al. Exploiting the Mutanome for Tumor Vaccination. *Cancer Research* **2012**, *72*, 1081–1091, doi:10.1158/0008-5472.CAN-11-3722.
376. Rojas, J.J.; Guedan, S.; Searle, P.F.; Martinez-Quintanilla, J.; Gil-Hoyos, R.; Alcayaga-Miranda, F.; Cascallo, M.; Alemany, R. Minimal RB-responsive E1A Promoter Modification to Attain Potency, Selectivity, and Transgene-arming Capacity in Oncolytic Adenoviruses. *Molecular Therapy* **2010**, *18*, 1960–1971, doi:10.1038/mt.2010.173.

377. Blair, G.E.; Dixon, S.C.; Griffiths, S.A.; Zajdel, M.E. Restricted replication of human adenovirus type 5 in mouse cell lines. *Virus Res.* **1989**, *14*, 339–346, doi:10.1016/0168-1702(89)90026-9.
378. Young, A.-M.; Archibald, K.M.; Tookman, L.A.; Pool, A.; Dudek, K.; Jones, C.; Williams, S.L.; Pirlo, K.J.; Willis, A.E.; Lockley, M.; et al. Failure of Translation of Human Adenovirus mRNA in Murine Cancer Cells Can be Partially Overcome by L4-100K Expression In Vitro and In Vivo. *Molecular Therapy* **2012**, *20*, 1676–1688, doi:10.1038/mt.2012.116.
379. Holtkamp, S.; Kreiter, S.; Selmi, A.; Simon, P.; Koslowski, M.; Huber, C.; Türeci, Ö.; Sahin, U. Modification of antigen-encoding RNA increases stability, translational efficacy, and T-cell stimulatory capacity of dendritic cells. *Blood* **2006**, *108*, 4009–4017, doi:10.1182/blood-2006-04-015024.
380. Kreiter, S.; Vormehr, M.; van de Roemer, N.; Diken, M.; L?wer, M.; Diekmann, J.; Boegel, S.; Schr?rs, B.; Vascotto, F.; Castle, J.C.; et al. Mutant MHC class II epitopes drive therapeutic immune responses to cancer. *Nature* **2015**, *520*, 692–696, doi:10.1038/nature14426.
381. Kreiter, S.; Selmi, A.; Diken, M.; Sebastian, M.; Osterloh, P.; Schild, H.; Huber, C.; Türeci, Ö.; Sahin, U. Increased Antigen Presentation Efficiency by Coupling Antigens to MHC Class I Trafficking Signals. *J Immunol* **2008**, *180*, 309–318, doi:10.4049/jimmunol.180.1.309.
382. Woller, N.; Gürlevik, E.; Fleischmann-Mundt, B.; Schumacher, A.; Knocke, S.; Kloos, A.M.; Saborowski, M.; Geffers, R.; Manns, M.P.; Wirth, T.C.; et al. Viral Infection of Tumors Overcomes Resistance to PD-1-immunotherapy by Broadening Neoantigenome-directed T-cell Responses. *Molecular therapy : the journal of the American Society of Gene Therapy* **2015**, *23*, 1630–40, doi:10.1038/mt.2015.115.
383. Rincón, E.; Cejalvo, T.; Kanojia, D.; Alfranca, A.; Rodríguez-Milla, M.Á.; Gil Hoyos, R.A.; Han, Y.; Zhang, L.; Alemany, R.; Lesniak, M.S.; et al. Mesenchymal stem cell carriers enhance antitumor efficacy of oncolytic adenoviruses in an immunocompetent mouse model. *Oncotarget* **2017**, *8*, 45415–45431, doi:10.18632/oncotarget.17557.
384. Bett, A.J.; Prevec, L.; Graham, F.L. Packaging capacity and stability of human adenovirus type 5 vectors. *Journal of Virology* **1993**, *67*, 5911–5921, doi:10.1128/JVI.67.10.5911-5921.1993.
385. Lichtenstein, D.L.; Doronin, K.; Toth, K.; Kuppuswamy, M.; Wold, W.S.M.; Tollefson, A.E. Adenovirus E3-6.7K protein is required in conjunction with the E3-RID protein complex for the internalization and degradation of TRAIL receptor 2. *J. Virol.* **2004**, *78*, 12297–12307, doi:10.1128/JVI.78.22.12297-12307.2004.
386. Bruder, J.T.; Jie, T.; McVey, D.L.; Kovesdi, I. Expression of gp19K increases the persistence of transgene expression from an adenovirus vector in the mouse lung and liver. *Journal of Virology* **1997**, *71*, 7623–7628.
387. Tanaka, Y.; Tevethia, S.S. Differential effect of adenovirus 2 E3/19K glycoprotein on the expression of H-2Kb and H-2Db class I antigens and H-2Kb- and H-2Db-restricted SV40-specific CTL-mediated lysis. *Virology* **1988**, *165*, 357–366, doi:10.1016/0042-6822(88)90580-6.

388. Bortolanza, S.; Bunuales, M.; Alzuguren, P.; Lamas, O.; Aldabe, R.; Prieto, J.; Hernandez-Alcoceba, R. Deletion of the E3-6.7K/gp19K region reduces the persistence of wild-type adenovirus in a permissive tumor model in Syrian hamsters. *Cancer Gene Ther* **2009**, *16*, 703–712, doi:10.1038/cgt.2009.12.
389. Schmidt, J.; Guillaume, P.; Dojcinovic, D.; Karbach, J.; Coukos, G.; Luescher, I. In silico and cell-based analyses reveal strong divergence between prediction and observation of T-cell–recognized tumor antigen T-cell epitopes. *J Biol Chem* **2017**, *292*, 11840–11849, doi:10.1074/jbc.M117.789511.
390. Akram, A.; Inman, R.D. Immunodominance: A pivotal principle in host response to viral infections. *Clinical Immunology* **2012**, *143*, 99–115, doi:10.1016/j.clim.2012.01.015.
391. Schöne, D.; Hrycak, C.P.; Windmann, S.; Lapuente, D.; Dittmer, U.; Tenbusch, M.; Bayer, W. Immunodominance of Adenovirus-Derived CD8+ T Cell Epitopes Interferes with the Induction of Transgene-Specific Immunity in Adenovirus-Based Immunization. *J Virol* **2017**, *91*, doi:10.1128/JVI.01184-17.
392. Schirmbeck, R.; Reimann, J.; Kochanek, S.; Kreppel, F. The Immunogenicity of Adenovirus Vectors Limits the Multispecificity of CD8 T-cell Responses to Vector-encoded Transgenic Antigens. *Molecular Therapy* **2008**, *16*, 1609–1616, doi:10.1038/mt.2008.141.
393. Frahm, N.; DeCamp, A.C.; Friedrich, D.P.; Carter, D.K.; Defawe, O.D.; Kublin, J.G.; Casimiro, D.R.; Duerr, A.; Robertson, M.N.; Buchbinder, S.P.; et al. Human adenovirus-specific T cells modulate HIV-specific T cell responses to an Ad5-vectored HIV-1 vaccine. *J Clin Invest* **2012**, *122*, 359–367, doi:10.1172/JCI60202.
394. Lopes, A.; Feola, S.; Ligot, S.; Fusciello, M.; Vandermeulen, G.; Préat, V.; Cerullo, V. Oncolytic adenovirus drives specific immune response generated by a poly-epitope pDNA vaccine encoding melanoma neoantigens into the tumor site. *J Immunother Cancer* **2019**, *7*, doi:10.1186/s40425-019-0644-7.
395. D'Alise, A.M.; Leoni, G.; Cotugno, G.; Troise, F.; Langone, F.; Fichera, I.; De Lucia, M.; Avalle, L.; Vitale, R.; Leuzzi, A.; et al. Adenoviral vaccine targeting multiple neoantigens as strategy to eradicate large tumors combined with checkpoint blockade. *Nat Commun* **2019**, *10*, 2688, doi:10.1038/s41467-019-10594-2.
396. Larson, C.; Oronsky, B.; Varner, G.; Caroen, S.; Burbano, E.; Insel, E.; Hedjran, F.; Carter, C.A.; Reid, T.R. A practical guide to the handling and administration of personalized transcriptionally attenuated oncolytic adenoviruses (PTAVs). *Oncoimmunology* **2018**, *7*, e1478648, doi:10.1080/2162402X.2018.1478648.
397. AdAPT Oncolytic Virus Platform | EpicentRx.
398. Bridle, B.W.; Hanson, S.; Lichty, B.D. Combining oncolytic virotherapy and tumour vaccination. *Cytokine & Growth Factor Reviews* **2010**, *21*, 143–148, doi:10.1016/j.cytogfr.2010.02.009.
399. Pol, J.G.; Acuna, S.A.; Yadollahi, B.; Tang, N.; Stephenson, K.B.; Atherton, M.J.; Hanwell, D.; El-Warrak, A.; Goldstein, A.; Moloo, B.; et al. Preclinical evaluation of a MAGE-A3 vaccination utilizing the oncolytic Maraba virus currently in first-in-human trials. *OncoImmunology* **2019**, *8*, e1512329, doi:10.1080/2162402X.2018.1512329.

400. Olson, B.; Li, Y.; Lin, Y.; Liu, E.T.; Patnaik, A. Mouse Models for Cancer Immunotherapy Research. *Cancer Discov* **2018**, *8*, 1358–1365, doi:10.1158/2159-8290.CD-18-0044.
401. Ropponen, K.; Tammi, M.; Parkkinen, J.; Eskelinen, M.; Tammi, R.; Lipponen, P.; Agren, U.; Alhava, E.; Kosma, V.M. Tumor cell-associated hyaluronan as an unfavorable prognostic factor in colorectal cancer. *Cancer Res.* **1998**, *58*, 342–347.
402. Auvinen, P.; Tammi, R.; Parkkinen, J.; Tammi, M.; Agren, U.; Johansson, R.; Hirvikoski, P.; Eskelinen, M.; Kosma, V.M. Hyaluronan in peritumoral stroma and malignant cells associates with breast cancer spreading and predicts survival. *Am. J. Pathol.* **2000**, *156*, 529–536, doi:10.1016/S0002-9440(10)64757-8.
403. Bertrand, P.; Girard, N.; Delpech, B.; Duval, C.; d'Anjou, J.; Dauce, J.P. Hyaluronan (hyaluronic acid) and hyaluronectin in the extracellular matrix of human breast carcinomas: comparison between invasive and non-invasive areas. *Int. J. Cancer* **1992**, *52*, 1–6, doi:10.1002/ijc.2910520102.
404. Munson, J.M.; Shieh, A.C. Interstitial fluid flow in cancer: implications for disease progression and treatment. *Cancer Manag Res* **2014**, *6*, 317–328, doi:10.2147/CMAR.S65444.
405. Nakazawa, H.; Yoshihara, S.; Kudo, D.; Morohashi, H.; Kakizaki, I.; Kon, A.; Takagaki, K.; Sasaki, M. 4-methylumbelliferone, a hyaluronan synthase suppressor, enhances the anticancer activity of gemcitabine in human pancreatic cancer cells. *Cancer Chemother. Pharmacol.* **2006**, *57*, 165–170, doi:10.1007/s00280-005-0016-5.
406. Litwiniuk, M.; Krejner, A.; Speyrer, M.S.; Gauto, A.R.; Grzela, T. Hyaluronic Acid in Inflammation and Tissue Regeneration. *Wounds* **2016**, *28*, 78–88.
407. Dominguez-Gutierrez, P.R.; Crispen, P.; Kusmartsev, S.A. Abstract 1521: Tumor-produced hyaluronan contributes to the formation tolerogenic immunosuppressive microenvironment. *Cancer Res* **2019**, *79*, 1521–1521, doi:10.1158/1538-7445.AM2019-1521.
408. Váradi, T.; Mersich, T.; Auvinen, P.; Tammi, R.; Tammi, M.; Salamon, F.; Besznyák, I.; Jakab, F.; Baranyai, Z.; Szöllősi, J.; et al. Binding of trastuzumab to ErbB2 is inhibited by a high pericellular density of hyaluronan. *J. Histochem. Cytochem.* **2012**, *60*, 567–575, doi:10.1369/0022155412448070.
409. Duran-Reynals, F. TISSUE PERMEABILITY AND THE SPREADING FACTORS IN INFECTION : A Contribution to the Host:Parasite Problem. *Bacteriol Rev* **1942**, *6*, 197–252.
410. Weber, G.C.; Buhren, B.A.; Schrumpf, H.; Wohlrab, J.; Gerber, P.A. Clinical Applications of Hyaluronidase. In *Therapeutic Enzymes: Function and Clinical Implications*; Labrou, N., Ed.; Advances in Experimental Medicine and Biology; Springer: Singapore, 2019; pp. 255–277 ISBN 9789811377099.
411. Provenzano, P.P.; Cuevas, C.; Chang, A.E.; Goel, V.K.; Von Hoff, D.D.; Hingorani, S.R. Enzymatic targeting of the stroma ablates physical barriers to treatment of pancreatic ductal adenocarcinoma. *Cancer Cell* **2012**, *21*, 418–429, doi:10.1016/j.ccr.2012.01.007.

412. Breaking the Barrier—PEGylated Recombinant Human Hyaluronidase (PEGPH20)—A New Therapeutic Approach to the Treatment of Pancreatic Ductal Adenocarcinoma. *touchONCOLOGY* 2017.
413. Halozyme Announces HALO-301 Phase 3 Study Fails To Meet Primary Endpoint Available online: https://www.halozyme.com/investors/news-releases/news-release-details/2019/Halozyme-Announces-HALO-301-Phase-3-Study-Fails-To-Meet-Primary-Endpoint/default.aspx (accessed on May 8, 2020).
414. Michl, P.; Gress, T.M. Improving drug delivery to pancreatic cancer: breaching the stromal fortress by targeting hyaluronic acid. *Gut* **2012**, *61*, 1377–1379, doi:10.1136/gutjnl-2012-302604.
415. Farrera-Sal, M.; Fillat, C.; Alemany, R. Effect of Transgene Location, Transcriptional Control Elements and Transgene Features in Armed Oncolytic Adenoviruses. *Cancers* **2020**, *12*, 1034, doi:10.3390/cancers12041034.
416. Kelly, T.J.; Lewis, A.M. Use of Nondefective Adenovirus-Simian Virus 40 Hybrids for Mapping the Simian Virus 40 Genome. *Journal of Virology* **1973**, *12*, 643–652, doi:10.1128/JVI.12.3.643-652.1973.
417. Flint, S.J.; Wewerka-Lutz, Y.; Levine, A.S.; Sambrook, J.; Sharp, P.A. II. RNA Sequences Complementary to Simian Virus 40 and Adenovirus 2 DNA in Ad2+NDr- and Ad2+ND3-Infected Cells. **1975**, *16*, 12.
418. Berkner, K.L.; Sharp, P.A. Generation of adenovirus by transfection of plasmids. *Nucl Acids Res* **1983**, *11*, 6003–6020, doi:10.1093/nar/11.17.6003.
419. Chanda, P.K.; Natuk, R.J.; Mason, B.B.; Brat, B.M.; Greenberg, L.; Dheer, S.K.; Molnar-kimber, K.L.; Mizutani, S.; Lubeck, M.D.; Davis, A.R.; et al. High level expression of the envelope glycoproteins of the human immunodeficiency virus type I in presence of rev gene using helper-independent adenovirus type 7 recombinants. *Virology* **1990**, *175*, 535–547, doi:10.1016/0042-6822(90)90438-W.
420. Haj-Ahmad, Y.; Graham, F.L. Development of a helper-independent human adenovirus vector and its use in the transfer of the herpes simplex virus thymidine kinase gene. *J Virol* **1986**, *57*, 267–274.
421. Saito, I.; Oya, Y.; Yamamoto, K.; Yuasa, T.; Shimojo, H. Construction of nondefective adenovirus type 5 bearing a 2.8-kilobase hepatitis B virus DNA near the right end of its genome. *Journal of Virology* **1985**, *54*, 711–719.
422. Kretschmer, P.J.; Jin, F.; Chartier, C.; Hermiston, T.W. Development of a transposon-based approach for identifying novel transgene insertion sites within the replicating adenovirus. *Molecular Therapy* **2005**, *12*, 118–127, doi:10.1016/j.ymthe.2005.03.019.
423. Jin, F.; Kretschmer, P.J.; Hermiston, T.W. Identification of novel insertion sites in the Ad5 genome That utilize the Ad splicing machinery for therapeutic gene expression. *Molecular Therapy* **2005**, *12*, 1052–1063, doi:10.1016/j.ymthe.2005.07.696.
424. Wang, Y.; Hallden, G.; Hill, R.; Anand, A.; Liu, T.-C.; Francis, J.; Brooks, G.; Lemoine, N.; Kirn, D. E3 gene manipulations affect oncolytic adenovirus activity in immunocompetent tumor models. *Nat Biotechnol* **2003**, *21*, 1328–1335, doi:10.1038/nbt887.

425. Suzuki, K.; Alemany, R.; Yamamoto, M.; Curiel, D.T. The Presence of the Adenovirus E3 Region Improves the Oncolytic Potency of Conditionally Replicative Adenoviruses. 13.
426. García-Castro, J.; Martínez-Palacio, J.; Lillo, R.; García-Sánchez, F.; Alemany, R.; Madero, L.; Bueren, J.A.; Ramírez, M. Tumor cells as cellular vehicles to deliver gene therapies to metastatic tumors. *Cancer Gene Ther* **2005**, *12*, 341–349, doi:10.1038/sj.cgt.7700801.
427. Robinson, M.; Ge, Y.; Ko, D.; Yendluri, S.; Laflamme, G.; Hawkins, L.; Jooss, K. Comparison of the E3 and L3 regions for arming oncolytic adenoviruses to achieve a high level of tumor-specific transgene expression. *Cancer Gene Ther* **2008**, *15*, 9–17, doi:10.1038/sj.cgt.7701093.
428. Nettelbeck, D.M. Cellular genetic tools to control oncolytic adenoviruses for virotherapy of cancer. *J Mol Med* **2008**, *86*, 363–377, doi:10.1007/s00109-007-0291-1.
429. Suzuki, T.; Sakurai, F.; Nakamura, S.; Kouyama, E.; Kawabata, K.; Kondoh, M.; Yagi, K.; Mizuguchi, H. miR-122a-regulated expression of a suicide gene prevents hepatotoxicity without altering antitumor effects in suicide gene therapy. *Mol. Ther.* **2008**, *16*, 1719–1726, doi:10.1038/mt.2008.159.
430. Card, P.B.; Hogg, R.T.; Gil Del Alcazar, C.R.; Gerard, R.D. MicroRNA silencing improves the tumor specificity of adenoviral transgene expression. *Cancer Gene Ther.* **2012**, *19*, 451–459, doi:10.1038/cgt.2012.16.
431. Geisler, A.; Fechner, H. MicroRNA-regulated viral vectors for gene therapy. *World J Exp Med* **2016**, *6*, 37–54, doi:10.5493/wjem.v6.i2.37.
432. Davis, J.J.; Wang, L.; Dong, F.; Zhang, L.; Guo, W.; Teraishi, F.; Xu, K.; Ji, L.; Fang, B. Oncolysis and suppression of tumor growth by a GFP-expressing oncolytic adenovirus controlled by an hTERT and CMV hybrid promoter. *Cancer Gene Ther* **2006**, *13*, 720–723, doi:10.1038/sj.cgt.7700944.
433. Lee, Y.J.; Galoforo, S.S.; Battle, P.; Lee, H.; Corry, P.M.; Jessup, J.M. Replicating adenoviral vector–mediated transfer of a heat-inducible double suicide gene for gene therapy. *Cancer Gene Ther* **2001**, *8*, 397–404, doi:10.1038/sj.cgt.7700310.
434. Rivera, A.A.; Wang, M.; Suzuki, K.; Uil, T.G.; Krasnykh, V.; Curiel, D.T.; Nettelbeck, D.M. Mode of transgene expression after fusion to early or late viral genes of a conditionally replicating adenovirus via an optimized internal ribosome entry site in vitro and in vivo. *Virology* **2004**, *320*, 121–134, doi:10.1016/j.virol.2003.11.028.
435. Cascante, A.; Abate-Daga, D.; Garcia-Rodríguez, L.; González, J.R.; Alemany, R.; Fillat, C. GCV modulates the antitumoural efficacy of a replicative adenovirus expressing the TAT8-TK as a late gene in a pancreatic tumour model. *Gene Ther* **2007**, *14*, 1471–1480, doi:10.1038/sj.gt.3303008.
436. Donnelly, M.L.L.; Mehrotra, A.; Gani, D.; Hughes, L.E.; Luke, G.; Li, X.; Ryan, M.D. Analysis of the aphthovirus 2A/2B polyprotein 'cleavage' mechanism indicates not a proteolytic reaction, but a novel translational effect: a putative ribosomal 'skip.' *Journal of General Virology* **2001**, *82*, 1013–1025, doi:10.1099/0022-1317-82-5-1013.
437. Szymczak, A.L.; Workman, C.J.; Wang, Y.; Vignali, K.M.; Dilioglou, S.; Vanin, E.F.; Vignali, D.A.A. Correction of multi-gene deficiency in vivo using a single "self-

cleaving" 2A peptide–based retroviral vector. *Nat Biotechnol* **2004**, *22*, 589–594, doi:10.1038/nbt957.

438. Funston, G.M.; Kallioinen, S.E.; de Felipe, P.; Ryan, M.D.; Iggo, R.D. Expression of heterologous genes in oncolytic adenoviruses using picornaviral 2A sequences that trigger ribosome skipping. *Journal of General Virology* **2008**, *89*, 389–396, doi:10.1099/vir.0.83444-0.
439. Quirin, C.; Rohmer, S.; Fernández-Ulibarri, I.; Behr, M.; Hesse, A.; Engelhardt, S.; Erbs, P.; Enk, A.H.; Nettelbeck, D.M. Selectivity and Efficiency of Late Transgene Expression by Transcriptionally Targeted Oncolytic Adenoviruses Are Dependent on the Transgene Insertion Strategy. *Human Gene Therapy* **2011**, *22*, 389–404, doi:10.1089/hum.2010.100.
440. Berget, S.M.; Moore, C.; Sharp, P.A. Spliced segments at the 5′ terminus of adenovirus 2 late mRNA. *Proc Natl Acad Sci USA* **1977**, *74*, 3171–3175, doi:10.1073/pnas.74.8.3171.
441. Muhlemann, O.; Yue, B.-G.; Petersen-Mahrt, S.; Akusjarvi, G. A Novel Type of Splicing Enhancer Regulating Adenovirus Pre-mRNA Splicing. *Molecular and Cellular Biology* **2000**, *20*, 2317–2325, doi:10.1128/MCB.20.7.2317-2325.2000.
442. Fernández-Ulibarri, I.; Hammer, K.; Arndt, M.A.E.; Kaufmann, J.K.; Dorer, D.; Engelhardt, S.; Kontermann, R.E.; Hess, J.; Allgayer, H.; Krauss, J.; et al. Genetic delivery of an immunoRNase by an oncolytic adenovirus enhances anticancer activity: ImmunoRNase-expressing oncolytic adenovirus. *Int. J. Cancer* **2015**, *136*, 2228–2240, doi:10.1002/ijc.29258.
443. Provenzano, P.P.; Hingorani, S.R. Hyaluronan, fluid pressure, and stromal resistance in pancreas cancer. *Br. J. Cancer* **2013**, *108*, 1–8, doi:10.1038/bjc.2012.569.
444. Josefsson, A.; Adamo, H.; Hammarsten, P.; Granfors, T.; Stattin, P.; Egevad, L.; Laurent, A.E.; Wikström, P.; Bergh, A. Prostate cancer increases hyaluronan in surrounding nonmalignant stroma, and this response is associated with tumor growth and an unfavorable outcome. *Am. J. Pathol.* **2011**, *179*, 1961–1968, doi:10.1016/j.ajpath.2011.06.005.
445. Baumgartner, G.; Gomar-Höss, C.; Sakr, L.; Ulsperger, E.; Wogritsch, C. The impact of extracellular matrix on the chemoresistance of solid tumors--experimental and clinical results of hyaluronidase as additive to cytostatic chemotherapy. *Cancer Lett.* **1998**, *131*, 85–99.
446. Pillwein, K.; Fuiko, R.; Slavc, I.; Czech, T.; Hawliczek, G.; Bernhardt, G.; Nirnberger, G.; Köller, U. Hyaluronidase additional to standard chemotherapy improves outcome for children with malignant brain tumors. *Cancer Lett.* **1998**, *131*, 101–108, doi:10.1016/s0304-3835(98)00205-5.
447. Infante, J.R.; Korn, R.L.; Rosen, L.S.; LoRusso, P.; Dychter, S.S.; Zhu, J.; Maneval, D.C.; Jiang, P.; Shepard, H.M.; Frost, G.; et al. Phase 1 trials of PEGylated recombinant human hyaluronidase PH20 in patients with advanced solid tumours. *Br J Cancer* **2018**, *118*, 153–161, doi:10.1038/bjc.2017.327.
448. Habermann, E.; Neumann, W.P.; Neumann, W. Reinigung der Phospholipase A von Bienengift. *Naturwissenschaften* **1956**, *43*, 84–84, doi:10.1007/BF00631863.

449. Barker, S.A.; Bayyuk, S.I.; Brimacombe, J.S.; Palmer, D.J. Characterization of the Products of the Action of Bee Venom Hyaluronidase. *Nature* **1963**, *199*, 693–694, doi:10.1038/199693a0.
450. Gmachl, M.; Kreil, G. Bee venom hyaluronidase is homologous to a membrane protein of mammalian sperm. *Proc. Natl. Acad. Sci. U.S.A.* **1993**, *90*, 3569–3573, doi:10.1073/pnas.90.8.3569.
451. Soldatova, L.N.; Crameri, R.; Gmachl, M.; Kemeny, D.M.; Schmidt, M.; Weber, M.; Mueller, U.R. Superior biologic activity of the recombinant bee venom allergen hyaluronidase expressed in baculovirus-infected insect cells as compared with Escherichia coli. *Journal of Allergy and Clinical Immunology* **1998**, *101*, 691–698, doi:10.1016/S0091-6749(98)70179-4.
452. Villanueva, E.; Martí-Solano, M.; Fillat, C. Codon optimization of the adenoviral fiber negatively impacts structural protein expression and viral fitness. *Sci Rep* **2016**, *6*, 27546, doi:10.1038/srep27546.
453. Núñez-Manchón, E.; Farrera-Sal, M.; Castellano, G.; Medel, D.; Alemany, R.; Villanueva, E.; Fillat, C. Transgene codon usage drives viral fitness and therapeutic efficacy in oncolytic adenoviruses. *bioRxiv* **2020**, 2020.06.19.161026, doi:10.1101/2020.06.19.161026.
454. Plotkin, J.B.; Robins, H.; Levine, A.J. Tissue-specific codon usage and the expression of human genes. *Proceedings of the National Academy of Sciences* **2004**, *101*, 12588–12591, doi:10.1073/pnas.0404957101.
455. McBride, W.H.; Bard, J.B. Hyaluronidase-sensitive halos around adherent cells. Their role in blocking lymphocyte-mediated cytolysis. *J. Exp. Med.* **1979**, *149*, 507–515, doi:10.1084/jem.149.2.507.
456. Singha, N.C.; Nekoroski, T.; Zhao, C.; Symons, R.; Jiang, P.; Frost, G.I.; Huang, Z.; Shepard, H.M. Tumor-Associated Hyaluronan Limits Efficacy of Monoclonal Antibody Therapy. *Mol Cancer Ther* **2015**, *14*, 523–532, doi:10.1158/1535-7163.MCT-14-0580.
457. Thompson, C.B.; Shepard, H.M.; O'Connor, P.M.; Kadhim, S.; Jiang, P.; Osgood, R.J.; Bookbinder, L.H.; Li, X.; Sugarman, B.J.; Connor, R.J.; et al. Enzymatic depletion of tumor hyaluronan induces antitumor responses in preclinical animal models. *Mol. Cancer Ther.* **2010**, *9*, 3052–3064, doi:10.1158/1535-7163.MCT-10-0470.

ANNEX

Supplementary Table 1. Oligonucleotides used in this thesis for generating PCR fragments.

Primer	Sequence 5' to 3'
sPH20 Fwd	CCACCGGTGCCACCATGGG
sPH20 Rv	AACGCGGCCGCTTTATTAGTGGTGGTGGTGGTGGTGGGGGCCCTGGAACAGC ACCTCCAGAGATAGTGTGGAGGGTGAAGC
BHyal Fwd	ATCCACCGGTCCACCATGTCTCGGCCTCTCGTGAT
BHyal Rv	CGCGGCGGCCGCTTTAGTGGTGGTGGTGGTGGTGGGGGCCCTGGAACAGCAC CTCCAGCACTTGGTCCACGCTCACGTC
40PH20af Fwd	ATCGTTTGTGTTATGTTTCAACGTGTTTATTTTTCAATTGGCAGGCGCAATCTTC GCATTTCTTTTTTCCAGCCACCATGGGAGTGCTAAAATTCAA
40PH20af Rv	GCTATACTACTGAATGAAAAATGACTTGAAATTTTCTGCAATTGAAAAATAAAG TTTATTAAGATAGTGTGGAGGGTG
E4-IIIaPH20 Fwd	CTTCCTCAAATCGTCACTTCCGTTTTCCCACGTTACGTCACGTACTAAGCGGTGA TGTTTCTGATCAGCCACCATGGGAGTGCTAAAATTCAA
E4-40PH20 Fwd	CTTCCTCAAATCGTCACTTCCGTTTTCCCACGTTACGTCACGCAGGCGCAATCTT CGCATTTCTTTTTTCCAGCCACCATGGGAGTGCTAAAATTCAA
40PH20 Rv	GTAGGTTTTAGGGCGGAGTAACTTGTATGTGTTGGGAATTGTAGTTTTCTTAAA ATGTTTATTAAGATAGTGTGGAGGGTG
E1A-RpsL Fwd	GAGGACTTGCTTAACGAGCCTGGGCAACCTTTGGACTTGAGCTGTAAACGCCC CAGGCCAGGCCTGGTGATGATGGCG
E1A-RpsL Rv	CATCAACTCATTCAGCAAACAAAGGCGTTAACCACACACGCAATCACAGGTTTA CACCTTATCAGAAGAACTCGTCAAG
E1PH20 F1	GAGGACTTGCTTAACGAGCCTGGGCAACCTTTGGACTTGAGCTGTAAACGCCC CAGGCCAGGAAGCGGAGCTACTAAC

E1PH20 F2	CTTGAATTTTAGCACTCCCATAGGTCCAGGGTTCTCCTCCACGTCTCCAGCCTGC TTCAGCAGGCTGAAGTTAGTAGCTCCGCTTCC
E1PH20 Rv	CATCAACTCATTCAGCAAACAAAGGCGTTAACCACACACGCAATCACAGGTTTA CACCTTAAGATAGTGTGGAGGGTGA
IIIaBHyalwt af Fwd	ATCGTTTGTGTTATGTTTCAACGTGTTTATTTTTCAATTGGTACTAAGCGGTGAT GTTTCTGATCAGCCACCATGTCTCGGCCTCTCGTGA
BHyalwt af Rv	GCTATACTACTGAATGAAAAATGACTTGAAATTTTCTGCAATTGAAAAATAAAG TTTATTACACTTGGTCCACGCTCA
E4-IIIaBHyal wt Fwd	CTTCCTCAAATCGTCACTTCCGTTTTCCCACGTTACGTCACGTACTAAGCGGTGA TGTTTCTGATCAGCCACCATGTCTCGGCCTCTCGTGA
E4-BHyalwt Rv	GTAGGTTTTAGGGCGGAGTAACTTGTATGTGTTGGGAATTGTAGTTTTCTTAAA ATG*TTTA*TTACACTTGGTCCACGCTCA
CMVpRpsL Fwd	CTATATAAGCAGAGCTGGTTTAGTGAACCGTCAGCAGTGCCACCGGCCTGGTG ATGATG
AfterFiRpsL Rv	TTGAAATTTTCTGCAATTGAAAAATAAACACGTTGAAACATTTATCAGAAGAAC TCGTCA
CMVTMG Fwd	GGCGTGTACGGTGGGAGGTCTATATAAGCAGAGCTGGTTTAGTGAACCGTAC ATTTGCTTCTGACACA
CMVTMG Rv	AATGACTTGAAATTTTCTGCAATTGAAAAATAAACACGTTGAAACAGCAATGAA AATAAATGTTT
Fi-RpsLneo Fwd	GTCAGTTTCCTCCTGTTCCTGTCCATCCGCACCCACTATCTTCATGTTGTTGCAG GGCCTGGTGATGATGGCGG
Fi-RpsLneo Rv	GGGCTATGAACTAATGACCCCGTAATTGATTACTATAACACAAACGATTCTTTA TCAGAAGAACTCGTCAAGAAGGCG
Fi-RGD Fwd	GTCAGTTTCCTCCTGTTCCTGTCCATCCGCACCCACTATCTTCATGTTGTTGCAG

	ATGAAGCGCGCAAGACCGTCT
Fi-RGD Rv	GGGCTATGAACTAATGACCCCGTAATTGATTACTATAACACAAACGATTCTTTA TTCTTGGGCAATGTATGAAAAAGTGTAAG
CMV-RpsLNeo2 Fwd	GGGCGGTAGGCGTGTACGGTGGGAGGTCTATATAAGCAGAGCTGGTTTAGTG AACCGTGGCCTGGTGATGATGGCGG
CMV-RpsLNeo2 Rv	ACTACTGAATGAAAAATGACTTGAAATTTTCTGCAATTGAAAAATAAACACGTT GAAACATCAGAAGAACTCGTCAAGAAGGCG

Supplementary Table 2. Titers of purified viruses in this thesis. Vp: viral particles, TU: transfecting units.

Purified viruses	**Physical Titer (vp/mL)**	**Function Titer (TU/mL)**	**Vp/TU Ratio**
ICO15-del6.7/19K	8,28E+11	9,51E+10	8,7
ICO15-del6.7/19K-B16TMG	2,76E+12	3,43E+11	8,0
ICO15-del6.7/19K-B16TMG2	3,75E+12	5,63E+11	6,7
ICO15-del6.7/19K-B16TMG2.Linker	4,52E+12	7,83E+11	5,8
ICO15-del6.7/19K-CMT64.6TMG	3,48E+12	4,62E+10	75,3
ICO15K	3,93E+12	4,92E+11	8,0
VCN01 engineering run	1,18067E+12	7,83E+10	15,1
ICO15K-40SAPH20/2 - UPV1444	4,150E+12	3,75E+11	11,07
ICO15KE1aP2APH20/2 - UPV1445	4,600E+12	4,18E+11	11
ICO15K-E4.IIIaBhyal wt	7,40667E+11	1,23E+11	6,0

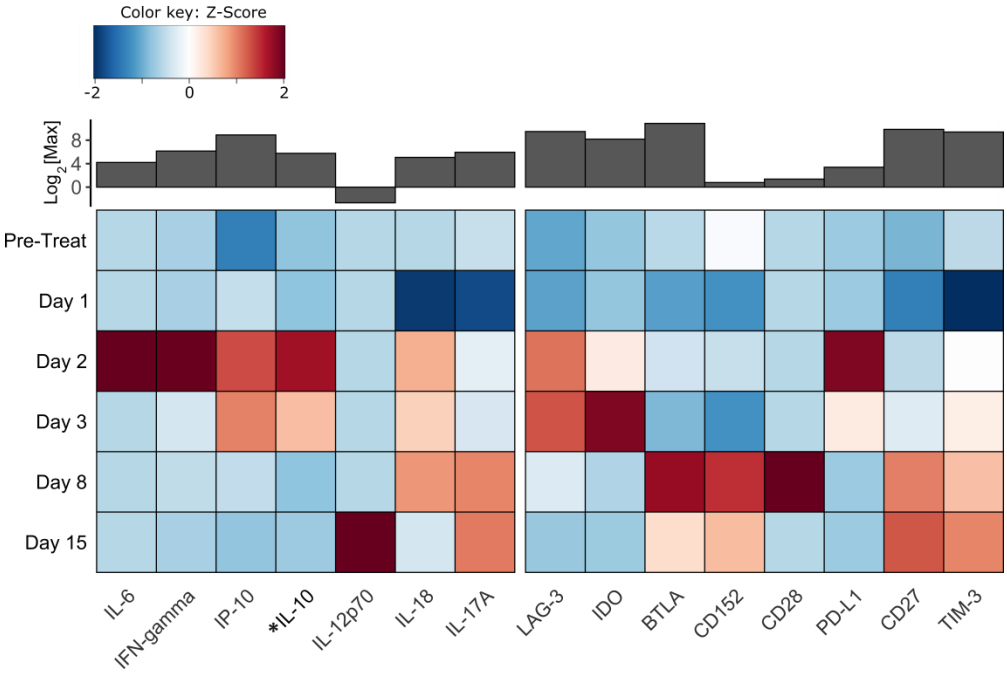

Supplementary Figure 1. Soluble immune markers variation after P-VCNA-001:II treatment. Serums from patients treated with VCN-01 concomitant with chemotherapeutic regime (P-VCNA-001:II, n=7) were analyzed. The log2 of the maximum concentration detected per analyte is represented on the top of the graph by grey bars. The Z-score within each analyte is represented in the heatmap. Analytes that significantly variate compared to the pre-treatment values are highlighted with and asterisk in the column name (*p<0.05 by paired-Wilcoxon test).

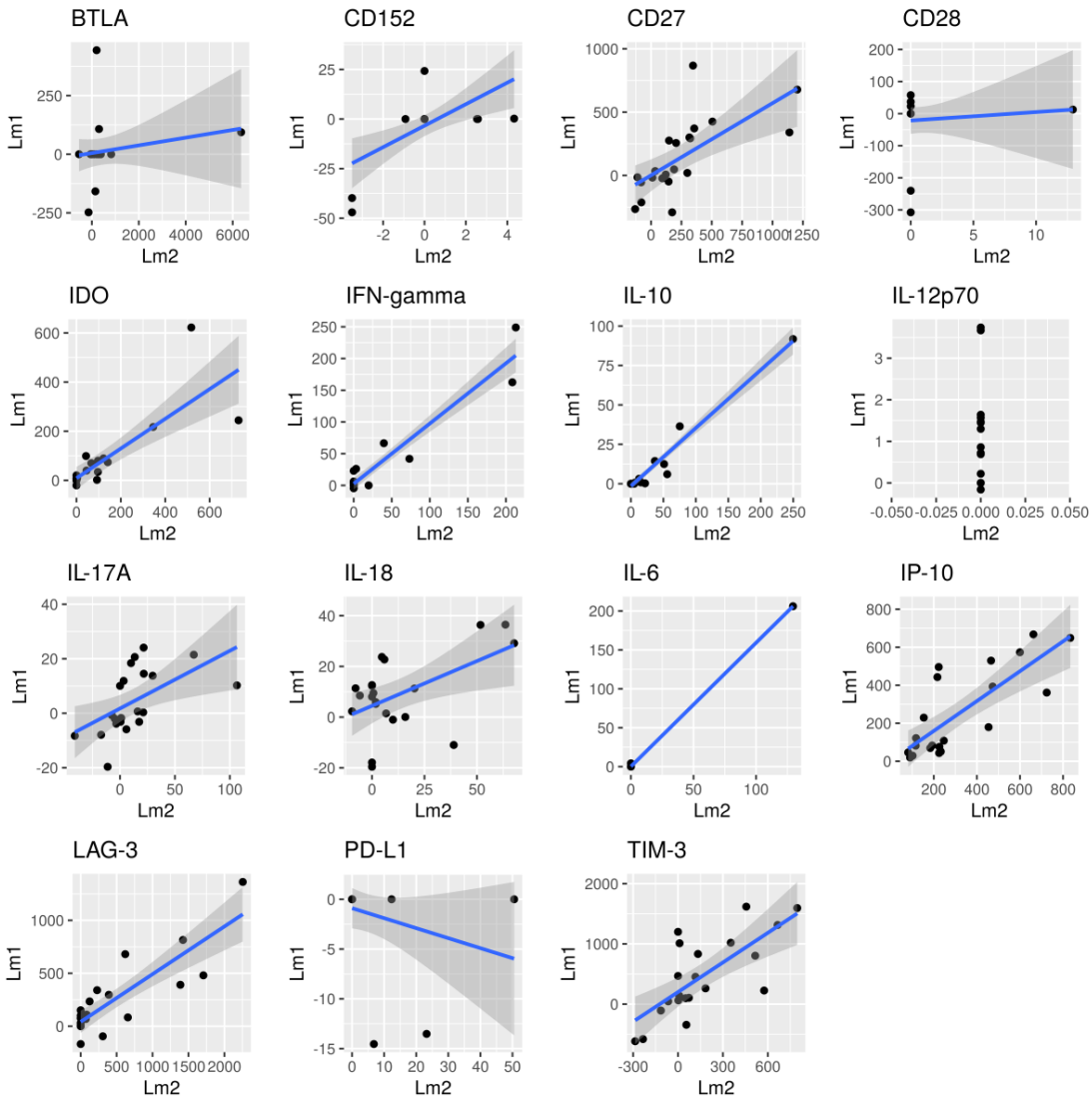

Supplementary Figure 2. Inter-experiment variability of Luminex assay. The difference between all the values from P-VCNA-001:II patients and their respective pre-treatment values were compared between the first 34-Multiplex Luminex and the second 18-Multiplex Luminex in order to assess the inter-experiment variability of this technique.

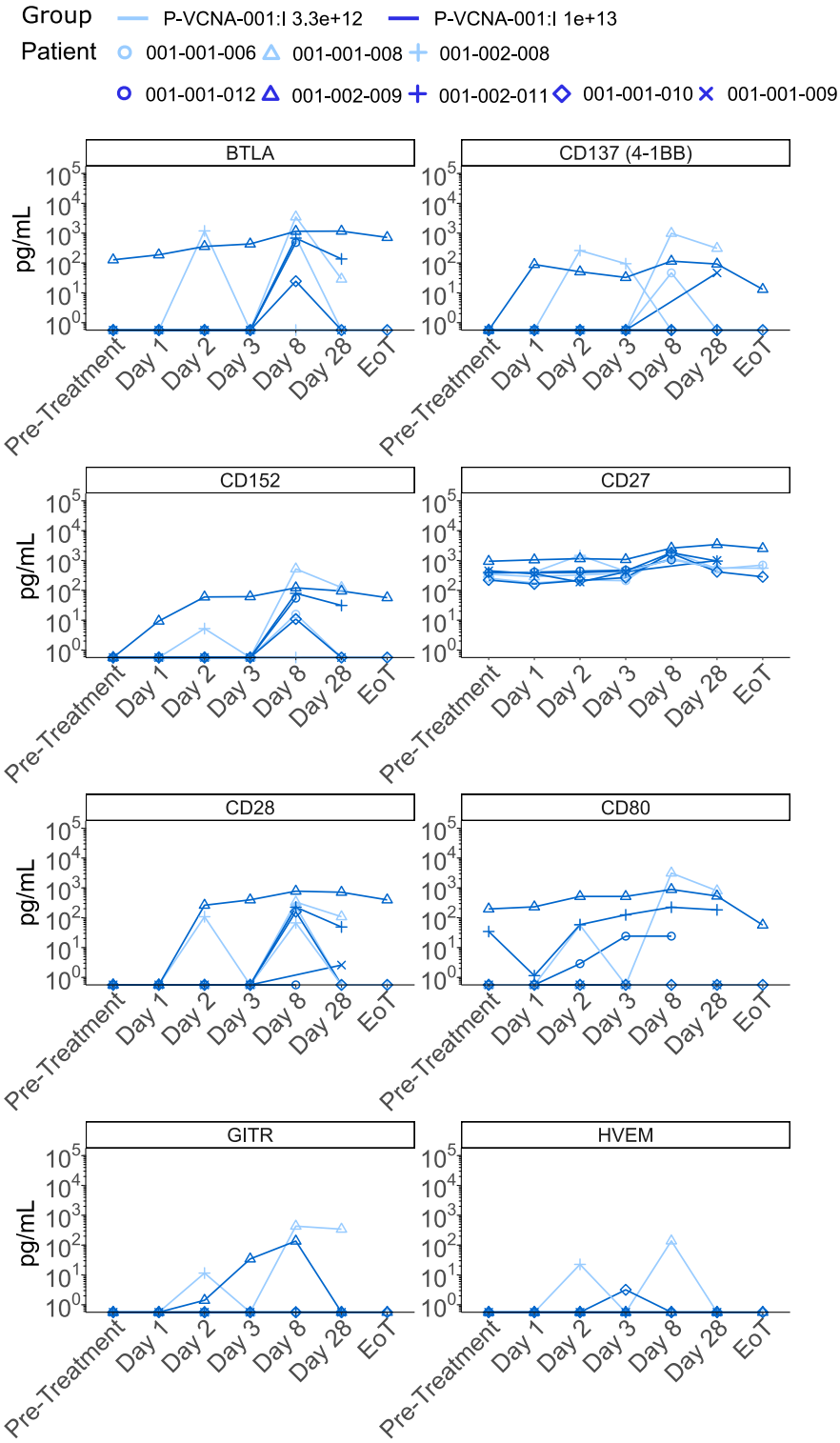
Group
P-VCNA-001:I 3.3e+12
P-VCNA-001:I 1e+13
Patient
001-001-006
001-001-008
001-002-008
001-001-012
001-002-009
001-002-011
001-001-010
001-001-009
BTLA
CD137 (4-1BB)
CD152
CD27
CD28
CD80
GITR
HVEM
pg/mL
Pre-Treatment
Day 1
Day 2
Day 3
Day 8
Day 28
EoT

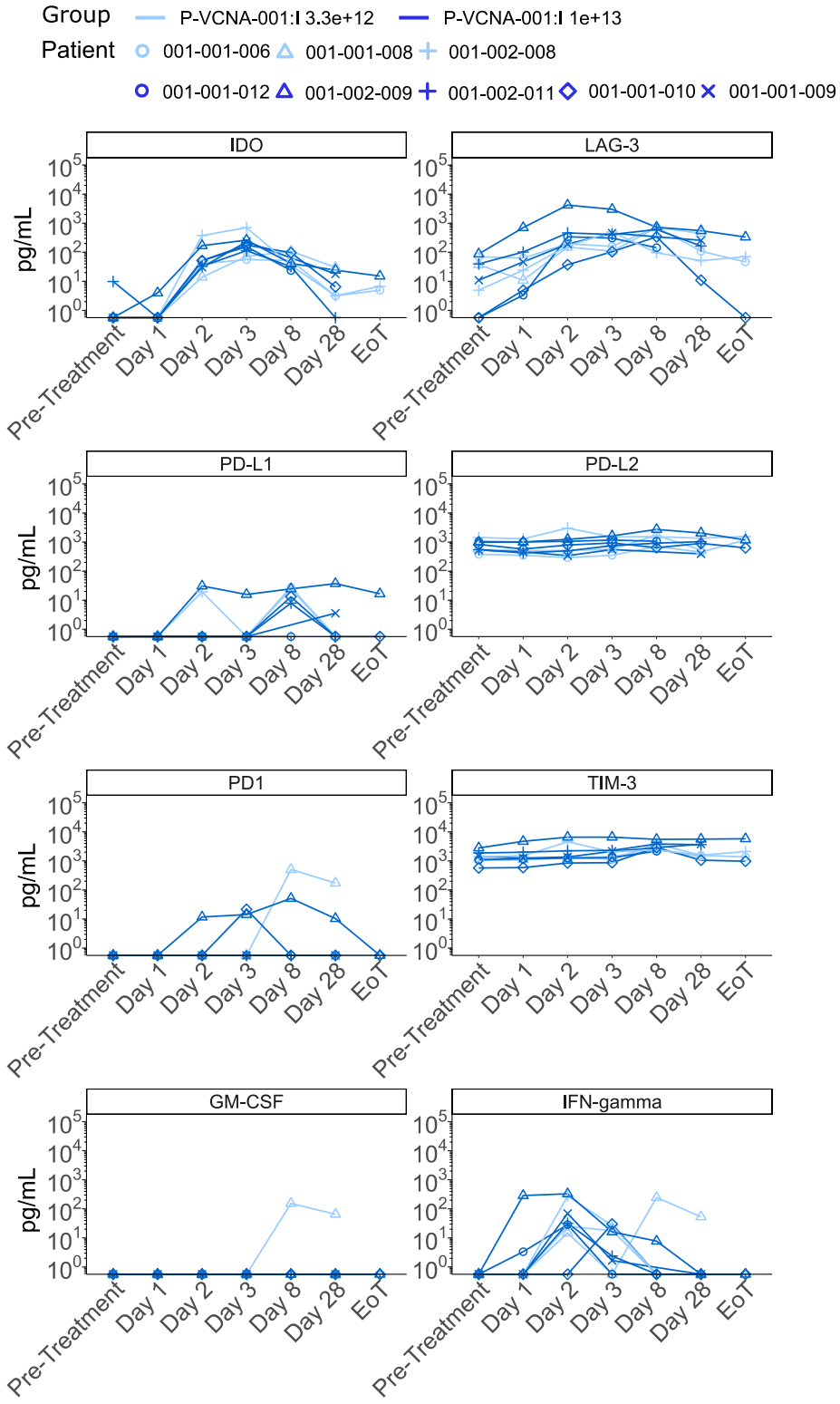
Group
P-VCNA-001:I 3.3e+12
P-VCNA-001:I 1e+13
Patient
001-001-006
001-001-008
001-002-008
001-001-012
001-002-009
001-002-011
001-001-010
001-001-009
IDO
LAG-3
PD-L1
PD-L2
PD1
TIM-3
GM-CSF
IFN-gamma
pg/mL
Pre-Treatment
Day 1
Day 2
Day 3
Day 8
Day 28
EoT

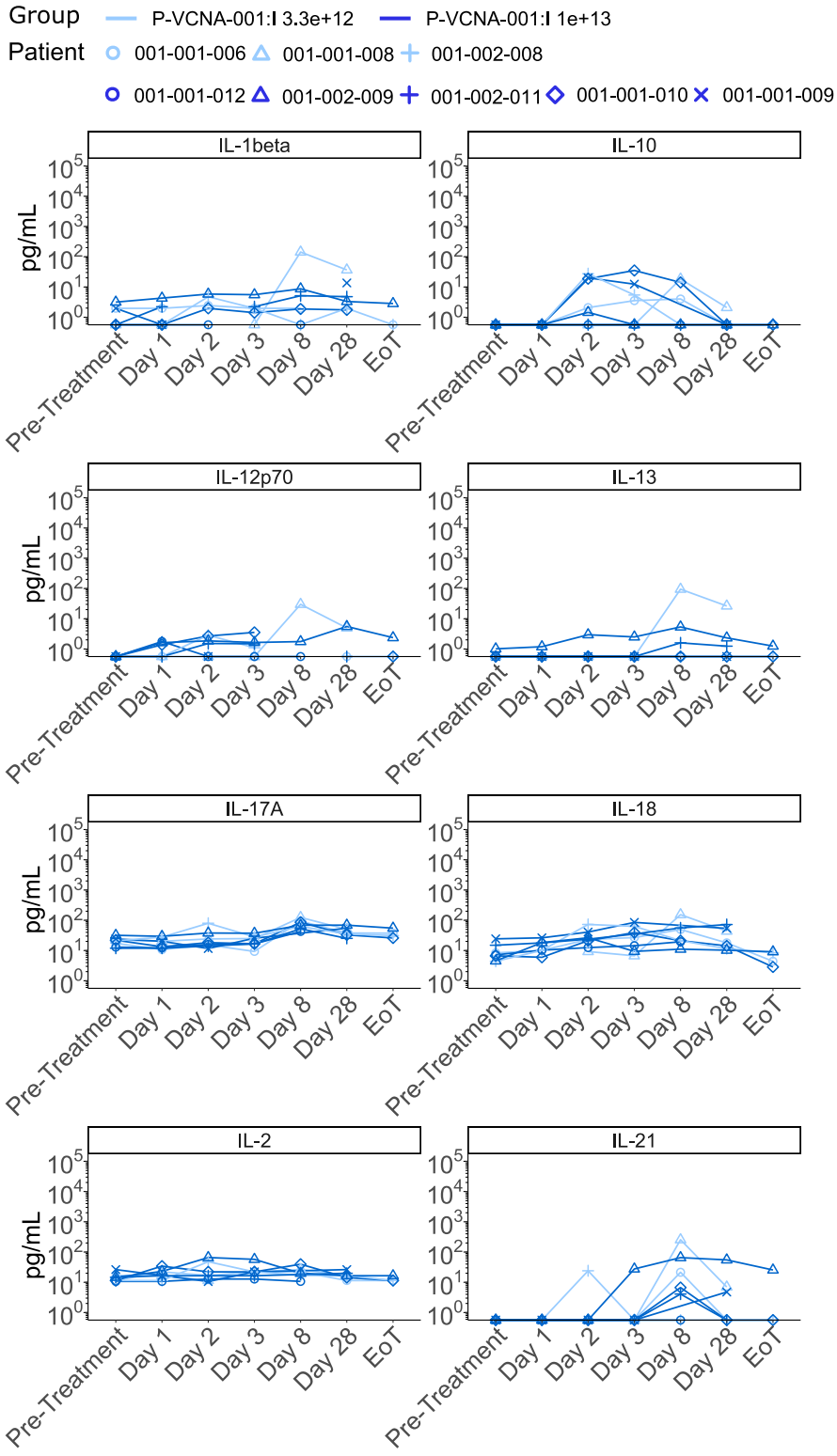
Group
P-VCNA-001:I 3.3e+12
P-VCNA-001:I 1e+13
Patient
001-001-006
001-001-008
001-002-008
001-001-012
001-002-009
001-002-011
001-001-010
001-001-009
IL-1beta
IL-10
IL-12p70
IL-13
IL-17A
IL-18
IL-2
IL-21
pg/mL
Pre-Treatment
Day 1
Day 2
Day 3
Day 8
Day 28
EoT

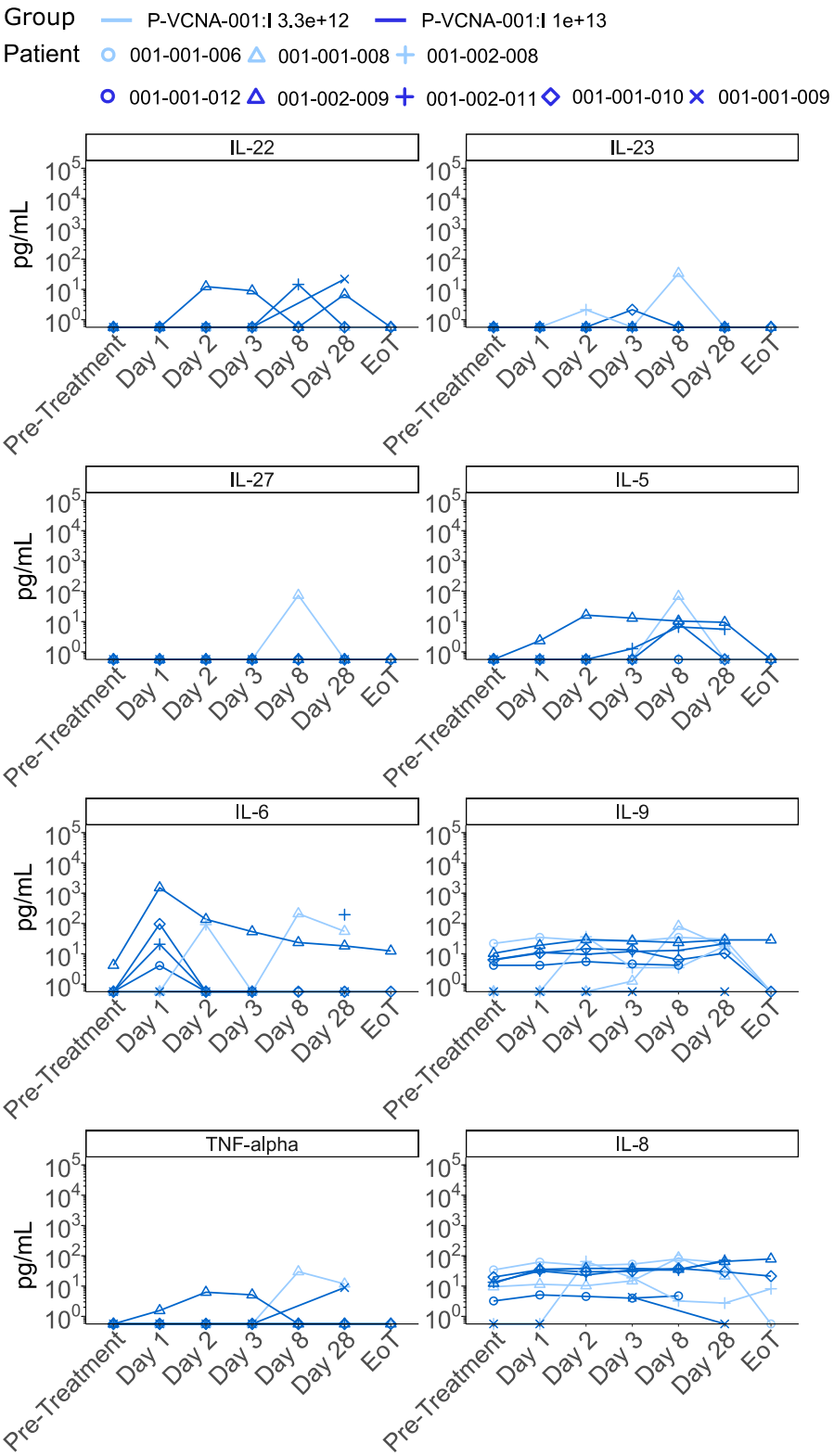
Group
P-VCNA-001:I 3.3e+12
P-VCNA-001:I 1e+13
Patient
001-001-006
001-001-008
001-002-008
001-001-012
001-002-009
001-002-011
001-001-010
001-001-009
IL-22
IL-23
IL-27
IL-5
IL-6
IL-9
TNF-alpha
IL-8
pg/mL
Pre-Treatment
Day 1
Day 2
Day 3
Day 8
Day 28
EoT

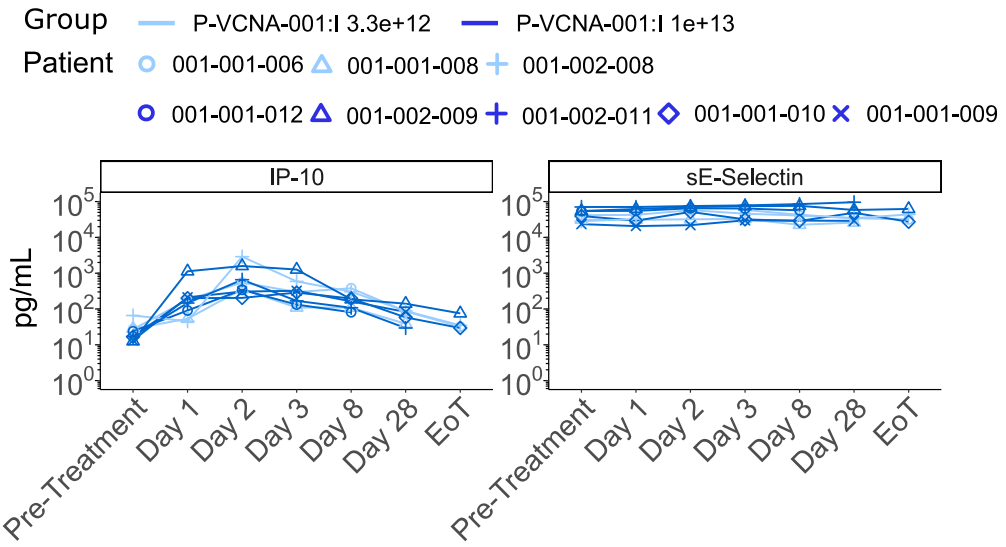

Supplementary Figure 3. P-VCNA-001:I Kinetics. Sera from patients treated with VCN-01 in monotherapy were analyzed for the levels of represented immune markers over the time: Pre-Treatment, Day 1 (6h), Day 2 (24h), Day 3 (48h), Day 8, Day 28 and End of Treatment (EoT, this timepoint could not be the same for the different patients).

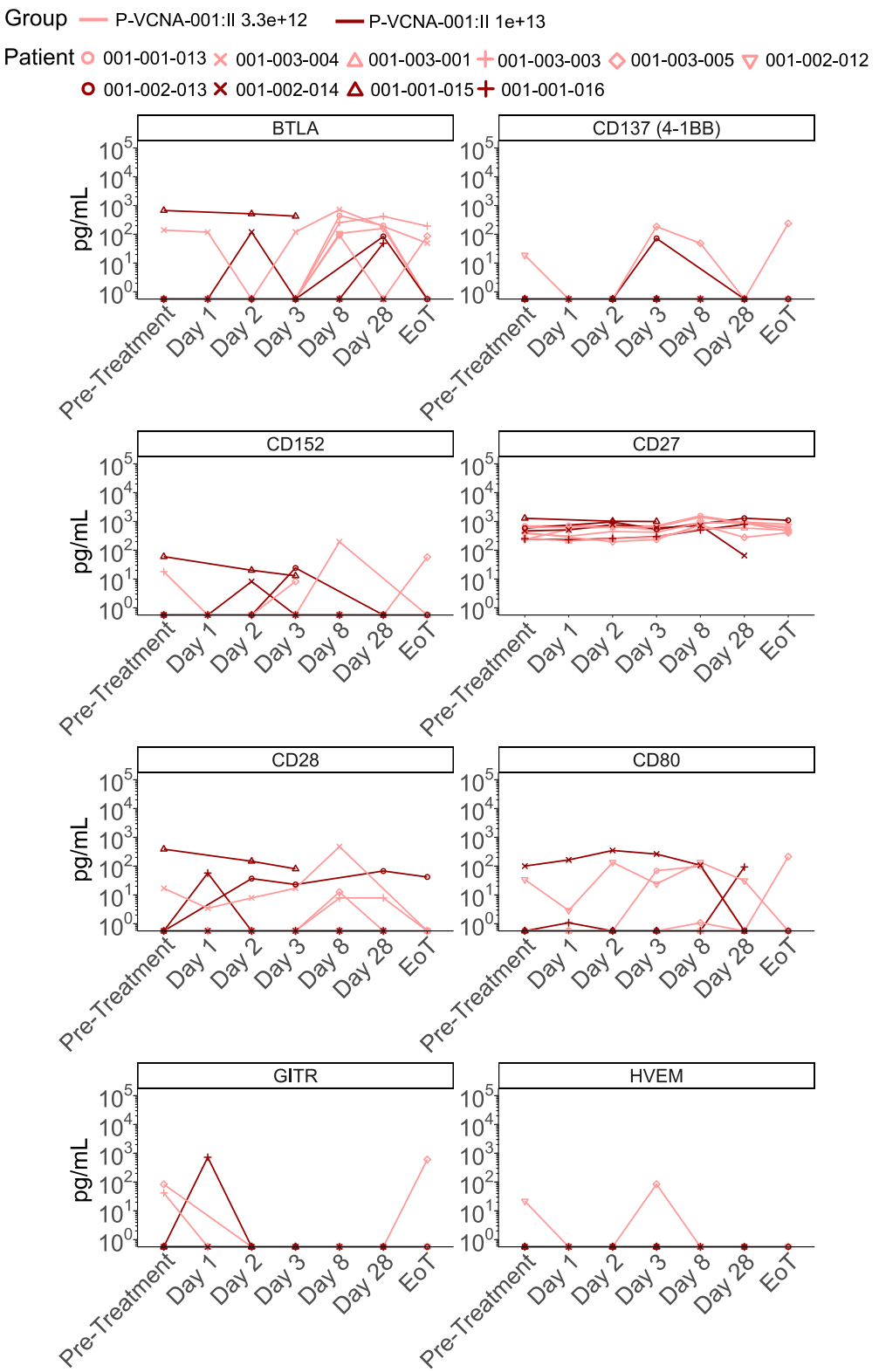
Group
P-VCNA-001:II 3.3e+12
P-VCNA-001:II 1e+13
Patient
001-001-013
001-003-004
001-003-001
001-003-003
001-003-005
001-002-012
001-002-013
001-002-014
001-001-015
001-001-016
BTLA
CD137 (4-1BB)
CD152
CD27
CD28
CD80
GITR
HVEM
pg/mL
Pre-Treatment
Day 1
Day 2
Day 3
Day 8
Day 28
EoT

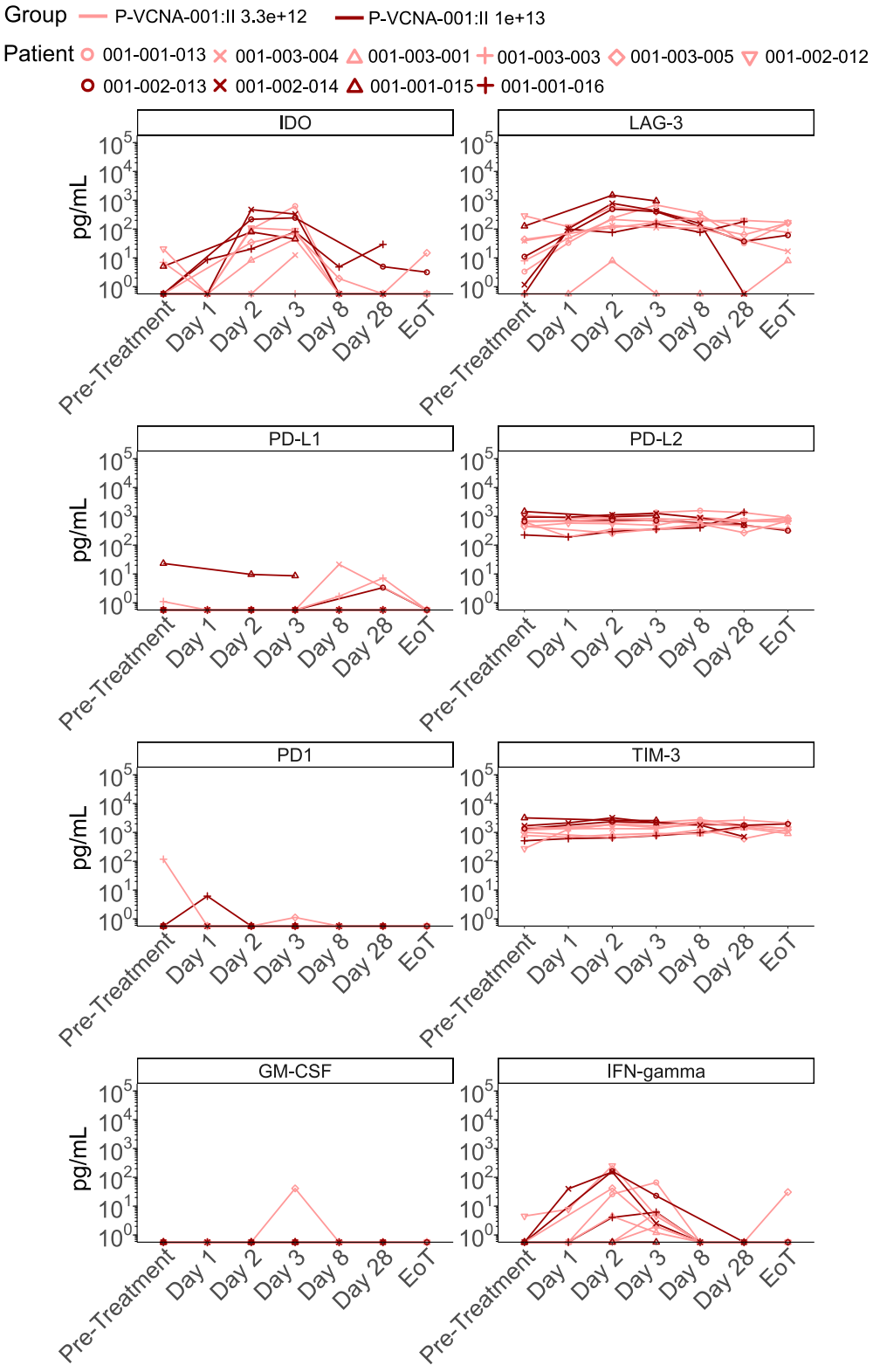
Group
P-VCNA-001:II 3.3e+12
P-VCNA-001:II 1e+13
Patient
001-001-013
001-003-004
001-003-001
001-003-003
001-003-005
001-002-012
001-002-013
001-002-014
001-001-015
001-001-016
IDO
LAG-3
PD-L1
PD-L2
PD1
TIM-3
GM-CSF
IFN-gamma
pg/mL
Pre-Treatment
Day 1
Day 2
Day 3
Day 8
Day 28
EoT

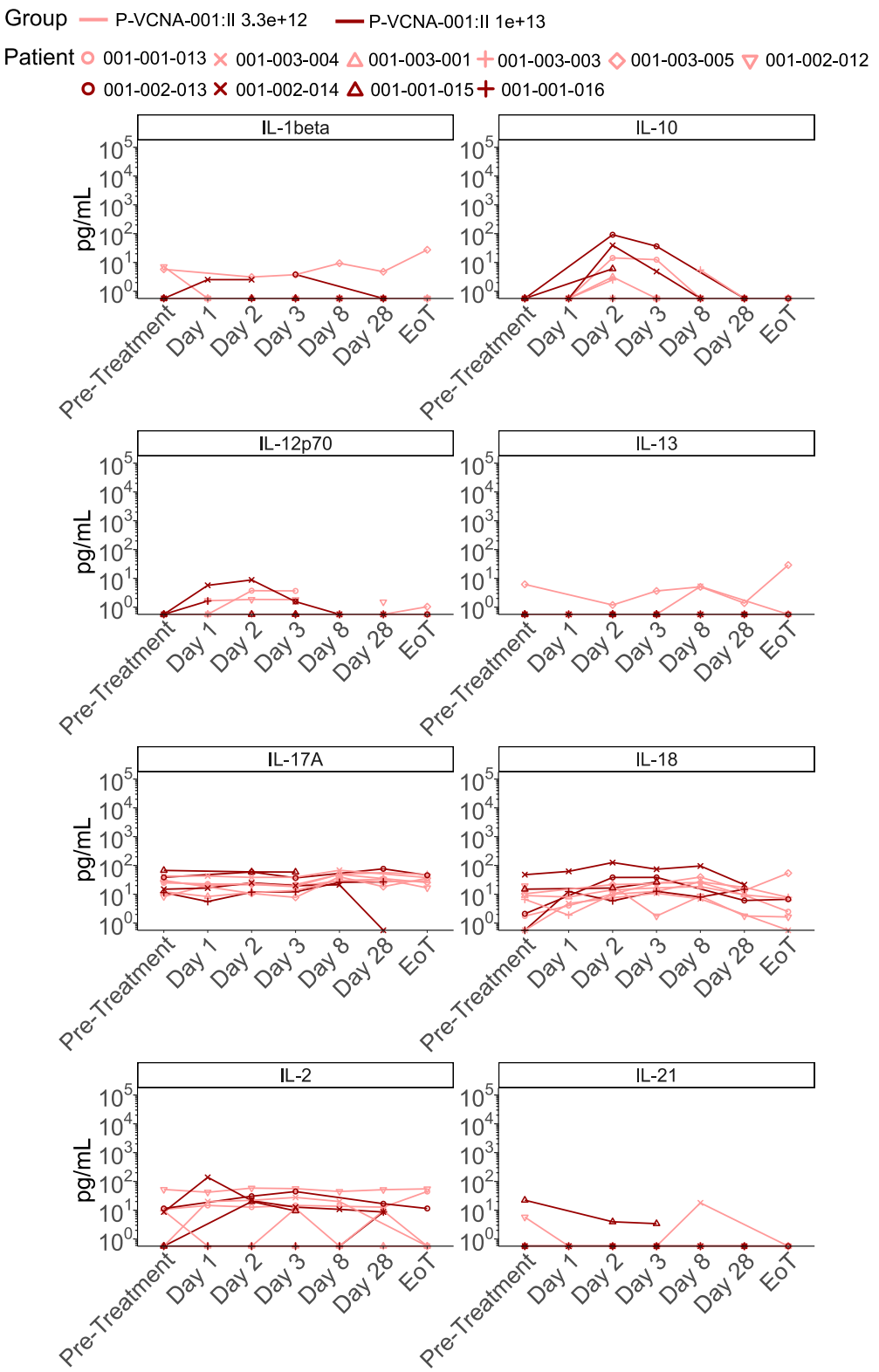
Group
P-VCNA-001:Il 3.3e+12
P-VCNA-001:Il 1e+13
Patient
001-001-013
001-003-004
001-003-001
001-003-003
001-003-005
001-002-012
001-002-013
001-002-014
001-001-015
001-001-016
IL-1beta
IL-10
IL-12p70
IL-13
IL-17A
IL-18
IL-2
IL-21
pg/mL
Pre-Treatment
Day 1
Day 2
Day 3
Day 8
Day 28
EoT

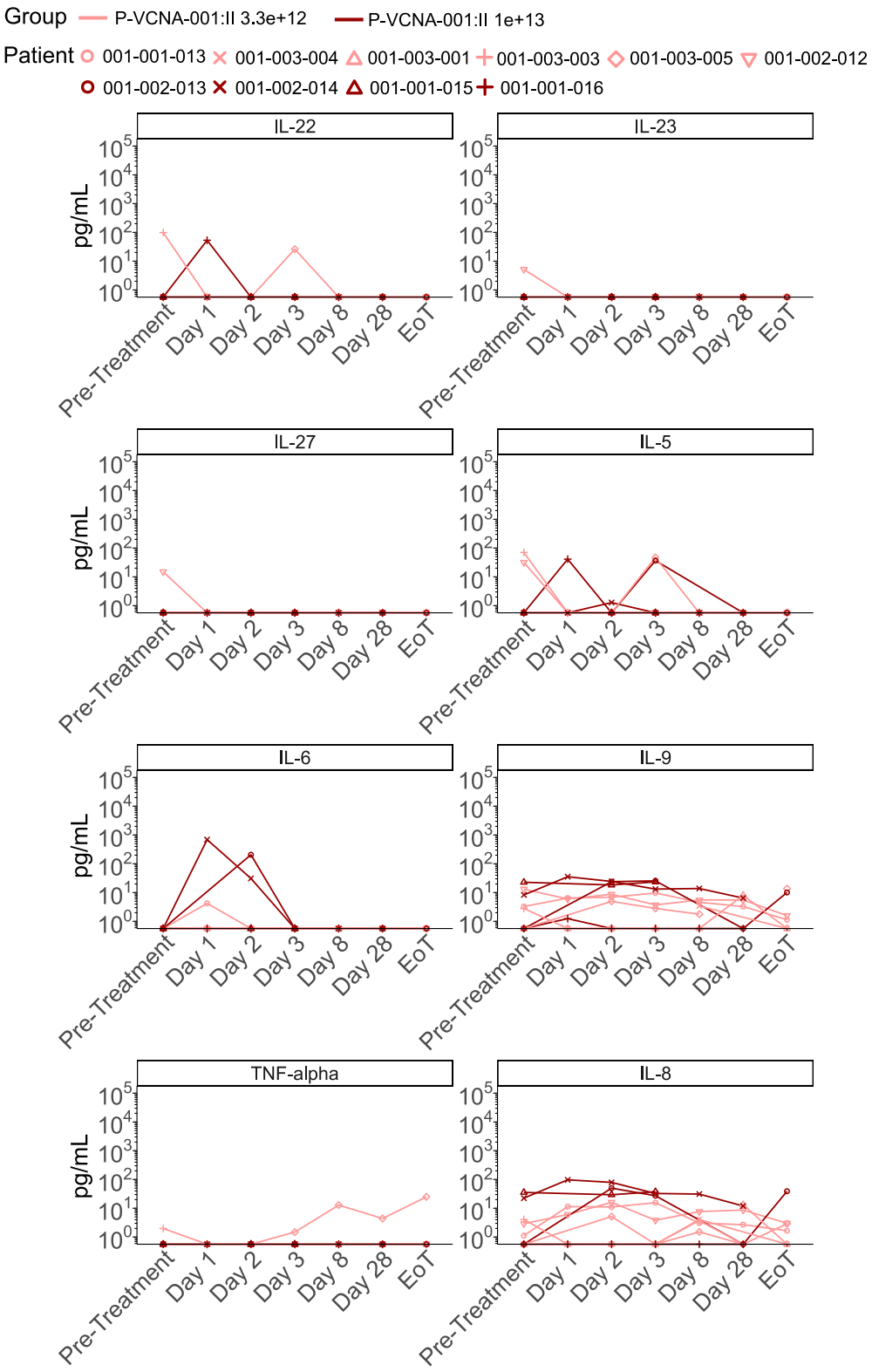
Group
P-VCNA-001:II 3.3e+12
P-VCNA-001:II 1e+13
Patient
001-001-013
001-003-004
001-003-001
001-003-003
001-003-005
001-002-012
001-002-013
001-002-014
001-001-015
001-001-016
IL-22
IL-23
IL-27
IL-5
IL-6
IL-9
TNF-alpha
IL-8
pg/mL
Pre-Treatment
Day 1
Day 2
Day 3
Day 8
Day 28
EoT

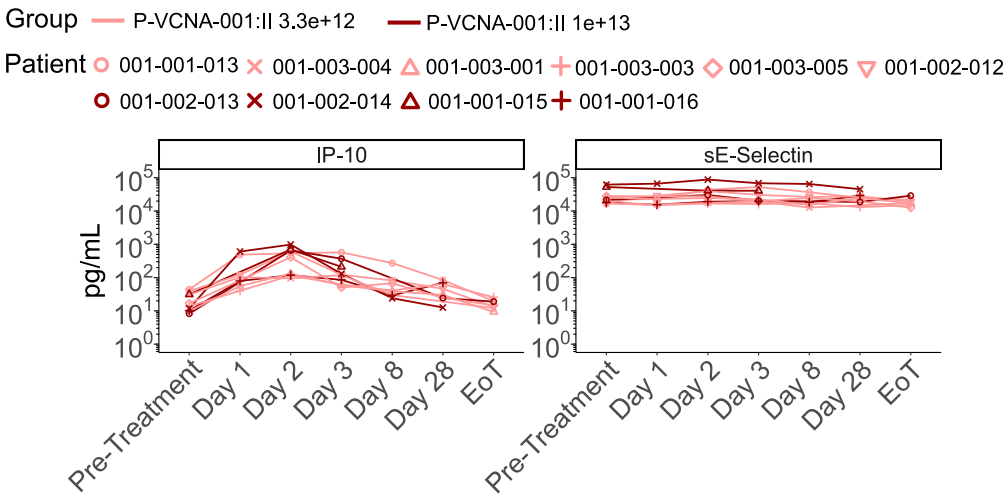

Supplementary Figure 4. P-VCNA-001:II Kinetics. Sera from patients treated with VCN-01 concomitant with Gemcitabine/Abraxane were analyzed for the levels of represented immune markers over the time: Pre-Treatment, Day 1 (6h), Day 2 (24h), Day 3 (48h), Day 8, Day 28 and End of Treatment (EoT, this timepoint could not be the same for the different patients).

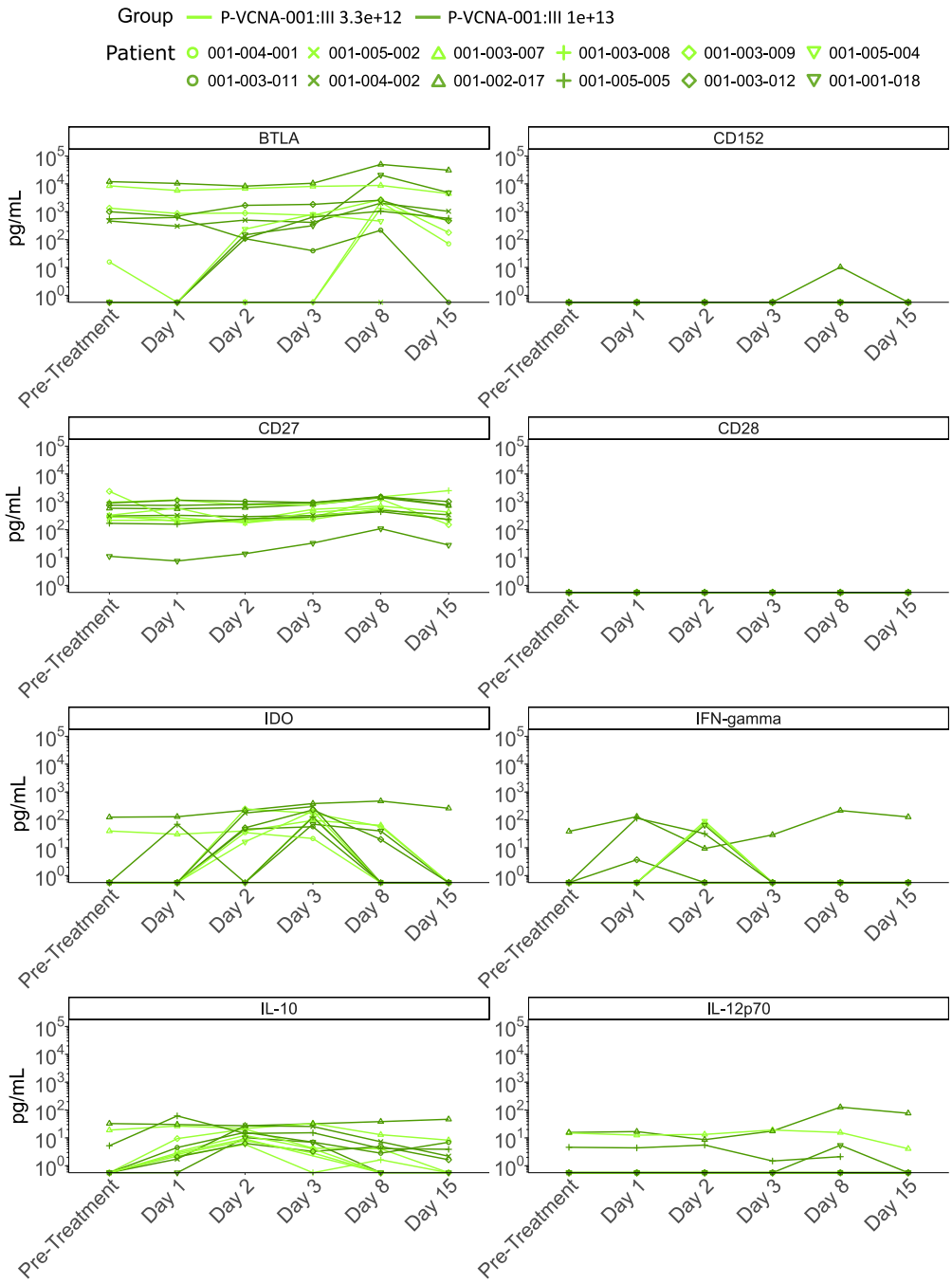
Group
P-VCNA-001:III 3.3e+12
P-VCNA-001:III 1e+13
Patient
001-004-001
001-005-002
001-003-007
001-003-008
001-003-009
001-005-004
001-003-011
001-004-002
001-002-017
001-005-005
001-003-012
001-001-018
BTLA
CD152
CD27
CD28
IDO
IFN-gamma
IL-10
IL-12p70
pg/mL
Pre-Treatment
Day 1
Day 2
Day 3
Day 8
Day 15

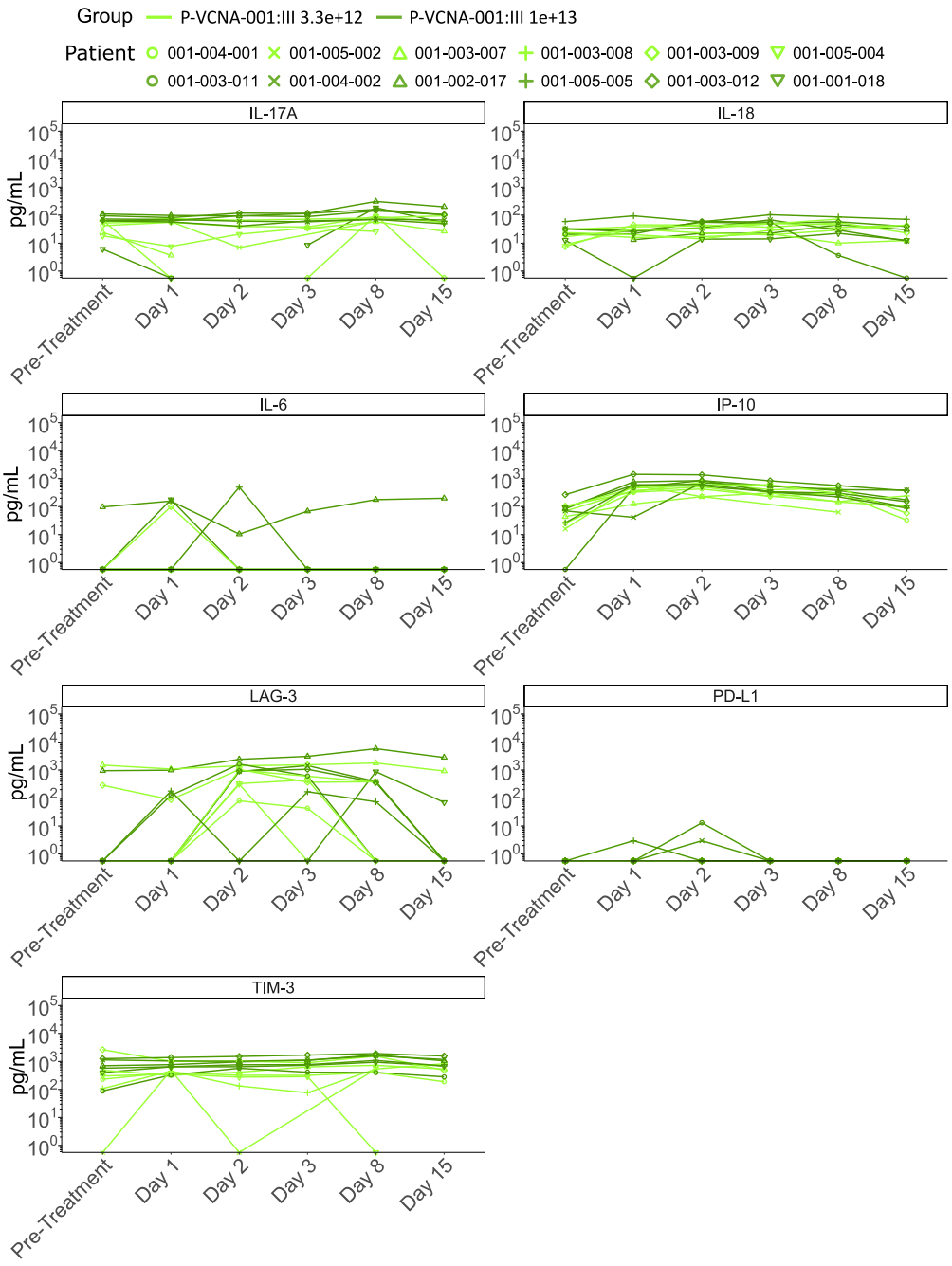

Supplementary Figure 5. P-VCNA-001:III Kinetics. Sera from patients treated with VCN-01 and decalated regime of chemotherapy were analyzed for the levels of represented immune markers over the time: Pre-Treatment, Day 1 (6h), Day 2 (24h), Day 3 (48h), Day 8, Day 28 and End of Treatment (EoT, this timepoint could not be the same for the different patients).

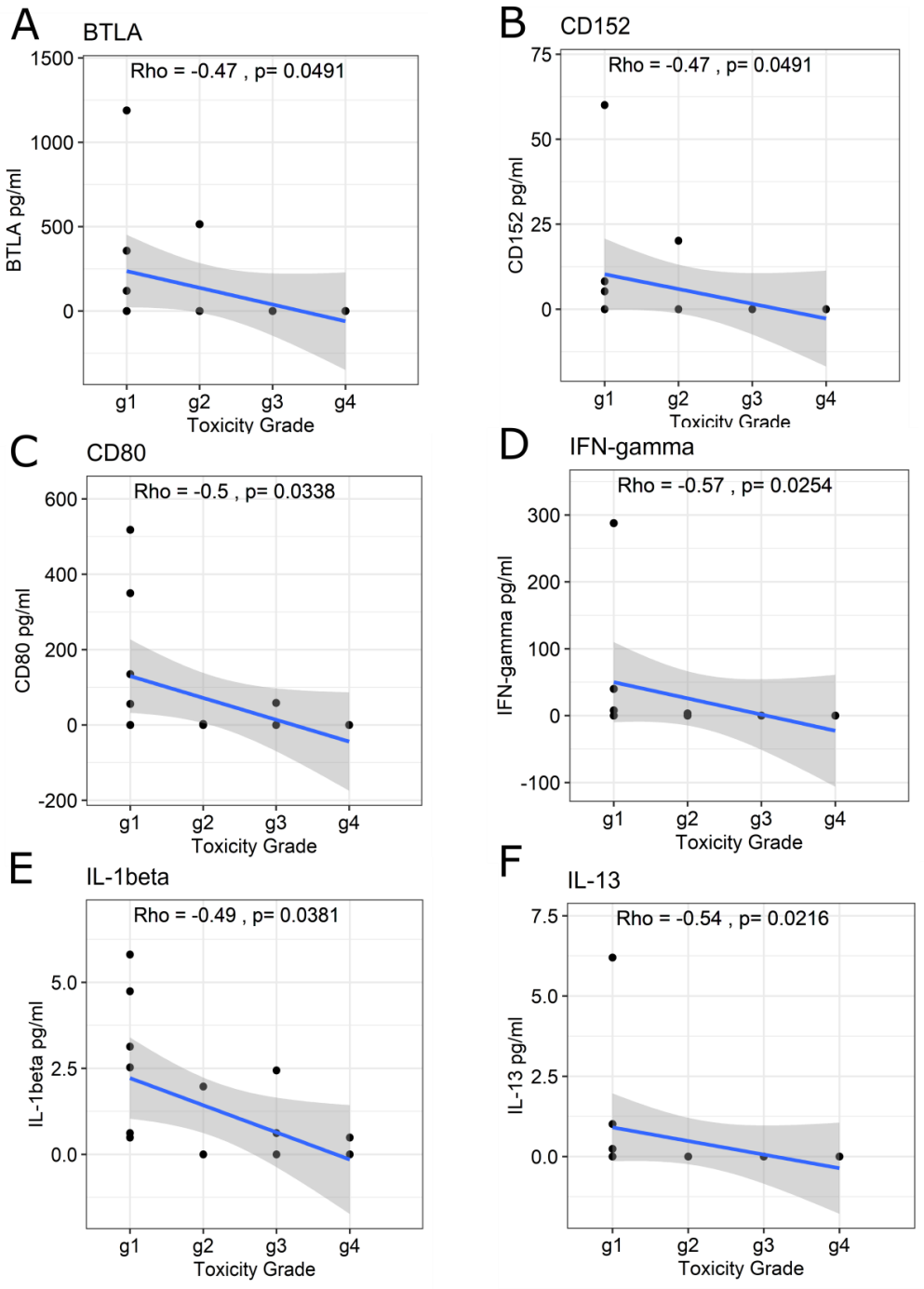

Supplementary Figure 6. Toxicity correlations between the maximum toxicity grade per patient within the first 15 days of treatment and (A) BTLA serum levels ón day 2, **(B)** CD152 levels at day 2, **(C)** CD80 on day 2, (D) IFNγ on day 1, (E) IL-13 on day 3 and (F) IL-13 on Pre-treatment. Spearman correlation was performed and rho coefficient and p-value are reported in the graph.

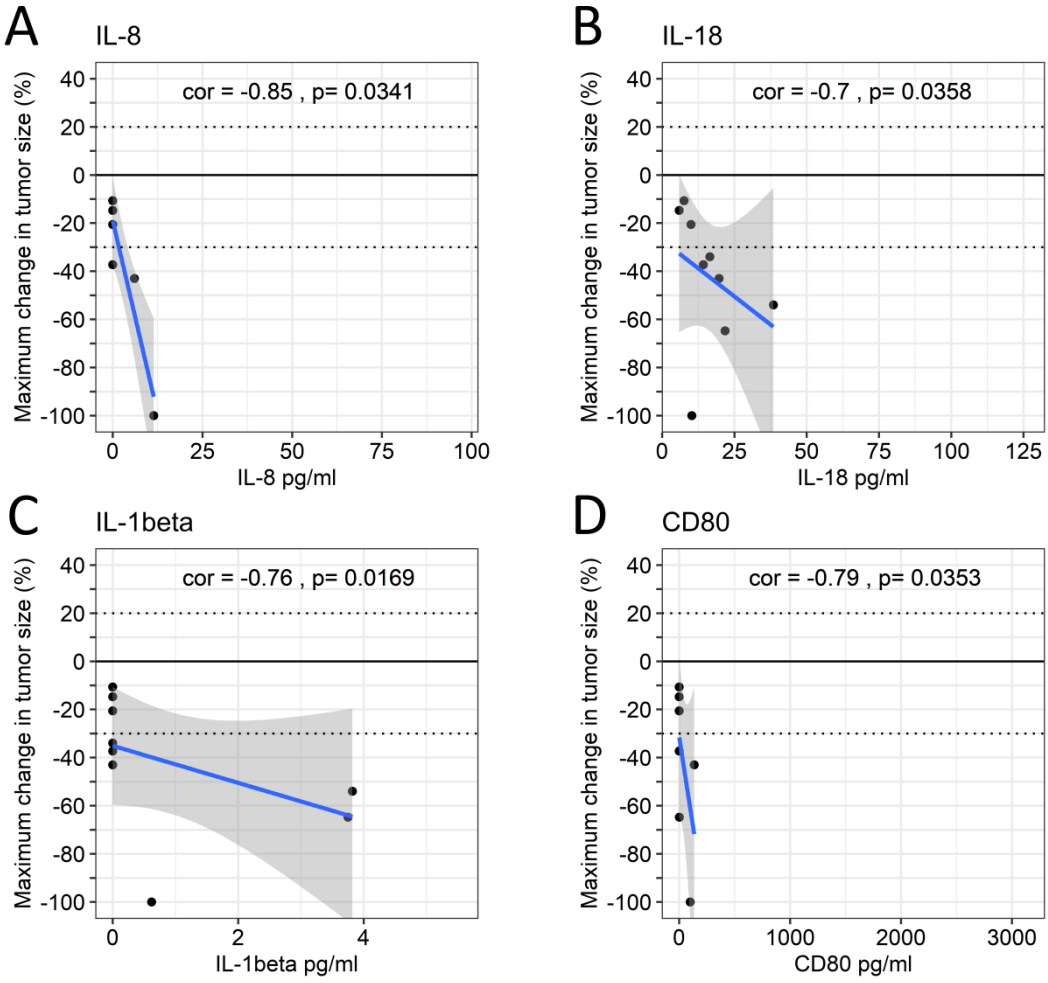

Supplementary Figure 7. Efficacy correlation in P-VCNA-001:II patients. (A) the levels of IL-8 at day 1, (B) the serum concentration of IL-18 at day 2, **(C)** IL-1β levels at day 3 and **(D)** CD80 at day 8 were correlated with maximum change in tumour size. Spearman correlations were performed, correlation factor (cor) and p-value (p) are presented in the graph.

Supplementary Table 3. Detailed sequence of Ova257 and Ova 323 and corresponding NetMHCpan prediction.

Identity	Peptide	Core	H2	Affinity	Rank(%)
Ova257	SIINFEKL	SIINFEKL	Kb	19.37	0.06
Ova323	ISQAVHAAHAEINEAGR	ISQAVHAA	Kb	15506.3	20

Supplementary Table 4. *In silico* prediction of B16-F10 neoantigens and their counterparts with NetMHCpan. Peptides highlighted in red were included into the tandem minigene. Peptides highlighted in bold were previously published in Castle et al.[375].

Identity	Mutated peptide	H2	Affinity (nM)	Rank (%)	Exp	Wild-type peptide	H2	Affinity (nM)	Rank (%)
LINES	RMLQNSDTL	Db	6.29	0.01	2.93	RMLQNSDKL	Db	21.17	0.01
NR1H2	SGFRYNVL	Kb	6.33	0.01	6.07	SGFHYNVL	Kb	16.66	0.05
NDUS6	AALTFRRL	Kb	6.64	0.02	6.67	AVLTFRRL	Kb	7.33	0.02
PNPH	VVMEYENL	Kb	6.69	0.02	3.34	VVMDYENL	Kb	11.71	0.04
AT11A	LGFTYLRL	Kb	7.63	0.02	6.16	LGFTYLRL	Kb	7.63	0.02
F2Z4A3	IAMQNTTQL	Db	8.2	0.01	4.12	IAIQNTTQL	Db	6.37	0.01
Q6NZL1	SSVLFKGL	Kb	8.31	0.03	4.09	SSVLFKEL	Kb	15	0.05
HSF2	YGFRNVVHI	Db	14.13	0.01	4.01	YGFRKVVHI	Db	3278.68	0.9
SYTC	TVYRCGHL	Kb	14.52	0.05	5.50	TVYRCGPL	Kb	10.84	0.03
AT11A	QSLGFTYL	Kb	14.63	0.05	6.16	QRLGFTYL	Kb	2057.91	3.5
RFWD3	VIYSHLQV	Kb	14.78	0.05	4.33	VIYSHLQG	Kb	1903.93	3
ARVC	VVHLYLSL	Kb	17.89	0.05	2.90	VVRLYLSL	Kb	18.26	0.06
HJURP	SSSRFQTL	Kb	19.62	0.06	5.56	SSSRFQTL	Kb	19.62	0.06
CATD	VSFANAVVL	Db	20.12	0.01	10.11	VGFANAVVL	Db	55.58	0.04
SRBP2	SALEYLKL	Kb	22.2	0.07	5.32	SALEYLKL	Kb	22.2	0.07
SPN90	QNLCYSAL	Kb	22.67	0.07	2.70	QKLCYSAL	Kb	840.83	1.6
ARVC	VVHLYLSLL	Kb	22.93	0.07	2.90	VVRLYLSLL	Kb	23.51	0.07
AL1B1	TSYSTAAV	Kb	27.46	0.08	2.11	TSYSTAAA	Kb	474.16	1
TULP2	ASVTNFQIV	Db	31.87	0.03	2.53	ASVKNFQIV	Db	77.68	0.05
ORC2	VVPSFSAEI	Kb	32.67	0.1	5.02	FVPSFSAEI	Kb	180.04	0.5
DCA15	FSFYIYHL	Kb	32.75	0.1	4.01	FSFYIYHL	Kb	32.75	0.1
NDUS6	AALTFRRLL	Kb	36.53	0.12	6.67	AVLTFRRLL	Kb	48.51	0.15
DHX57	LGYHVASL	Kb	38.74	0.12	3.22	LGYHLASL	Kb	22.32	0.07
TECT3	VSVRQTNL	Kb	38.93	0.12	3.14	VSFRQTNL	Kb	5.5	0.01
NSUN2	KILRMSPL	Kb	39.75	0.12	5.45	KILRKSPL	Kb	264.78	0.7
HSF2	NMYGFRNV	Kb	41.06	0.12	4.01	NMYGFRKV	Kb	318.35	0.8
PCMD1	VSFAPLVQL	Kb	46.6	0.15	3.77	VSFAPLVQP	Kb	5210.06	7
WSB2	TTYQVLAL	Kb	47.3	0.15	7.01	TTYQVLAL	Kb	47.3	0.15
LRC28	FTFVYPTI	Kb	47.64	0.15	3.42	FTFVYPKI	Kb	61.64	0.17
AL1B1	TSYSTAAVL	Kb	47.95	0.15	2.11	TSYSTAAAL	Kb	14.53	0.05
B3GT6	VHYLRLSL	Kb	50.59	0.15	2.16	VHYLRLSR	Kb	3730.94	5.5
TT39C	VSFLNAMI	Kb	**51.15**	**0.15**	2.82	VSFLNAMM	Kb	24.89	0.08
ANGE2	SVMSYNIL	Kb	51.23	0.15	3.80	SVMSYNIL	Kb	51.23	0.15
HERC6	SSPPYLIL	Kb	52.05	0.15	4.16	SSPPYLIL	Kb	52.05	0.15
TNPO3	**LAYLMKGL**	**Kb**	**53.52**	**0.17**	**6.13**	**LGYLMKGL**	**Kb**	**96.53**	**0.3**
PNPH	SLITNKVVM	Db	54.77	0.04	3.34	SLITNKVVM	Db	54.77	0.04
PDE1C	STFTRQMGM	Kb	63.89	0.2	2.48	STFTRQMGM	Kb	63.89	0.2
DOCK1	RSRVLFNQL	Kb	68.88	0.2	3.81	RSRVLFNQL	Kb	68.88	0.2

Q6NV99	VARNRFVQI	Kb	72.41	0.2	3.02	VARNRFLQI	Kb	86.06	0.25
EF2	ESFAFTADL	Kb	73.82	0.25	10.49	ESFGFTADL	Kb	139.85	0.4
TM39A	IDYYLAAL	Kb	76.79	0.25	5.40	IDYYLAAF	Kb	1174.9	2
DIP2A	LVFVVGRL	Kb	78.03	0.25	3.45	LVFVVGKL	Kb	317.18	0.8
FZD7	VAHVAAFL	Kb	81.52	0.25	4.78	VAHVAGFL	Kb	552.27	1.2
NDUS6	LTFRRLLTL	Kb	83.09	0.25	6.67	LTFRRLLTL	Kb	83.09	0.25
NDUS6	AAALTFRRL	Kb	85.38	0.25	6.67	AAVLTFRRL	Kb	46.18	0.15
0A087WR45	SSLRAAAEL	Kb	97.81	0.3	ND	SSLRAAPEL	Kb	548.85	1.2
EI3JA	KSLYYASCL	Kb	99.37	0.3	4.27	KSLYYASFL	Kb	35	0.12
WIPI2	QGRAFAAV	Kb	101.34	0.3	4.94	QGRAFATV	Kb	195.29	0.5
Q8C7T0	VLFVMPLL	Kb	102.32	0.3	0.36	VLFVMPLL	Kb	102.32	0.3
RAD9B	ANLILATL	Kb	103.47	0.3	3.09	ANFILATL	Kb	17.83	0.05
WDR82	TNGSFIRL	Kb	104.83	0.3	4.87	TNGSFIRL	Kb	104.83	0.3
M3K6	VCFDYTFAL	Kb	108.47	0.3	3.53	VCFHYTFAL	Kb	120.74	0.4
TT39C	SFVSFLNAM	Kb	111.94	0.3	2.82	SFVSFLNAM	Kb	111.94	0.3
HIPK3	ATLTFEGM	Kb	116.14	0.3	3.49	ATLTSEGM	Kb	8234.68	11
XPC	TVRPYRSL	Kb	117.92	0.4	4.01	TLRPYRSL	Kb	870.16	1.6
TM39B	FNLLMVTPI	Db	118.63	0.07	2.20	FNLLMVTAI	Db	707.26	0.3
MAP1S	VFLRVRAL	Kb	119.32	0.4	4.42	FFLRVRAL	Kb	832.35	1.6
TM246	TSPAAMPL	Kb	123.91	0.4	1.93	TSPAAMLL	Kb	526.6	1.1
WIPI2	RAFAAVRL	Kb	125.31	0.4	4.94	RAFATVRL	Kb	175.45	0.5
SPN90	QNLCYSALV	Kb	126.16	0.4	2.70	QKLCYSALV	Kb	1800.33	3
HERC2	FGQMFAKM	Kb	129.13	0.4	3.22	FGQMCAKM	Kb	7741.34	10
DPOE1	MMKKFFLQL	Kb	129.34	0.4	3.22	MMKKLFLQL	Kb	1065.04	1.9
HTR5A	VLILHAAAL	Kb	130.19	0.4	2.75	ALILHAAAL	Kb	520.07	1.1
LRC28	FVYPTIFPL	Kb	131.88	0.4	3.42	FVYPKIFPL	Kb	70.81	0.2
AP3D1	TNFEWCISI	Kb	132.52	0.4	6.04	TNFEWYISI	Kb	37.86	0.12
XPC	TVRPYRSLL	Kb	140	0.4	4.01	TLRPYRSLL	Kb	759.45	1.5
MGRN1	SAYRYPPK	Kb	140.27	0.4	7.29	SAYRYPPK	Kb	140.27	0.4
ACTN4	VTFQAFIDV	Kb	140.28	0.4	7.10	VTFQAFIDF	Kb	272.3	0.7
PLOD2	**VWQIFENPV**	**Kb**	**144.58**	**0.4**	**4.65**	**FWQIFENPV**	**Kb**	**598.27**	**1.2**
F6SAC3	YMHRFAAYF	Kb	146.38	0.4	ND	YMYRFAAYF	Kb	17.96	0.05
MCES	VAAHYNEL	Kb	146.84	0.4	4.13	VAAHYNEL	Kb	146.84	0.4
EMAL5	STHPYLPI	Kb	147	0.4	3.88	ATHPYLPI	Kb	443.68	1
BRAF	VNYDQLDLL	Kb	152.96	0.4	3.99	VNYDQLDLL	Kb	152.96	0.4
SOX6	ISLREQLL	Kb	156.91	0.4	3.83	ISLREQLL	Kb	156.91	0.4
ARVC	VHLYLSLL	Kb	160	0.4	2.90	VRLYLSLL	Kb	640.52	1.3
HSF2	LNMYGFRNV	Kb	161.71	0.5	4.01	LNMYGFRKV	Kb	596.09	1.2
XYLB	MGFYFDVM	Kb	173.7	0.5	2.50	LGFYFDVM	Kb	353.02	0.8
TM39A	ITVMLARRL	Kb	177.05	0.5	5.40	ITVMLARRL	Kb	177.05	0.5
CATD	VSFANAVV	Kb	180.67	0.5	10.11	VGFANAVV	Kb	902.57	1.7
ANGE2	FSVMSYNIL	Db	181.69	0.1	3.80	FSVMSYNIL	Db	181.69	0.1
FZD7	VAVAHVAAF	Kb	185.7	0.5	4.78	VAVAHVAGF	Kb	215.97	0.6
HERC2	QMFAKMSSF	Kb	187.17	0.5	3.22	QMCAKMSSF	Kb	2320.77	3.5

CATD	VSFANAVVL	Kb	188.51	0.5	10.11	VGFANAVVL	Kb	534.35	1.1
MGRN1	SAYRYPPNS	Kb	194.3	0.5	7.29	SAYRYPPKS	Kb	926.95	1.7
MFAP3	ASFLPSIEL	Kb	195.13	0.5	3.90	ASFLPSFEL	Kb	183.7	0.5
SRBP2	SSALEYLKL	Kb	195.25	0.5	5.32	SSALEYLKL	Kb	195.25	0.5
WDR82	TNGSFIRLL	Kb	198.93	0.5	4.87	TNGSFIRLI	Kb	621.46	1.3
EIF3H	SQFSYQHTI	Kb	202.03	0.5	8.38	SQFSYQHAI	Kb	166.01	0.5
TOPK	AAVILRDAL	Db	203.83	0.12	2.85	AAVILRVAL	Db	848.38	0.4
PEX6	SSQPRLAHV	Kb	204.07	0.5	4.78	SSQPRLAQV	Kb	339.7	0.8
SYTC	TTVYRCGHL	Kb	208.31	0.5	5.50	TTVYRCGPL	Kb	143.81	0.4
DDB1	VLMINGEEV	Db	307.48	0.15	6.34	VLMLNGEEV	Db	295.63	0.15
C99L2	RAQSNPMEL	Db	357.83	0.17	3.98	RAPSNPMEL	Db	21.4	0.01
LINES	MLQNSDTL	Db	373.88	0.17	2.93	MLQNSDKL	Db	2574.57	0.7
DEN5A	RHIQNIGEI	Db	436.1	0.2	6.62	RHIQNIGEI	Db	436.1	0.2
EF2	YLPVNESFA	Db	451.88	0.2	10.49	YLPVNESFG	Db	4988.74	1.3
ACOT2	RGLAMASFL	Db	558.19	0.25	5.05	LGLAMASFL	Db	1667.89	0.5
RL13A	AAIVGKQVL	Db	586.1	0.25	11.60	AAIVAKQVL	Db	1550	0.5
KLH22	YILKNVVAF	Db	626.3	0.25	5.74	YILKNFVAF	Db	374.82	0.17
F2Z4A3	AMQNTTQL	Db	642.84	0.25	4.12	AIQNTTQL	Db	500.29	0.25
AL1B1	TAAVLPNPI	Db	659.13	0.3	2.11	TAAALPNPI	Db	1201.6	0.4
CBPD	YLQTNFFEV	Db	704.18	0.3	3.61	YLQTNCFEV	Db	3949.91	1.1
0A087WR45	AAAELETPL	Db	733.93	0.3	ND	AAPELETPL	Db	83.82	0.06
INT11	**FANNPGPM**	**Db**	**734.5**	**0.3**	**4.57**	**FADNPGPM**	**Db**	**5161.03**	**1.3**

Supplementary Table 5. *In silico* prediction of CMT64.6 neoantigens with NetMHCcons. SB: strong binder, WB: weak binder. Peptides highlighted in red were selected for the tandem minigene. Peptides highlighted in bold were previously published in Woller et al. [180].

Identity	Mutated peptide	Allele	Affinity (nM)	Rank (%)	Binding Level	Expression
D3Z496	VHFSFFTFF	H-2-Kb	26.97	0.07	SB	0.97819563
NDUS6	LTFRRLLTL	H-2-Kb	35.73	0.1	SB	6.32714841
E9PZ36	VTFSRLAVV	H-2-Kb	45.58	0.15	SB	**1.40053793**
E9Q4Y4	SAYHQRTHL	H-2-Kb	50.78	0.17	SB	3.40053793
J3QPX0	KAFARLSSF	H-2-Kb	60.06	0.25	SB	0
D3Z496	SFFTFFSDF	H-2-Kb	82.64	0.3	SB	0.97819563
NEIL3	FMYFGHRAL	H-2-Kb	91.58	0.4	SB	2.11769504
EFHC1	KVLCYLAAL	H-2-Kb	94.61	0.4	SB	1.40053793
ARHGA	**RSFIRTRSL**	**H-2-Kb**	**104.28**	**0.4**	**SB**	**4.08831124**
ITAV	SSILYVKSL	H-2-Kb	112.49	0.4	SB	**5.12225857**
NDUS6	AALTFRRLL	H-2-Kb	113.71	0.5	SB	6.32714841
PIAS2	ISAMLLQRL	H-2-Kb	123.99	0.5	SB	3.8409667
ITFG2	SSVSYVQRV	H-2-Kb	125.34	0.5	SB	3.70043972
KIF15	FVFDYVADM	H-2-Kb	126.7	0.5	SB	3.63691458

UB2L6	SSYYANVLV	H-2-Kb	139.66	0.5	SB	2.07382023
SBP2	CGPGYSTPL	H-2-Kb	147.43	0.8	WB	
F6YJW4	KSRFWYFVL	H-2-Kb	159.03	0.8	WB	
SPP2A	VLGGYWSGL	H-2-Kb	167.87	0.8	WB	
MUC4	SAPITYTHI	H-2-Db	168.78	0.17	SB	
WDR7	HNALRLARL	H-2-Kb	172.47	0.8	WB	
HJURP	STLVRESWL	H-2-Kb	175.29	0.8	WB	
PIAS2	SVYLVRQLI	H-2-Kb	185.03	0.8	WB	
S35F5	FFVWFLANL	H-2-Kb	185.03	0.8	WB	
ATMIN	LNFSAQNGL	H-2-Kb	189.08	0.8	WB	
J3QPX0	KAFALLSSL	H-2-Kb	191.14	0.8	WB	
E9Q4Y4	GAICSREFL	H-2-Db	198.52	0.2	SB	
D3Z5L4	KAFASHSYL	H-2-Kb	203.96	0.8	WB	
SPP2A	VIAVFTVVL	H-2-Kb	229.74	1	WB	
S35F5	SFFFFFVWF	H-2-Kb	232.24	1	WB	
MUC4	SAPITYTHI	H-2-Kb	242.51	1	WB	
W4VSP4	QMMFKKSTF	H-2-Kb	260.18	1	WB	
D3Z496	SVHFSFFTF	H-2-Kb	268.76	1	WB	
PLIN2	MLVDQYFPL	H-2-Kb	282.17	1.5	WB	
E9Q4Y4	IVVKRLRAV	H-2-Kb	348.45	1.5	WB	
F6YJW4	VAKSRFWYF	H-2-Kb	398.91	1.5	WB	
NDUS6	AAALTFRRL	H-2-Kb	405.44	1.5	WB	
F6YJW4	HFWYFVSQL	H-2-Kb	418.82	1.5	WB	
SCD3	IFIDCMAAL	H-2-Kb	418.82	1.5	WB	
Q9DAV6	ANSTFAIHL	H-2-Kb	423.37	1.5	WB	
F264	VVAANFVQV	H-2-Kb	425.67	1.5	WB	
HJURP	ESRSRFQTL	H-2-Kb	425.67	1.5	WB	
I20L2	NAVLNSTQA	H-2-Db	437.34	0.3	SB	
UB2L6	YANVLVWHM	H-2-Db	471.75	0.4	SB	
SCD3	RWHINFTTI	H-2-Db	528.51	0.4	SB	
Q9EQC8	LAPALPPPL	H-2-Db	598.54	0.4	SB	
D3Z5L4	KAFASHSYL	H-2-Db	723.31	0.5	SB	
SYLM	RQLVSGPPV	H-2-Db	864.68	0.5	SB	
ARHGA	**ADPANTAWI**	**H-2-Db**	**968.71**	**0.8**	**WB**	4.088
E9Q4Y4	**QIINNSVTL**	**H-2-Db**	**995.27**	**0.8**	**WB**	3.4
MUC4	SAPIISTHI	H-2-Db	1376.93	0.8	WB	
ASH1L	RSPRLVACM	H-2-Db	1414.68	0.8	WB	
J3QPX0	KAFALLSSL	H-2-Db	1445.63	0.8	WB	
TB182	AALPVLEPV	H-2-Db	1593.49	0.8	WB	
E9Q4Y4	FQIINNSVT	H-2-Db	1884.44	1	WB	
E9Q4Y4	FLTWGGVPL	H-2-Db	1915.27	1	WB	
MUC4	TAPSTTHIL	H-2-Db	2032.71	1	WB	
F264	VVAANFVQV	H-2-Db	2122.61	1.5	WB	
NEIL3	FMYFGHRAL	H-2-Db	2302.04	1.5	WB	
GCSH	YSLRTALAF	H-2-Db	2664.09	1.5	WB	
A0A0G2JG52	FNSSNTSHL	H-2-Db	2678.54	1.5	WB	

HJURP	STPQTASTL	H-2-Db	2766.91	1.5	WB	
D3Z496	FTFFSDFVI	H-2-Db	2812.19	1.5	WB	
Q9EQC8	AAPMPEPTL	H-2-Db	2858.2	1.5	WB	
V9GXQ2	FETFNTPAM	H-2-Db	3000.81	1.5	WB	
E9Q4Y4	SAYHQRTHL	H-2-Db	3066.45	1.5	WB	
V9GXQ2	NTPAMYNAI	H-2-Db	3254.47	1.5	WB	
RAB13	**SDKKNNKCL**	**H-2-Kb**	**33504.88**	**50.00**	-	**4.094**
BIR1B	**CPLLNRFQL**	**H-2-Db**	**4936.17**	**3.00**	-	**2.72**
NEST	**SIEENLGTV**	**H-2-Db**	**6829.04**	**3.00**	-	**1.64**
NDUS1	**ILAAVSNMV**	**H-2-Kb**	**8119.76**	**16.00**	-	**5.27**

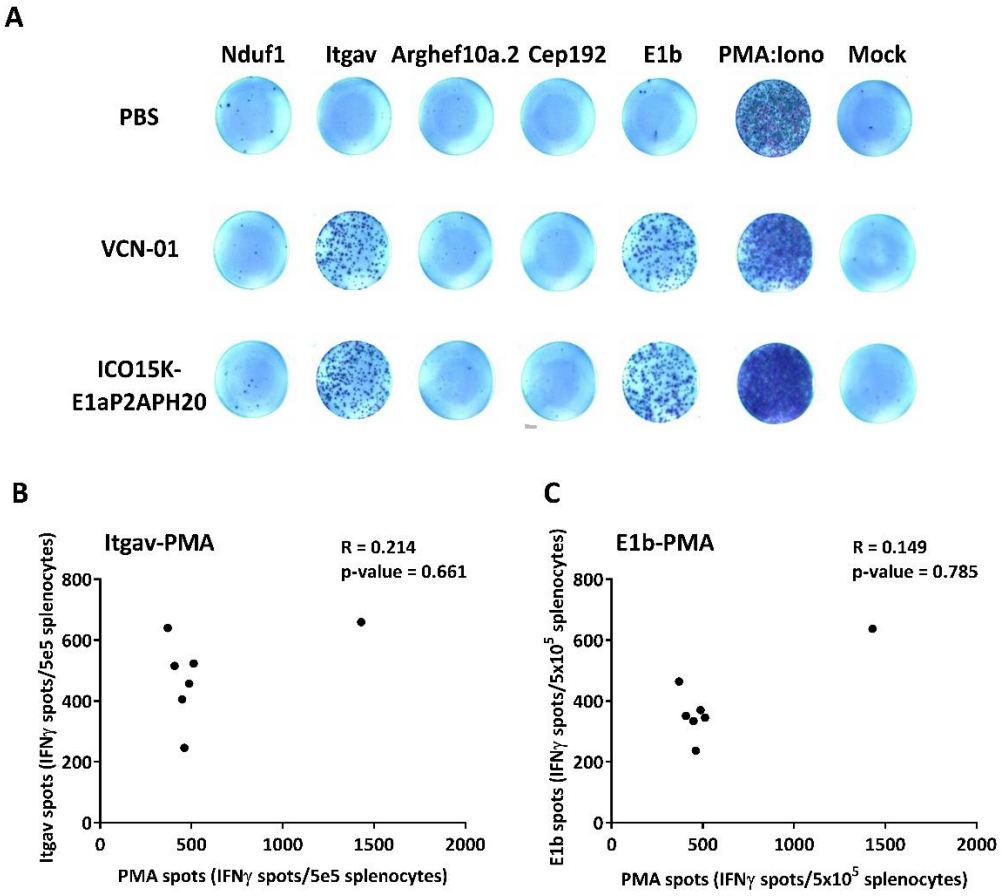

Supplementary Figure 8. Immune response in E138/18. (A) Representative images ELISPOT wells for every group. PMA:Iono was used as a control positive of stimulation, and Mock as a negative control. **(B)** Spearman correlation of IFNγ-spots after stimulating with Itgav or PMA:Iono. **(C)** Spearman correlation between of IFNγ-spots after stimulating with viral E1b or PMA:Iono. The correlation coefficient (R) and p-value is presented in each graph.